DESIGN OF MILLIMETER MICROWAVE DEVICES USING METAMATERIALS AND ELECTROMAGNETIC BANDGAP STRUCTURES

A thesis submitted to

Delhi Technological University

for the Award of Degree of

Doctor of Philosophy

in

Electronics and Communication Engineering

by

KARTEEK VISWANADHA

(Enrollment No.: 2K16/Ph.D/EC/11)

Under the Supervision of

Dr. N. S. RAGHAVA

Professor

Department of Electronics and Communication Engineering

Delhi Technological University (Formerly DCE)

Bawana Road, Delhi - 110042, India.

November, 2022.

DECLARATION

I declare that the research work reported in this thesis entitled "**Design of Millimeter Microwave Devices using Metamaterial and Electromagnetic Bandgap Structures**" for the award of the degree of *Doctor of Philosophy in Electronics and Communication Engineering* has been carried out by me under the supervision of Prof. N.S. Raghava, Department of Electronics and Communication Engineering, Delhi Technological University, Delhi, India.

The research work embodied in this thesis, except where otherwise indicated, is my original research. This thesis has not been submitted by me earlier in part or full to any other University or Institute for the award of any degree or diploma. This thesis does not contain other person's data, graphs or other information, unless specifically acknowledged.

Date: 17/03/2025

(Karteek Viswanadha)
Enrollment no.: 2K16/PhD/EC/11
Department of ECE
Delhi Technological University,
Delhi-110042, India

DELHI TECHNOLOGICAL UNIVERSITY

(Formerly Delhi College of Engineering)

Shahbad Daulatpur, Bawana Road,

Delhi- 110042, India

CERTIFICATE

This is to certify that the research work embodied in the thesis entitled **" Design of Millimeter Microwave Devices using Metamaterial and Electromagnetic Bandgap Structures"** submitted by **Mr. Karteek Viswanadha** with enrollment number **(2K16/Ph.D/EC/11)** is the result of his original research carried out in the Department of Electronics and Communication Engineering, Delhi Technological University, Delhi, for the award of **Doctor of Philosophy** under the supervision of **Prof. N.S. Raghava.**

It is further certified that this work is original and has not been submitted in part or fully to any other University or Institute for the award of any degree or diploma.

This is to certify that the above statement made by the candidate is correct to the best of our knowledge.

(Prof. N.S. Raghava)
Supervisor
Department of ECE
Delhi Technological University
Delhi-110042

ACKNOWLEDGEMENTS

Any job in this world cannot be accomplished without the assistance of others. First of all, I would like to thank the God for providing me the strength to complete this work. I also feel a deep sense of gratitude in thanking all those who helped me to carry this work to its eventual fruition.

I would like to express my gratitude to my able and invaluable research supervisor Dr.N.S.Raghava, Professor, Electronics & Communication Engineering, Delhi Technological University, Delhi (India), for giving me an opportunity to pursue this research work under his supervision. It has been my honor to work under his guidance and the words cannot express his invaluable support he has provided me over the years. I appreciate all his contribution of time and ideas to make my Ph.D experience productive and simulating. The joy and enthusiasm he has for his research was contagious and motivational for me.

I would like to thank to Dr. B.T.P. Madhav, K.L. University, Vijayawada for his help in my research journey.

I would like to thank Professor S. Indu, and Professor Neeta Pandey for continuous support throughout my Ph.D.

It is my pleasure to thank all the faculty members of the Department of Electronics and Communication Engineering and Technical staff for their help.

I would like to thank Mr.O.P.Gupta I.A.S (Controller General of patents and designs) for permitting me to pursue part time Ph.D. Without his immense support, I would not have carried out research work at the right time.

Above all, I would like to express my heartiest thanks to all my family members whose blessings and affection have been remained constant source of inspiration. I have no words to express my gratitude to my father-in-law late.Mr.Pappu Satyanarayana, my grandmother late. Viswanadha Lakshmi, my paternal grandfather Mr. Viswanadha Appala Narasimha Murthy, mother-in-law Ms.Pappu Nagamani, my maternal grandmother Ms.Ayyalasomayajula Lakshmi, and brother Mr.Vivek Viswanadha, last and never the least, my son Satya Krishang Viswanadha.

Words cannot express my deep sense of gratitude to my life partner “Pappu Deepti” for her encouragement, motivation, understanding, cooperation and positive support during every stage of this work. I might not be able to reach at this stage without her. She is always there cheering me up and stood by me through the good and bad times equally. Last, but not least, I would like to dedicate my thesis to my beloved wife and loving parents for their endless love, patience and understanding.

Date : 17/03/2025 **(Karteek Viswanadha)**

Place : Delhi, India.

DEDICATED TO MY BELOVED PARENTS

&

GRANDFATHER

Viswanadha Surya Rama Sarma

Viswanadha Jayaprabha

&

Late. Ayyalasomayajula Suryanarayana

CONTENTS

Abstract

Microstrip patch antennas are planar in nature with a radiating patch printed on the top of the substrate and the whole structure is mounted on the ground plane. These antennas can be easily integrated with very large scale integrated (VLSI) circuits. The compactness of these antennas can be achieved by using techniques such as varying substrate thickness, stubs, slots, shorting pins, Defective Ground Structures (DGS), Electromagnetic Bandgap Structures (EBG) and metamaterials thereby making them suitable candidates for High Frequency (30MHz-300MHz) communications. But these antennas are prone not only to ohmic and radiation losses but also suffer from unstable gains and radiation patterns.

A large co-polarization radiation component is desired in conventional patch antennas especially in beam-forming and beam switching applications. But unstable radiation patterns and gains in patch antennas decrease the co-polarization levels and increase cross-polarization levels. Cross-polarization levels depend on the surface current distribution of higher frequency modes. These modes are responsible for generation of surface waves in the antennas and thus deviating radiation from antenna boresight. Cross-polarization levels are usually reduced by thinning the substrate thickness and/or by connecting shorting pins to the antenna. But these techniques offer limited solution to reduce cross-polarization level in antennas. Using different techniques mentioned in the first paragraph, the cross-polarization levels can be reduced. The antennas for different applications such as C-band, WLAN, WMAX, X-band, K-band, Ku-band applications etc are designed in this thesis.

In the first chapter, various types of fundamental antennas like rectangular, semi-circular, square, oval and circular are studied analysing different performance parameters. Due to the planar nature, these antennas radiate in z-direction due to fringing fields when they are placed in x-y plane. The analysis of near and far fields using cavity model is discussed. Cavity model is used to analyse the electric and magnetic fields in the fabricated antenna discussed in the further chapters. The structures of the antenna are further modified by the above-mentioned techniques and their performance parameters are studied in the further chapters.

In second chapter, different types of stubs loaded small antennas are designed and discussed. These stubs loaded antennas act as solution to the problems encountered by the antennas in the first chapter. In this chapter, a ‘L’ shaped stub loaded serpentine shaped patch antenna and a ‘L’-shaped stub and meander shaped stub loaded oval shaped patch antenna are discussed. To

miniaturize the antennas and make them operate at lower giga-hertz frequencies, the antennas are attached with 'L'-shaped stubs and folded meander lines. The effect of stubs on the antenna's performance parameters is studied. Folded stub line loaded serpentine shaped patch antenna possesses the simulated bandwidths of 662MHz, 1.6GHz and measured bandwidths of 660MHz and 1.52GHz. Measured gains of 3.2dBi, 5.42dBiand 5.56dBi along with the efficiencies of 82.1%, 86.3% and 88.1% are obtained at 6.8GHz, 9.51GHz and 9.89GHz respectively. The radiation patterns of the fabricated prototype are unidirectional E- and H-planes at 6.8GHz. At 9.51GHz, the radiation patterns are omnidirectional in H-plane and unidirectional in E-plane. The radiation patterns are unidirectional in E- and H-planes at 9.89GHz. Stub loaded oval ring patch antenna resonates at 6.21GHz, 9.4GHz, 16.78GHz and 25GHz. The simulated and measured values of performance parameters of the proposed antenna are obtained. The measured gain values are observed to be 1.01dBi at 6.21 GHz, 1.2dBi at 9.4 GHz and 5.6dBic at 16.78GHz. At 25GHz, there is a gain of 8.1dBi. The efficiencies of 60.14% is obtained at 6.21GHz, 74.3% at 9.4GHz and 78.6% at 16.78GHz. Similarly, an efficiency of 83.64% is obtained at 25GHz. The radiation patterns of the proposed patch are unidirectional in all the planes at 6.21GHz, 9.4GHz, 16.78GHz and 25GHz.The proposed prototype is circularly polarized at 16.78GHz and linearly polarized at other frequencies of operation.

Antennas discussed in the second chapter suffer from unstable gain and higher order modes. To overcome these problems, antennas designed in the third chapter act as a solution. In this chapter, a study on dumbbell shaped High Impedance Surfaces (HIS) is carried out. Stub loaded oval-shaped patch antenna is mounted on dumbbell-shaped metamaterials (MTM), electromagnetic bandgap structures (EBG), and defective ground structures and the effect of the latter on the earlier is discussed. Effect of the ground plane on the metamaterial is discussed. The selection of particular HIS based on the application's requirement is discussed. These structures are used along with the stub loaded oval-shaped patch antenna to further enhance the performance parameters. Metamaterial antenna possesses high bandwidths in the frequency ranges 12.72GHz – 14.23GHz (1.51GHz) and 16.52GHz – 18.71GHz (2.19GHz). EBG mounted patch antenna is used to achieve further miniaturization and DGS mounted patch antenna is used to achieve high gain at all its resonant frequencies.

Though HIS loaded antennas show superior performance, these antennas show degradation in the performance when more high impedance cells are loaded in the antenna structure. The

antenna designed in the fourth chapter discusses the holistic approach to achieve the improved performance with reasonable gain, efficiency and bandwidth. This chapter discusses the design and analysis of ultra-wideband, dual polarized and highly efficient dual feed dumbbell shaped patch antenna. The design of splattered ring EBG is discussed. The effects of using EBG on the antenna and the variation in the performance parameters are described. Total dimensions of the proposed antenna are 25 x 30 x 1.524mm^3. The axial ratio of the antenna at 11.78GHz is 2.1dB and 4dB at remaining frequencies of operation. A wide-bandwidth of 20.2GHz (171.4%) along with a varying gain in the range of 6.21dB to 9.03dB in the range of frequencies 10.8GHz to 31GHz is achieved by the proposed structure. A wide range of efficiencies varying from 88.34% to 91.06% is achieved. Another antenna discussed in this chapter is swastika EBG mounted slotted antenna. This antenna is designed to radiate at 21.29GHz. The proposed antenna is simulated using Advanced Design System-2016. Gain and bandwidth of the proposed antenna are observed to be 11.92dB and 3.2GHz respectively.

The purpose of achieving the miniaturization at lower gigahertz range is served by the antenna discussed in the fifth chapter. The antenna is designed by placing circular patches of different radii along the circumference of a central circular patch and thereby forming the proposed flower-shaped patch antenna. The design of proposed antenna is inspired from kissing circles theorem in geometry. The proposed structure is mounted on and loaded with Double Negative (DNG) triple Complementary Split Ring Resonator cells. The overall dimensions of the patch are 23.5 × 16 x 1.6 mm^3. This antenna operates at 5.2GHz as well as 8.25GHz. This also owns a wider bandwidth of 1.2 GHz (24.1%) in the ranges of 4.95 to 6.15 GHz and also a wider bandwidth of 2.2 GHz (26.5%) in the ranges of 7.1 to 9.3 GHz. There is a gain of 3.93 dBi and 5.02 dBi observed in the frequency ranges of operation. The radiating electric, magnetic fields and the green's function are analysed using cavity model. The designed structure is useful for several applications, such as WLAN, WiMAX, and ISM band.

Important parameters in modern day wireless communications are beam switching and low cross-polarization levels. This feature cannot be achieved with the antenna discussed in the previous chapter. Hence, chapter five provides the solution to the above requirements. This chapter throws the light on design and analysis of a meta post loaded slotted waveguide antenna array. The resonant frequencies of the proposed structure are 3.1GHz, 3.3GHz, and 4.1GHz. The simulated gains of 11.3dBi, 14.1dBi and 12.6dBi are observed at these frequencies. The proposed antenna operates in the frequency ranges of 3.01GHz to 3.12GHz, 3.2GHz to

3.44GHz and 3.91GHz to 4.45GHz. Also, the meta post loaded slotted waveguide antenna array exhibits beam switching feature in E-plane with the side lobe level with low cross-polarization levels.

Meta post loaded slotted array waveguide antenna is an excellent candidate for high gain applications. But complex and bulky nature of this antenna makes it prone to high ohmic losses and radiation deflections. Hence, stable radiation patterns cannot be achieved with these types of structures. The solution to these problems is to design concatenated antennas as discussed in the seventh chapter. The patch antenna presented in the second chapter is loaded on a serpentine shaped EBG ground is described in this chapter. Here, the radiation element is an oval shaped patch antenna and serpentine shaped patch slots are etched on the ground. Overall dimensions of the proposed patch antenna are 18 x 18 x 0.8mm^3. The structure is miniaturized by 89.1%. The resonant frequencies of the proposed patch are 4.28GHz, 6.15GHz, 6.78GHz and 12.15GHz. The peak gains at the frequency of operations are 1.1dBi, 1.3dBi, 2.8dBi and 2dBi. The radiation patterns are seen to be stable at the resonant frequencies.

In miniaturized antennas, it is difficult to maintain high gain up to higher frequencies and at the same time it is difficult to maintain stable radiation patterns. Artificial intelligence devices must be used to direct the radiation leakages towards the antennas. These artificial devices direct the current on the patch with improved power gain and reduce the eddy current losses. Further, many techniques can be developed to improve the quality of communication from one place to another by introducing MIMO, fractal antennas, superstrates, Substrate Integrated Waveguide etc.

List of Figures

List of Tables

CHAPTER 1

Introduction to different microstrip patch antennas

1.1. Introduction

Antennas are one of the important devices in the front and back ends of the transceivers. Many antennas line horn antenna, helical antenna, parabolic antenna etc. are introduced to get high data rates which are highly essential in the recent technologies. But these antennas are bulky and cannot meet the specifications of large- scale integration. To meet the large-scale integration requirements, microstrip antennas are used. These devices are planar and easy to integrate. Easy integration of these antennas makes them suitable for Ultra Large Scale Integrated (ULSI) circuits. The overall dimensions of these antennas are further optimized to meet the higher generation communication requirements. Though these antennas enjoy various advantages, they often prone to radiation leakage losses at the interfaces. Therefore, the structure of conventional patch antenna is further modified by attaching radiating stubs, inserting slots, attaching shorting pins and/ or modifying the ground plane. These modified structures are aimed to achieve features like wide bandwidth, beam-forming, beam-switching, high gain etc. which are essential for higher generation communication technologies. Though these antennas fit into ULSI technology, they often suffer from high radiation spillages. To overcome these drawbacks, slotted waveguide antenna arrays are deployed to achieve high gains and to meet the requirements of 5G/6G technologies.

This antenna radiates through the slots which are etched on its top surface. The spacing between two slots must be an integral multiple of guided wavelength. By choosing so, the antenna will be free from radiation leakages. Directivity is enhanced by choosing the dimensions and position of the slot. The dimensions and number of the slots decides the gain, efficiency and bandwidth of the slotted waveguide antenna array. Increase in the number of slots increase gain, and co-polarization radiation levels. Increase in the gain and co-polarization levels may not assure stable radiation patterns in the desired directions. This unstable radiation patterns lead to increase in the cross-polarization levels. Cross-polarization levels depend on the surface current distribution of higher frequency modes. These modes are responsible for generation of surface waves in the antennas and thus deviating radiation from antenna

boresight.

This chapter discusses various types of fundamental antennas like rectangular, semi- circular, square, oval, slotted waveguide antenna array and circular are studied analyzing different performance parameters. The analysis of near and far fields using cavity model is discussed. Cavity model is used to analyze the fields in the fabricated antenna as discussed in the further chapters. The structures of the antenna are further modified by the above-mentioned techniques and their performance parameters are studied in the further chapters.

1.2. Microstrip patch antenna

Microstrip patch antennas were first designed Deschamps in the year 1953. A microstrip antenna consists of a metallic patch printed on a grounded substrate. However practical antennas were fabricated only after 20 years as advanced fabrication techniques for copper or aluminium layered dielectric substrates with different relative permittivites, thermal conductivities, electrical conductivities and dielectric losses were introduced. The antenna was first fabricated in the 1970's by Howell and Munson. Aftermath many advanced developments and designs in the field of microstrip antennas have led to diversified applications due to their superior features over large antennas such as planar nature, compactness, conformality with the monolithic microwave integrated circuits (MMICs). Due to the above advantages, these antennas are implemented in vehicular and wireless communications. These antennas are integrated in low power VLSI devices and thus making them suitable for low power communication systems and high data rate wireless devices. The popularity of Microstrip antennas is increasing due to their low-key nature. Hence, making them more compatible with embedded antennas used in handheld devices. The antennas on modern wireless devices and telemetry need to be compact and highly integrable. These are often microstrip patch antennas which meet the above requirements. The features discussed above make these antennas apt for space communication applications. It comprises of a conductor which acts a radiating element printed on a dielectric substrate and the whole structure is mounted on a ground plane. The radiating element can be of any shape depending on the type of application.

Fringing fields in the patch contribute to the radiating fields in the patch. The electric and magnetic fields in microstrip patch antenna are analysed by different methods. These methods include transmission line model, cavity model and full wave analysis. Full wave analysis is based on Finite Element Method (FEM). The transmission line model is easiest and simplest

of all, but it is less accurate. The performance of a patch antenna depends on the type of dielectric substrate used. Usually, the relative permittivities of these substrates vary from 1 to 10. Lower dielectric constant provides higher radiation efficiency, wide bandwidth and reasonable gain as fields are loosely confined inside the substrate. But all these features are achieved at an expense of area of the patch.

1.3. Different types of patch antennas

In the recent times, varieties of patch antennas are proposed. Widely used patch antennas are rectangular, circular and oval type. Ease of design and compactness of these antennas make them suitable for many wireless applications. These antennas usually possess reasonable gain, efficiency, bandwidth and circular polarization which is necessary in the modern wireless communications. Different patch antennas are discussed in the further sections.

1.3.1. Rectangular patch antenna

These antennas are easy to design and integrate with VLSI systems. Apart from the above features, these antennas are easy to analyse. A conventional rectangular microstrip patch antenna is presented in Figure 1.1.

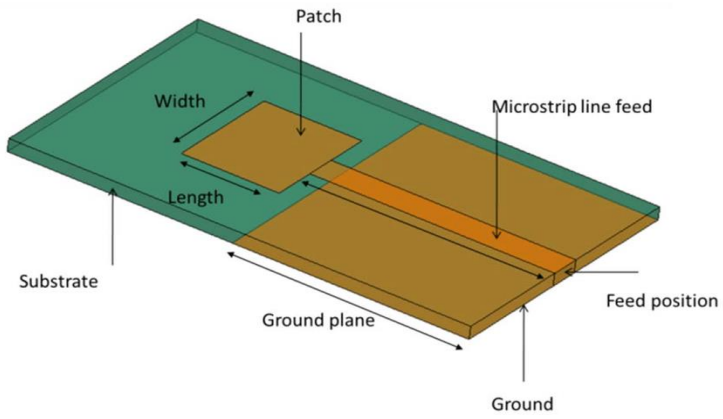

Fig.1.1. Structure of rectangular microstrip patch antenna

The resonant frequency of the antenna varies with its length. The length of the antenna is inversely proportional to the operational frequency [1].

Frequency of the patch (f_r) = $\frac{C}{2L\sqrt{\varepsilon_r}}$ (1.1)

Where ‘c’ represents the speed of light

‘L’ represents length of the patch antenna

‘ε_r’ represents relative permittivity

The opposing edges of the patch antenna are treated as slots. These edges do not radiate as long as the feed position is not at the centre of the edges. Thus, it is observed that a rectangular patch is modelled as two slots fed by a transmission line. A slot is equivalent to parallel resonant tank circuit. Figure.1.2. presents the equivalent circuit of a conventional antenna.

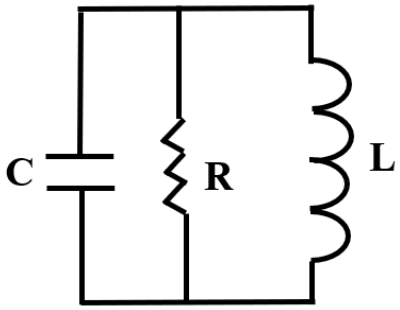

Fig.1.2. Lumped element equivalent of rectangular patch antenna

However, this equivalent circuit does not model mutual inductance between the two radiating edges. Hence, this model becomes inaccurate while analysing non-rectangular patch antennas.

The input impedance of a patch is inversely proportional to its width. The width ‘W’ of the microstrip antenna not only controls its impedance but also radiation patterns. Apart from the parameters, the position of the feed line determines the impedance of a patch. Feed line provides a wide range of frequencies to the antenna. The impedance or operational bandwidth of a patch antenna is the band of frequencies for which impedance of the feed line is matched with the input impedance of the patch. Usually, lower input impedance patches occupy higher space. Moreover, rectangular patch antenna supports single mode. Square shaped patch antenna offers better features like multi-frequency, multiband for the same length as that of the rectangular patch antenna. However, conventional rectangular/ square patch antennas are not compact at lower gigahertz frequencies. Therefore, circular patch antenna is used to achieve miniaturization at lower gigahertz frequencies.

1.3.2. Circular patch antenna

Circular patches provide high quality factors when compared to rectangular patch antennas. Circular patches not only possess high quality factors but also high gains and directivities. Figure.1.3. shows the circular patch antenna.

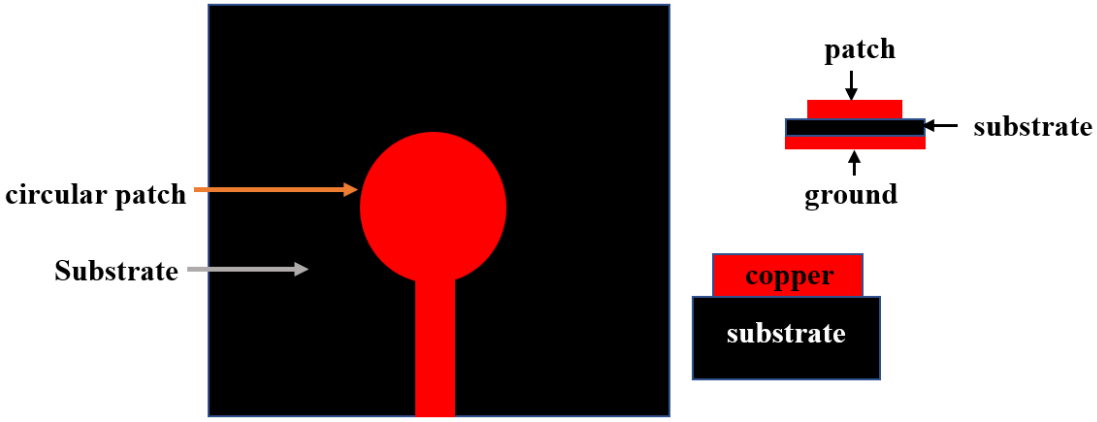

Fig.1.3. Circular patch antenna

The resonant frequency (f_r') of circular patch antenna depends on the effective radius (r_e) of the patch [2].

$$f_r' = \frac{1.8412 * c}{2\pi(r_e)\sqrt{\varepsilon_r}} \tag{1.2}$$

$$r_e = r\left[1 + \frac{2h}{\pi r \varepsilon_r}\left\{\ln\left(\frac{r}{2h}\right) + (1.41\varepsilon_r + 1.77) + \frac{h}{r}(0.268\varepsilon_r + 1.65)\right\}\right]^{\frac{1}{2}} \tag{1.3}$$

Where 'r' represents the radius of the patch

'ε_r' represents the relative permittivity

'h' represents height of the substrate.

Effective radius of the patch depends on the relative permittivity of substrate, radius of the patch and thickness of the substrate.

Larger is the radius, lower is the resonant frequency. To reduce the space occupied by the circular patch antenna, semi-circular patch antenna is opted. This patch operates at the same frequency as that of circular patch antenna with half of the total area as that of circular patch antenna. Apart from the compactness, semicircular patch antenna does not offer any other advantages.

The antenna designed in 5th chapter is based on the concept of circular patch antenna. This antenna is obtained by placing a circular patch in the middle and small circular patches with different radii around the circumference of central circular patch. Though different types of circular patches are designed, their radii limit the bandwidth. Radius of the circular patch not only limits the bandwidth but also limits the frequency of operation. Due to this reason, only single mode is supported by circular patch antenna. To make circular patch antenna radiate at multiple frequencies, oval shape patch antenna is designed.

1.3.3. Oval shape patch antenna

Oval shape patch antenna is obtained by attaching semi-circular patches at the ends and rectangular or square patch in the middle. This antenna has multiple degrees of freedom such as length of major and minor axis and is highly flexible. This patch antenna possesses enhanced bandwidth. This introduces multiple frequencies of operation. This antenna is usually used for circular polarization applications. Figure.1.4. shows the oval shaped patch antenna.

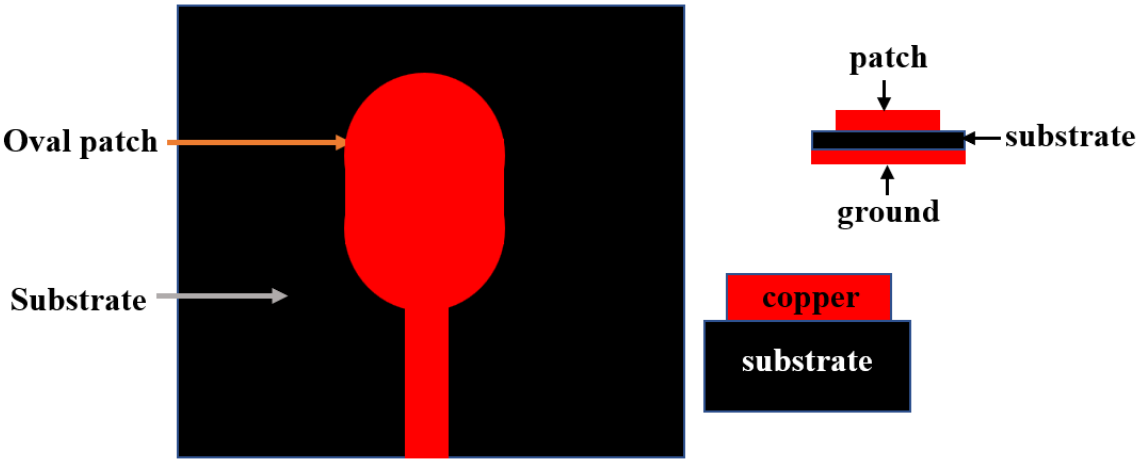

Fig.1.4. Oval shaped patch antenna

The operational frequency depends on the length of major axis. The resonant frequency of the patch is obtained from eq.1.3.

Though different shapes of conventional antennas are designed, these antennas suffer from certain limitations such as narrow bandwidth, low efficiency, and possibility of excitation of surface waves.

To provide the solutions to the problems faced by conventional patch antennas, different types of stub-loaded and High Impedance Surface (HIS), SIW antennas are designed in the recent literatures. These antennas are discussed in the literature review presented in the next section.

1.4. Literature Review

Aakash Bansal *et.al.* in [3]: presents a review on different feeding techniques to feed patch antennas such as inset feed, coaxial feed and edge feed to improve antenna's gain.

Zhan-Hong Zeng *et.al.* in [4]: presents a technique to reshape the surface currents, pattern corrections and polarization reversal. Slot loading disturbs the surface currents on the patch and thereby increasing the electrical length of each mode.

Ali I.Aabdalla *et.al.* in [5]: presents a square shaped slotted patch antenna. M-slot is etched on the patch and the structure is mounted on the ground plane with rectangular slot etched on it. The structure resonates at 2.4GHz, 4.55GHz, and 7.63GHz.

Ajay Yadav in *et.al.* in [6]: presents a circular patch antenna with rectangular slot DGS. The designed antenna resonates at 5.5GHz. Stubs attached to the metallic patch makes it polarization reconfigurable.

K.P.Ray *et.al.* in [7]: presents a circular patch antenna with an electrically small slot cut along the feed axis. The slotted patch resonates at 1800MHz and 2400MHz and is deployed for GSM and Bluetooth applications.

Amir Jafargholi *et.al.* in [8]: presents a capacitively loaded loop (CLL) metamaterial (MTM) to attenuate surface waves. The patch possesses gain and efficiency of 7.8dBi and 95%i at 3.18GHz.

Hilal M. El Misilmani,Mohammed *et.al.* in [9]: presents a planar slotted waveguide antenna arrays. The antenna resonates at 3.97GHz with a peak gain of 26dBi. Slots and the waveguide walls are displaced to control the side-lobe levels.

Wai Yan Yong *et.al.* in [10]: presents a bandwidth enhanced 8 x 8 cavity-backed slotted array antenna. The antenna consists of four 2 x 2 subarrays fed by ridge gap waveguide and a modified bow-tie coupling slot in the cavity layer. The proposed antenna resonates at 24GHz, 26GHz, 28GHz, and 30GHz. The proposed possesses a gain peak gain of 24.6dBi.

E.Baum Carl in [11]: presents a slotted waveguide antenna array with slots etched on its sidewalls. Aa brief analysis on placement of slots, and slot dimensions is presented.

Li.J-Y. *et.al.* in [12]: presents a detailed mathematical analysis on radiating fields in slotted waveguide antenna array using Metho of Moments (MoM). The variation in the radiation is observed with the narrow-wall slots cut at various angles of inclination.

Itoh Keiichi *et.al.* in [13]: presents a waveguide slot antenna with dielectric lenses. Micro-genetic algorithm (MGA) with the real-coded gene is implemented to optimize the slot length and offset parameters. Aperture fields are observed to be uniform and side lobe levels (SLL) are improved.

Sekretarov .S *et.al.* in [14]: presents a wideband slotted waveguide antenna array for X-band applications. The longitudinal slots on the antenna are optimized to achieve improved performace. The antenna possesses beam and gain of 4^o x 6^o and 30dB respectively.

Qiang Fu *et.al.* in [15]: presents an ultra-broad band radar cross section reduction slotted waveguide antenna array. The waveguide is loaded orthogonal double split ring resonators. The antenna achieved 17.81 dB at 8.68 GHz for x-polarized incidence and 21.79 dB at 6.25 GHz for y-polarized waves.

Keltouma Nouri *et.al.* in [16]: presents a slotted waveguide antenna array. This antenna has a vertical row of slots along the length of a vertical waveguide, with the array of slots increasing the gain by flattening the vertical beam. The whole array antennas including two slots and feeding element is completely constructed at a single substrate by using substrate integrated waveguide technique and tapered micro-strip transition.

Yousefbeigi M. *et.al.* in [17]: presents a 2 x 8 microstrip antenna array fed by SIW feed system. The antenna possesses a gain of 17.9dBi in the frequency range of 17.4GHz to 18GHz.

Clauzier.S *et.al.* in [18]: presents a slotted waveguide antenna array possessing near-field focused beam in E- plane. The antenna illuminates a linear array as reflect- or transmit-array antenna with a small width (100 mm) and a very large length (1530 mm) located in the near-field region.

G.Srivastava *et.al.* in [19]: presents a differential substrate integrated waveguide (SIW) antenna with good common-mode (CM) suppression and high gain. The designed antenna uses an H-shaped slot backed by SIW cavity and is differentially excited by two microstrip feedlines from two opposite sides of the cavity. The differential impedance bandwidth of the proposed antenna is 10.19–11.03 GHz with CM suppression below 2dB.

Mehmet.A.Belen *et.al.* in [20]: presents a brief design of octagonal and circular patch antennas. These antennas are designed on SIW for X-band applications. These antennas possess high gain, directivity and high degree of miniaturization.

Sama Leme *et.al.* in [21]: presents a SIW slot antenna fed through a cavity. The antenna radiates in such a way that the antenna patterns are confined to the hemisphere depending on the slot orientation from the boy and thereby affecting the directivity.

Massimiliano Casaletti *et.al.* in [22]: presents an SIW-based antenna utilising full wave analysis. The antenna implements a hybrid method-of moments and mode-matching approach. Entire-domain basis functions are chosen to minimize the number of unknowns, and an efficient computation of Green functions for large radial distances is granted by means of a radial-transmission-line representation.

The antennas discussed in the literature review possesses enhanced performance parameters. Usually, these parameters are enhanced by the multiple modes supported by the patch antennas. These multiple modes are viewed as higher order modes which usually analysed through surface current distributions. Surface current distributions are studied using modal analysis.

1.5. Modal analysis

Modal analysis gives the surface current distribution at different frequencies at which patch antenna resonates and the radiation pattern corresponding to these resonant frequencies. Modal analysis or The Characteristic Modes (TCM) is an eigen value problem where the surface current on the patch is treated as eigen vector and its value is treated as eigen value. Characteristic modes are mathematically analysed on the copper conductor [23].

$$[\Lambda(J)E^{i}]^{tan} = 0 \tag{1.4}$$

Where Λ is a linear operator with tan representing the tangential fields on the patch. Linear operation of is sum of vector and scalar potentials. Vector potential is due to magnetic field and scalar potential is due to electric field. The linear operator is given by:

$$\Lambda(J) = j\omega A(J) + \Delta\phi(J) \tag{1.5}$$

where A (K) and Φ (K) are vector and scalar potentials respectively. The term Λ (K) is electric field intensity at any point in space. This means that the operator Λ in (1) has the dimension of impedance:

$$Imp(K) = \Lambda(K)_{tan} \quad (1.6)$$

The operator of space impedance Imp is complex from [1], and it can be written as,

$$Imp(K) = Res(K) + jReact(K) \quad (1.7)$$

The characteristic current modes are obtained from the eigen value problem given by

$$X(\overrightarrow{J_n}) = \lambda_n R\ (\overrightarrow{J_n}) \quad (1.8)$$

where 'Res' and 'React' are resistance and reactance parts of impedance operator Imp=Res+jReact, λ_n is eigen value, $\overrightarrow{J_n}$ is eigen function. The above relation shows the distribution of surface currents on the patch depending on its shape. Thus, modal analysis is useful in calculating surface currents and the corresponding radiating fields. After studying the modal analysis, different models are discussed to analyse fields and radiating fields in the patch antenna. Further, modal analysis is used to obtain different modes in the patch antenna designed in chapter-2.

1.6. Analysing methods

Microstrip patch antennas are analysed using different models such as transmission line model, cavity model and full wave analysis model which includes Finite Element Method(FEM). Transmission model is teasy to analyse and is useful in calculating the resonant frequency of a patch antenna. This model is inaccurate and fails for complex models of patch antennas. Cavity model is precise of all the analysing methods and at the same time complex to compute. Full wave models are more precise and can analyse complex models using Finite Element Method (FEM), Method of Moments (MoM). Transmission line and cavity models are discussed in the next section.

1.6.1. Transmission line model

As explained in the introduction section, patch antenna is treated as slotted antenna with the slots etched along the width 'W' and the length 'L' with the thickness equal to the height of the substrate 'h'. Microstrip line is sandwiched between two dielectrics i.e. air and substrate. Due to this, microstrip line become a non-homogenous transmission line as shown in figure.1.5.

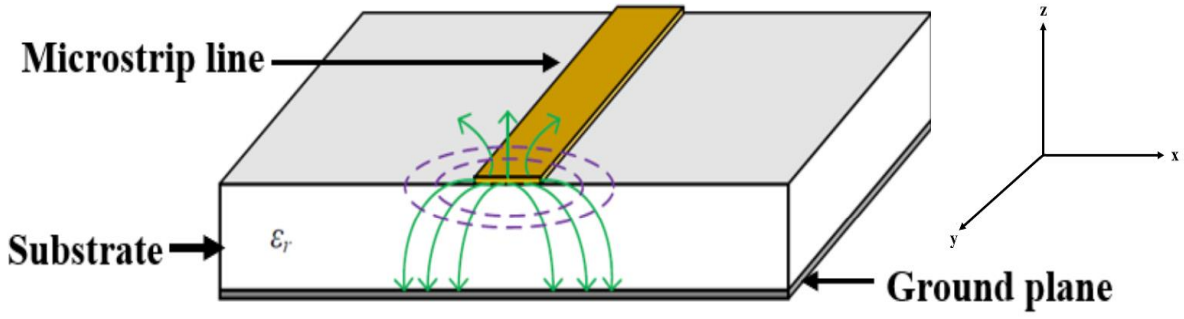

Fig.1.5. Microstrip transmission line

It is further observed from figure.1.5 that electric field spills in to the air without getting confined to the substrate. As a result, there is a discontinuity in the magnitude of electric field in the two media. Therefore, microstrip strip cannot support pure transverse electro-magnetic (TEM) waves. Moreover, phase velocities of the wave are different in air and substrate. Part of the electric field is confined inside the substrate and rest in the air. As a result, wave supported by microstrip lines are labelled as quasi-TEM waves. Hence, an effective dielectric constant (ε_{eff}) must be calculated taking fringing fields and fields confined in the substrate into consideration. The value of ε_{eff} is less than relative dielectric constant (ε_r) because of the discontinuity of electric fields at the air-substrate boundary.

The effective dielectric constant is obtained as:

$$\varepsilon_{eff} = \frac{\varepsilon_r+1}{2} + \frac{\varepsilon_r-1}{2}\frac{1}{\sqrt{1+12\frac{h}{W}}} \tag{1.9}$$

Where ε_{eff} is effective dielectric constant

ε_r is relative dielectric constant of substrate

h is the height of dielectric substrate

W is width of the microstrip line

Figure.1.6. shows a rectangular patch antenna of length 'L', width 'W' and mounted on a substrate of height 'h'. Patch is placed in x-y plane and facing towards z-direction. The dominant mode in patch antenna is TM_{10} mode [24]. TM_{10} mode signifies that there is one half wave-length variation along x-axis and no variation along y-axis. Patch antenna supports this mode if its length is slightly less than half wavelength ($\lambda/2$). Wavelength of the mode propagating beneath the patch is equal to $\lambda_o/\sqrt{\varepsilon_{eff}}$ where λ_o is the free space wavelength. Figure 1.6 shows the fringing field effect in the patch antenna. As discussed before, patch antenna is

represented by two slots along the width 'W' i.e. in x-direction and separated by a transmission line of length 'L' along y-direction. Voltage is maximum and current is minimum at the slots. The fields are split into normal and tangential components with respect to ground plane.

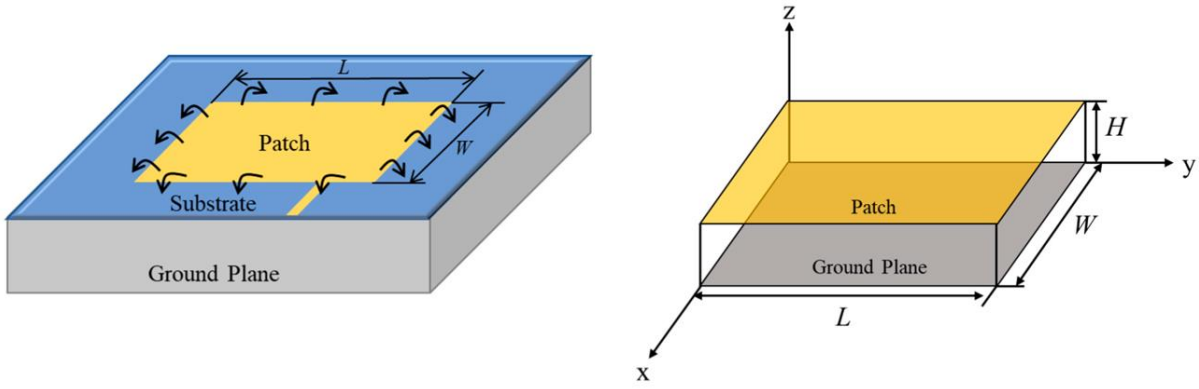

Fig.1.6. Fringing fields in patch antenna

From figure 1.6, it is seen that components of electric fields along the widths cancel each other as the incident and reflected electric field along the width are out of phase. This happens the path traced by electric field is half wavelength long and hence the fields are shorted in the broadside direction. The electric fields along length 'L' contribute for the radiating fields and in the process, electric spills out of the patch. The fringing field effect increases the effective length of the patch by a distance ΔL, which is given empirically as:

$$\Delta L = 0.412h\frac{(\varepsilon_{eff}+0.3)\left(\frac{W}{h}+0.264\right)}{(\varepsilon_{eff}-0.258)\left(\frac{W}{h}+0.8\right)} \quad (1.10)$$

$L_{eff} = L + 2\,\Delta L$

For a given resonant frequency f_o, effective length is obtained as:

$$L_{eff} = \frac{c}{2f_o\sqrt{\varepsilon_{eff}}} \quad (1.11)$$

For rectangular patch antenna, resonant frequency of a TM_{mn} mode is given as:

$$f_o = \frac{c}{2\sqrt{\varepsilon_{eff}}}\left[\left(\frac{m}{L}\right)^2 + \left(\frac{n}{W}\right)^2\right]^{\frac{1}{2}} \quad (1.12)$$

1.6.2. Cavity model

The cavity model computes electric and magnetic fields which contribute to the radiation mechanism of a patch antenna. This model assumes patch antenna as a rectangular or circular cavity depending on the size of the patch. The cavity if loaded with a dielectric material. The patch and ground layer are assumed to perfect electric conductors and the sidewalls of the substrate as perfect magnetic conductors [25].

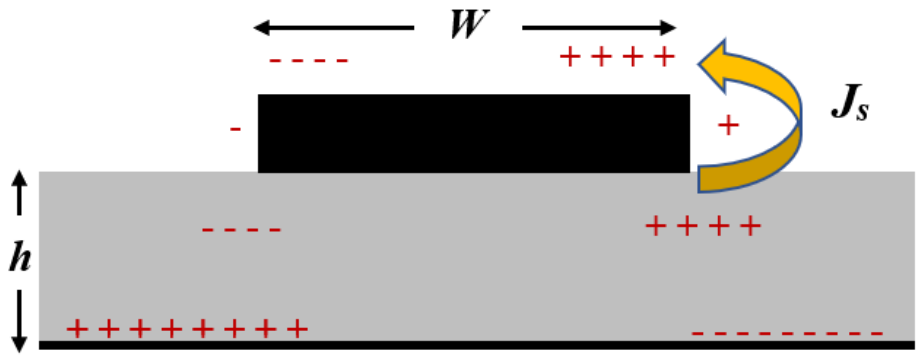

Fig.1.7. Cavity model of patch antenna

From figure 1.7, the patch is excited with a microwave source. The source imparts charges on the top and bottom surfaces of the radiator and the ground layer. The charge dispensation is governed by attractive and repulsive mechanisms. The attractive mechanism between lower surface of the patch and the top of the ground plane keeps the charges intact. Repulsive mechanism pushes the charges from bottom of the patch to the top of the patch. The charge movement generates the current on the patch. But this current is negligible because height of the substrate to the width of the patch ratio is small. This small ratio keeps the attractive mechanism dominant and as a result most of the current is concentrated beneath the patch. Thus, all the sidewalls are assumed to be perfect magnetic conductors. Therefore, TM_z modes are considered inside the cavity.

1.7. Motivation and objective of the thesis

In the modern wireless communications, there is an extensive requirement of enhanced gain, wide bandwidth, multi-band, compactness and beam-switching. Moreover, modern day wireless applications are demanding for high directionality and efficient antennas at sub-6GHz band. To mee the above specifications, many methods like different patch shapes, dual feed, slots, shorting pins are introduced. However, these methods are proven less efficient for enhancing the performance parameters of antennas. To overcome the above problems, the

whole antenna structure has to modified in order to meet the designer's requirements.

The literature survey in the section 1.2 reveals that many types of antennas are designed to obtain miniaturization, high gain, bandwidth, efficiency and radiation patterns. Though extensive research is carried to achieve above parameters, designers are successful to some extent. Due to the above requirements, our research work mostly concentrates on miniaturization, multi-band, gain enhancement, efficiency improvement and beam switching etc. with different stubs and high impedance surfaces. The following challenges are motivating factors to conduct research work on millimeter microwave antennas:

- Introducing different stub loading techniques to achieve miniaturization, high gain and multi-band feature.
- Reduce cross-polarization levels in the miniaturized antennas.
- Introduce different Electromagnetic Bandgap (EBG) structures, Metamaterials (MTMs) to achieve wide bandwidth

On the basis of the above factors, the main objective of this thesis is to design and analyze different stub loaded antennas and HIS loaded antennas.

The main objectives of this thesis are listed below:

- To study the tunability in metamaterial structure i.e. minimization or maximization can be obtained in the frequency shifting by tuning the substrate thickness and also by changing the material of the substrate used.
- To find out the improvements and trade-offs in designing metamaterial and EBG inspired microwave devices.
- To utilize EBG structures in different types of microstrip patch antenna design, thereby, improving the antenna properties such as gain, bandwidth, directivity, radiation and antenna efficiency.
- To study the tunability in metamaterial structure i.e. minimization or maximization can be obtained in the frequency shifting by tuning the substrate thickness and also by changing the material of the substrate used.

- ❖ To simulate the design of these antennas using CST studio simulator.
- ❖ To do comparative analysis of the results obtained from FEM based CST microwave studio and CAD based calculations in MATLAB.

1.8. Design guidelines of the antenna

Figure 1.8: shows the work plan in flow chart format and divides the whole work into subsections shown below:

- ❖ Identify the type of application, choose the frequency, and select the substrate.
- ❖ Mathematically compute the resonant frequency.
- ❖ Study the appropriate techniques to improve the performance parameters of proposed antennas.
- ❖ Design the antennas in CST-Microwave studio and their corresponding lumped element model in Agilent-ADS.
- ❖ Conduct parametric analysis to identify the design parameters which effect the antenna's performance.
- ❖ Fabricate the antenna prototype after the antenna is designed and studied.
- ❖ Measure and validate the results of fabricated antenna.

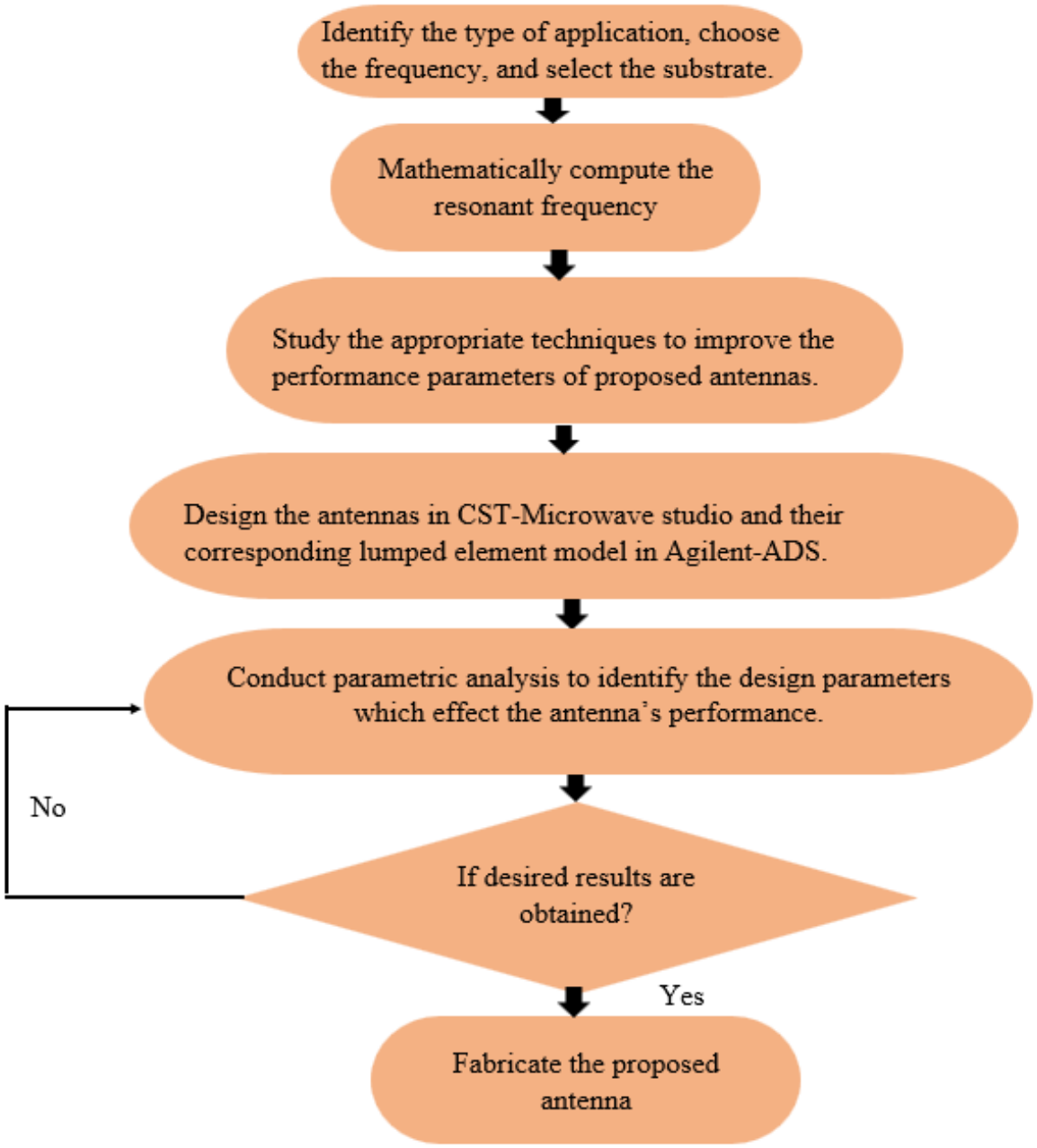

Fig.1.8. Design methodology of the proposed antennas.

1.9. Organization of the Thesis

The thesis has been divided into eight chapters which are given as:

Chapter-1: In the first chapter, various types of fundamental antennas like rectangular, semi-circular, square, oval and circular are studied analysing different performance parameters. Due to the planar nature, these antennas radiate in z-direction due to fringing fields when they are placed in x-y plane. The analysis of near and far fields using cavity model is discussed. Cavity model is used to analyse the electric and magnetic fields in the fabricated antenna discussed in the further chapters. The structures of the antenna are further modified by the above mentioned techniques and their performance parameters are studied in the further chapters.

Chapter-2: In second chapter, different types of stubs loaded small antennas are designed and discussed. These stubs loaded antennas act as solution to the problems encountered by the antennas in the first chapter. In this chapter, a 'L' shaped stub loaded serpentine shaped patch antenna and a 'L'-shaped stub and meander shaped stub loaded oval shaped patch antenna are discussed. To miniaturize the antennas and make them operate at lower giga-hertz frequencies, the antennas are attached with 'L'-shaped stubs and folded meander lines. The effect of stubs on the antenna's performance parameters is studied.

Chapter-3: Antennas discussed in the second chapter suffer from unstable gain and higher order modes. To overcome these problems, antennas designed in the third chapter act as a solution. In this chapter, a study on dumbbell shaped High Impedance Surfaces (HIS) is carried out. Stub loaded oval-shaped patch antenna is mounted on dumbbell-shaped metamaterials (MTM), electromagnetic bandgap structures (EBG), and defective ground structures and the effect of the latter on the earlier is discussed. Effect of the ground plane on the metamaterial is discussed. The selection of particular HIS based on the application's requirement is discussed.

Chapter-4: Though HIS loaded antennas discussed in the third chapter show superior performance, these antennas show degradation in the performance when more high impedance cells are loaded in the antenna structure. The antenna designed in the fourth chapter discusses the holistic approach to achieve the improved performance with reasonable gain, efficiency and bandwidth. This chapter discusses the design and analysis of ultra-wideband, dual polarized and highly efficient dual feed dumbbell shaped patch antenna. The design of splattered ring EBG is discussed. The effects of using EBG on the antenna and the variation in the performance parameters are described. Total dimensions of the proposed antenna are 25 x

30 x 1.524mm^3. The axial ratio of the antenna at 11.78GHz is 2.1dB and 4dB at remaining frequencies of operation. A wide-bandwidth of 20.2GHz (171.4%) and the gain ranging between 6.21dB and 9.03dB in the frequency ranges of 10.8GHz to 31GHz is achieved using the proposed structure. A wide range of efficiencies varying from 88.34% to 91.06% is achieved. Another antenna discussed in this chapter is swastika EBG mounted slotted antenna. This antenna is designed to radiate at 21.29GHz. The antenna is developed using ADS-2016. Gain of the antenna is 11.29dB and bandwidth is 3.2GHz.

Chapter-5: Though the antennas discussed in the fourth chapter show superior performance, the purpose of achieving the miniaturization at lower gigahertz range is served by the antenna discussed in the fifth chapter. The antenna is designed by placing circular patches of different radii along the circumference of a central circular patch and thereby forming the proposed flower-shaped patch antenna. The design of proposed antenna is inspired from kissing circles theorem in geometry. The proposed structure is mounted on and loaded with Double Negative (DNG) triple Complementary Split Ring Resonator cells. The overall dimensions of the patch are 23.5 × 16 x 1.6 mm^3. The antenna operates at 5.2GHz and 8.25GHz. This also possesses a wider bandwidth of 1.2 GHz (24.1%) and 2.2 GHz (26.5%) in the ranges of 4.95 GHz to 6.15 GHz and 7.1GHz to 9.3 GHz respectively. The gains of 3.93 dBi and 5.02 dBi are observed in the frequency ranges of operation. The radiating electric, magnetic fields and the green's function are analysed using cavity model. The designed structure is useful for several applications, such as WLAN, WiMAX, and ISM band.

Chapter-6: Important parameters in modern day wireless communications are beam switching and low cross-polarization levels. This feature cannot be achieved with the antenna discussed in the previous chapter. Hence, chapter five provides the solution to the above requirements. This chapter throws the light on design and analysis of a meta post loaded slotted array waveguide antenna. The resonant frequencies of the proposed structure are 3.1GHz, 3.3GHz, and 4.1GHz. The simulated gains of 11.3dBi, 14.1dBi and 12.6dBi are observed at these frequencies. The proposed antenna is resonant in the frequency ranges of 3.01GHz to 3.12GHz, 3.2GHz to 3.44GHz and 3.91GHz to 4.45GHz. Further, the proposed meta post loaded slotted waveguide antenna array exhibits beam switching feature in E-plane with the side lobe level with low cross-polarization levels.

Chapter-7: Meta post loaded slotted array waveguide antenna is an excellent candidate for high gain applications. But complex and bulky nature of this antenna makes it prone to high

ohmic losses and radiation deflections. Hence, stable radiation patterns cannot be achieved with these types of structures. The solution to these problems is to design concatenated antennas as discussed in the seventh chapter. The patch antenna presented in the second chapter is loaded on a serpentine shaped EBG ground is described in this chapter. Here, the radiation element is an oval shaped patch antenna and serpentine shaped patch slots are etched on the ground. Overall dimensions of the proposed patch antenna are 18 x 18 x 0.8mm^3. The structure is miniaturized by 89.1%. The resonant frequencies of the proposed patch are 4.28GHz, 6.15GHz, 6.78GHz and 12.15GHz. The peak gains at the frequency of operations are 1.1dBi, 1.3dBi, 2.8dBi and 2dBi. The radiation patterns are observed to be stable at the resonant frequencies.

Chapter-8: In the end, the eighth chapter consists of the overall conclusion and future scope of the thesis. In this thesis, we designed various antennas like stub-loaded, EBG loaded, Metamaterial loaded, DGS loaded antennas, meta post loaded slotted array waveguide antennas to achieve high gain, bandwidth, stable radiation patterns and efficiency. These antennas are designed to cover frequencies ranging from 4GHz -25GHz and will be deployed for C-band, X-band, K-band, K_u-band, WLAN applications.

In this way, this thesis will discuss gain enhancement, miniaturization, beam switching using stubs, DGS, metamaterials, EBG and meta posts.

Published work

Journals

1. Karteek Viswanadha and N.S.Raghava, "Design and Analysis of a Meander Line Cornered Microstrip Patch Antenna with Square Slotted EBG Structure for ISM/WLAN Applications", *International Journal of Advanced Science and Technology*,Vol.113, Issue.10, 2018, pp.93-102. DOI: 10.14257/ijast.2018.113.10 (Scopus-Indexed)
2. Karteek Viswanadha and N.S.Raghava, "Design of High Gain, Bandwidth and Efficient Double Split Ring Slotted Antenna with Swastika Shape EBG Structures at 21.29GHz for High Data Rate Communications", *International Journal of Computer Applications*, Vol.180, Issue.11, 2018, pp.35-38. DOI: 10.5120/ijca2018916232.
3. Karteek Viswanadha and N.S.Raghava, "Design and Analysis of a Multi-band Flower Shaped Patch Antenna for WLAN/WiMAX/ISM Band Applications", *Wireless Personal Communications*, Springer Nature, Vol.111, 2020, pp.1-24. https://doi.org/10.1007/s11277-02007078-8 (SCI-E Indexed).
4. Karteek Viswanadha and N.S.Raghava, "Design and Analysis of a Compact Dual-band Serpentine-shaped Patch Antenna with Folded Stub Lines for C- and X-band Applications", *Journal of Communications Technology and Electronics*, Springer Nature, Vol.65, Issue.10, 2020, pp.1-23. DOI: 10.1134/S106422692010006X. (SCI & SCI-E Indexed).
5. Karteek Viswanadha and N.S.Raghava, "Design and analysis of a dual- polarization multiband oval ring patch antenna with L- stubs and folded meander line for C-band/X-band/ Ku-band/ K- band communications", *International Journal of Electronics*, Taylor and Francis, Vol.108, issue.4, 2021, pp.647-663. https://doi.org/10.1080/00207217.2020.1793411. (SCI &SCI-E Indexed).
6. Karteek Viswanadha and N.S.Raghava, "Design and analysis of a compact asymmetrical CPW fed stubs loaded hook-shaped patch antenna for upper 5G- and data collection applications", *Wireless Personal Communications, Springer (SCI-E)* **(Communicated)**
7. Karteek Viswanadha and N.S.Raghava, "Design and analysis of a compact triple-band circularly polarized meta-atom and stub loaded patch antenna for Bluetooth, WLAN and X-band applications", *Journal of Engineering Research (SCI-E)***(Communicated)**

Conferences

1. Karteek Viswanadha and N.S.Raghava, "Study of high gain configurations of double split ring slotted patch antenna for GSAT applications", *IEEE-Nirma University International Conference on Engineering (NUiCONE)*, 2017, pp.1-6. DOI: 10.1109/NUICONE.2017.8325617(Scopus-Indexed Conference).
2. Karteek Viswanadha and N.S.Raghava, "Design and Mathematical Analysis of Microstrip Bandpass Power Divider for Ku Band Communications", *2nd IEEE International Conference on Power Electronics, Intelligent Control and Energy Systems (ICPEICES)*, 2019, pp.1000-1005. DOI: 10.1109/ICPEICES.2018.8897280. (Scopus Indexed Conference).
3. Karteek Viswanadha and N.S.Raghava, "Design and analysis of a slotted waveguide antenna array with double broken ring Meta posts for 5G (India) and C-band applications", *1st International Conference on Signal Processing, VLSI and Communication Engineering (ICSPVCE)*, 2020, pp.1-6. DOI:10.1109/ICSPVCE46182.2019.9092807. (Scopus Indexed Conference).

4. Karteek Viswanadha and N.S.Raghava, “Review on implementation of Silicon-on-Insulator Technology for Slot Antennas”, International Conference on Contemporary Issues in Science, Engineering and Management(ICCI-SEM), 2017, pp.270-274.
5. Karteek Viswanadha and N.S.Raghava, “Design of a dual polarized ultra wideband dual feed dumb-bell patch antenna with splattered ring EBG”, Indian Conference on Antennas and Propagation(InCAP), 2020, pp.1-6. DOI: 10.1109/InCAP47789.2019.9134652.
6. Karteek Viswanadha and N.S.Raghava, “Design of multiband stub loaded oval ring patch antenna with serpentine shaped EBG for C- and Ku-band communications”, *Wireless, Antenna and Microwave Symposium* (WAMS-2022), N.I.T, Rourkela,2022. (Scopus-Indexed).

Book Chapters

1. Karteek Viswanadha and N.S.Raghava, “Design of a Narrow- Band Pass Asymmetric Microstrip Coupled-Line Filter with Distributed Amplifiers at 5.5 GHz for WLAN Applications”, *Applications of Artificial Intelligence Techniques in Engineering*, Springer-Singapore, Vol.697, 2018, pp.181-187. DOI: https://doi.org/10.1007/978-981-13-1822-1_17. (Scopus-Indexed).
2. Karteek Viswanadha and N.S.Raghava, “Study of Performance Parameters of Stub Loaded Oval-Shaped Patch Antenna Using Metamaterials, Electromagnetic Bandgap Structures, and DGS of Dumbbell Shape”, *Planar Antennas, CRC Press,* 2021, pp.49-62 (Scopus-Indexed).

CHAPTER 2

Design of stub-loaded patch antennas

2.1 Introduction

With the technology moving towards high data rates, antennas designed in the recent times are expected to have high gain and directionality with reasonable degree of miniaturization. Miniaturization may degrade gain and directivity. Hence, active areas of patch antennas must be modified many techniques are introduced in the recent times to achieve miniaturization without degrading gain and directionality. These techniques include modification of ground plane, introducing slots, attaching shorting pins etc. But these techniques degrade efficiency. Stub-loaded patch antennas are suitable candidates for achieving high gain, bandwidth and efficiency without compromising the degree of miniaturization.

Hence, stub-loaded antennas play pivotal role in the next generation wireless communication systems.

In literature, many types of stubs loaded patch antennas are designed to improve the performance parameters of the patch antennas [26]. Several designs have been proposed to improve the gain and reduce the cross-polarization levels in miniaturized antennas [27]-[28]. In this work, to improve the degree of miniaturization, enhance the gain and bandwidth, two types of stubs loaded antennas designed on RO-4003C (ε_r=3.8) and RT/duroid-6202 (ε_r=2.94) are proposed. The antennas proposed in this work are:

- Design of folded stub line loaded serpentine-shaped patch antenna.
- Design of a stub loaded oval ring patch antenna.

Figure.2. presents the design methodology of the proposed antenna.

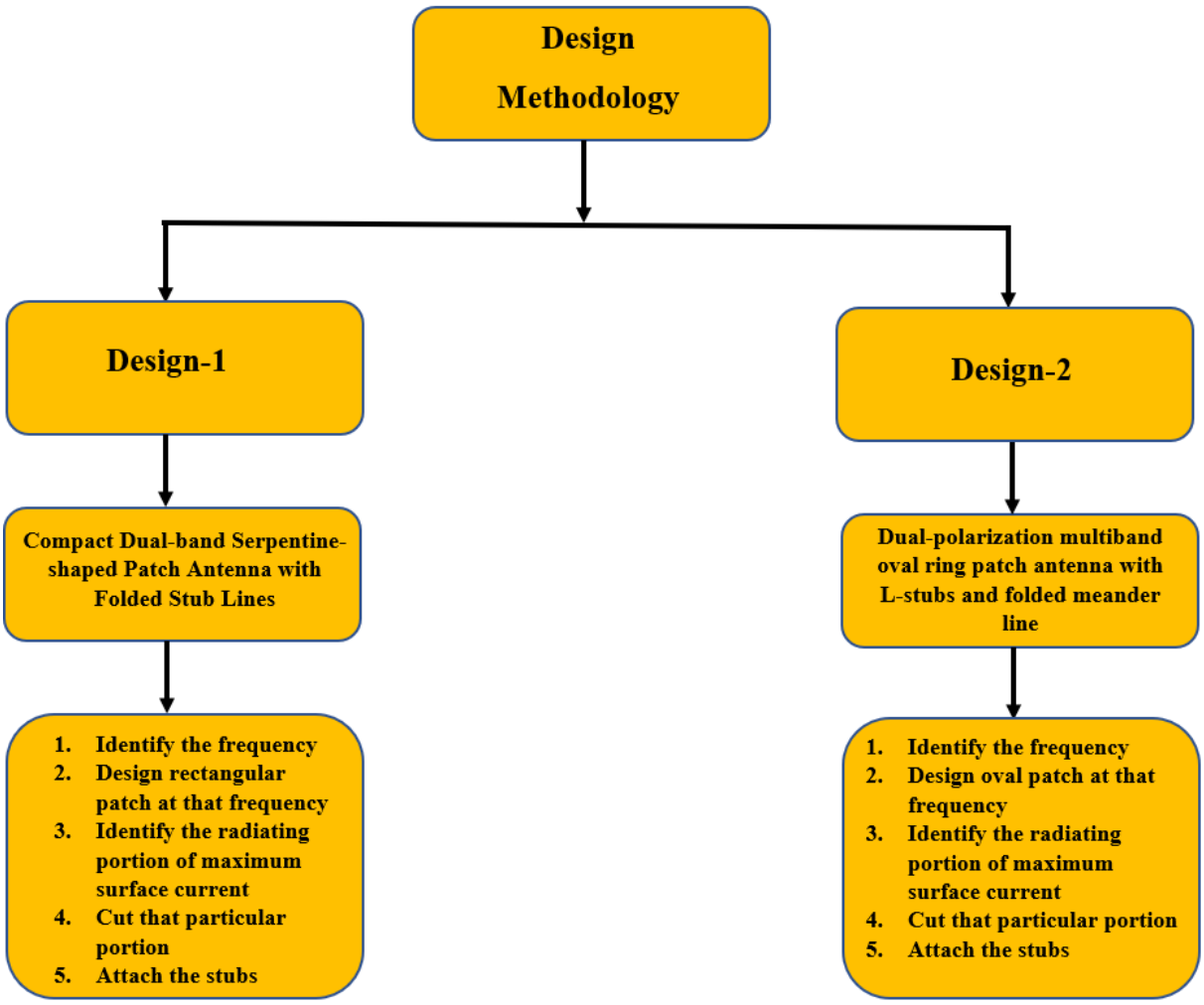

Fig.2. Design methodology of antennas in chapter-2

2.2. Design of folded stub line loaded serpentine-shaped Patch Antenna

Figure.2.1 presents the design of the proposed antenna. The patch is printed on a single side of RO-4003C substrate which is 1.524 mm thick, with a relative permittivity of 3.38 and loss tangent of 0.027. At the beginning, a basic serpentine patch antenna is fed by a 50 Ω microstrip line.Its impedance bandwidth is observed. The patch resonates at 9.61GHz. The bandwidth obtained in this structure is not high as desired. Bandwidth of the structure is increased by attaching strip-line and stub-line of quarter-wavelength to the antenna. Stub-line radiates at operational frequency of 6.82GHz and strip-line radiates at resonant frequency of 10.1GHz. The whole structure is printed on the partial ground layer with the volume of 10 x 6.5 x 0.035mm^3.

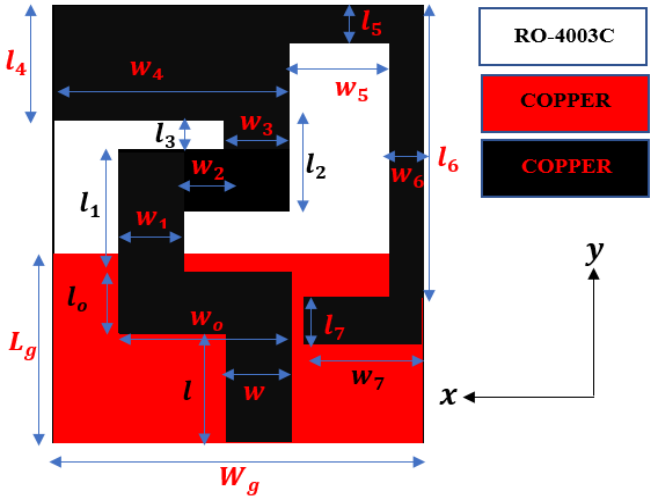

Fig.2.1. Structure of the designed antenna

The design features of the serpentine patch are presented in Table 2.1.

Table 2.1. Detailed dimensions of the antenna

Dimension	l	W	l_0	w_0	l_1
Value (mm)	3.5	2	1.5	8	2.75
Dimension	w_1	l_2	w_2	l_3	w_3
Value (mm)	2	2.5	2	1	2
Dimension	L_g	W_g	w_5	l_6	w_6
Value (mm)	6.5	10	2	6.5	1.5
Dimension	l_4	w_4	l_5	l_7	w_7
Value (mm)	4.25	6.5	1.5	4.5	3.5

The proposed patch antenna resonates at four frequencies (f_1, f_2, and f_3). First, second, and third frequencies are 6.96GHz, 9.61GHz, and 10.1GHz respectively.

The frequency of resonance of the radiating stub segment is calculated by:

$$f_1 = \frac{c}{4l_6\sqrt{\varepsilon_{eff}}} \ , \tag{2.1}$$

where :

- c represents velocity of the light,
- l_6 represents length of radiating stub
- ε_{eff} represents effective dielectric constant obtained from eq.(1.9).
- ε_r represents the relative permittivity
- h represents height of the dielectric
- w represents the width of the feed line.

Similarly, the frequency of resonance of the serpentine segment is calculated by:

$$f_2 = \frac{c}{2(l_0+l_1+l_3+l_4)\sqrt{\varepsilon_{eff}}} \ . \tag{2.2}$$

The frequency of resonance of the strip line is calculated by:

$$f_3 = \frac{c}{4l_7\sqrt{\varepsilon_{eff}}} \ . \tag{2.3}$$

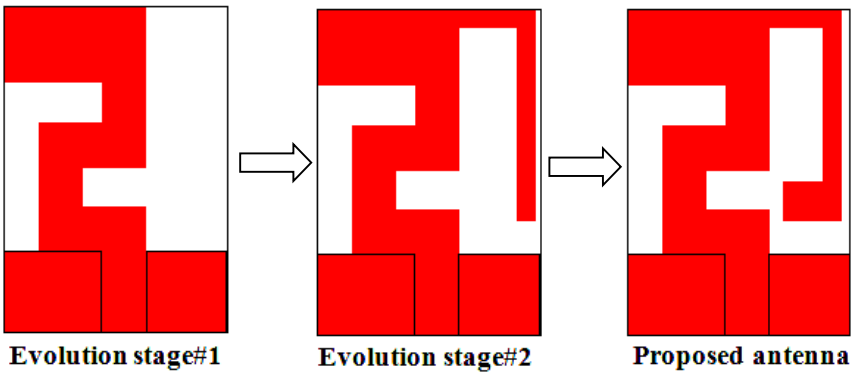

Fig.2.2. Development stages of the proposed antenna.

Figure.2.2 presents the development of the proposed patch antenna. The impedance bandwidth curves of these antennas are presented in figure.2.3. The basic antenna presented in the 1st development stage resonates at 9.65GHz with its return loss represented in blue dotted curve.

The impedance or operational bandwidth (S11<-10dB) of 763MHz is seen in the frequency range of (9.27GHz~10.03GHz).

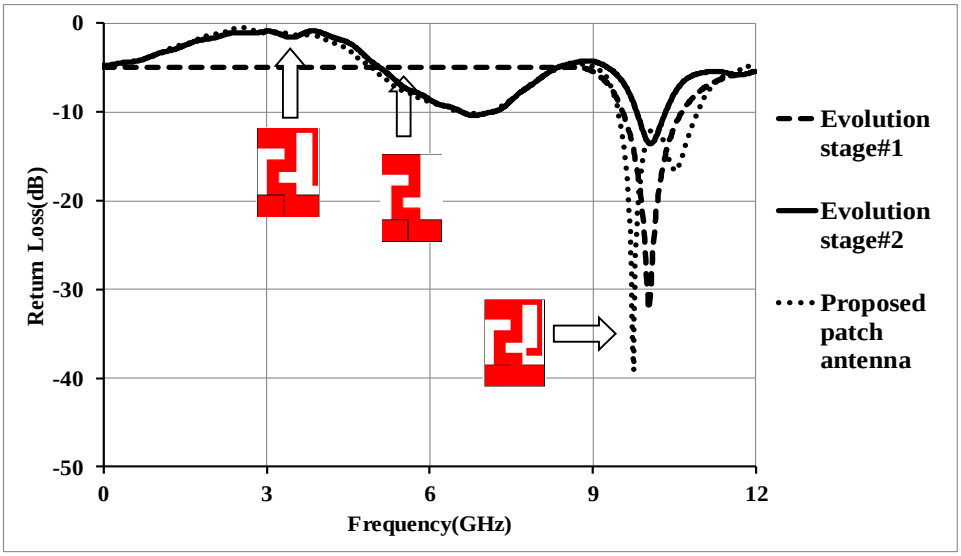

Fig.2.3. Return losses of evolution stages of proposed patch antenna

When a bent stub-line with the length equal to λ/4 is attached to basic patch antenna in the 1st evolution stage, the resultant patch operates at 6.52GHz and 9.58GHz as given in Figure 2.3 (shown as a red dotted curve). The operational bandwidths of 150MHz and 352MHz are seen in the frequency ranges of operation. Further, a strip line added to bent stub makes the patch antenna resonate at 6.8GHz, 9.6GHz and 10.03GHz with the impedance bandwidths 662MHz and 1.6GHz respectively as shown in figure 2.3 (represented in green dotted curve). The simulated and measured plots of impedance of the antenna are presented in figure. 2.4. The resistive component of the impedance is almost 50Ω in the frequency ranges of 6.6GHz~7.2GHz and 8.8GHz~10.4GHz. It can be seen that the impedances of the antenna and feed line are perfectly matched. The reactive component of the impedance is in close proximity to zero ohms in the resonant frequency bands. There is a concurrance between simulated and measure values of impedances. The values of electrical elements in the model shown in figure 2.5 are extracted from the impedance plots presented in figure.2.4. Iterations and tunings are carried on electrical elements to achieve the desired results. The simulated models in CST and ADS are in close proxmity.

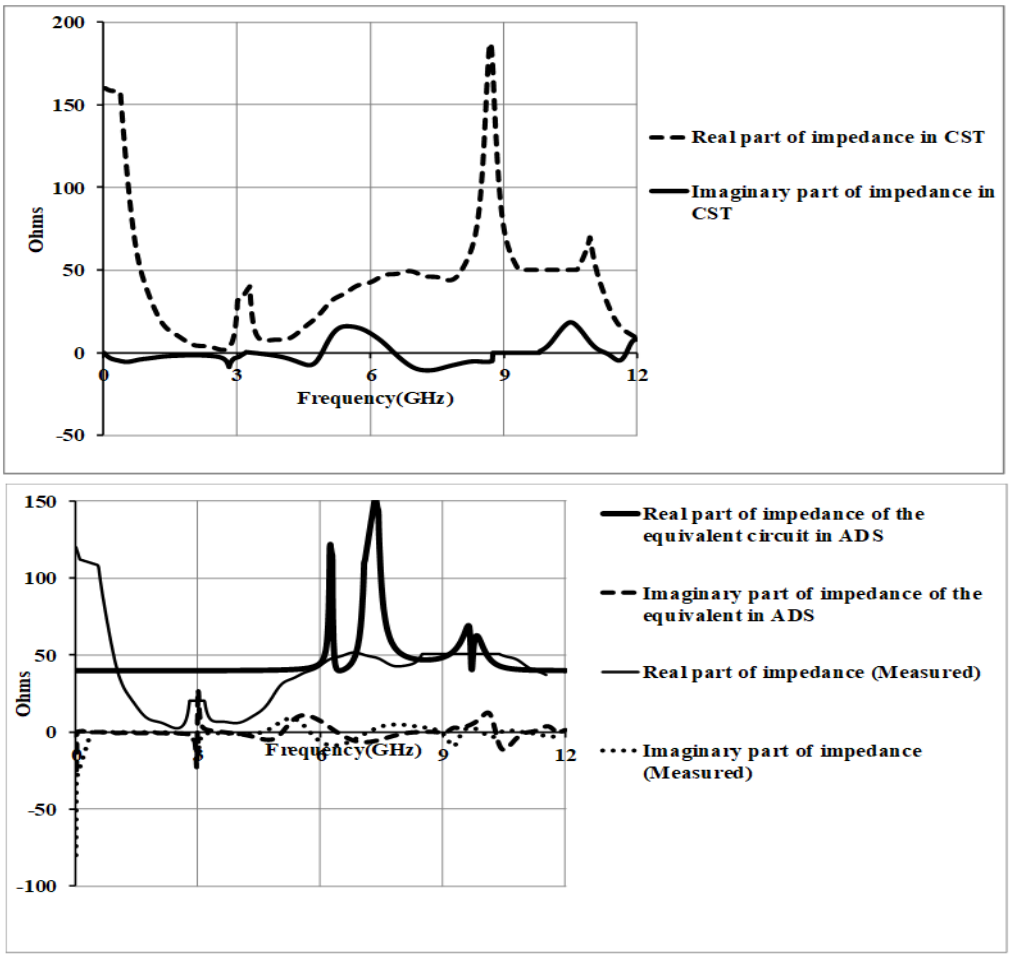

Fig.2.4. Impedance of the antenna structure

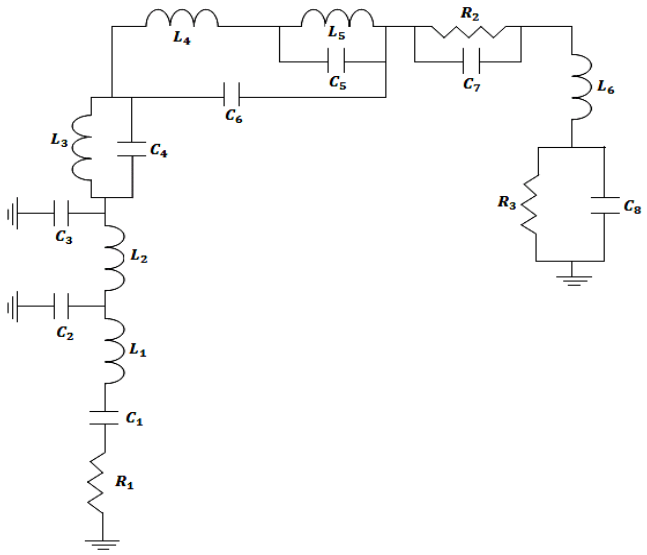

Fig.2.5. Electrical model of the designed antenna structure

The electrical equivalent of the antenna is presented in figure.2.5. The lumped elements (L_3, L_4, & C_4) represent serpentine portion. The lumped elements (R_2, L_5, C_5, & C_7) represent stub-line portion and (L_1, C_1, R_1, L_2, C_2, &C_3) represent feed line portion. C_6 corresponds to the gap

capacitance between the serpentine and stub- line portions. The section (L_6, R_3, &C_8) correspond to the strip line. The reflection coefficient of the electrical model of the antenna is presented in figure.2.6. Table.2.2 presents the optimized values of electrical elements obtained from Agilent-ADS by tuning the lumped elements. Initially, the electrical element values are obtained from antenna's impedance plots presented in figure.2.4.

Table.2.2 Values of elements in electrical model of the proposed antenna.

Lumped element	**L_1(nH)**	**L_2(nH)**	**L_3(nH)**	**L_4(nH)**	**L_5(nH)**	**L_6(nH)**	**C_1(pF)**
Value	1	1.1	0.15	35.529	0.27	3.6	1
Lumped element	**C_2(pF)**	**C_3(pF)**	**C_4(pF)**	**C_5(pF)**	**C_6(pF)**	**C_7(pF)**	**C_8(pF)**
Value	0.66	0.786	4	0.968	0.1	20	0.3
Lumped element	**R_1(Ω)**	**R_2(Ω)**	**R_3(Ω)**				
Value	40	59.25	19				

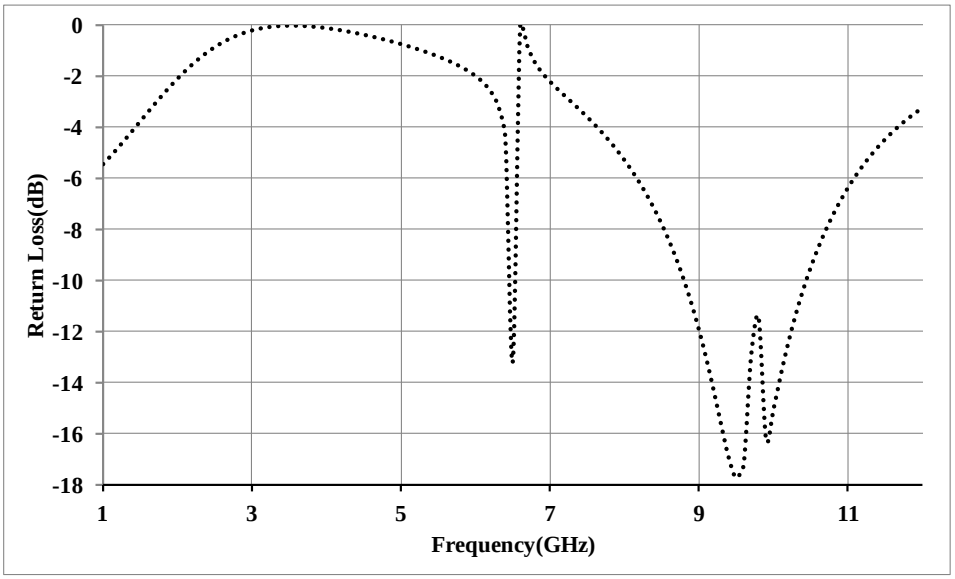

Fig.2.6. Return loss of electrical model

The circuit exhibits resonance at 6.72GHz, 9.61GHz, and 10.05GHz. An operational bandwidth of 1.61GHz is seen in the frequency band of 8.8GHz~10.04GHz.

2.2.1 Parametric Analysis

The performance parameters of the serpentine antenna depend on various design features of the antenna. The area of the antenna and the radiating stubs play vital role in achieving the desired performance parameters. The variation in the reflection coefficient with the change in various parameters of the designed antenna is observed through simulations in CST. The observations are studied through parametric analysis. Figure 2.7.(a) presents the impact of the length of the antenna on the impedance bandwidth. When the length is 2mm, the patch resonates at 6.81GHz and 10.69GHz. The impedance bandwidths in the band are 312MHz and 1.2GHz. When the section length is increased to 3mm, the proposed patch resonates at 6.79GHz, 9.52GHz and 10.81GHz. The impedance bandwidths in the operational bands are 512MHz, 451MHz and 856MHz. Increase in the length of the patch to 5mm pushes the resonant frequencies to 6.83GHz, 9.72GHz and 10.5GHz with the impedance bandwidths of 631MHz and 1.41GHz respectively. Further increase in the antenna length deteriorates the operational bandwidth. Therefore, there is a need for optimization of the length (l) of the serpentine portion, which is optimized and found to be 4.25mm.

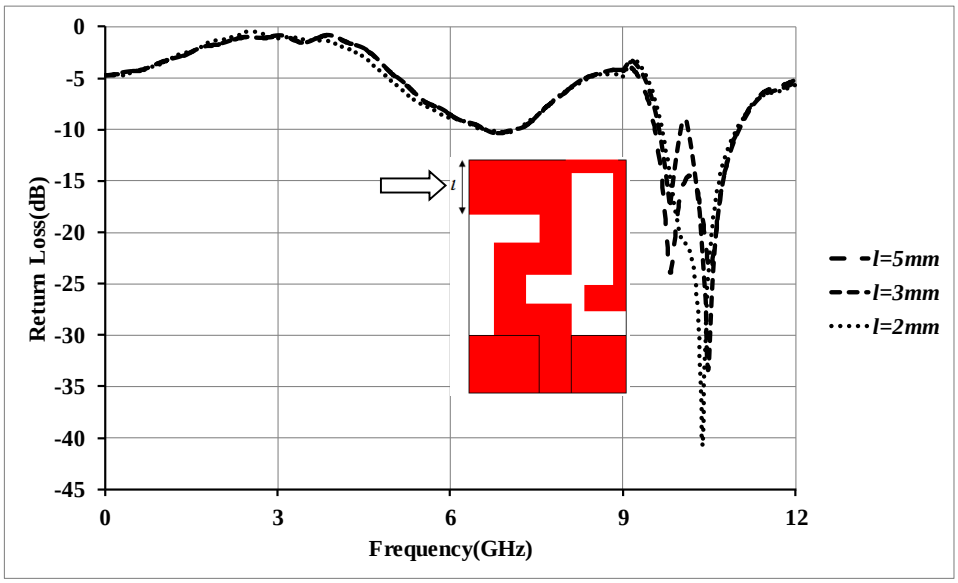

(a)

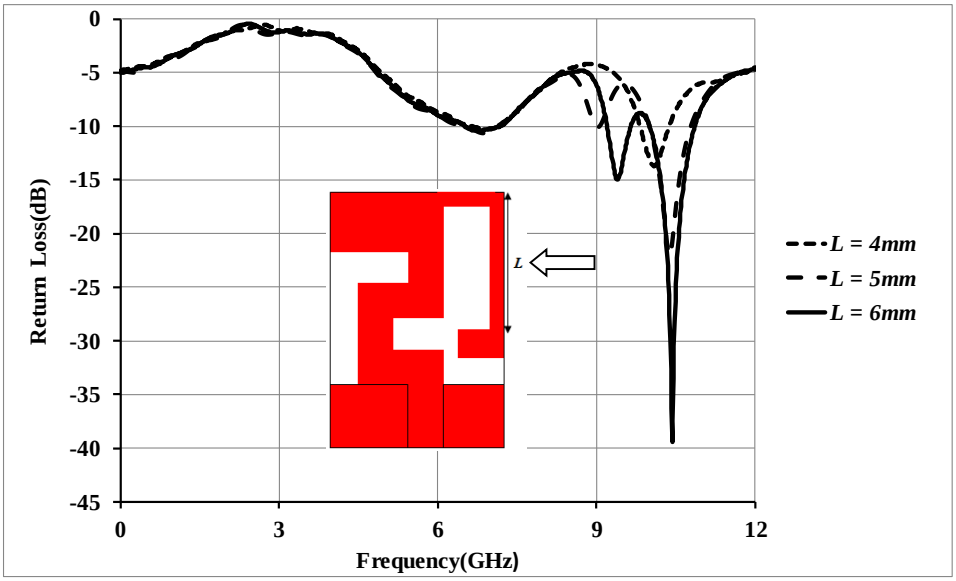

(b)

Lengths of the stub-line and strip-line highly impact the operational bandwidth of the designed antenna. The length of the radiating stub-line is altered from 4mm to 6mm to observe the change in the impedance bandwidth of the antenna. Figure 2.7.(b) presents the change in the return loss with the alteration in the length of the stub-line. When the length is 4mm, the antenna radiates at 6.81GHz and 9.43GHz with impedance bandwidths of 611MHz and 223MHz respectively. A 1mm increase in the stub length makes the patch antenna resonates at 6.81GHz, 9.02GHz and 9.82GHz with the bandwidths of 612MHz, 435MHz and 1.25GHz respectively. When the length is further increased to 6mm, the patch operates at 6.8GHz, 9.62GHz and 9.83GHz. The impedance bandwidths observed in the operational bands are 640MHz, 72MHz and 1.23GHz. Further increment in the stub length produces undesired results and hence, those results are not presented. Hence, the stub length is optimized to 6.5mm.

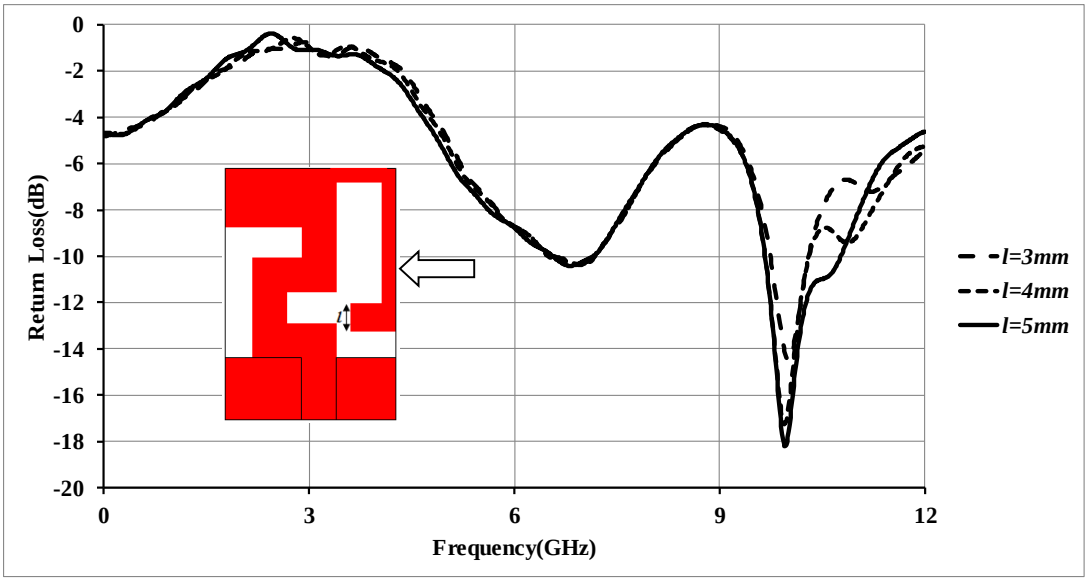

(b)

Figure 2.7.(c) presents the variation in the impedance bandwidth with the change in the strip line length. When the strip line length is 3mm, the patch resonates at 6.66GHz and 9.87GHz with the impedance bandwidths of 223MHz and 760MHz respectively. If the length of the strip line is increased to 4mm then the patch antenna resonates at 6.62GHz and 9.8GHz respectively. The patch antenna possesses impedance bandwidths of 110MHz and 664MHz. When the length is further increased to 5mm, the patch radiates at 6.5GHz and 10.62GHz with impedance bandwidths of 212MHz and 1.1GHz respectively.

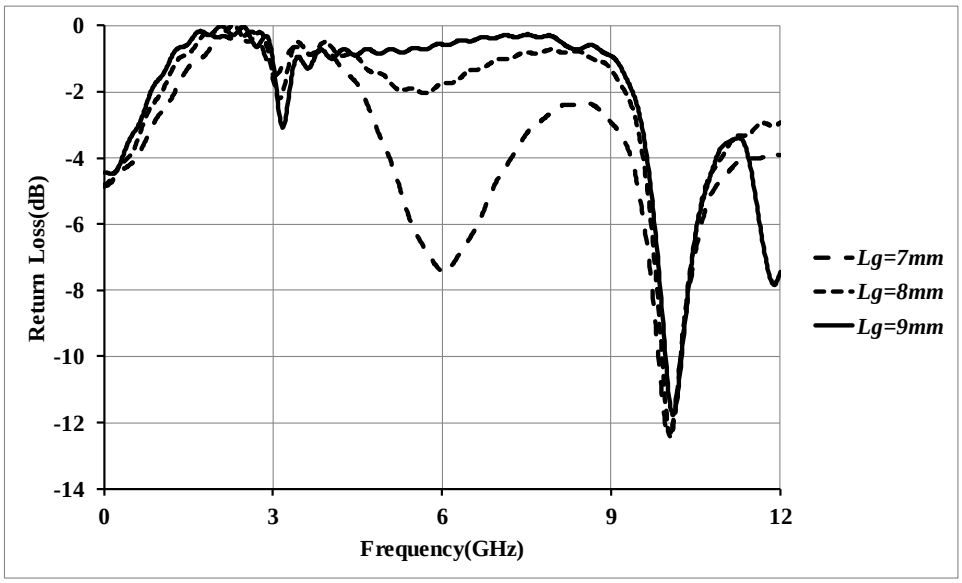

(d)

Figure 2.7.(d) presents the impact of dimension of the ground plane particularly its length over the impedance bandwidth. When the length is 7mm, the patch radiates at 10.16GHz having the

impedance bandwidth of 276MHz. If the length is changed to 8mm then the patch antenna operates at 10.21GHz with the bandwidth of 271MHz. If the ground plane length is increased to 9mm then impedance bandwidth is 312MHz. Further increase in the length of the ground produces higher modes and hence, those results are not presented in this section. Figure 2.7.(e) presents the change in the operational bandwidth with the variation in the width of the serpentine section. When the width of the serpentine section is 1mm, the antenna resonates at 9.42GHz with the impedance bandwidth of 1.1GHz. If the width is increased to 2mm then the antenna resonates at 9.42GHz with the impedance bandwidth of 186MHz. If the width of the serpentine section is further increased to 4mm then the patch antenna resonates at 8.02GHz and 9.44GHz with the impedance bandwidth of 1.49GHz.

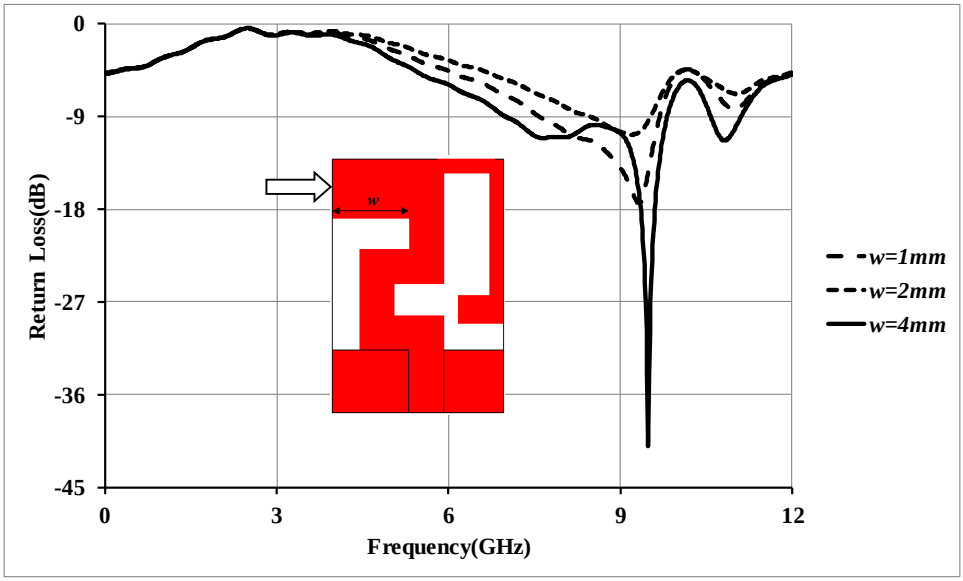

(e)

The variation in the return loss is studied by changing the width of the designed antenna. The area of the designed antenna varies with change in the width of the antenna. The impact of variation in the area of the patch on the impedance bandwidth is studied and analysed. When the patch area is 117mm^2, the antenna resonates at 7.63GHz, 9.65GHz and 11.72GHz with the impedance bandwidths of 312MHz, 176MHz and 1GHz respectively. When the active area of the patch is 104mm^2, the antenna resonates at 8.32GHz and 10.82GHz with the impedance bandwidths of 1.01GHz and 412MHz respectively. When the active area of the patch is 96mm^2, the antenna resonates at 8.51GHz and 10.93GHz with the operational bandwidths of 1.19GHz and 232MHz respectively. Further reduction in the area of the patch produces undesired results and hence, those results are not presented in this chapter.

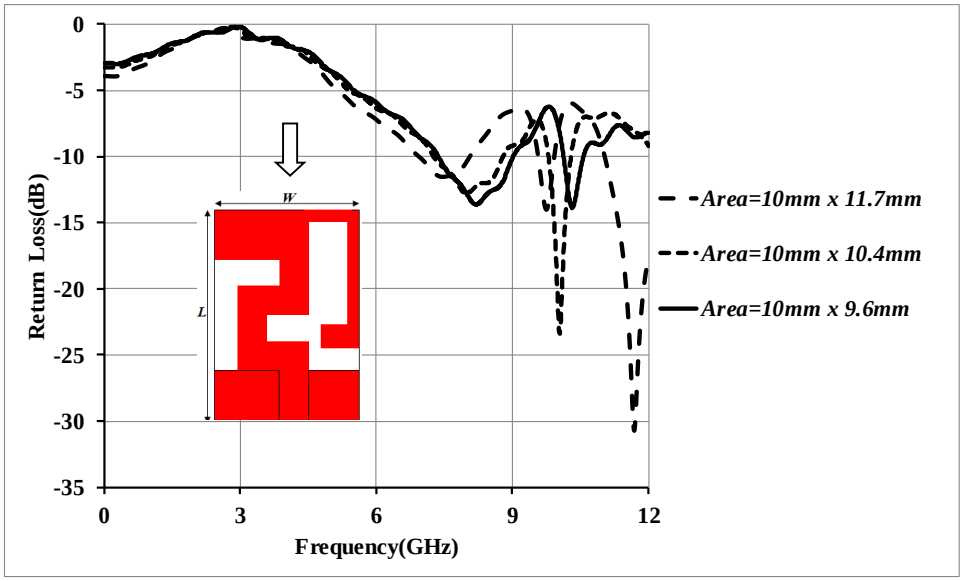

(f)

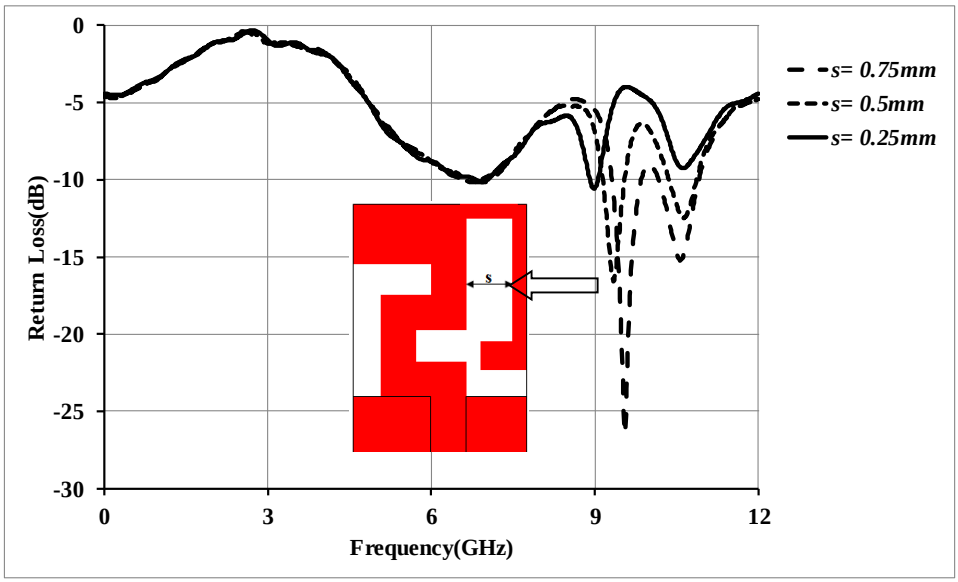

(g)

Fig.2.7. (a). Impact of the length of serpentine section over the impedance bandwidth of patch antenna.**(b).** Impact of length of the stub-line over the impedance bandwidth of the antenna. **(c).** Impact of length of strip line on the impedance bandwidth of the proposed antenna. **(d).** Impact of length of the ground plane on the impedance bandwidth of the proposed antenna. **(e).** Impact of width of serpentine section on the impedance bandwidth of the proposed antenna. **(f).** Impact of the overall active area of the patch on the return loss of the proposed antenna. **(g).** Impact of the gap between the serpentine portion and the stub-line section on the impedance bandwidth of the proposed antenna.

The change in the magnitude of the return loss is analysed by changing the gap between the serpentine section and the radiating bent stub-line. When the gap is 0.25mm, the patch radiates at 9GHz with the impedance bandwidth of 89MHz.When the gap is increased to 0.5mm, the patch radiates at 6.62GHz, 9.73GHz and 10.77GHz with the impedance bandwidths of 101MHz, 623MHz and 712MHz respectively. When the gap is further increased to 0.75mm,

the patch antenna radiates at 6.62GHz, 9.62GHz and 10.76GHz with the impedance bandwidths of 101MHz, 712MHz and 801MHz respectively.

2.2.2 Outcomes and Disquisitions

The antenna is devised and fabricated with parameters obtained in table.2.1. Figure 2.8 presents the fabricated antenna. Figure.2.9 presents the results of impedance bandwidths of the developed prototype. The measured results are in close proximity with the simulated results. The minor variations are due to structural discontinuities, the quality of the feed and any fabrication inaccuracies. The operational bandwidths of the antenna are 602.1MHz and 1.52 GHz in the bands of 6.6GHz~7.21GHz and 8.84GHz ~10.36GHz respectively. The resonant frequencies are further studied with the help of current distributions.

Fig.2.8. Fabricated prototype

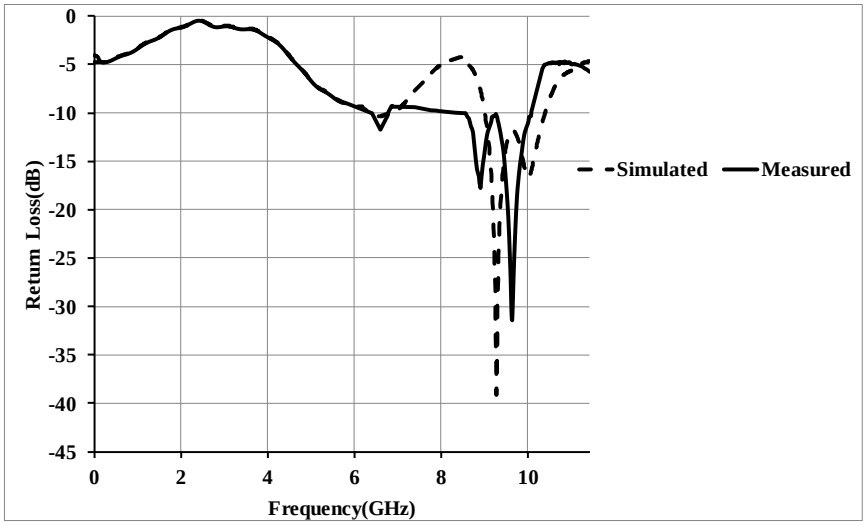

Fig.2.9. Return losses of the designed antenna

Figure.2.10 presents the current densities at resonant frequencies. It is seen that current density is confined on the radiating lines and ground plane at 6.8GHz. At 9.51GHz, surface current is diverted towards serpentine segment and the magnitude of current on the ground layer is decreased. At 9.89GHz, the surface current is concentrated on the strip line.

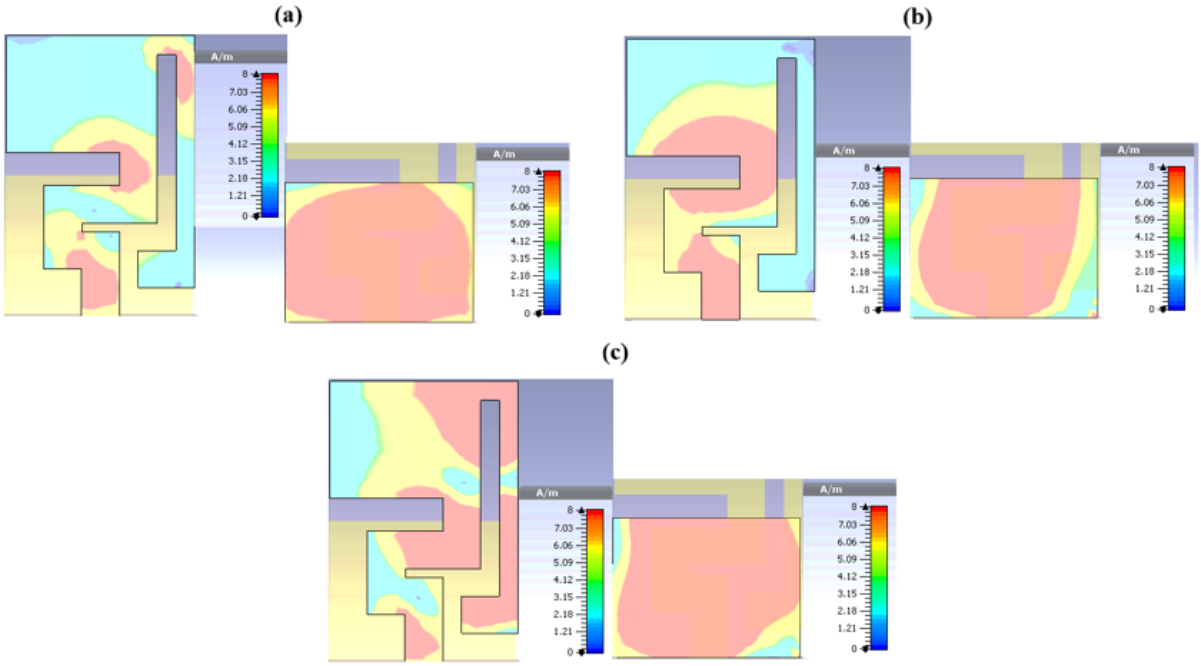

Fig.2.10. Surface current densities over the antenna (left) and ground plane (right)

(a). 6.8 GHz. **(b).**9.51 GHz **(c).** 9.89 GHz

Figure.2.11 presents the efficiencies of the designed antenna. Efficiencies are observed to be varying between 81.6% to 88.4%. Efficiency is constant across the frequency bands of operation.

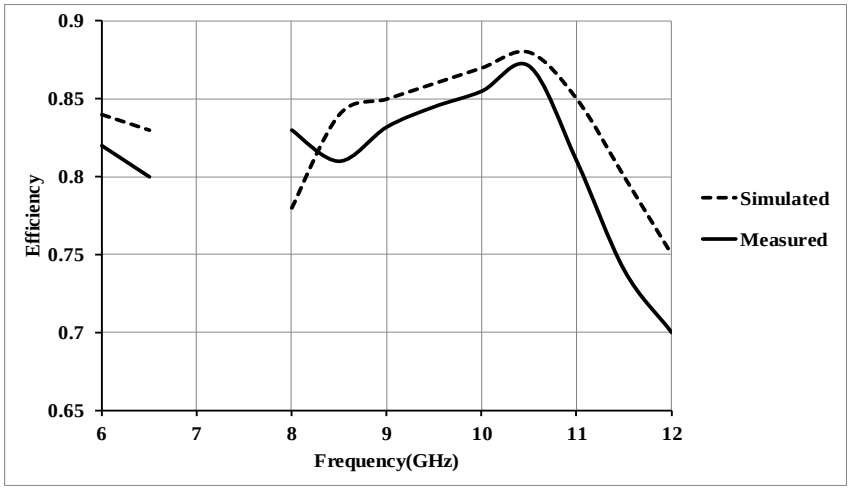

Fig.2.11. Efficiencies of the patch antenna

Figure.2.12 presents the plots of peak gains of the designed antenna. The gains are observed to be ranging from 3.34dBi to 5.6dBi with the peak gains ranging from 3.2dBi to 5.56dBi across the frequency bands of operation.

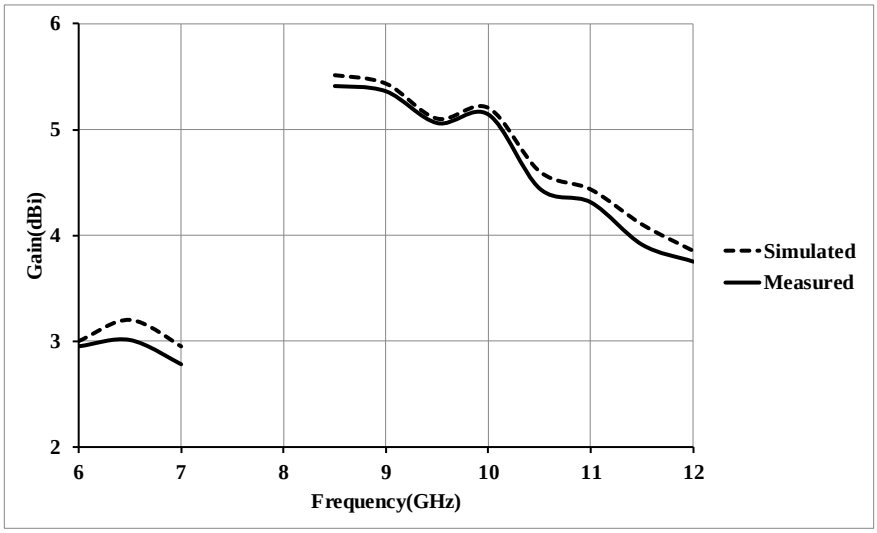

Fig.2.12. Gains of the patch antenna

The antenna patterns corresponding to all the radiating planes are simulated in CST-Microwave Studio and measurement is accomplished using double-ridge horn as the testing antenna. Antenna patterns in E- and H-planes at 6.8GHz, 9.51GHz, and 9.89GHz are presented in figures 2.13.(a), 2.13.(b), and 2.13.(c) respectively. The antenna patterns in E- and H-planes at 6.82GHz are unidirectional. At 9.51GHz, the radiation patterns in E-plane are unidirectional and the antenna patterns in H-plane are omnidirectional. The antenna patterns are unidirectional in both the radiating planes at 9.89GHz. The cross-polarization levels of -8dB and -8.78dB are observed at 6.8GHz. Higher values of cross-polarization at 6.8GHz is due to the propagation of spurious modes in the patch. At 9.51GHz, cross-polarization levels of -13.2dB and -14.38dB are observed in the E- and H-planes. At 9.89GHz, cross-polarization levels of -14.6dB and -14.08dB are observed in the E- and H-planes. The difference in simulated and measured results is due to human and measurement equipment errors.

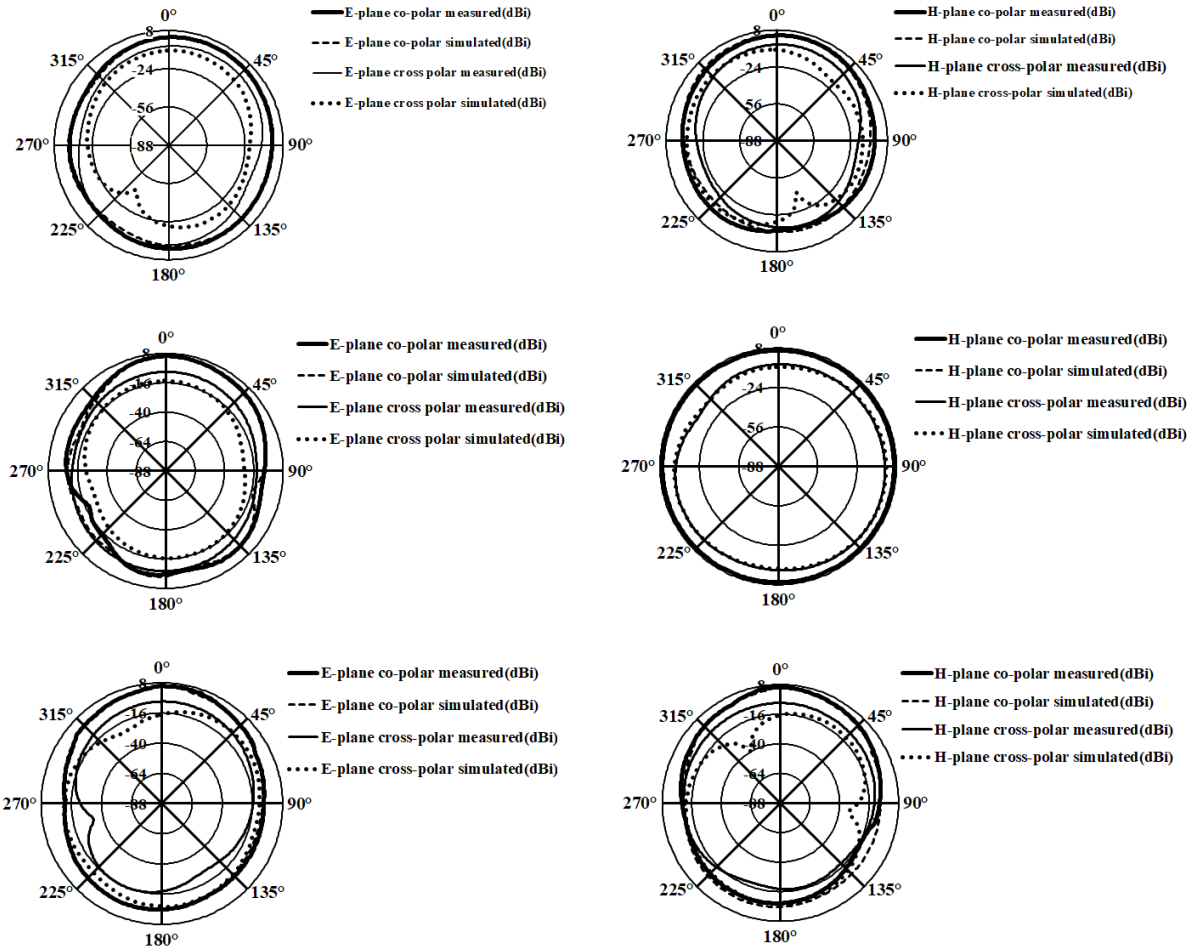

Fig.2.13. Co- and cross-polarization plots of the designed antenna at (a).6.8GHz (b).9.51GHz. (c).9.89GHz

The present design is weighed up with the antennas in the existing literature resonating in C- and X-bands. Table 2.2 presents the detailed contrast between the present design and the preceding designs. This possesses improved performance parameters compared to that of existing antennas. The volume proposed antenna structure is 198.12mm^3 with an active area of 70.74mm^2.

Table 2.3. Weighing up the patch antenna with some existing at C, and X-band

Ref	Dimension (mm^3)	Volume (mm^3)	Active area of the patch (mm^2)	Frequencies (GHz)	Gain (dBi)	Bandwidth (MHz)	Efficiency (%)	Application (s)
[29]	27.31 x 37.4 x 1.58	1625.4	1021.394	3.9& 8.9	8.15	Not Mentioned	Not Mentioned	C-and X-bands
[30]	20 x 15 x 1.5	450	300	5.8	2.78	621	Not Mentioned	C-band
[31]	16 x 18 x 1.6	460.8	77	7.47 & 11.01	5.46 &4.65	400 & 190	Not Mentioned	C- and X-bands
[32]	32.015 x 32.015 x 1.6	1639.93	1024.96	9	6.5	2500	Not Mentioned	X-band
[33]	14.3 x 14.3 x 2	408.98	56.8	8.96, 14.4, & 18.97	6.32, 6.32, & 6.32	650, 800, & 1420	80.91, 80.91, & 80.91	C- and X-bands
[34]	25.6 x 23.63 x 1.6	967.88	466.176	9.19, & 10.82	1.44, & 2.03	540, & 1600	68.9, & 71.2	X-band
[35]	40.29 x 35.1 x 0.78	1113.59	1414.179	7.75, 9.72 & 11.92	5.59, 6.67 & 3.72	180, 270 & 300	84.14, 85.6 & 86.3	C- and X-band
[36]	30 x 30 x 3	2700	400	9.5	4.46	1560	81.1	X-band
[37]	35 x 30 x1.6	1680	450	10.3	7.62	2110	83.2	X-band
[38]	28.33 x 31.34 x 1.6	1420.57	793.21	9.96, 10.81, & 11.56	3.32, 2.84, & 1.16	470, 590, & 420	Not Mentioned	X-band
[39]	20 x 20 x 0.2	80	80	7.5	0.59	1500	Not Mentioned	C-band
[40]	20 x 17.2 x1.6	550.4	344	8.95, 11.06 & 11.85	4.45, 3.99, & 4.17	450, 1010 & 450	90.90, 87.89 & 88.32	X-band
[41]	40 x 40 x 1.6	2650	1600	10.25 & 11.54	4.31	1590	78.8	X-band
This work	**10 x 13 x1.524**	**198.12**	**70.74**	**6.8, 9.51 & 9.89**	**3.2, 5.41 & 5.56**	**660.2 and 1600**	**82.1, 86.3 & 88.1**	**C- and X-bands**

2.3. Design of a stub loaded oval ring patch antenna

Figure.2.14.(a) shows the design of the proposed patch antenna. The patch is printed on one side of RT/Duroid-6202 substrate (ε_r = 2.94) and having thickness of 1.524 mm. Initially, a basic oval ring patch antenna is excited through a microstrip feed line having an impedance of 50Ω. The impedance bandwidth is observed after the patch is excited. The patch resonates at 30GHz. The bandwidth obtained in this structure is as high as 2.2GHz but the required miniaturization is not achieved in this design. An enlarged bandwidth is achieved by attaching two L-stubs and folded meander line of quarter wavelength to the oval ring patch. The required multi-band and wide-bandwidth features are achieved by attaching the stubs to oval ring patch antenna. L- shaped stub lines radiate at operational frequency of 6.12GHz and 9.42GHz. Folded meander line stub resonates at 15.6GHz. The developed structure possesses a total volume of 10 x 12 x 0.035mm^3.

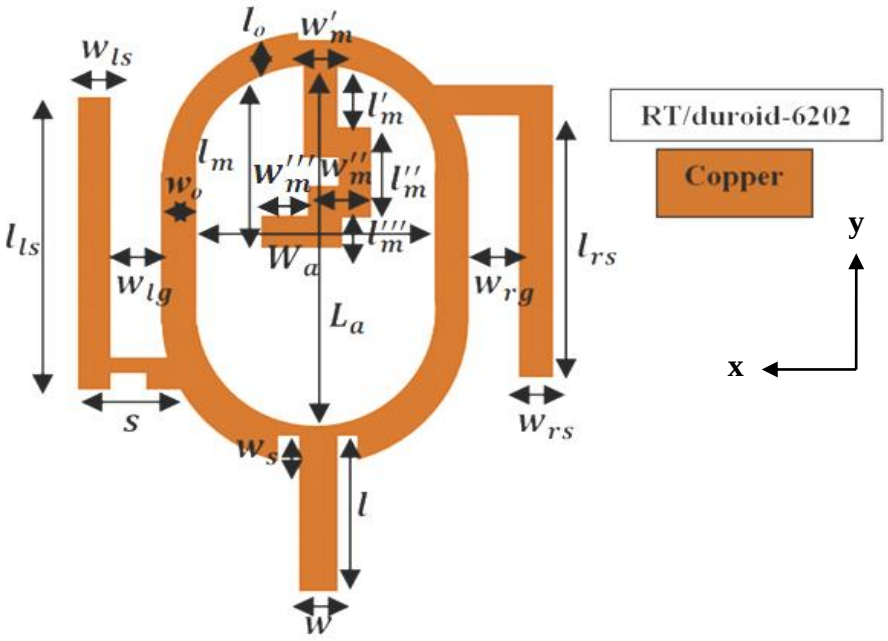

Fig.2.14.(a). Structure of the designed antenna

Figure.2.14.(b) shows the fabricated prototype.

Fig.2.14.(b). Fabricated prototype

Table.2.4 presents the optimized design values of the proposed antenna structure.

Table 2.4. Detailed design values of the designed antenna

Dimension	L_a	W_a	l_m	l'_m	l''_m
Value(mm)	6	4	3.25	2	0.75
Dimension	l'''_m	w'_m	w''_m	w_{rg}	w_{lg}
Value(mm)	0.5	0.5	1	1	1
Dimension	L_g	W_g	w_{ls}	w_{rs}	l_{ls}
Value(mm)	12	10	1	1	5.5
Dimension	l_{rs}	s	l	w	w_s
Value(mm)	7.75	2.5	2.5	1	0.5
Dimension	w_o	l_o	w''_m		
Value(mm)	1	1	1.5		

The proposed patch antenna resonates at four frequencies (f_1, f_2, f_3, and f_4). First, second, third, and fourth frequencies are 6.12GHz, 9.42GHz, 15.6GHz, and 25GHz respectively.

The resonant frequency of the radiating stub line is calculated by:

$$f_1 = \frac{c}{4(l_{rs})\sqrt{\varepsilon_{eff}}} \tag{2.4}$$

- $'l_{rs}'$ is the length of the right stub

Similarly, the resonant frequency of the radiating stub section is calculated by:

$$f_2 = \frac{c}{4(l_{ls})\sqrt{\varepsilon_{eff}}} \tag{2.5}$$

The frequency of the radiating meander line is calculated by:

$$f_3 = \frac{c}{4(l_m)\sqrt{\varepsilon_{eff}}} \tag{2.6}$$

The frequency of the oval ring is calculated by:

$$f_4 = \frac{c}{\pi(l_o)_{eff}\sqrt{\varepsilon_{eff}}} \tag{2.7}$$

Where 'l_o' is the perimeter of the oval ring

$$l_{o\,eff} = l_o\left[1 + \left(\frac{2h}{l_o \pi \varepsilon_r}\right)\left[\ln\left(\frac{a}{2h}\right) + (1.41\varepsilon_r + 1.77) + \frac{h}{l_o}(0.265\varepsilon_r + 1.65)\right]\right]^{\frac{1}{2}} \tag{2.8}$$

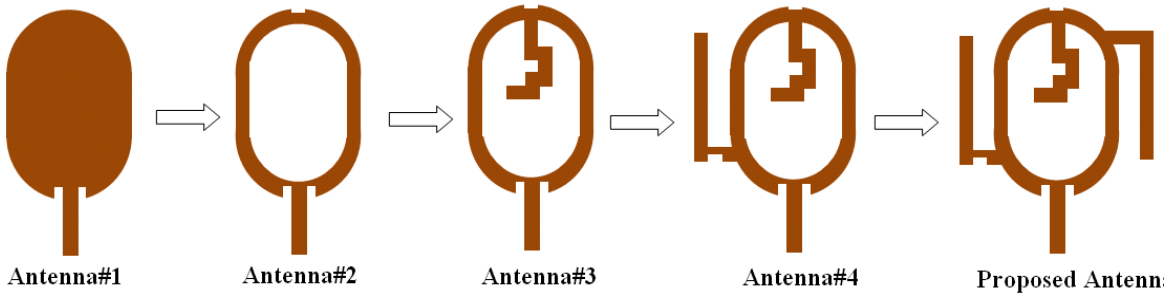

(a)

Figure.2.15.(a) Stages of development of the patch antenna. Figure.2.15.(b) represents the impedance bandwidth plots of development stages of the antenna. Initially, an oval shaped patch antenna as denoted by antenna#1 is designed and simulated. This antenna resonates at 25.5GHz and 30GHz as plotted in red. Impedance bandwidths of 1.1GHz and 1.52GHz are seen in the frequency ranges of (25GHz~26.1GHz) and (28.52GHz~30GHz).

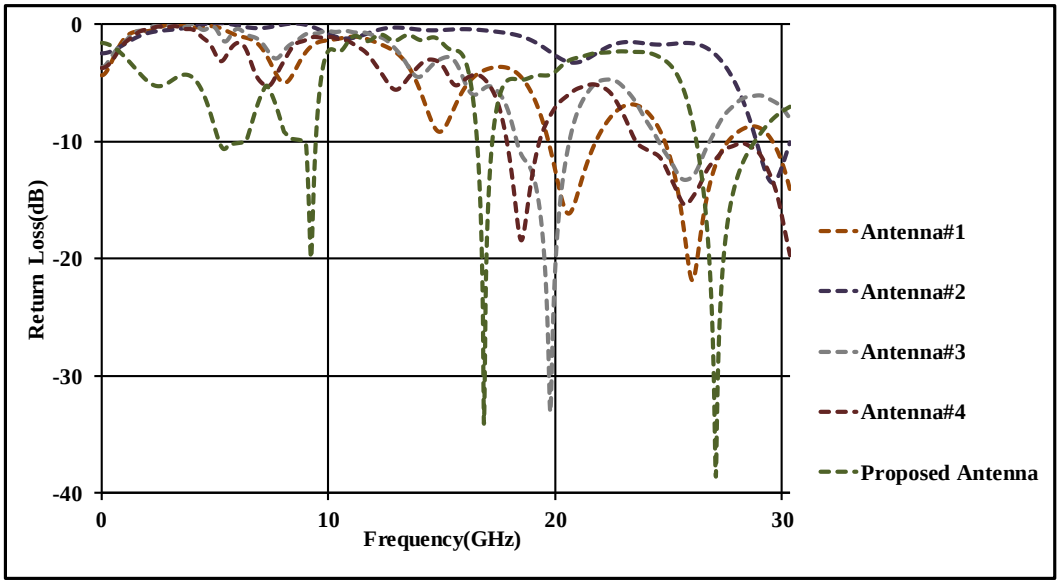

(b)

Antenna#2 is evolved by etching the inner circumference of the antenna presented in the first stage. The antenna evolved resonates at 30GHz with the impedance bandwidth of 2.2GHz Antenna#3 is evolved by attaching folded meander line stub to the antenna presented in stage-2. This antenna resonates at 21.63GHz and 26.5GHz with the impedance bandwidths of 4.1GHz (18.53GHz~22.63GHz) and 3.23GHz (25GHz~28.23GHz). Next stage of antenna is formed by attaching stub to the left side of the design as presented in stage 3. The antenna thus formed is named as antenna#4. This antenna resonates at 18.6GHz, 27.1GHz and 30GHz. This exhibit operational bandwidths of 2.23GHz (17.5GHz~19.7GHz) and 8.1GHz (21.9GHz~30GHz). Proposed antenna is evolved by attaching another L-shaped stub to the right side to the structure as presented in stage-4. The antenna operates at 6.12GHz, 9.42GHz, 15.6GHz and 25GHz. It possesses impedance bandwidths of 321MHz (5.97GHz~6.29GHz), 684MHz (9.32GHz~9.98GHz), 430MHz (15.71GHz~16.01GHz) and 3.3GHz (23.5GHz~26.8GHz). Figure. 2.15.(c) shows the variations of input impedance of the designed antenna structure with the frequency. The input impedance is observed through simulations and measured after the fabrication. The values of the resistive part of input impedance are close to 50Ω in the frequency ranges 5.57GHz~6.29GHz, 9.32GHz~9.98GHz, 15.71GHz~16.01GHz and 23.5GHz~26.8GHz respectively. Thus showing that the required reflectionless matching is achieved in the band of interest. The values of reactance part of input impedance are close to zero in the frequency ranges of 5.57GHz~6.29GHz, 9.32GHz~9.98GHz, 15.71GHz~16.01GHz, and 23.5GHz~26.8GHz. The simulated and measured values of input impedance are in close agreement. Electrical models are helpful in analysing the multiband feature in antennas [42-43]. The values of lumped elements as shown in figure 2.15.(d) are

obtained from input impedance plots. The resistive impedance of electrical model is approximately 50Ω in the frequency ranges 5.57GHz~6.29GHz, 9.32GHz~9.98GHz, 15.71GHz~16.01GHz and 23.5GHz~26.8GHz. Whereas, the reactive impedance is in close proximity to zero in the desired frequency ranges. The impedance plots of lumped element equivalent are in close proximity with that of impedance plots of the designed antenna structure.

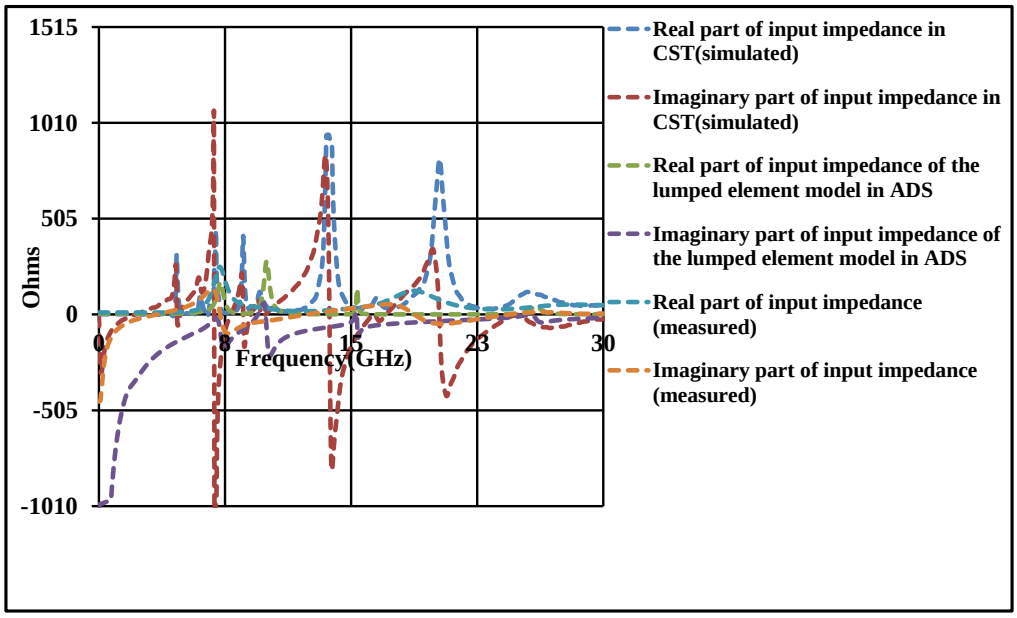

(c)

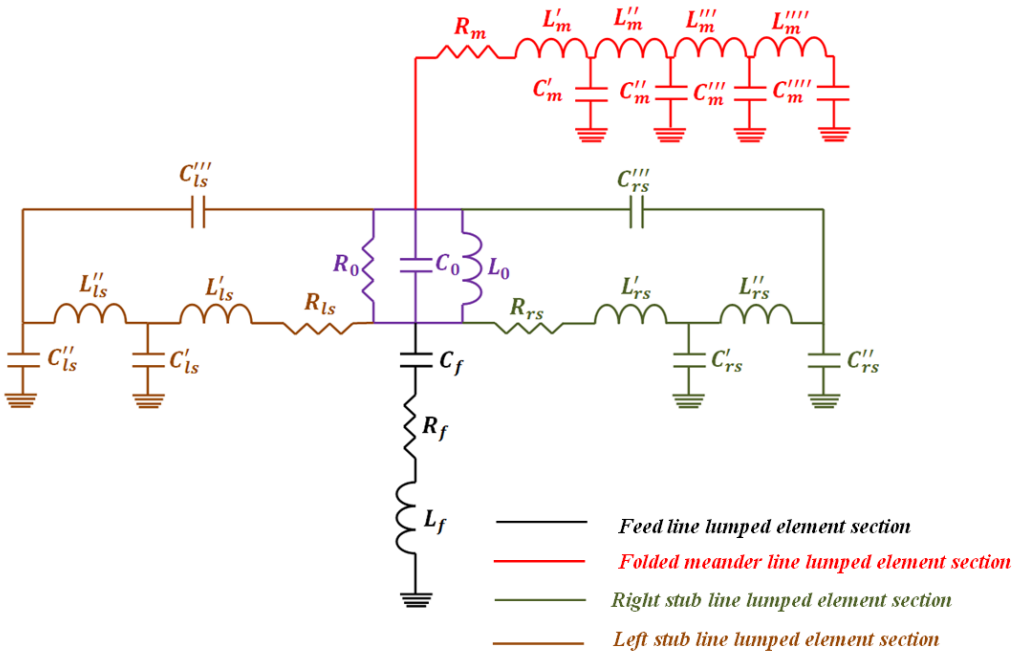

(d)

Figure 2.15.(d) represents the electrical model of the proposed antenna structure. The electrical elements (R_0, L_0, & C_0) represent oval portion. The electrical elements (R_{ls}, L'_{ls},L''_{ls}, C'_{ls},C''_{ls}, and C'''_{ls}) represent stub-line portion attached to the left side of the oval ring and the electrical elements (R_{rs}, L'_{rs}, L''_{rs}, C'_{rs},C''_{rs}, and C'''_{rs}) represent right stub-line section. (R_f, L_f, & C_f) corresponds to feed line section. The section (R_m, L'_m, L''_m,L'''_m,$L''''_m C'_m$,C''_m,C'''_m and C''''_m) represent the meander stub. Figure 2.15.(e) presents the operational bandwidth plot of the electrical model as presented in figure 2.15.(d). Table 2.5 presents the values of R-L-C elements in the electrical model. The intial values of the electrical elements are acquired from the input impedance plots simulated in CST-microwave studio. The electrical model is simulated in ADS after optimizing the lumped element values using ADS schematic tuner.

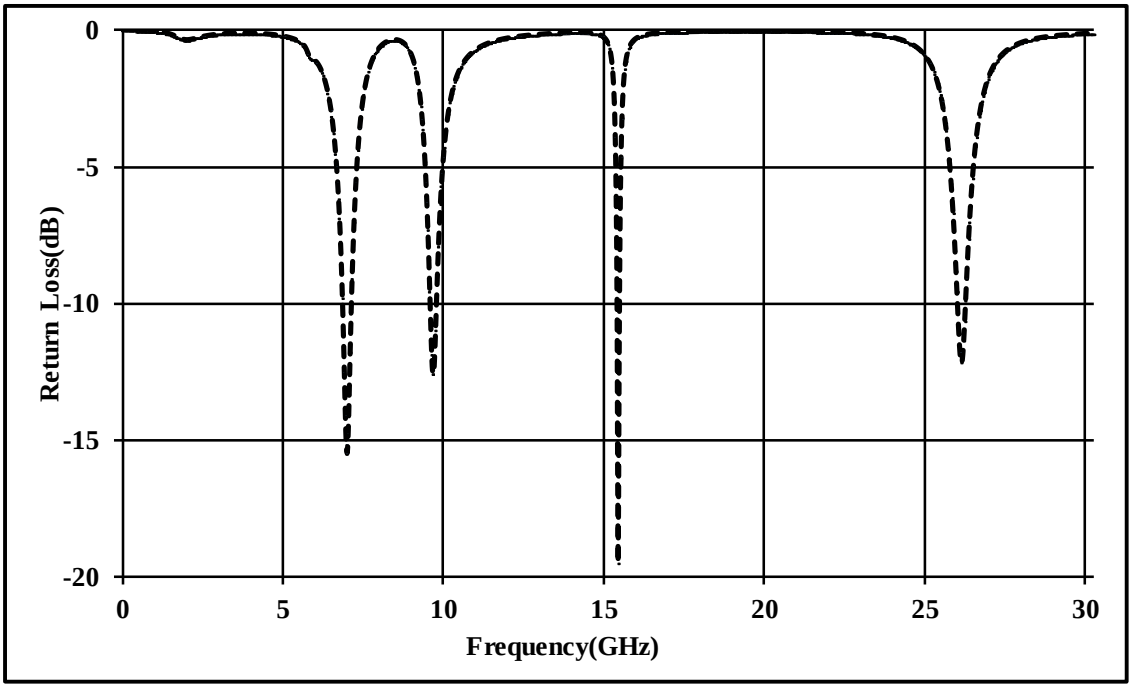

(e)

Fig.2.15.(a). Stages of development of the patch antenna. **(b).** Impedance bandwidth plots of development stages of the antenna. **(c).** Input impedance of the antenna and its electrical model. **(d).** An equivalent electrical model of the patch antenna **(e).** Impedance bandwidth of the electrical model in ADS.

In the plot shown in the figure 2.15.(e), resonant frequencies are observed at 6.21GHz, 9.61GHz, 15.73GHz and 25.63GHz with the impedance bandwidths of 313.1MHz, 423MHz, 419MHz and 1.31GHz respectively. Table 2.5 shows the values of elements of electrical model of the design.

Table.2.5 Values of electrical elements in the electrical model.

Electrical element	$R_f(\Omega)$	$R_0(\Omega)$	$R_{ls}(\Omega)$	$R_{rs}(\Omega)$	$R_m(\Omega)$	L_f(nH)	C_f(pF)
Value	0.1	10	150	30	4	3.6	0.24
Electrical element	L_0(nH)	C_0(pF)	L'_{ls}(nH)	L''_{ls}(nH)	C'_{ls}(pF)	C''_{ls}(pF)	C'''_{ls}(pF)
Value	10	50	5	0.8	1.22	6	0.13
Electrical element	L'_{rs}(nH)	L''_{rs}(nH)	C'_{rs}(pF)	C''_{rs}(pF)	C'''_{rs}(pF)	L'_m(nH)	L''_m(nH)
Value	5	1.34	0.36	0.94	0.576	0.422	0.408
Electrical element	L'''_m(nH)	L''''_m(nH)	C'_m(pF)	C''_m(pF)	C'''_m(pF)	C''''_m(pF)	
Value	0.5	0.69	0.1	0.1	0.5	0.24	

2.3.1 Parametric analysis

The multiband feature in the developed design is affected by the dimensions of the stubs especially their lengths (l_{ls} & l_{rs}) and the meander line (l_m). Figure 2.16.(a), 2.16.(b) and 2.16.(c) shows the variation of operational bandwidth of the designed antenna with the change in the design aspects of the antenna. The variation in the impedance bandwidth is observed by varying resonant length of the meander line from 3mm to 7mm. The proposed patch antenna resonates at 14.92GHz for the length of 3mm. The patch antenna resonates at 15.31GHz if the length is 5mm. The patch exhibits reflection co-efficient of -20.2dB at the said frequency. If length of the meander stub line is further increased to 6mm, the developed antenna operates at 15.52GHz. The patch antenna possesses return loss of -18.62dB at the resonant frequency. The patch resonates at 15.66GHz for the meander line length of 7mm. The patch possesses return loss of -18.12dB at the operational frequency.

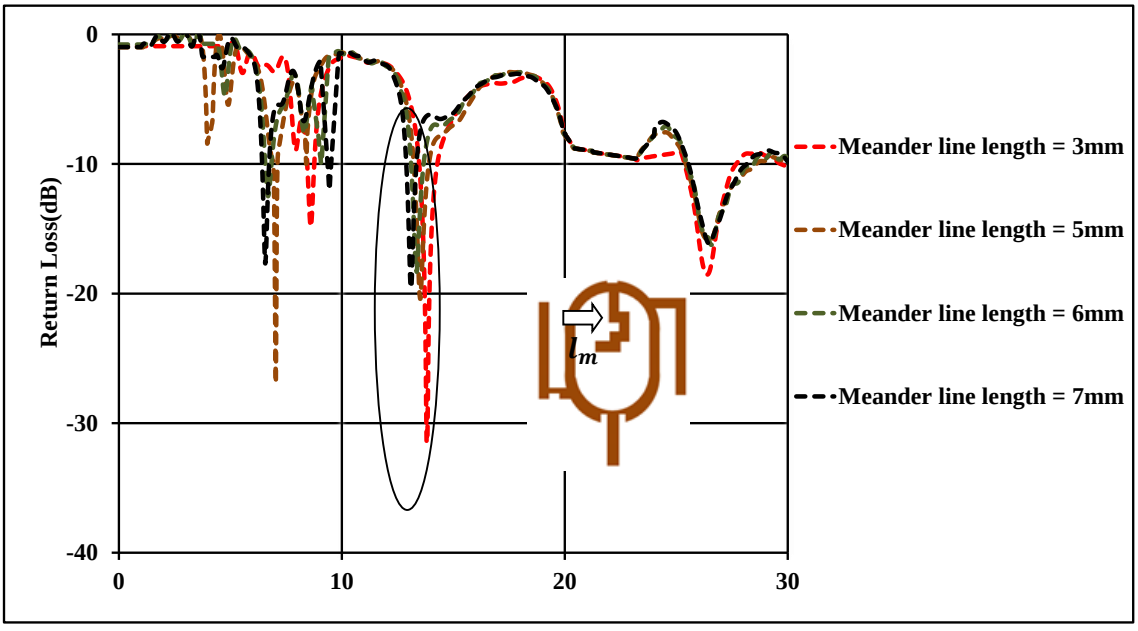

(a)

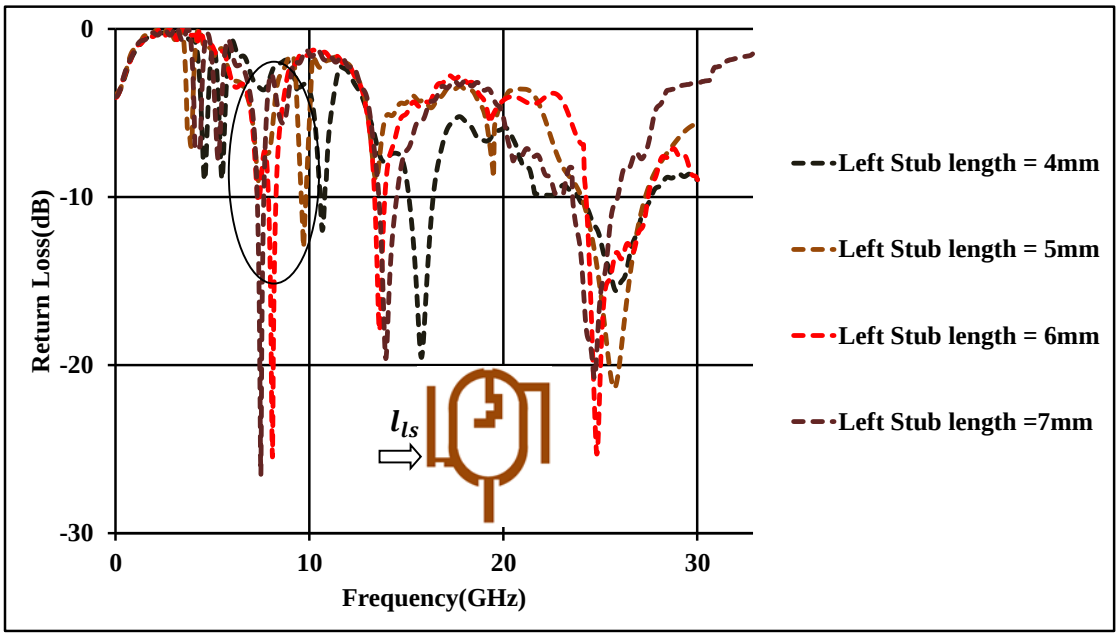

(b)

Figure.2.16.(b) presents the influence of stub length (l_{ls}) on the operational bandwidth of the structure. The left stub length is tuned from 4mm to 7mm. With the left stub dimension fixed at 4mm, the proposed patch resonates at 10.1GHz. This possesses reflection co-efficient of -12.58dB at the operational frequency. With the left stub dimension fixed at 5mm, the proposed patch resonates at 9.89GHz. With the left stub dimension fixed at 6mm, the proposed patch resonates at 8.2GHz. With the left stub dimension fixed at 7mm, the proposed patch resonates at 8.01GHz. From the above analysis, it can be inferred for l_{ls} of 5.5 mm, better results are obtained. Moreover, the fluctuation in the stub length deviates resonant frequencies namely 6.12GHz, 15.6GHz and 25GHz because of high capacitive loading between l_{ls}, l_m,l_{rs}, and l_o. Figure 2.16.(c) presents the impedance bandwidth plots of antenna for various l_{rs} values from 6 to 8mm. With the stub length (l_{rs}) fixed at 6mm, the antenna radiates at 7.35GHz and having reflection coefficient of -32.58dB. With the stub length (l_{rs}) fixed at 7mm, the designed structure radiates at 6.31GHz with the reflection co-efficient of -18.52dB. With the stub length (l_{rs}) fixed at 8mm, the antenna radiates at 6.03GHz with the reflection co-efficient of -22.72dB. The deviation in the operational frequencies is because of high capacitive loading between l_o, l_m, and l_{rs}.

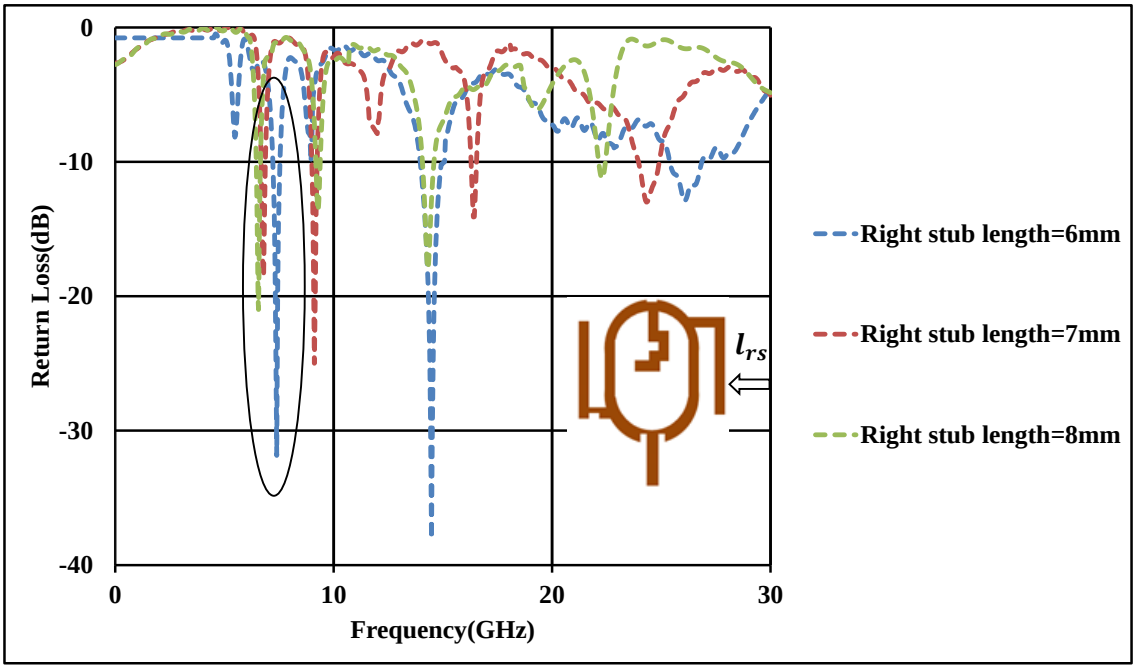

(c)

Fig.2.16.(a). Impact of length of the meander line on the impedance bandwidth of the antenna. **(b).** Impact of length of the left stub on the impedance bandwidth of the antenna **(c).** Impact of length of the right stub on the impedance bandwidth of the antenna

2.3.2. Outcomes and Disquisitions

The proposed prototype is devised in CST Microwave Studio and fabricated with parameters obtained in table.2.4. Figure 2.8 presents the fabricated antenna. Figure.2.9 presents the results of the impedance bandwidth. Both the results simulated and measured are in acceptable proximity. However, the variation in the simulated and measured results is because of fabrication, connector and substrate disruptions. The proposed patch resonates at 6.21GHz, 9.42GHz, 16.78GHz, and 25.4GHz. The designed antenna exhibits bandwidths of 315MHz (6.06GHz~6.31GHz), 671MHz (9.12GHz~9.79GHz), 441MHz (16.62GHz~17.29GHz), and 3.21GHz (24.4GHz~27.6GHz).

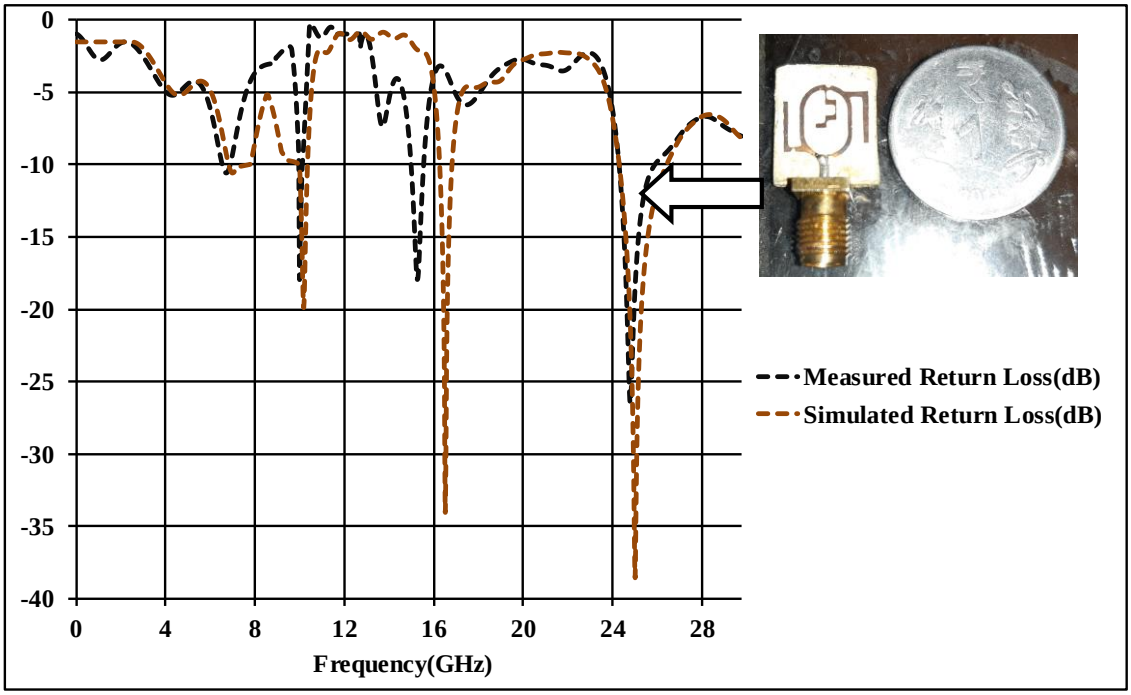

Fig.2.17. Impedance bandwidths of the stub loaded oval ring patch antenna

Figure 2.18 presents the surface current densities at 6.12GHz, 9.4GHz, 15.6GHz and 25GHz. At 6.12GHz, maximum current is directed along the right stub and a part is directed towards the oval ring and the ground layer. It is seen that current density is diverted towards the bent radiating stub at 6.8GHz and a significant magnitude of surface current is diverted towards the ground layer. At 9.4GHz, surface current is diverted towards the right stub and some part is directed towards ground layer. At 15.6GHz, the current in the right radiating stub is diverted towards meander line. At 25GHz, the surface current is distributed along the circumference of oval ring.

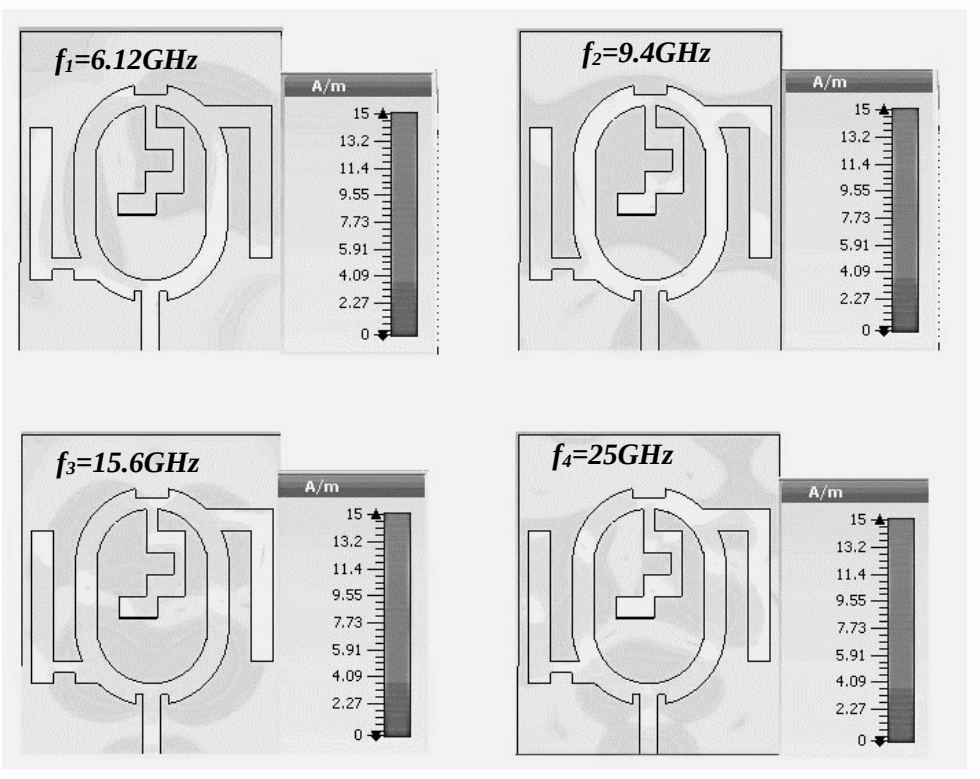

Fig.2.18. Surface current distributions of the proposed patch antenna at 6.12GHz, 9.4GHz, 15.6GHz and 25GHz

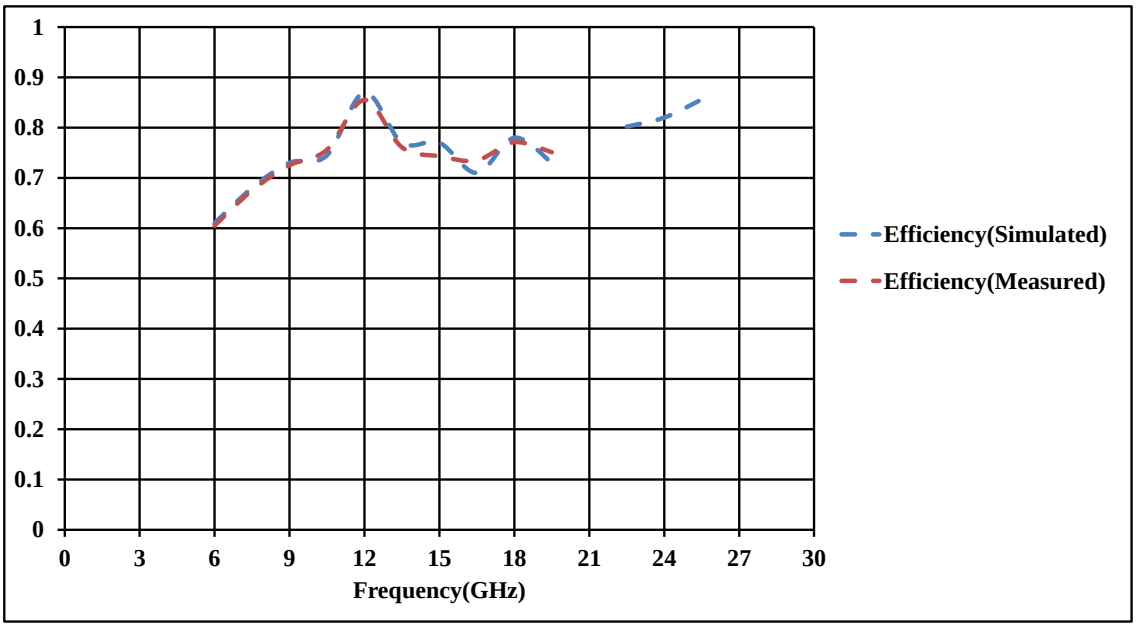

Fig.2.19. Simulated and measured efficiencies of the proposed patch antenna

Figure.2.19 presents the efficiency plots of stub loaded oval ring patch antenna. Efficiency is measured using antenna measurement set-up. Radiation efficiencies ranging from 60.14% to 78.6% are obtained at 6.21GHz, 9.4GHz, and 16.78GHz. Efficiency of 83.64% is obtained at 25GHz.

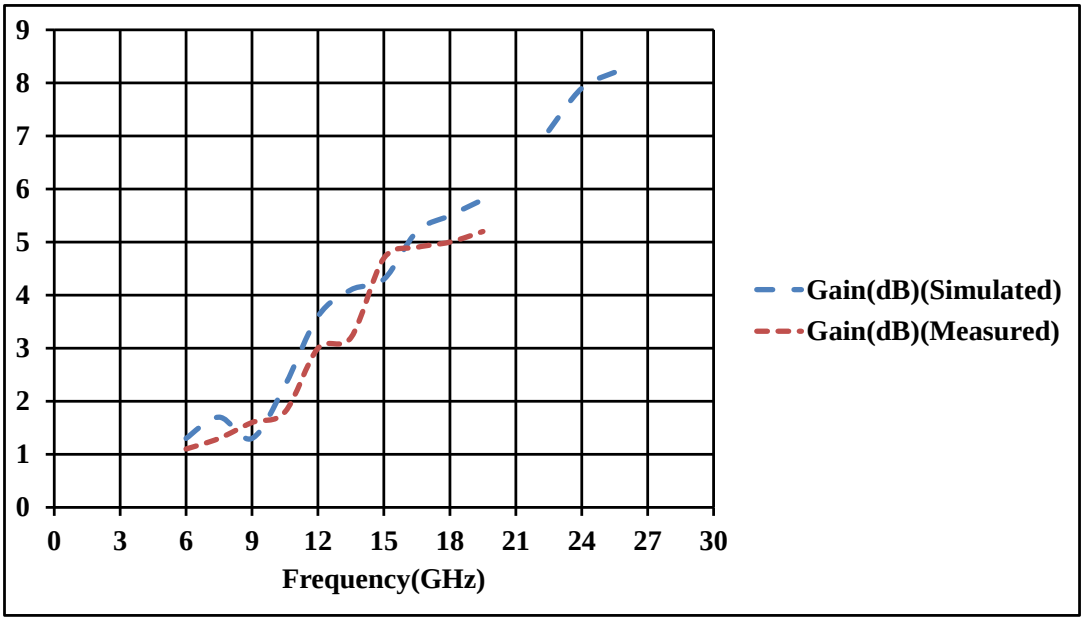

Fig.2.20. Gains of the stub loaded oval ring patch antenna.

The proposed antenna possesses peak gains in the operating bands as presented in figure.2.20. The gains vary from 1.1dBi to 8.09dBi at the operational frequencies. The simulated and measured gains are in close proximity with little deviation.

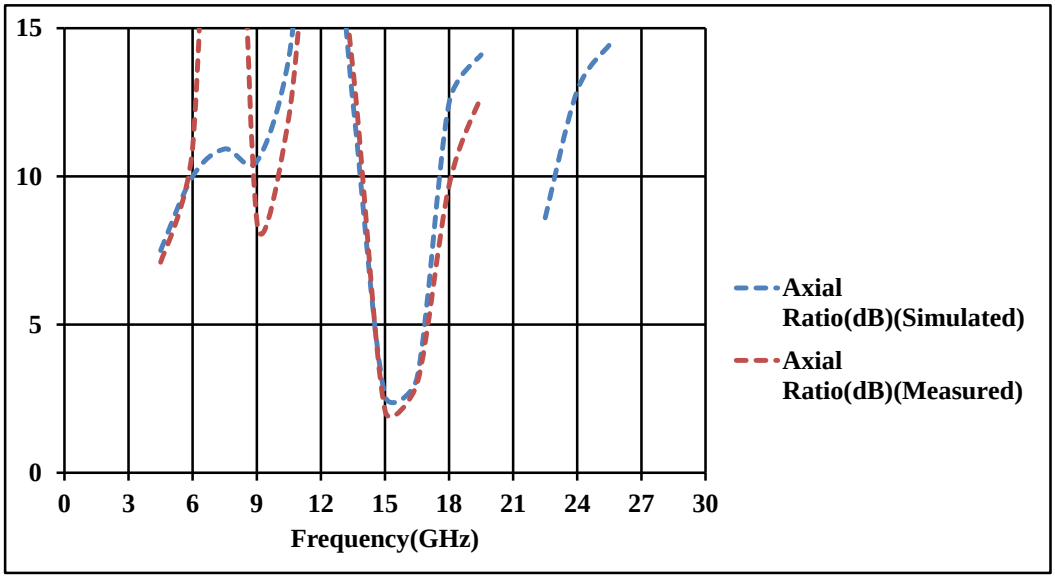

Fig.2.21. Simulated and measured axial ratios of the proposed patch antenna

The plots of axial ratio are presented in figure.2.21. At 6.21GHz, 9.4GHz, and 16.78GHz, measured axial ratio values are obtained as 11.02dB, 8.22dB, and 2.1dB. At 25GHz, simulated axial ratio of 13.65dB is observed. Axial ratio bandwidth of 1.82GHz is measured in the band of 15GHz~16.82GHz. In the remaining frequency ranges of operation, the proposed patch antenna possesses linear polarization. The patch possesses Right Hand Circular Polarization (RHCP) in the operational band of 15GHz~16.82GHz.

Antenna measurement system comprises of double-ridged horn antenna. Figure.2.22.(a) presents the measured antenna patterns in radiating planes at 6.21GHz. The radiation patterns in these planes are unidirectional. Figure.2.22.(b) presents the measured antenna patterns in radiating planes at 9.4GHz. The radiation patterns are unidirectional in both the planes. The antenna patterns of the antenna at 9.4GHz are presented in figure.2.22.(b). Both the radiating planes possesses antenna patterns of unidirectional type at 9.4GHz. Figure.2.22.(c) presents the measured antenna patterns in the radiating planes at 16.78GHz. The radiation patterns are unidirectional in shaped in E- and H-planes. Figure.2.22.(d) presents the antenna patterns at 25GHz. The measured antenna patterns are not shown due to the unavailability of anechoic chamber beyond 20GHz. E- and H-planes at this frequency possess unidirectional radiation patterns. Simulated and measured antenna patterns are in close proximity with high tolerance in measurement equipment.

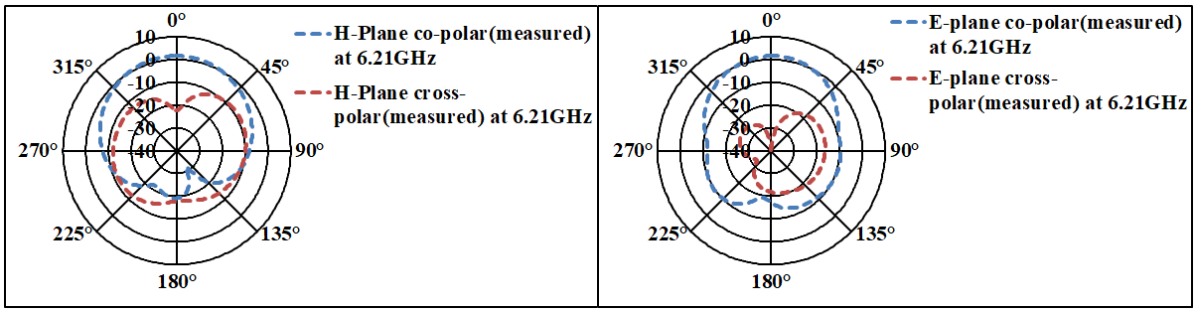

(a)

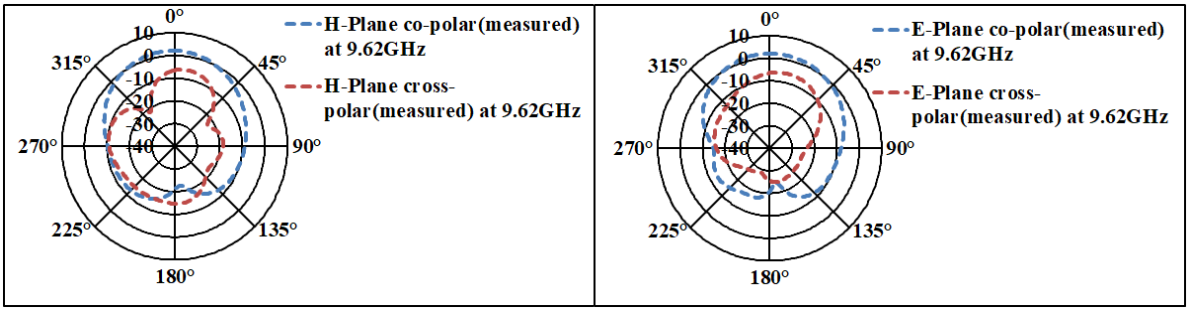

(b)

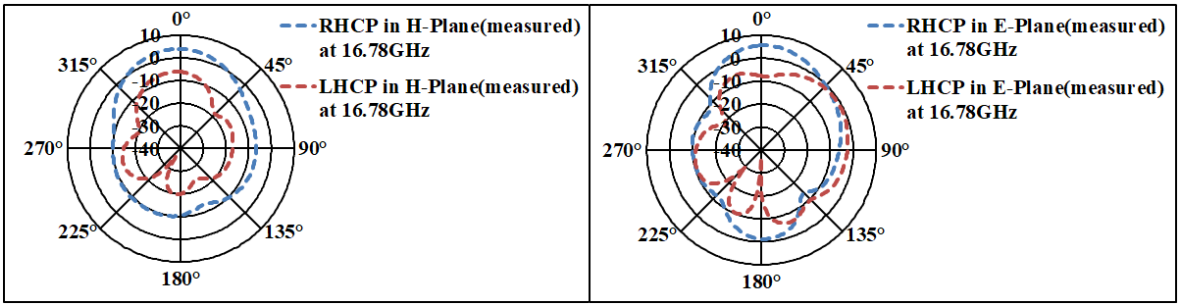

(c)

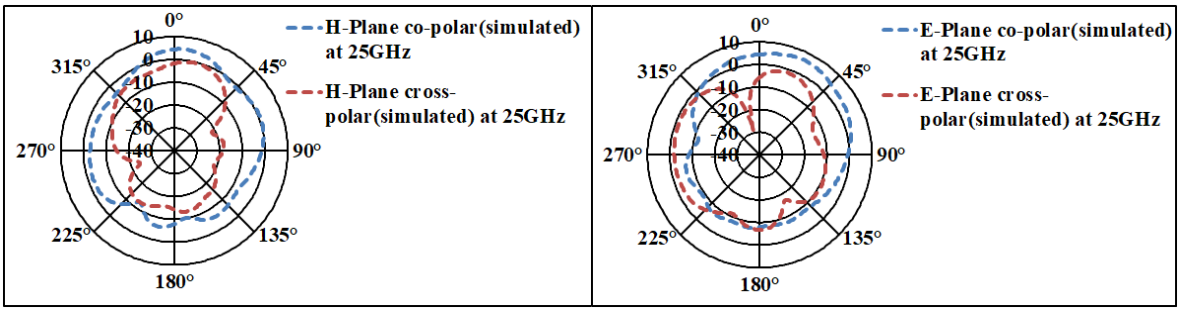

(d)

Fig.2.22. The antenna patterns at **(a).**6.21GHz **(b).**9.4GHz. **(c).**16.78GHz **(d).**25GHz

The increase in the cross-polarization levels is due to the propagation of undesired modes in the antenna structure. These spurious modes are responsible for the radiation leakages and distortions in the radiation patterns. At higher frequencies, the magnitude of cross-polarization levels is high in the antenna boresight as patch supports high frequency excitations in the form of higher propagation modes. The antenna is rested in the x-y plane and pointing towards z-axis shorts Transverse Electric modes (TE) and thereby supporting only TM modes. The supportive Transverse magnetic modes (TM) are obtained from the cavity model analysis as described in the preceding chapter. The higher order TM modes are solely responsible for radiation in unwanted directions. Resonance plots of the designed antenna are presented in figure.2.23. These higher order modes distort radiation patterns and increase cross-polarization levels. At the same time, higher order modes enhance performance parameters like bandwidth in the desired frequency range.

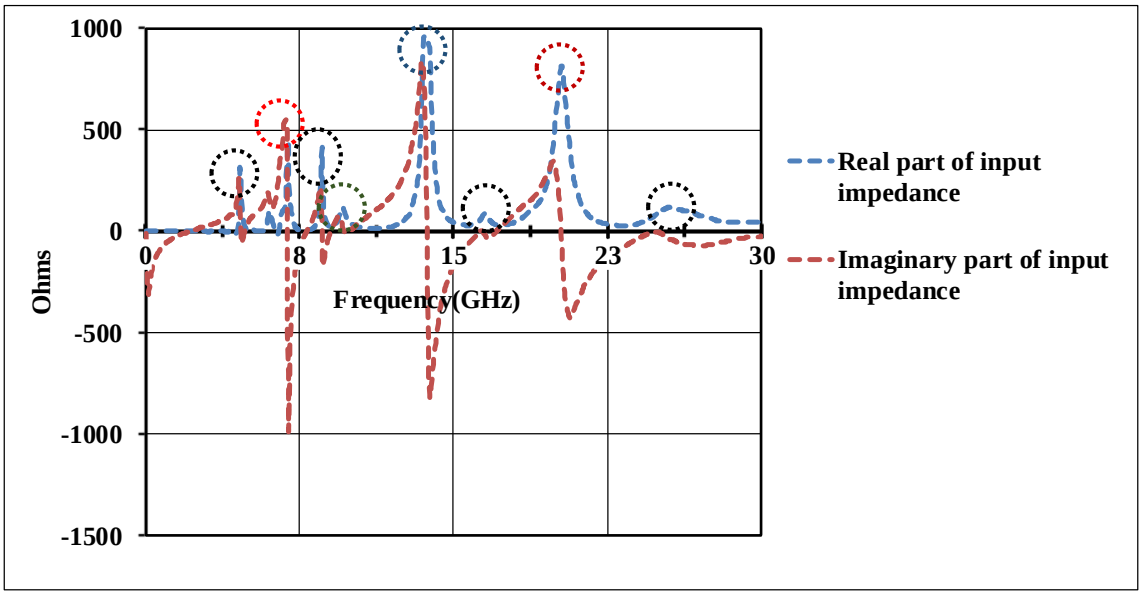

Fig.2.23. Resonant peaks of the designed antenna

Figure.2.24 presents the different propagation modes supported by the designed patch antenna. The supporting modes are obtained in CST-MW studio using Eigen mode solver. These modes are in close proximity with that of the modes presented in the resonance plots.

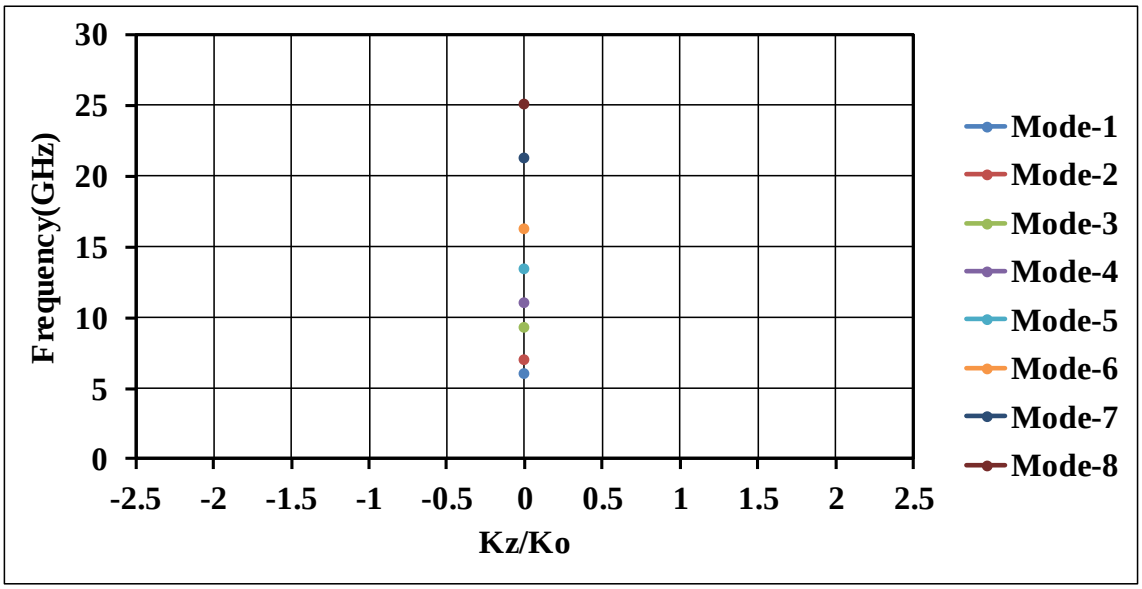

Fig.2.24. Modes observed using Eigen mode solver in CST MW-Studio.

The performance designed antenna are compared with that of preceding radiators at C-, X-, Ku-, and K-bands. From table.2.6, it is inferred that the developed structure shows superior performance than the antennas with good degree of miniaturization in the recent literatures. The design is miniaturized and has a total volume of 182.88mm^3. Further, the radiating area on the antenna is reduced to 70mm^2(excluding feed line) and 90mm^2(including feed line).

Table.2.6. Weighing up the proposed antenna with the existing ones

Ref	Dimensions (mm^3)	Volume (mm^3)	Area of the patch (mm^2)	Peak Gain(s) (dBi/dBic)	Frequencies (GHz)	Applications
[44]	8 x 8 x 2.702	172.8	64	8	16 & 30	K_u- and K-band
[45]	8 x 16 x 1.6	204.8	128	3.8, 8.3 & 8.4	8.7, 16.4 & 19.6	X-, K_u- and K-band
[46]	20 x 20 x1.575	630	400	1.87 & 3.87	15.56 & 20.41	K_u- and K-band
[47]	24 x 18 x 1.6	691.2	168	2.033 – 7.7	4.91, 7.76, 12.72 & 29.3	WiMAX, WLAN, 5 GHz U-NII, C-band, X-band, K_u-band, K-band and Ka-band
[48]	18 x 20 x1.58	568.8	77	4.91	11.5 & 12.5	X- and K_u-band
[49]	40 x 35 x 1.905	2667	1400	2.03 & 3.65	13 & 18.1	K_u- and K-band
[50]	20 x 20 x 0.787	314.8	400	6.96	4.5, 7, 9, 12, 15 & 18	C-, WLAN, X- and K_u-band
[51]	37.21 x 28.89 x 1.6	1719.99	1074.99	9.2	11.37, 12.13, 13.14 & 14.66	X- and K_u-band
[52]	15 x 15 x 1.6	360	225	1.56	8.8, 10.8, 13.02 & 15.23	X- and K_u-band
[53]	80 x 90 x 1.6	11520	1430	Not mentioned	11.44, 13.178, 15.482, 19.902 & 23.529	X-, K_u- and K-band
[54]	24.6 x 22.15 x 2	1089.78	544.89	9.6	8.5, 17.7, 20, 23.7 & 30	GPS, WLAN and military
[55]	11 x 15 x 1.6	264	165	1.65, 1.26, 2.4, 3.2, 4.57, 4.03	6.3, 7.1, 7.5, 8.7, 12.8, 17&21.3	C-, X-, K_u- and K-band
[56]	9.5 x 7.96 x 1.9	143.678	75.62	4.8, 6.42 & 3.9	15.33, 17.61 & 18.9	K- and K_u-band
[57]	28.8 x 28.8 x 0.8	663.552	92.16	6.60 & 5.80	9.56 & 14.46	X- and Ku-band
[58]	20 x 20 x 1.6	640	100	1.6-4.2	12.38 & 14.40	Ku-band
[59]	20 x 20 x 1.6	640	400	Not mentioned	6.18, 8.52, 14.7 &17.71	Mobile, Fixed-Satellite (Earth-to-space), Radiolocation
[60]	20 x 14 x 1.5	420	80	6.2	16.8	K- and K_u-band
[61]	20 x 20 x 1.6	640	400	8.5	15.4	K- and K_u-band
[62]	14 x 20 x 1.6	448	280	7.8	17.75	K_u-band
This work	**10 x 12 x 1.524**	**182.88**	**70**	**1.1, 1.23, 5.81 & 8.1**	**6.21, 9.42, 16.78 & 25**	**C-, X-, K_u- and K-band**

2.4. Conclusion

In this chapter, two types of antennas namely stub loaded serpentine patch antenna and stub loaded oval ring patch antenna are designed and analysed. These antennas are compact and possesses enhanced performance parameters.

The serpentine antenna with folded stubs possesses the simulated bandwidths of 662MHz, 1.6GHz and measured bandwidths of 660MHz and 1.52GHz. Measured gains of 3.2dBi, 5.42dBi and 5.56dBi along with the efficiencies of 82.1%, 86.3% and 88.1% are obtained at the resonant frequencies. The radiation patterns in all the planes are unidirectional at 6.8GHz. At 9.51GHz, omni-directional patterns are noticed in H-plane and unidirectional in E-plane. At 9.89GHz, unidirectional antenna patterns are noticed in all the radiating planes.

Stub loaded oval ring patch antenna resonates at 6.21GHz, 9.4GHz, 16.78GHz and 25GHz. Gains ranging from 1.01dBi to 8.1dBi are observed in the frequencies of resonance. The efficiencies ranging from 60.12% to 78.56% are obtained at the frequencies of operation. An efficiency of 83.64% is noticed at 25GHz. The antenna patterns are unidirectional in all the radiating planes at 6.21GHz, 9.4GHz, 16.78GHz and 25GHz. The designed structure is circularly polarized at 16.78GHz and linearly polarized at other frequencies of operation.

The performance parameters of the stub loaded antennas are further improved by using High Impedance Surfaces (HIS) which are discussed in the next chapter.

CHAPTER 3

Study and analysis of different dumbbell shaped high impedance surfaces

3.1. Introduction

In the last chapter, different stub-loaded patch antennas are discussed for obtaining reasonable gain, high bandwidth, and efficiency. These antennas possessed less active area with improved directionality. In the same chapter, higher modes which contribute to the enhancement of gain are analysed using modal analysis as discussed in chapter-1.

Stub-loaded antennas in the previous chapter suffered from low gains and high cross polarization levels. Stub-loaded in oval ring patch antenna supports higher order modes. These unwanted modes merge with the frequency of operation and a strong coupling occurs between these two. Due to which, power is coupled between the frequencies. This coupling reduces gains at the desired frequencies with the magnitude of cross-polarization being high. To overcome these problems, patch and/ or ground plane are loaded with Artificial Magnetic Conductor (AMC) [63]-[65]. In this chapter, a study on dumbbell shaped High Impedance Surfaces (HIS)/ AMC is conducted. oval-shaped antenna with radiating stubs is loaded with dumbbell-shaped metamaterials (MTM), electromagnetic bandgap structures (EBG), and defective ground structures and the effect of the latter on the earlier is discussed. The effect area of the ground layer on the metamaterial inspired structure is discussed. The selection of particular HIS based on the application's requirement is discussed.

Literature survey reveals, based on different HIS loaded antennas for improving antenna's performance parameters [66-81].

3.2. Literature survey

Debajyoti Chatterjee et.al. in [66] – presents an antenna loaded with slot and 3 x 3 SRR metamaterial for gain enhancement. The gain is highly improved with the implementation of metamaterial surface.

Parul Dawar et.al. in [67] – presents a miniaturized patch antenna loaded with 2-segment SRR metamaterial and operates at 4GHz. A miniaturization of 600% is achieved with the proposed metamaterial.

Parul Dawar et.al. in [68] – presents a meander strip line metamaterial loaded patch antenna resonating at 3.85GHz with degree of miniaturization of 84%. The designed patch antenna possesses a gain of 3dB.

Parul Dawar et.al. in [69] – presents a 'S'-shaped metamaterial loaded rectangular microstrip patch antenna having bandwidth of 4.7THz and peak gain of 3.79dBi.

Parul Dawar et.al. in [70] – presents a fractal antenna loaded with 4 x 4 'U-T' shaped metamaterial array. The antenna resonates at 7.5GHz with gain and directivity enhancement of 18% and 24% respectively.

Parul Dawar et.al. in [71] –presents a swastika metamaterial loaded patch antenna resonating at 3.85 THz. A miniaturization degree of 44% is achieved along with the proposed antenna resonating at 2.5THz and 1.9THz. The proposed patch exhibits bandwidth enhancement by 400%.

N.S.Raghava et.al. in [72] – presents a rectangular microstrip antenna printed on a square slotted EBG surface. This antenna resonates at 2.45GHz and possesses gain and efficiency of 4.63dBi and 96.53% respectively.

N.S.Raghava et.al. in [73] – presents a patch antenna mounted on cross-slotted EBG structure. This antenna resonates at 2.586GHz. This further possesses efficiency of 99.06%.

Anand Kumar et.al. in [74] – presents a metamaterial antenna loaded with multi-layered EBG surface comprising of metallic grids. This structure resonates at 11GHz. The gain is improved from gain to 5.64dBi to 9.21dBi.

Raimi Dewan et.al. in [75] – presents an antenna array loaded with EBG surface and exhibiting dual band feature. The characteristic of reconfigurability is achieved with the help EBG and the switching in the antenna pattern is observed. The antenna is reconfigurable in the first band i.e. 2.4GHz while keeping the second band i.e. 5.8GHz intact.

Kirti Inamdar et.al. in [76] – presents a patch antenna loaded with 3 x 3 criss-cross shaped metamaterial array. This structure resonates at 6GHz and its bandwidth is improved by 86.6%. The structure possesses gain of 4.61dBi.

A.Chaudary et.al. in [77] – presents a hexagonal shaped EBG surface loaded patch antenna. An airgap of 10.5mm is introduced between the patch and the ground layer. An improvement of 74% is achieved in the efficiency when compared to conventional microstrip patch antenna. Along with the efficiency, gain and directivity also improved by 10.5dB and 2dB respectively.

N.S.Raghava et.al. in [78] – presents a multilayer E-shaped antenna possessing improved efficiency and directivity. Aa 16% improvement in the gain and efficiency is observed with the proposed antenna. Both gain and efficiency of this modified antenna is increased by 16%. An enhancement in the bandwidth by 10.5% is obtained after the introduction oef EBG structure.

N.S.Raghava et.al. in [79] – presents a patch antenna stacked with the help of shorting pins and loaded on electromagnetic bandgap surface (EBG) which plays the role of a high impedance surface. The EBG surface comprises of square slots etched on the ground plane. The gain is enhanced by introducing reflector surface at a height of 8.5mm below the ground plane. The structure resonates at 2.57GHz and possesses gain and directivity of 3.46dBi and 4.64dBi respectively.

Karteek Viswanadha et.al. [80] – presents a multiband patch antenna loaded with radiating stubs. The designed antenna possesses operational bandwidth at the resonant frequency of 6.21GHz(315MHz), 9.4GHz(671MHz), 16.78GHz(441MHz), and 25GHz(3.21GHz) from the accomplished measurements. It is an apt candidate for various advanced and existing communications like C-band (4GHz-8GHz), X-band communications (8GHz-10GHz), K_u-band communications (16GHz-17GHz), and higher band communications especially K-band (24GHz-27.3GHz).

Rothwell, E. J. et.al in [81] – presents a Nicolson–Ross–Weir method to study S-parameters of different High Impedance Surfaces. This further presents the correlation of the complex part with the real part of refractive index, when the media impedance is either resistive or reactive.

The literature survey presented above on different HIS loaded patch antennas provided motivation to conduct study on oval shaped patch antenna loaded with dumbbell shaped HIS.

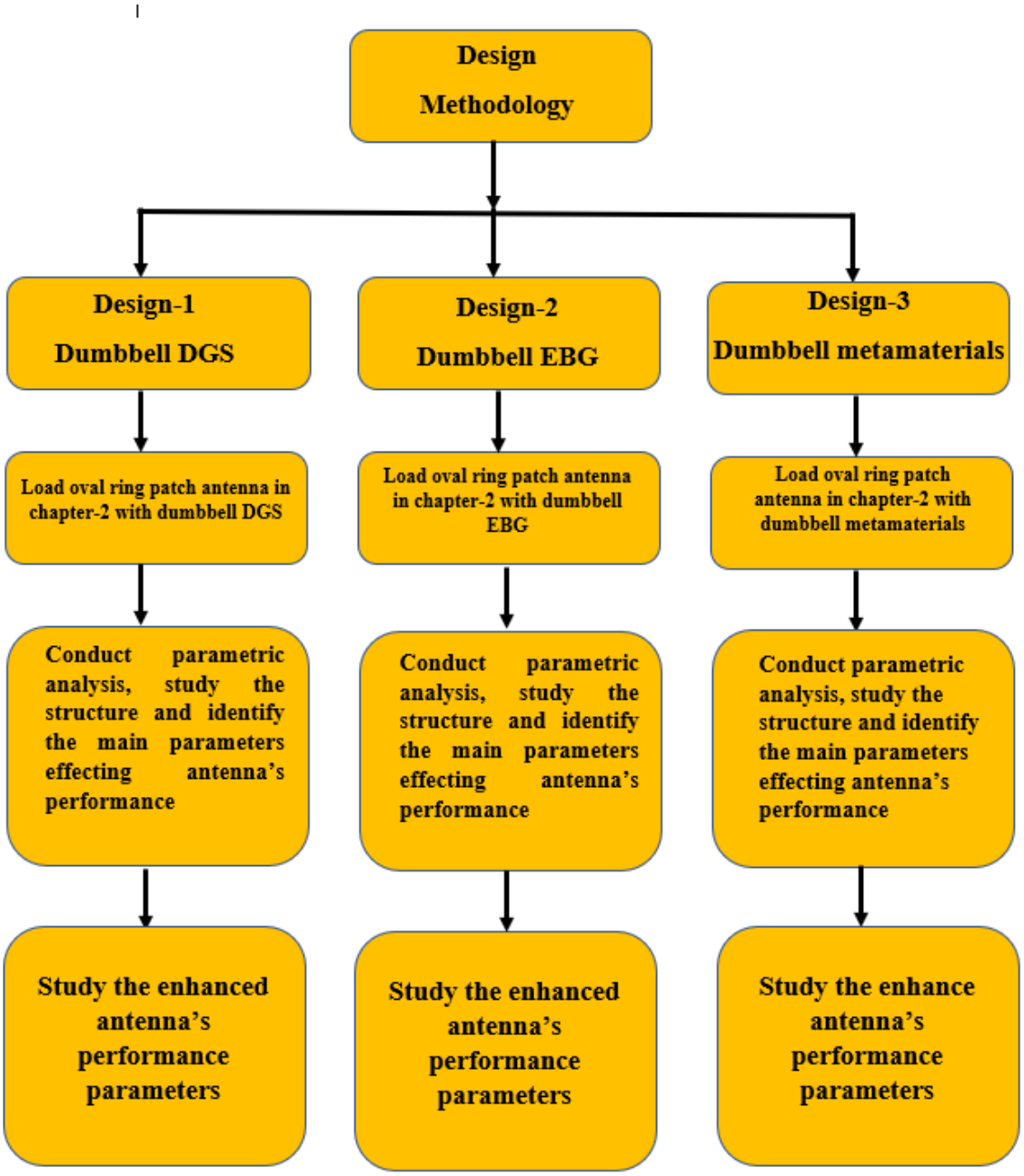

Fig.3. Design and study of antennas proposed in chapter-3

3.3. Oval shaped patch antenna loaded with stubs

The oval ring patch antenna designed in the preceding chapter is used as a reference to study its performance parameters when loaded with different High Impedance surfaces (HIS). Figure.3.1 shows the stub loaded oval shaped patch antenna.

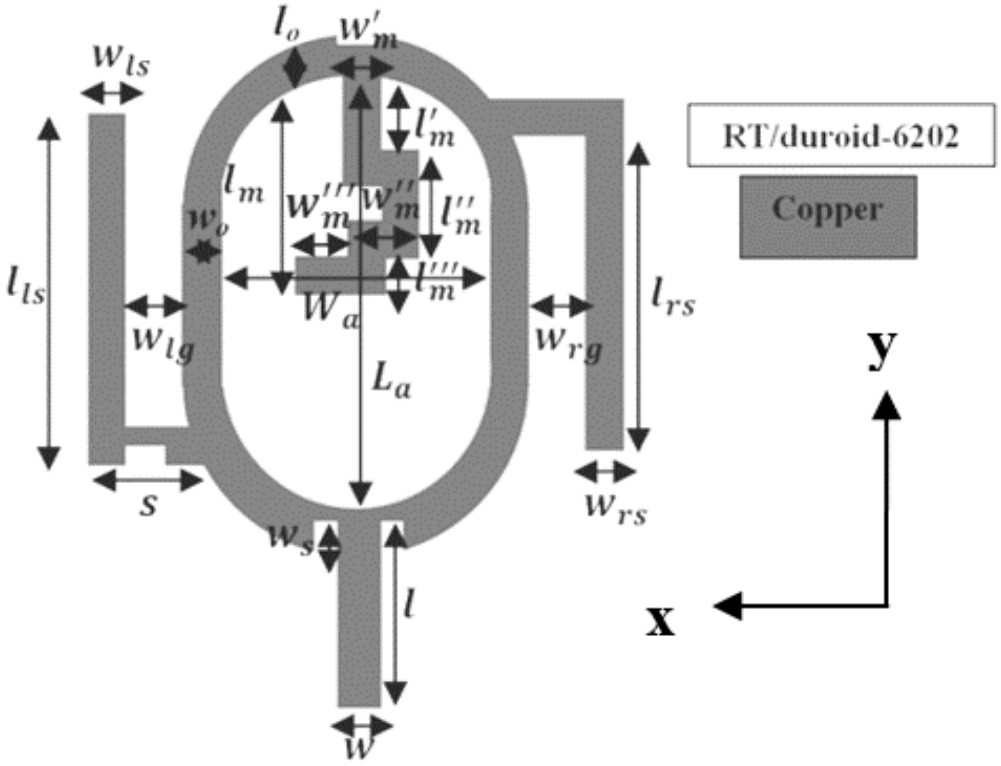

Fig.3.1. The geometry of the proposed patch antenna

3.3.1. Proposed high impedance surfaces

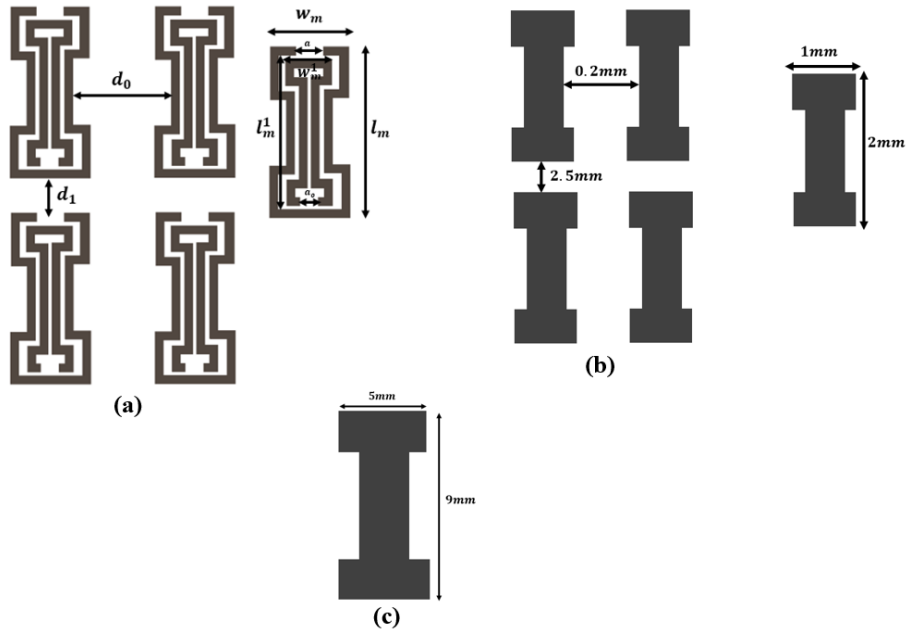

Fig.3.2. Proposed **a.** Metamaterials. **b.** EBG slots .**c**. DGS

Figure.3.2 shows the proposed structures. The antenna is loaded on a ground layer with the total volume of 10 x 6 x 0.035mm^3. The proposed oval patch antenna is loaded with 24 metamaterial cells. The reason for choosing 24 metamaterial cells is discussed in the parametric analysis section. Table.3.1 shows the design aspects of the designed unit metamaterial cell along with the vertical and horizontal spacings between two cells. The introduction of metamaterials not only miniaturizes the patch antenna but also introduces the multi-band feature.

Table.3.1 Dimensions of the proposed unit metamaterial cell

Parameter	d_o	d_1	l_m	w_m	a	a_o	l'_m	w'_m
Value(mm)	0.2	1.2	2	1	0.75	0.2	1.5	0.5

An oval patch antenna is loaded with EBG surface (full ground plane with the dimensions of 10 x 12 x 0.035mm^3) to study its performance characteristics. Final design is arrived by etching 14 EBG slots on the ground layer. The reason for etching 14 EBG cells is discussed in the parametric analysis section. To further study the change in the performance parameters, stub

loaded patch antenna is mounted on a dumbbell-shaped Defective Ground Structure (DGS) (full ground plane with the total volume of 10 x 12 x 0.035mm^3). The change in the return loss is studied by varying the total area of a DGS slot.

3.4. Study of different design aspects

This segment deals with the variation of impedance bandwidth and operational frequencies of the oval shaped antenna with the metamaterial cells, EBG slots and the dimensions of a DGS slot. Figure.3.3.(a) presents the variation in the impedance bandwidth with the number of metamaterials. A decrease in the number of metamaterials decreases bandwidths in two bands circled with brown and black dotted ovals. The decrease in the number of metamaterial cells not only deteriorates bandwidth in the desired frequency bands but also shifts operational frequencies. Additional resonant frequencies are introduced if 8 metamaterial cells are introduced (as circled with a green dotted oval). Therefore, the number of metamaterial cells are optimized to 24 to achieve better results.

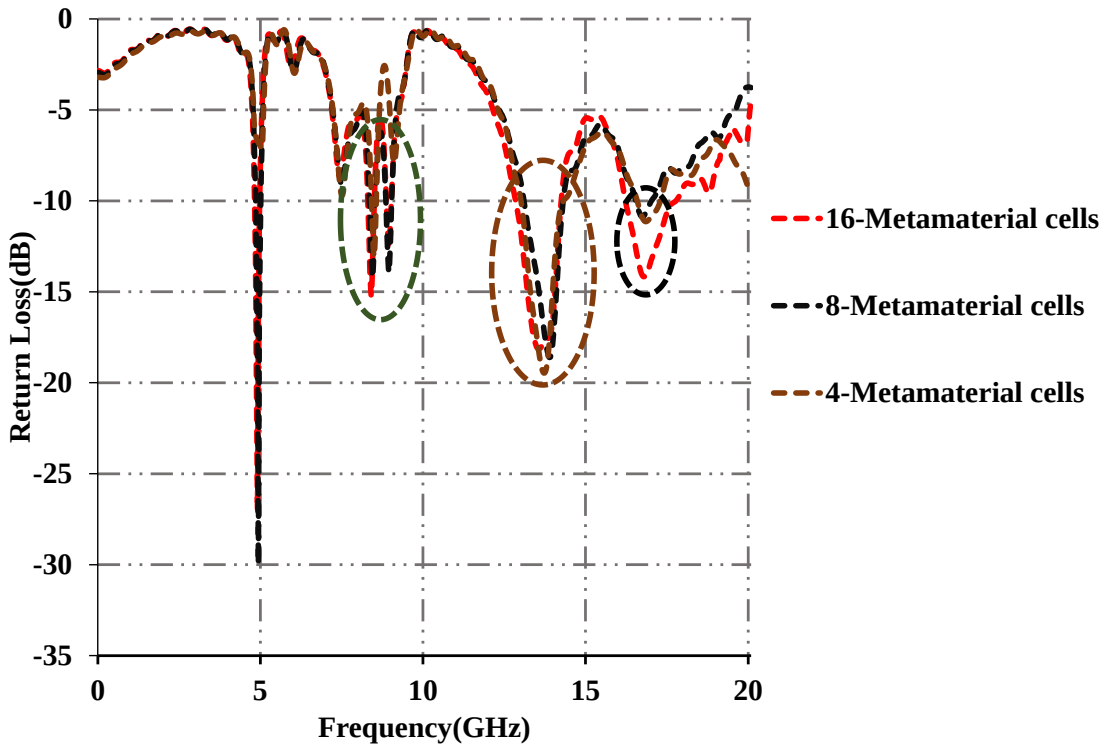

Fig.3.3.(a). Variation of return loss with the number of metamaterials

Figure.3.3.(b) presents the variation in the operational bandwidth with the EBG slots. With the decrease in the EBG cells, the operational frequency shifts towards higher frequencies. Therefore, the EBG slots are optimized to 14.

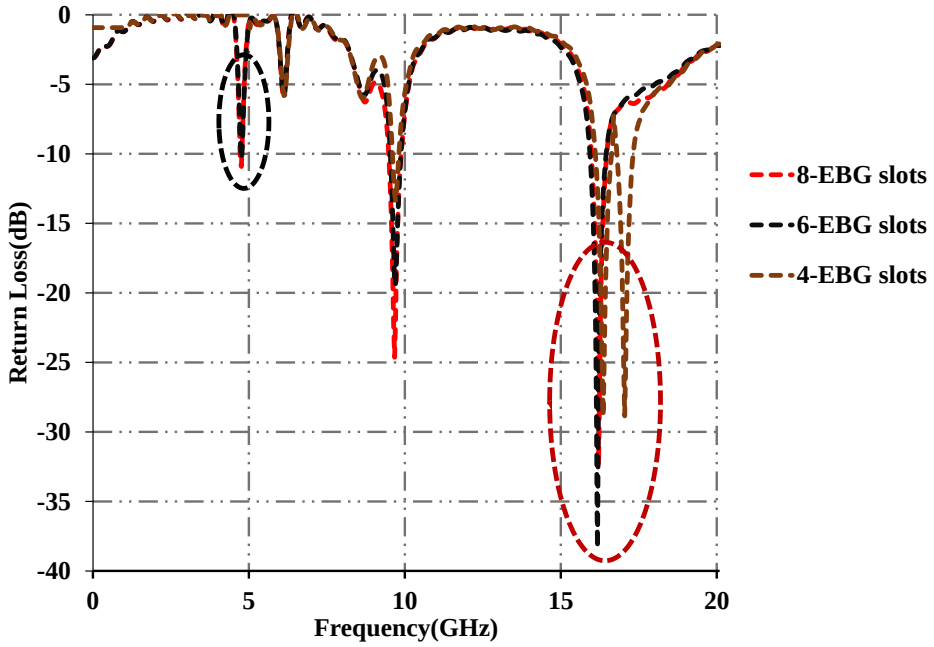

Fig.3.3.(b). Variation of return loss with the number of EBG slots

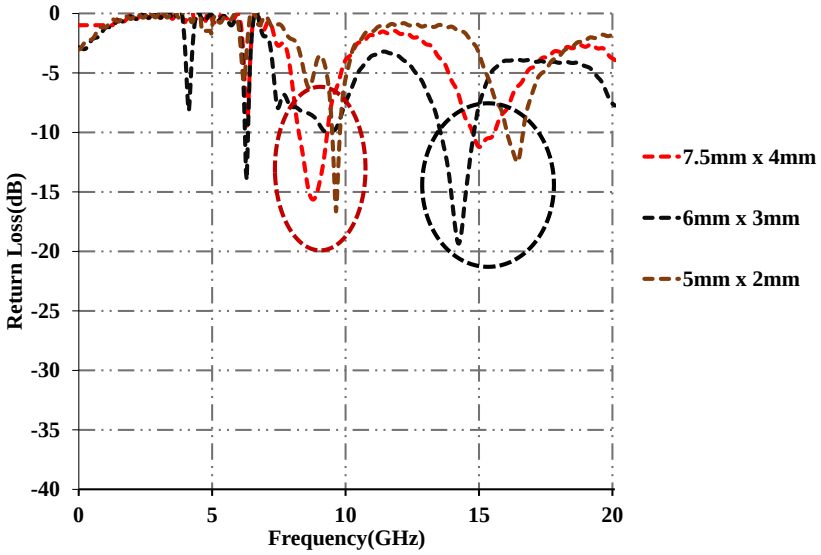

Fig.3.3.(c). Variation of return loss with the dimensions of the DGS slot.

Fig.3.3.(c). presents the variation in the impedance bandwidth with the dimensions of the DGS slot. Reducing the dimensions of the DGS slot not only decreases degree of miniaturization but also diminishes the multiband feature of the oval patch antenna. Hence, the dimensions of the DGS slot are optimized to 9mm x 5mm

3.5. Performance analysis of the proposed antenna structures

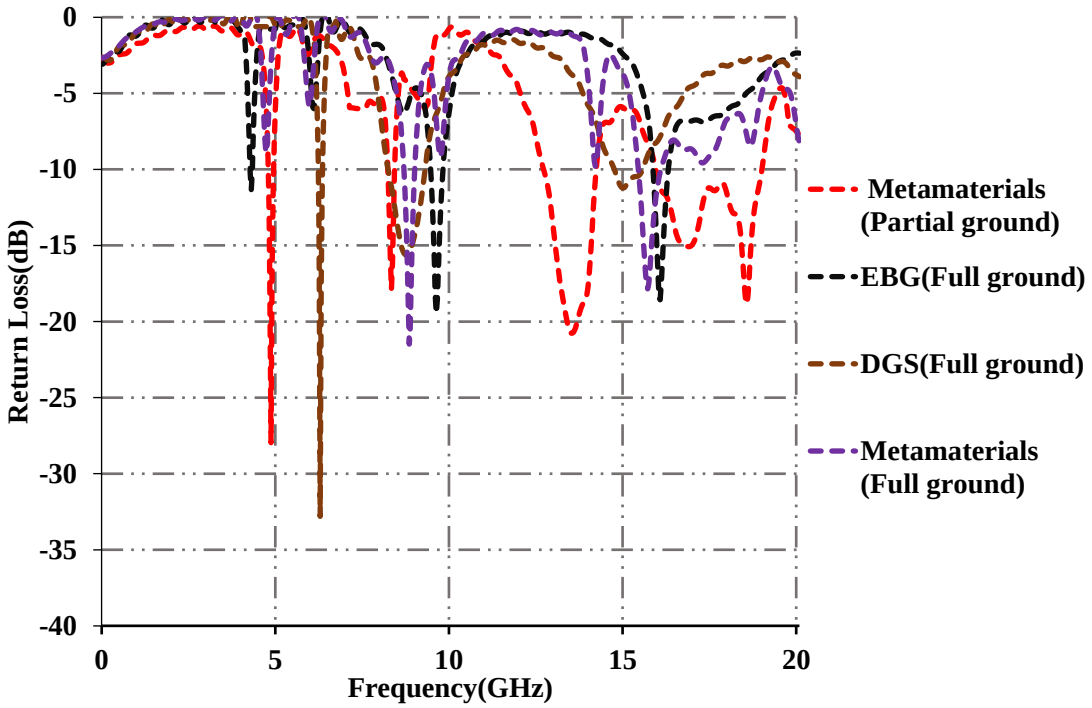

Fig.3.4. Return losses of the oval patch antenna with the proposed high impedance surfaces.

Figure.3.4 presents the operational bandwidths of the designed prototype loaded with metamaterials, EBG and DGS surfaces. When the oval patch is loaded with metamaterials, the structure resonates at 4.92GHz, 7.7GHz, 13.88GHz, 16.78GHz and 18.18GHz. The patch antenna not only retained its multiband characteristics but also enhanced its bandwidth in the frequency ranges of 12.72GHz – 14.23GHz (1.51GHz) and 16.52GHz – 18.71GHz (2.19GHz). When antenna is loaded with the EBG ground plane, it resonates at 4.74GHz, 9.62GHz, and 16.59GHz. Miniaturization of the patch antenna is improved. A basic stub loaded oval patch antenna with the dimensions of 7.5 x 9mm^2 has a lower resonant frequency of 6.12GHz and the same antenna when loaded with the designed EBG surface possesses the lower resonant frequency of 4.74GHz. Miniaturization of 74% is achieved with the basic patch antenna. Miniaturization is further improved to 84% after loading EBG surface. DGS loaded structure operates at 6.83GHz, 8.85GHz, and 15.01GHz. Bandwidth is highly reduced in the corresponding frequency bands. Conventional patch antenna resonates at 9.1GHz and 16.23GHz. The full ground plane shifts the resonant frequencies to a higher frequency range and reduces the gain. Therefore, the results are not presented in this chapter. Figure.3.5 presents the surface currents of metamaterial loaded, DGS and EBG mounted patch antenna. For

metamaterial antenna, the current is confined to the antenna, partial ground, and a part of the current is diverted towards metamaterials. As the frequency increases, the current is fully concentrated in metamaterials. When the EBG ground is loaded, the current is confined to the antenna and the EBG layer at a lower frequency. As the frequency increases, the current is confined to the stubs and center of the EBG ground layer. For the DGS mounted antenna, the current is concentrated on the stubs. With the increase in the frequency, the current is maximum on EBG and on the oval ring.

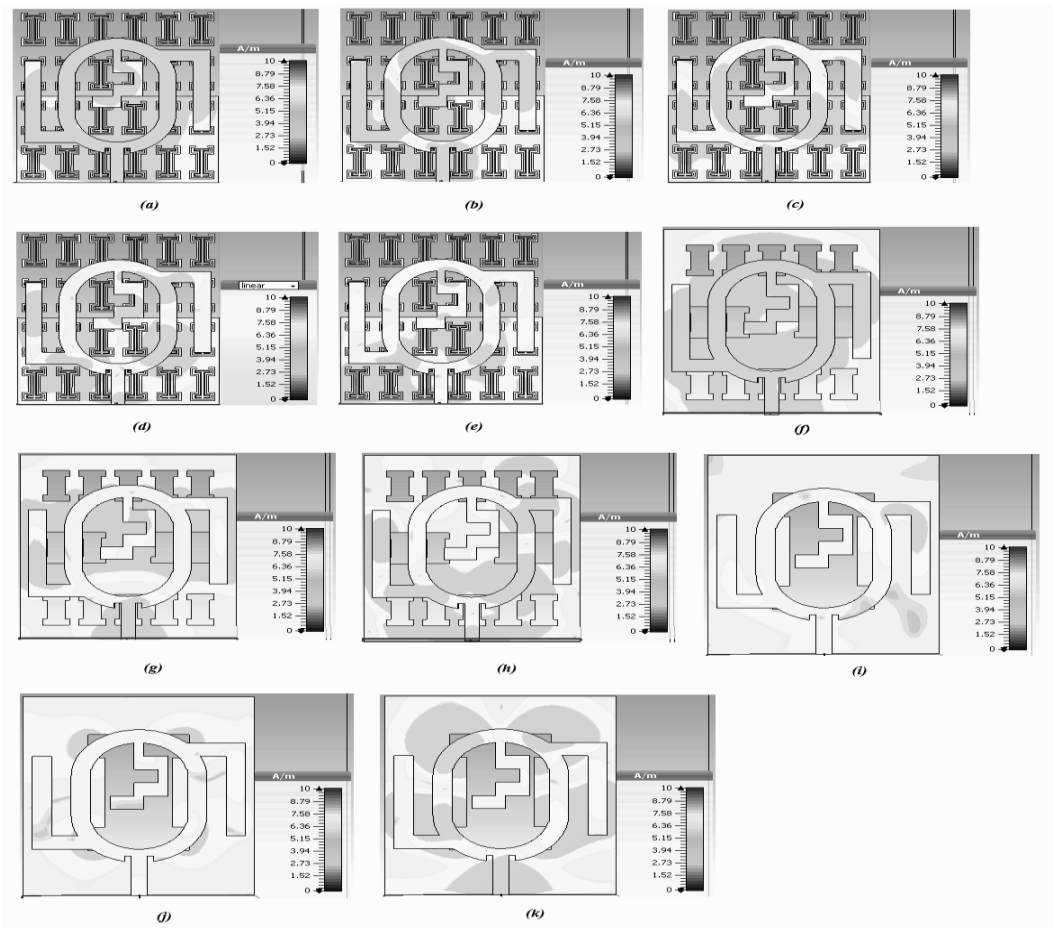

Fig.3.5. Surface currents with metamaterials at **a.** 4.92GHz**. b.** 7.7GHz. **c.** 13.88GHz. **d.** 16.78GHz. **e.** 18.18GHz. Surface currents with EBG ground plane at **f.** 4.74GHz. **g.** 9.62GHz. **h.** 16.59GHz. Surface currents with DGS ground plane at **i.** 6.83GHz**. j.** 8.85GHz**. k.** 15.01GHz.

Figure.3.6 presents the real and complex parts of permittivity and permeability which act as propagating parameters to calculate phase velocity. The propagating paranmeters are calculated with the help of Nicolson-Ross-Weir technque. The above technique is implemented in such a way that S-parameters are extracted from CST software and further,the calculations are carried out in MATLAB [81]. Permittivity is negative at 4.91GHz, 7.61GHz, 13.1GHz, 16.43GHz,

and 19.1GHz. Similarly, permeability is negative at 4.81GHz, 7.71GHz, 13.1GHz, and 16.38GHz. The proposed dumbbell metamaterial converts from Double Negative (DNG) to Epsilon Negative (ENG) at higher frequencies.

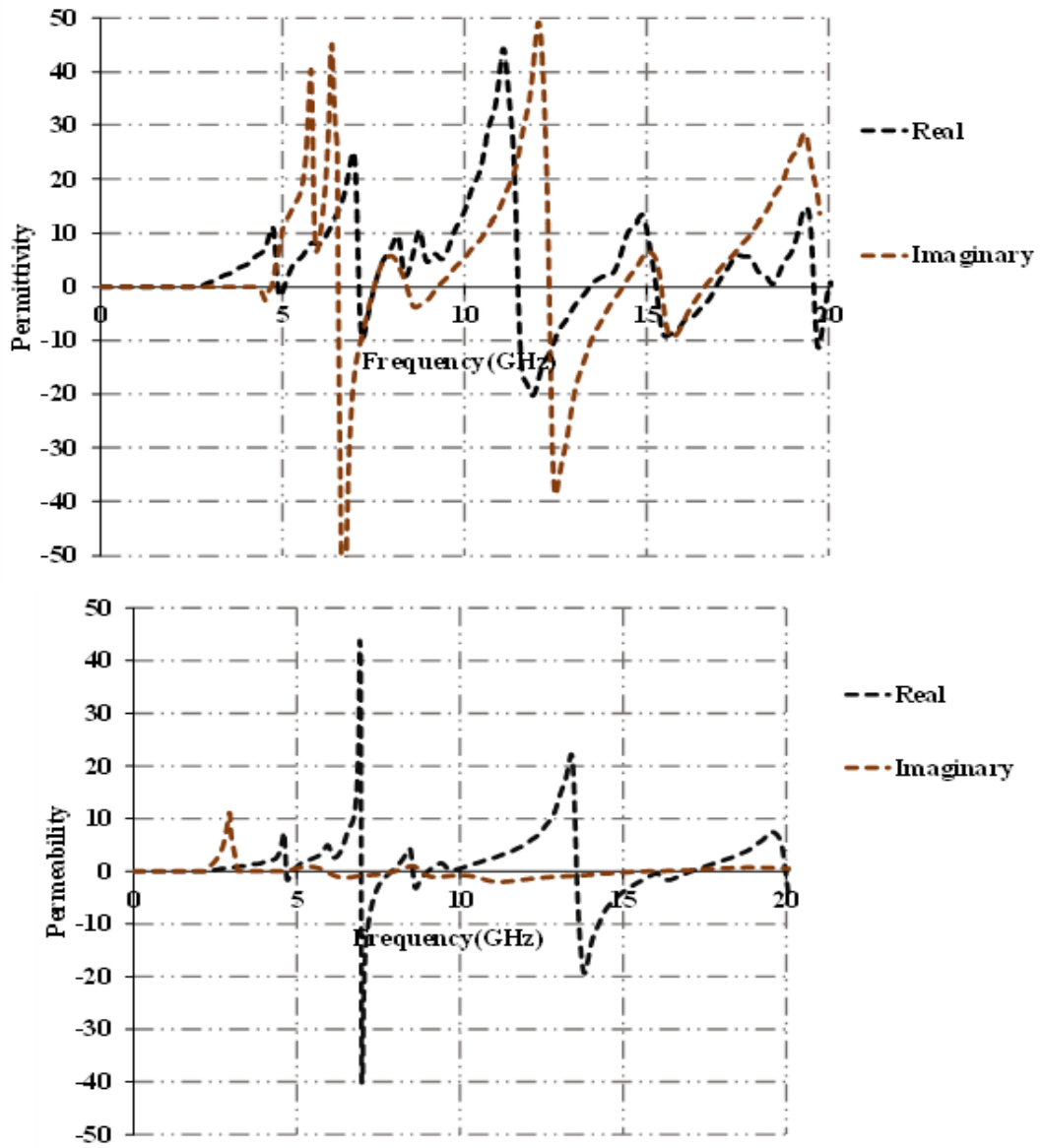

Fig.3.6. Real and imaginary parts of permittivity and permeability

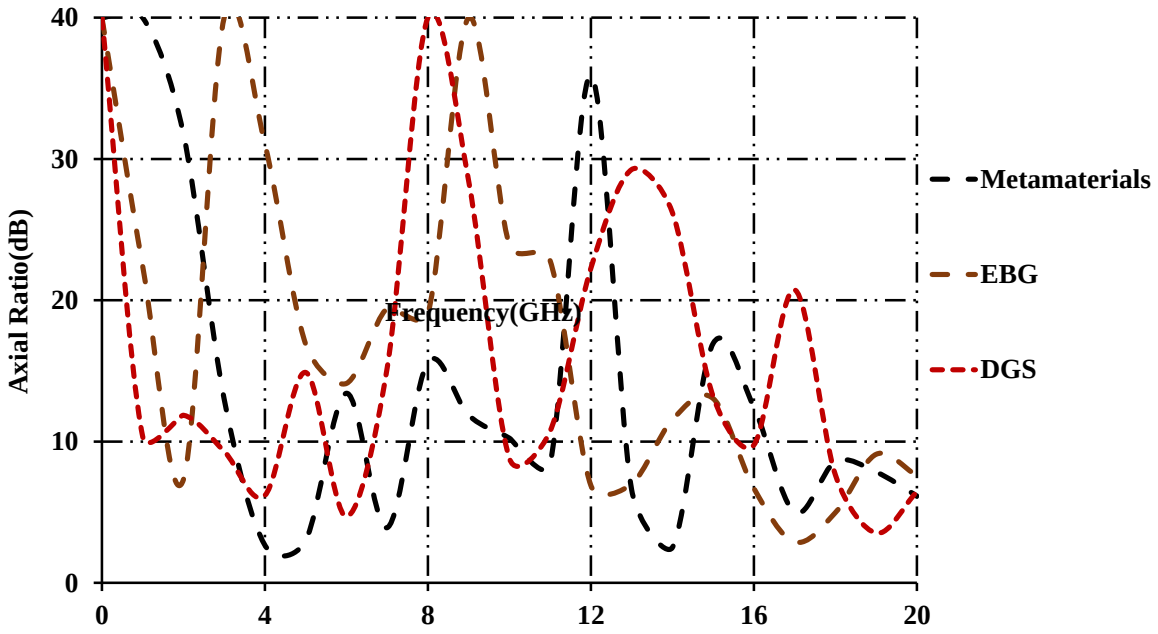

Fig.3.7. Axial ratios of oval patch antenna loaded/mounted with/on different structures

Figure.3.7 presents the axial ratio plots of different structures. Metamaterial inspired oval patch antenna is right-handed circularly polarized (Axial Ratio < 2dB) at 4.36GHz and 13.88GHz. It is elliptically polarized at 7.87GHz and 17.21GHz and linearly polarized at remaining frequencies. EBG ground plane is loaded to the antenna, it possesses circular polarization at 16.43GHz. When DGS slot is introduced on the ground layer, antenna exhibits elliptical polarization.

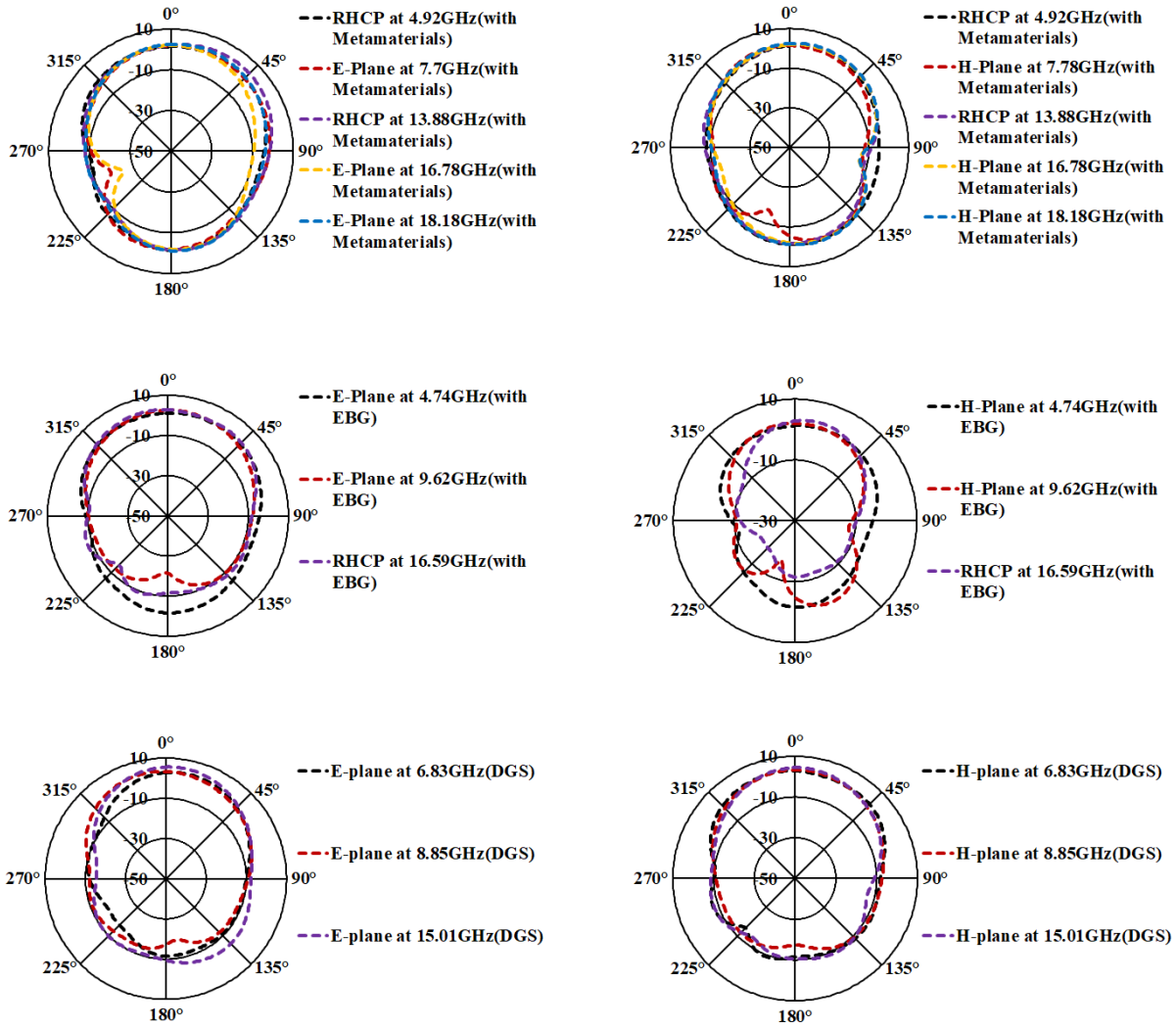

Fig.3.8. Radiation patterns of proposed antenna structures

Figure.3.8 presents the antenna patterns of Metamaterial-, EBG- and DGS-oval shaped patch antennas at their corresponding resonant frequencies. Metamaterial antenna resonates at 4.92GHz, 7.7GHz, 13.88GHz, 16.78GHz and 18.18GHz with the gains of 1.4dBic, 1.42dBi, 2.65dBic, 2.31dBi and 2.89dBi respectively. EBG-antenna resonates at 4.74GHz, 9.62GHz, and 16.59GHz with gains of 1.45dBi, 2.6dBi, and 2.85dBic respectively. DGS-antenna resonates at 6.83GHz, 8.85GHz, and 15.01GHz with the gains of 3.21dBi, 3.3.1dBi, and 4.38dBi respectively. Radiation patterns are unidirectional in all the planes.

Table.3.2 presents a weighing up of performance parameters of the designed antenna with the preceding. A suitable structure is chosen depending on the specifications of an application. Metamaterial antenna is chosen if high bandwidth and the multi-band is required for an

application. EBG-antenna is chosen if any further miniaturization of the oval patch antenna is required. DGS-antenna is chosen if a high gain is required for an application.

Table.3.2 Detailed contrast between the performance specifications of the designed antenna and preceding antenna

Type of antenna	Miniaturization (%)	Resonant frequencies (GHz)	Peak Gain (dBi/dBic)	Bandwidth (GHz)
[2]	25	4	4.99	2
[3]	25	3.85	3	Not mentioned
[5]	81	4.3	7.2	1
[6]	75	7	9.1	0.761
[7]	35	7.5	0.67	Not mentioned
[8]	72	8.5, 17.7, 20, 23.7 & 30	9.6	3
[18]	74	6.12, 9.4, 16.75 & 25	1.1, 1.34, 5.72 7 8.1	0.315, 0.671, 0.441 & 3.21
Metamaterial loaded	**81.2**	**4.92, 7.7,13.88,16.78 & 18.18**	**1.42, 1.48, 2.8, 2.45 & 3**	**0.2, 0.31, 1.51 & 2.19**
EBG-mounted	**84**	**4.74, 9.62 & 16.59**	**1.5, 2.7 & 2.9**	**0.12, 0.29 & 0.36**
DGS-mounted	**71.6**	**6.83, 8.85 & 15.01**	**3.3, 3.45 & 4.5**	**0.19, 1.2 & 0.43**

3.6. Conclusion

Performance characteristics of various patch antennas are studied. Dumbbell shapes structures (Metamaterials, EBG, and DGS) are promising enough to achieve miniaturization, high bandwidth, and gain. These structures are used along with the oval ring patch antenna loaded with radiating stubs to further enhance the performance parameters. Metamaterial antenna possesses high bandwidths in the frequency ranges 12.72GHz – 14.23GHz (1.51GHz) and 16.52GHz – 18.71GHz (2.19GHz). EBG mounted patch antenna is used to achieve further miniaturization and DGS mounted patch antenna is used to achieve high gain at all its resonant frequencies. These structures are used in various applications of satellite applications ranging from C-band to K-band. Further, the study of HIS in the present chapter is used as basis to design the antennas described in the fourth chapter.

CHAPTER 4

Design and analysis of different ultra-wide bandwidth Electromagnetic Bandgap structures mounted antennas

4.1. Introduction

In the last chapter, study on various dumbbell HIS was conducted to observe the variation in the different performance aspects of the oval ring antenna loaded with stubs. The study drew a brief comparison between various dumbbell HIS. Apart from the comparison, the study briefly presented the impact of these structures on different performance aspects of the oval ring antenna loaded with stubs. This study furthers provides flexibility to the designer to choose the appropriate structure to meet the application's specifications.

Conventional planar monopole antennas have low gain and efficiency and might not be suitable due to these limitations. To overcome these limitations, electromagnetic bandgap (EBG) structures act as an alternative to enhance throughput of antennas. Electromagnetic Bandgap structures are one of the high impedance surfaces which improve bandwidth of antennas.

Use of large number of EBG slots on the ground layer limits the bandwidth. This low bandwidth problem was approached in a systematic manner. Hence, to achieve high bandwidth without degradation in gain the antennas in [82-86] are designed to remove all these shortcomings. Literature survey reveals, there are several research attempts to enhance bandwidth using EBG structures in different types of antennas [87-96].

This chapter discusses about the enhancement of bandwidth of antennas using different EBG structures. This chapter discusses two different types of antennas.

- Design of a EBG loaded ultra-wideband dual feed dumb-bell patch antenna.
- Design of a EBG loaded double split ring slotted antenna.

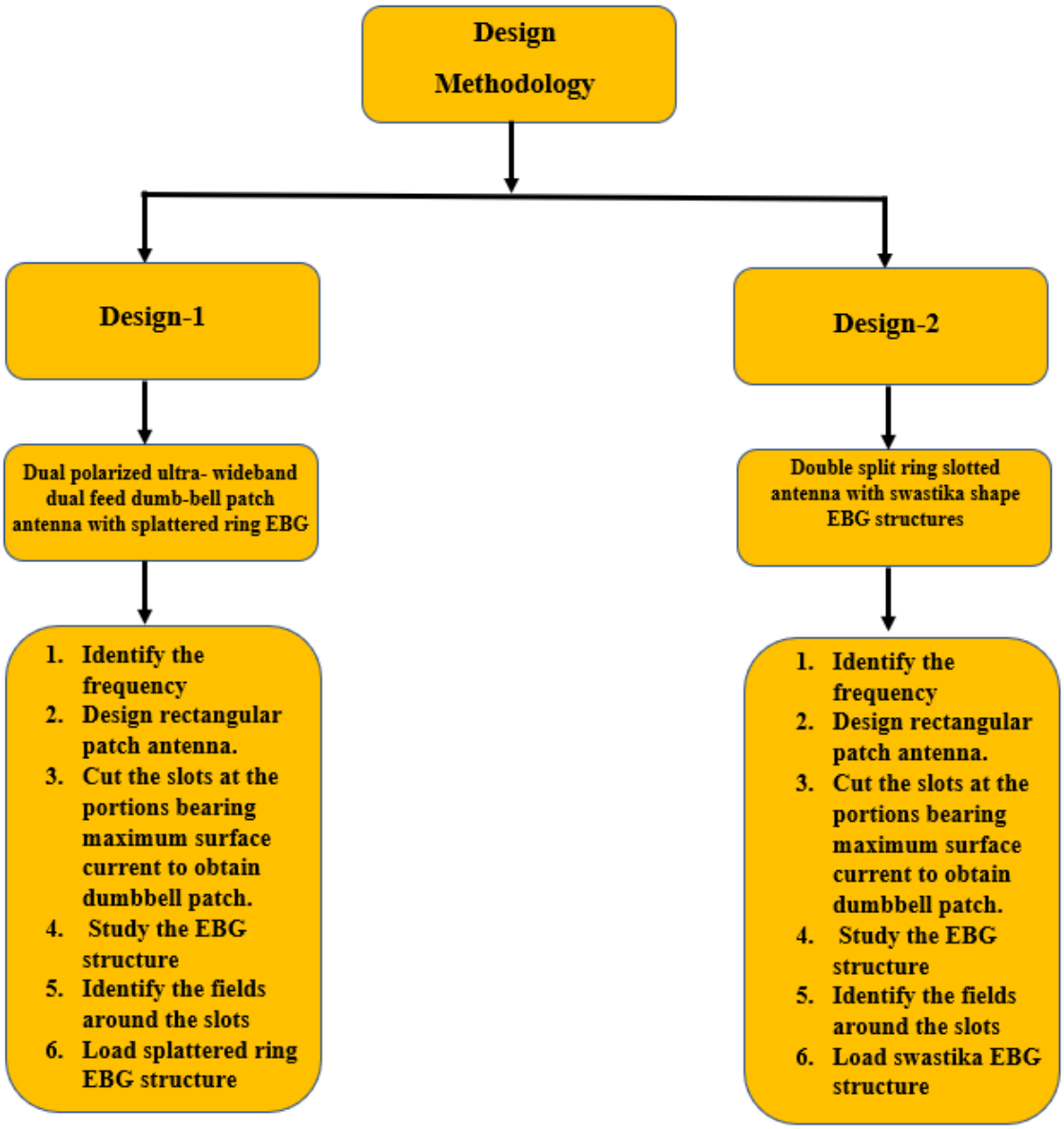

Fig.4. Design methodology of the proposed antennas in chapter-4.

4.2. Design of a EBG loaded ultra-wideband dual feed dumb-bell patch antenna

The evolution stages of the developed prototype are presented in figure.4.1. The evolution stages present the proposal procedure of the designed antenna.

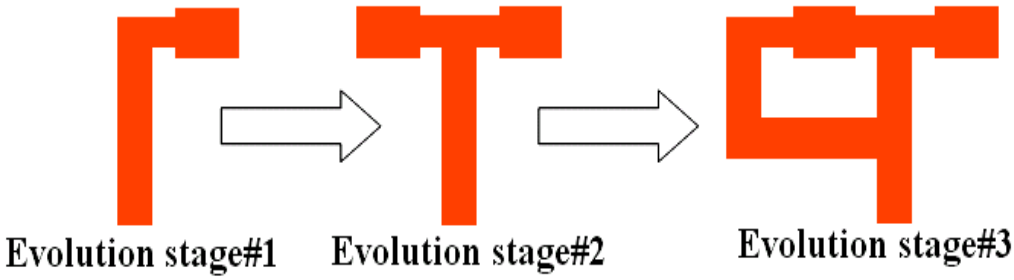

Fig.4.1. Development stages of the designed antenna

The operational bandwidth of the developed antenna is improved over the antennas presented in development stage-1 and development stage-2. The improvement is discussed through the impedance bandwidth curves presented in figure.4.2. Further addition of feed to the dumbbell patch yields undesired results. Hence, the triple feed design and its results are not presented in this chapter.

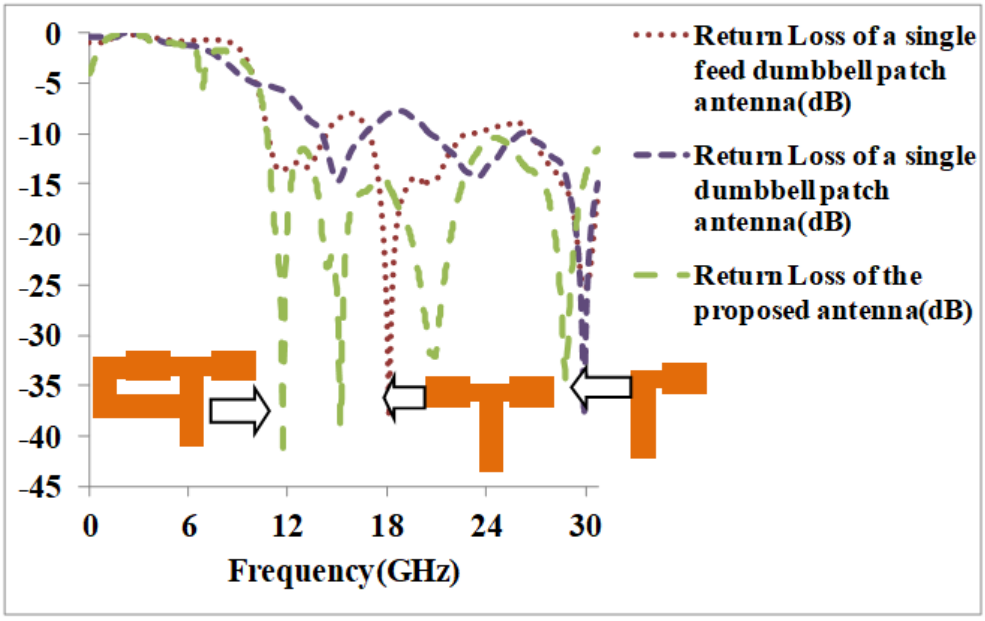

Fig. 4.2. Return loss curves of the evolution stages of the proposed patch

The development of the proposed antenna is studied through impedance bandwidth plots as presented in figure.4.2. The single dumbbell antenna as presented in the 1st development stage operates at 13.27GHz, 23.89GHz and 30GHz as presented in curve represented in purple. The

impedance bandwidths of 102.2MHz, 212.62MHz and 1.89GHz are noticed in the operational frequency bands. The antenna in the 2nd development stage resonates at 12.01GHz, 18GHz and 30GHz with the operational bandwidths of 2.62GHz, 4.72GHz and 2.14GHz in the operational frequency ranges as represented in dotted red graph. The designed antenna operates at 11.78GHz, 15.3GHz, 21GHz and 29GHz. It possesses an impedance bandwidth of 20.2GHz in the frequencies ranging from 10.8GHz to 31GHz. The whole structure is printed on a foam substrate (ε_r=1.01) with the total volume of 25mm x 30mm x 0.762mm^3. The antenna printed on the foam substrate is further loaded on the RT-Rogers-6202(lossy) substrate (ε_r=2.94) having height of 0.762mm. The area of the patch is 12 x 16mm^2 with the overall volume of ground plane being 25 x 30 x 0.035mm^3. The antenna is mounted on foam substrate (ε_r = 1.01) and RT-6202 (ε_r = 2.94). The multilayer substrates are used in this design to achieve the desired ultra-wide bandwidth along with the enhanced gain without distorting the radiation patterns. The detailed design of the proposed patch antenna is presented in figure.4.3. The two dumbbells on designed to radiate at two different frequencies. The right patch is devised to be functional at 15.2GHz and left patch is devised to be functional at 11.5GHz. The equivalent dielectric constant ($\varepsilon_{eq} = \left(2\frac{\varepsilon_{foam}*\varepsilon_{RT-6202}}{\varepsilon_{foam}+\varepsilon_{RT-6202}}\right)$) is 1.49. Subsequently, the effective permittivity is obtained as 1.1. The antenna is fed with quarter wavelength microstrip lines with dual feed to achieve circular polarization in the proposed antenna structure [97]. Hair pin line structure is used as a basis to implement the proposed splattered ring EBG structure. 132 EBG slots are etched on the ground plane with the portion beneath the patch remaining unetched. The dimensions of the ring and the spacing between the EBG cells is proportional to the performance specifications of the proposed antenna structure. Overall dimensions of the EBG cell are a fraction of operational wavelength. Horizontal and vertical spacings between the rings are $\frac{\lambda}{30}$ and $\frac{\lambda}{20}$ respectively. The number of EBG cells used on the ground plane has to be limited to suppress the surface waves and avoid the degradation of impedance bandwidth. Reduction in the EBG cells degrades efficiency and gain. This yields undesired results and therefore, these results are not presented in this chapter.

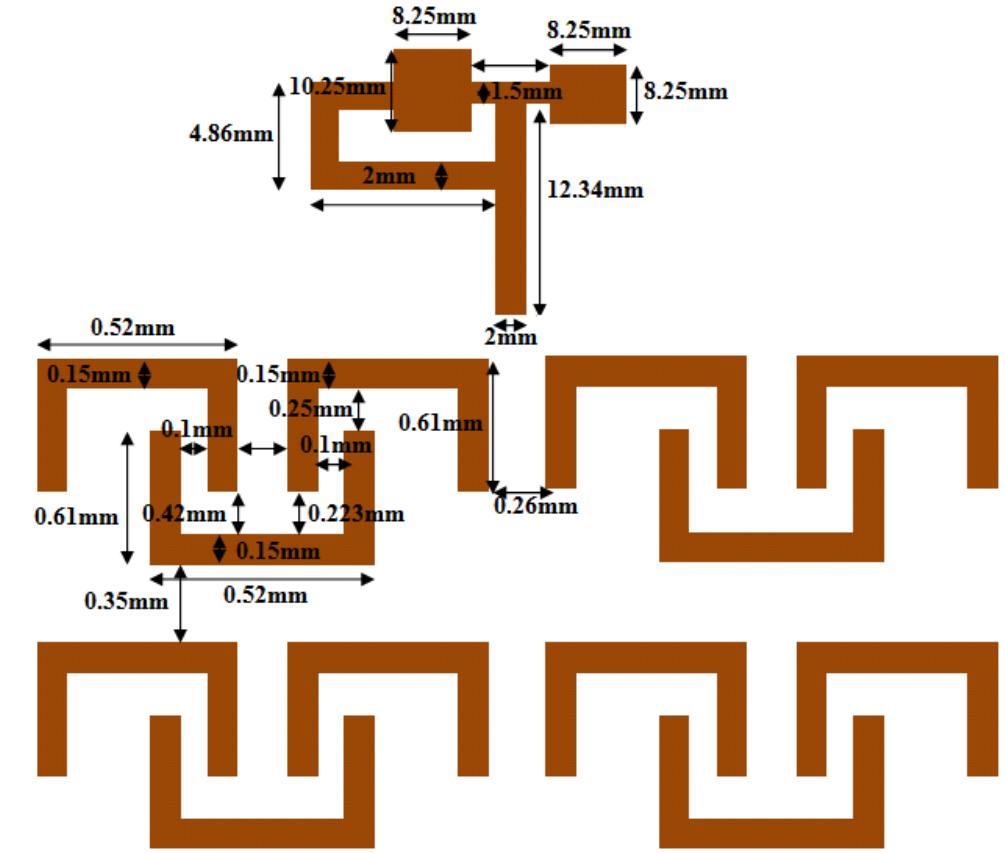

Fig.4.3. Structure of the proposed antenna

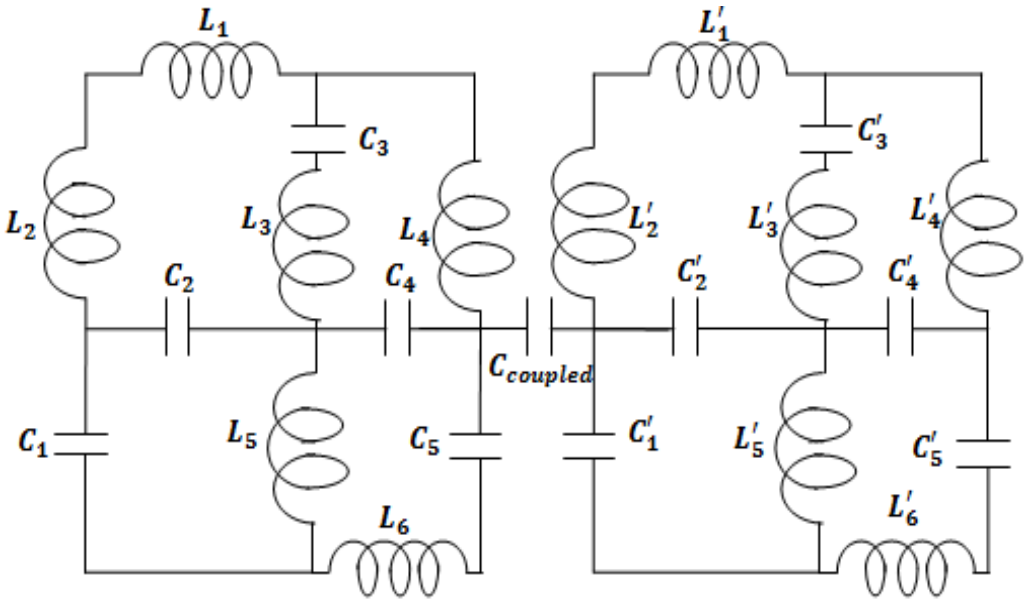

Fig.4.4. Electrical model of the proposed EBG structure.

The electrical model of the implemented EBG cell is presented in figure.4.4. Gap capacitance of the upper ring is modelled as $C_{coupled}$. The lumped elements L_1-L_6, L'_1-L'_6, C_1-C_5 and C'_1-C'_5 are efficacious in the operation frequency band. The purpose of L_3-C_3, L_6-C_5, L'_3-C'_3 and L'_6-C'_5

is to reduce radiation leakages and improve the antenna's bandwidth. Periodic placement of the equivalent circuits reduces surface waves and improves bandwidth.

4.2.1 Outcomes and disquisitions

The impedance bandwidths of the proposed patch antenna before and after loading of EBG structure is presented in figure.4.5.

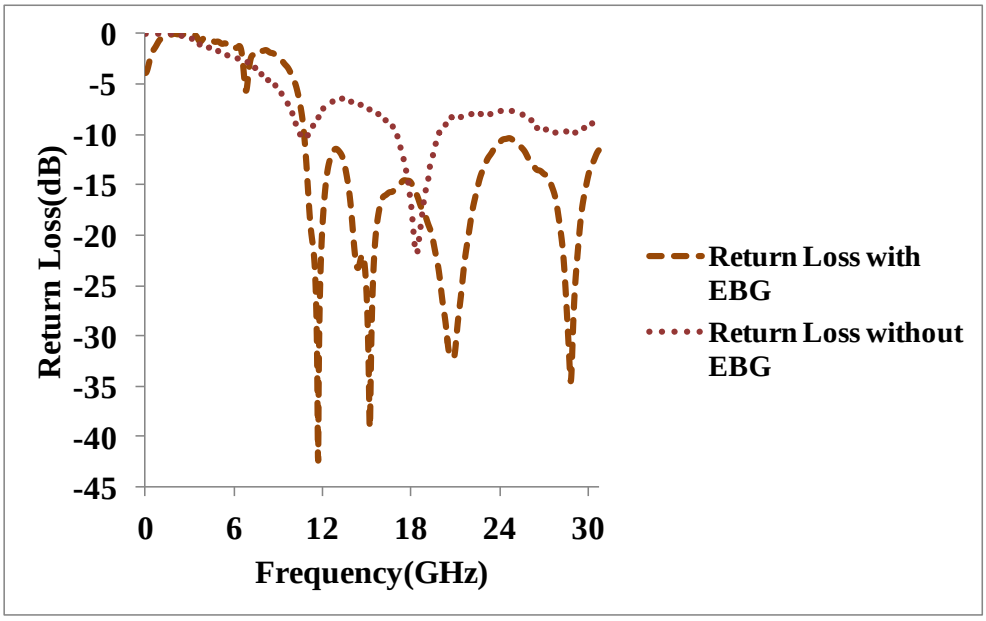

Fig.4.5. Plot of reflection co-efficient with and without EBG

Basic antenna radiates at 11.78GHz and 18.1GHz. It is characterised by the bandwidths of 112MHz and 1.92GHz in the frequencies ranging from 11.724GHz~11.836GHz and 16.6GHz~18.52GHz respectively. The designed antenna operates at 11.78GHz, 15.3GHz, 21GHz and 29GHz. The antenna is further characterised by a wide-bandwidth of 20.2GHz in the operational frequency ranges. By loading the antenna with the proposed EBG, the bandwidth is enhanced.

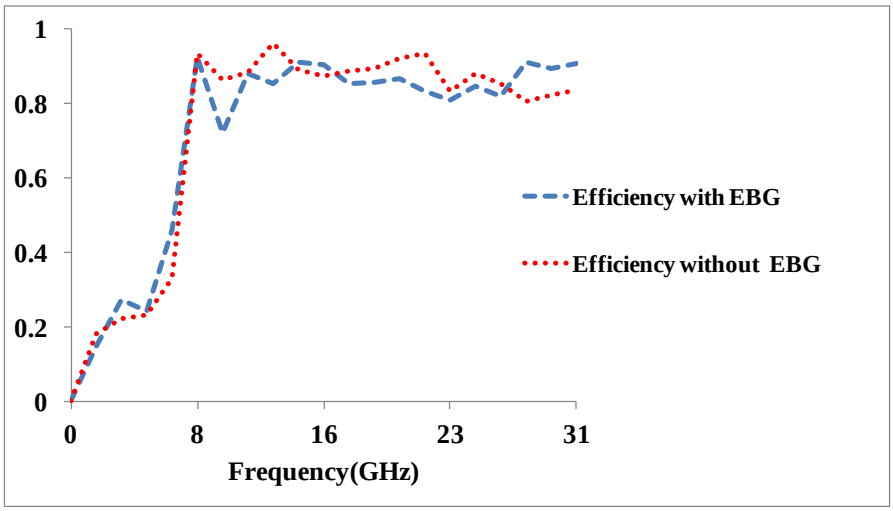

Fig.4.6. Impact of EBG structure on the efficiency.

The efficiencies of the EBG mounted antenna and the basic antenna are presented in figure.4.6. Without EBG, the efficiencies are nearly constant with the peak efficiency of 93% and having the deviation of ±2.2% in the bands of 11.724GHz to 11.836GHz and 16.6GHz to 18.52GHz. When the dumbbell patch is loaded on the EBG ground plane, the efficiencies fluctuate with the deviation of ±6.6% and having peak efficiency of 92.1% in the operation frequency range. The efficiency deteriorates with the enhancement in the impedance bandwidth.

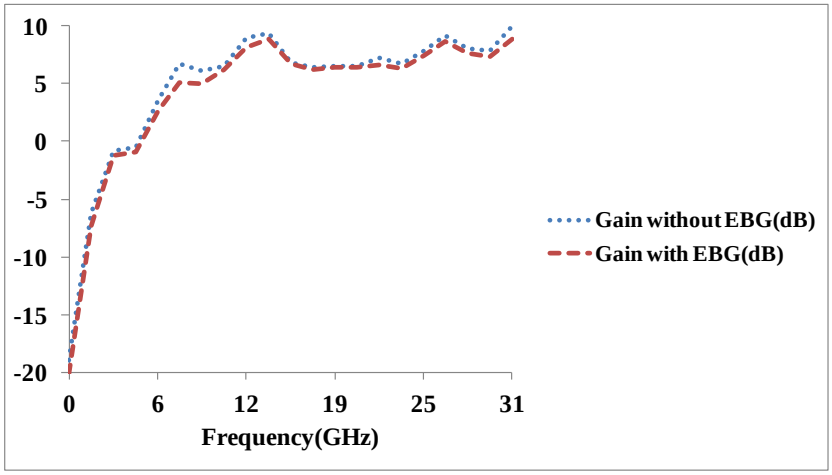

Fig.4.7. Impact of EBG structure on the gain.

The gains of EBG loaded dumbbell patch antenna and basic dumbbell patch antenna are presented in figure.4.7. Basic dumbbell patch antenna possesses the gain ranging from 7.75dB to 9.19dB and 6.59dB to 7.22dB at the frequencies of operation as that of the developed antenna. The gain of the designed antenna ranges from 6.18dB to 9dB in the operational frequency range. The decrease in the efficiency degrades the gain. Figure.4.8 presents the variation in the axial ratio before and after loading the EBG structure. Basic dumbbell patch

antenna is linearly polarized. The antenna possesses elliptical and linear polarizations in the frequencies of operation. The introduction of EBG structure makes the dumbbell antenna circularly polarized with the axial ratios of 2.1dB at 11.78GHz. The antenna possesses circular, elliptical and linear polarizations at the designed frequencies.

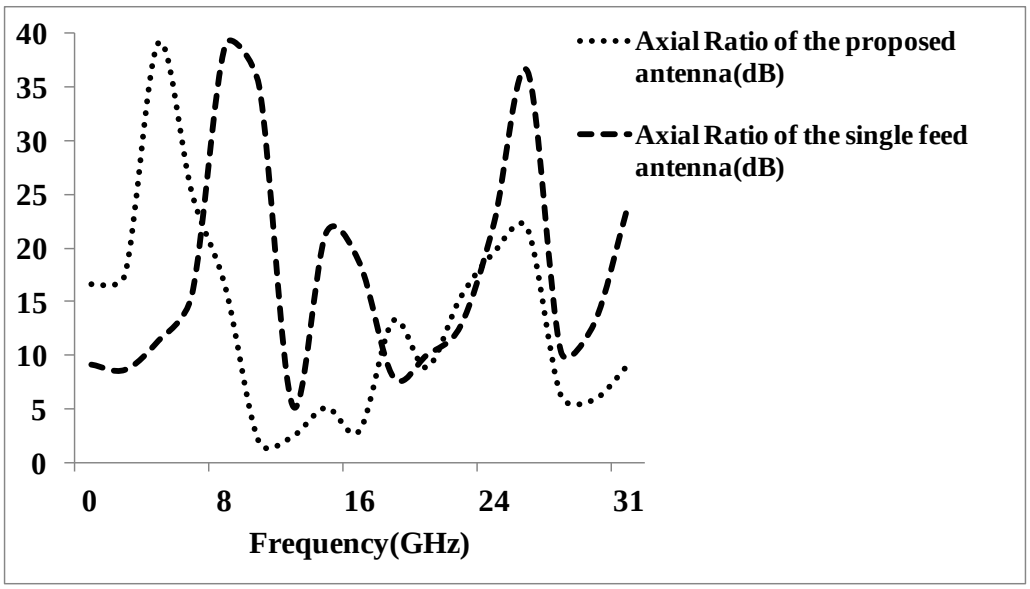

Fig.4.8. Impact of EBG structure on the axial ratio.

The antenna patterns in the radiating planes are simulated and presented. The antenna patterns in all the radiating planes at 11.78GHz are presented in figure.4.9.(a). The patterns are unidirectional in all the planes. The antenna patterns at 15.3GHz are illustrated using figure.4.9.(b). The antenna patterns are unidirectional in all the radiating planes. The antenna patterns in all the planes at 21GHz is illustrated using figure.4.9.(c). The antenna radiates unidirectionally in all the radiating planes. The antenna patterns at 29GHz are presented in figure.4.9.(d). These are unidirectional in all the radiating planes. The developed antenna exhibits stable antenna patterns of radiation at frequencies of operation.

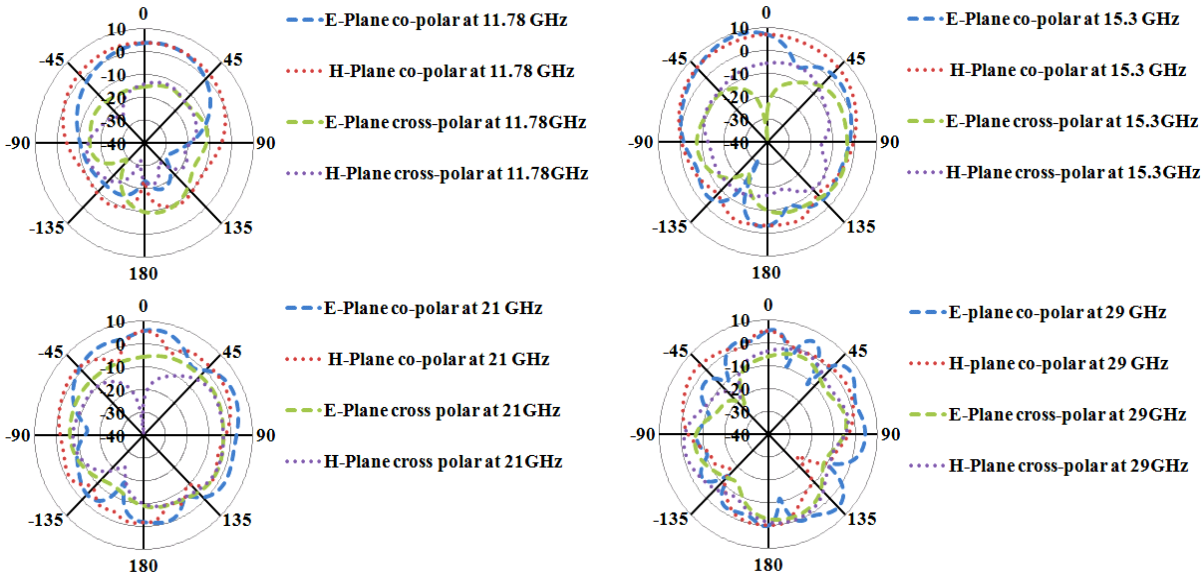

Fig.4.9. Radiation patterns of the designed antenna at (a).11.78GHz. (b).15.3GHz. (c).21GHz. (d).29GHz

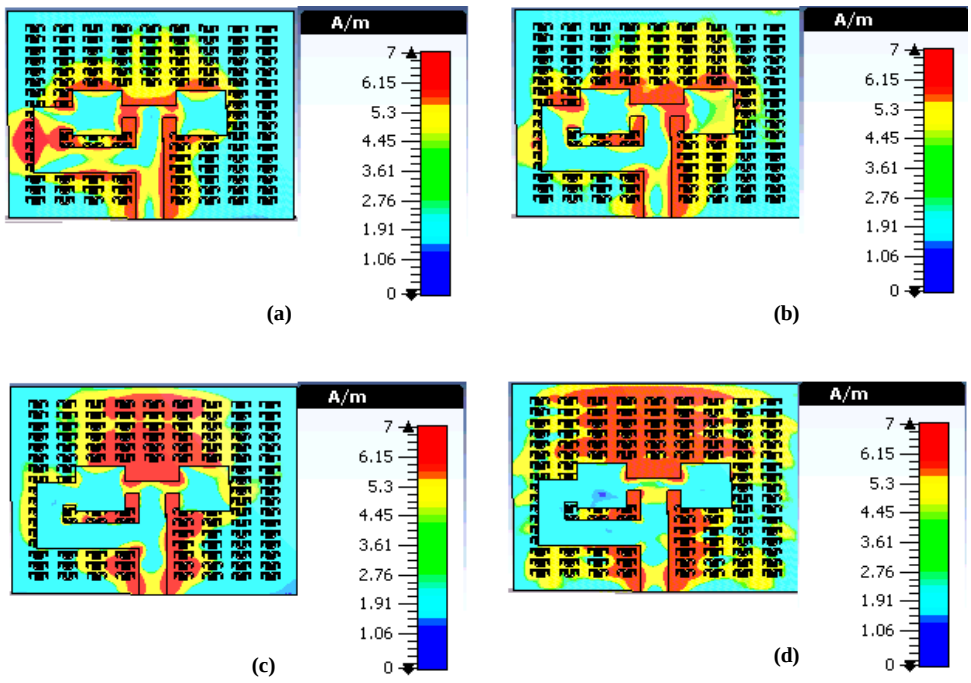

Fig.4.10. Distribution of surface current densities at (a).11.78GHz. (b).15.3GHz. (c).21GHz. (d).29GHz

The surface current distributions at all the operational frequencies are presented in figure.4.10(a), 4.10.(b), 4.10.(c), and 4.10.(d). At 11.78GHz, the current is directed towards the dumbbells and some part of current is confined to feed lines and ground layer. At 15.3GHz, current is mostly confined to the EBG ground plane. At 21GHz and 29GHz, current is directed towards ground plane due to propagation of higher order modes. Hence, EBG ground plane plays a pivotal role in the band of 20GHz~31GHz.

The detailed contrast between the developed prototype and the preceding ultra-wideband antennas is presented in table.4.1. From the comparison, we can infer that the developed antenna is superior in all the performance aspects.

Table.4.1. Weighing up the present work with the existing ultra-wideband antennas

Ref	Area (mm^2)	Peak Gain (dB)	Bandwidth (GHz)	Peak Efficiency (%)
[98]	300	4.5	21.52	68
[99]	300	4.1	10.57	71.1
[100]	500	4.9	14.2	74
[101]	750	5.2	11.9	Not Mentioned
[102]	900	5.6	10.1	Not Mentioned
[103]	625	12	17.1	91.6
Proposed antenna	**192**	**9.01**	**20.2**	**91.06**

4.3. Design of a EBG loaded double split ring slotted antenna

A patch antenna with five split rings i.e. four at the corners and one at the centre has been designed. Figure 4.11.(a) shows the dimensions of the ring which are obtained as 0.11mm and 0.01mm respectively. The spacing (s_1) of two rings is 0.127mm and the spacing (s) between the ring and the base is 0.127mm. The height of the rings (h) from the base is taken as 0.2mm. The slot acts as a band pass filter since the spacing between the rings is equivalent to an inductor and the width of the slot is equivalent to a capacitor. The dimensions of the patch are obtained as 7.7 mm and 11.81 mm. The inset feed of length (l_1) 6mm is attached to the antenna. Figure 1(b) shows the designed double split ring slotted antenna. The whole device is mounted on the ground plane on RT Rogers 5880 (ε_r=2.2) with the height of 2.5 mm. The developed prototype possesses and electrical length of 0.8881λ_ox 0.7298λ_o. Double split ring slotted patch antenna presented in the figure 4.11.(b) is designed to operate at 24.4 GHz.

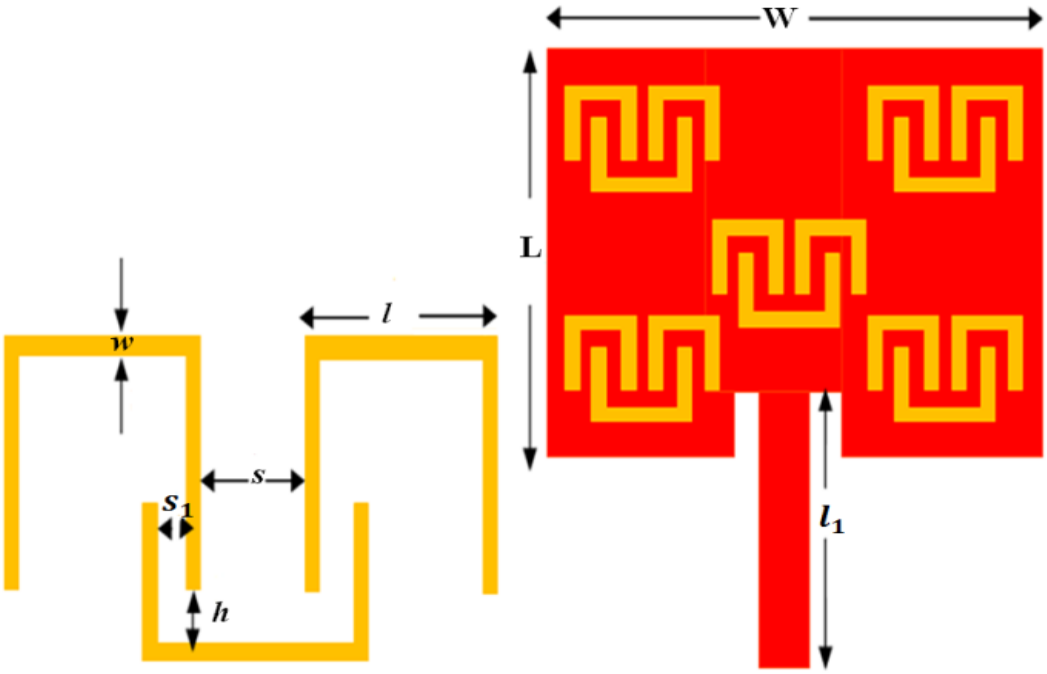

Fig.4.11.(a). Double split ring slot. **(b).** Double split ring slotted patch

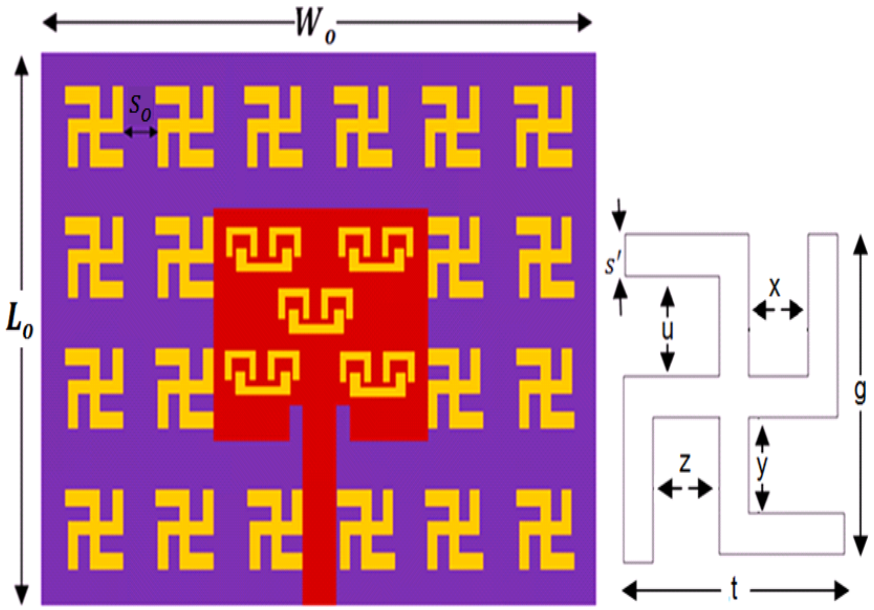

Fig.4.12.(a). Double split ring slotted antenna with swastika EBG**.(b).**Swastika slot

Figure.4.12.(a) shows the double spilt ring slotted antenna mounted on the ground plane etched with swastika shape slots commonly known as Electromagnetic Bandgap Structures (EBG). The proposed EBG structure is designed with total of 20 slots leaving the portion below the unetched portion. The dimensions of the ground plane are obtained as 29.525mm and 19.25mm respectively. As shown in figure.4.12 (b), the dimensions of the whole swastika slot are obtained as 2.5mm and 3.5mm respectively. Gap (x, z) between the vertically parallel arms are obtained as 0.4mm and 0.6mm respectively. Width (s') of all the arms of the slot is taken as 0.5mm. Spacing (y, u) between the horizontally parallel arms is chosen to be 1mm and 1mm respectively. Spacing (s_o) between two swastikas is taken as 0.75mm. Slotted patch is loaded exactly above the unetched portion of the EBG structure for the best results.

The electric model of a swastika slot is presented in figure.4.13.

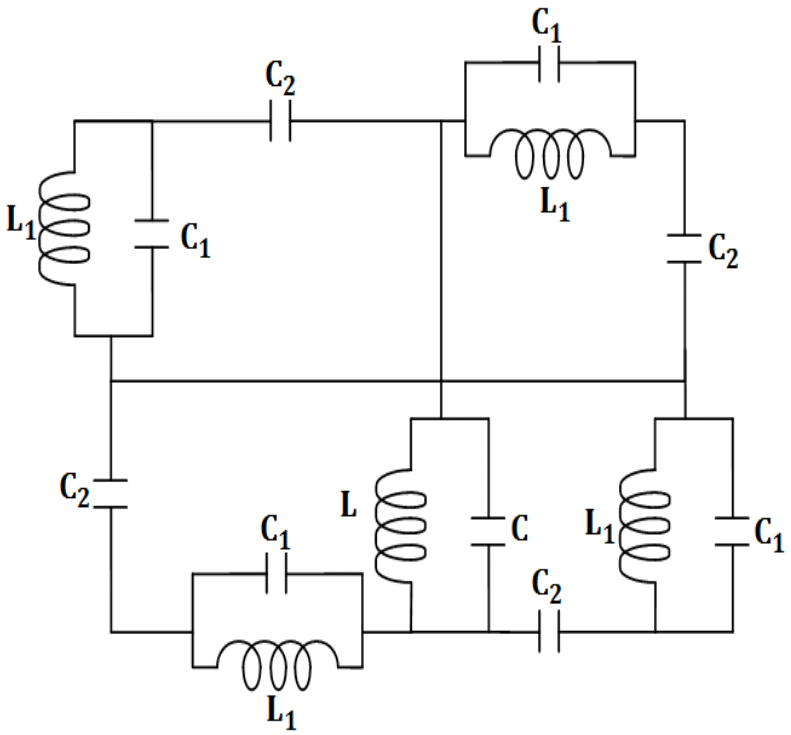

Fig.4.13. Electrical model of swastika slot

The system function of the model shown in figure.4.13 is given by:

$$H(s) = \frac{2LL_1s^4(C(C_1+C_2)+C_1C_2)+s^2(L_1(C_1+C_2)+LC)+1}{(LCL_1C_1s^4+s^2(LC+L_1C_1)+1)C_2s} \quad (4.1)$$

The approximate resonant frequencies of the slot are obtained as:

$$\omega_o' = \frac{1}{\sqrt{LC}} \ \& \ \omega_o'' = \frac{1}{\sqrt{L_1C_1}}$$

Resonant frequencies are calculated by assuming that swastika is symmetrical. As the proposed swastika is asymmetrical, the two resonant frequencies will coincide and thus making the EBG structure highly selective.

4.3.1. Outcomes and disquisitions

The antenna structure is developed through the simulations accomplished in ADS-2016 momentum and figure.4.14 presents the structure of the designed structure in radiating mode.

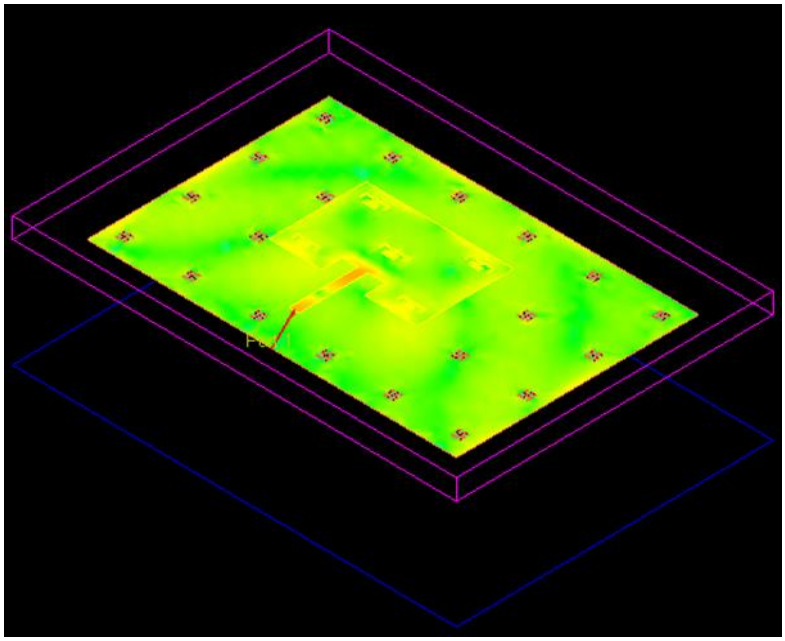

Fig.4.14. 3-D model of the proposed antenna.

Figure.4.15 presents the magnitude and phase plots of return losses.

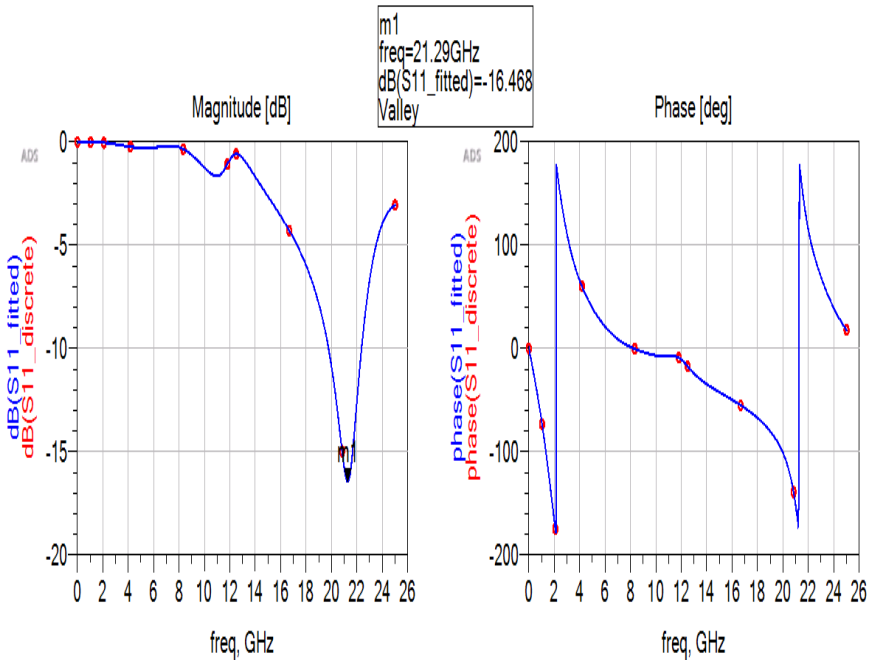

Fig.4.15. Magnitude and phase plots of reflection coefficient

Figure.4.16 shows the 2-D pattern of gain, directivity, electric and magnetic far fields.

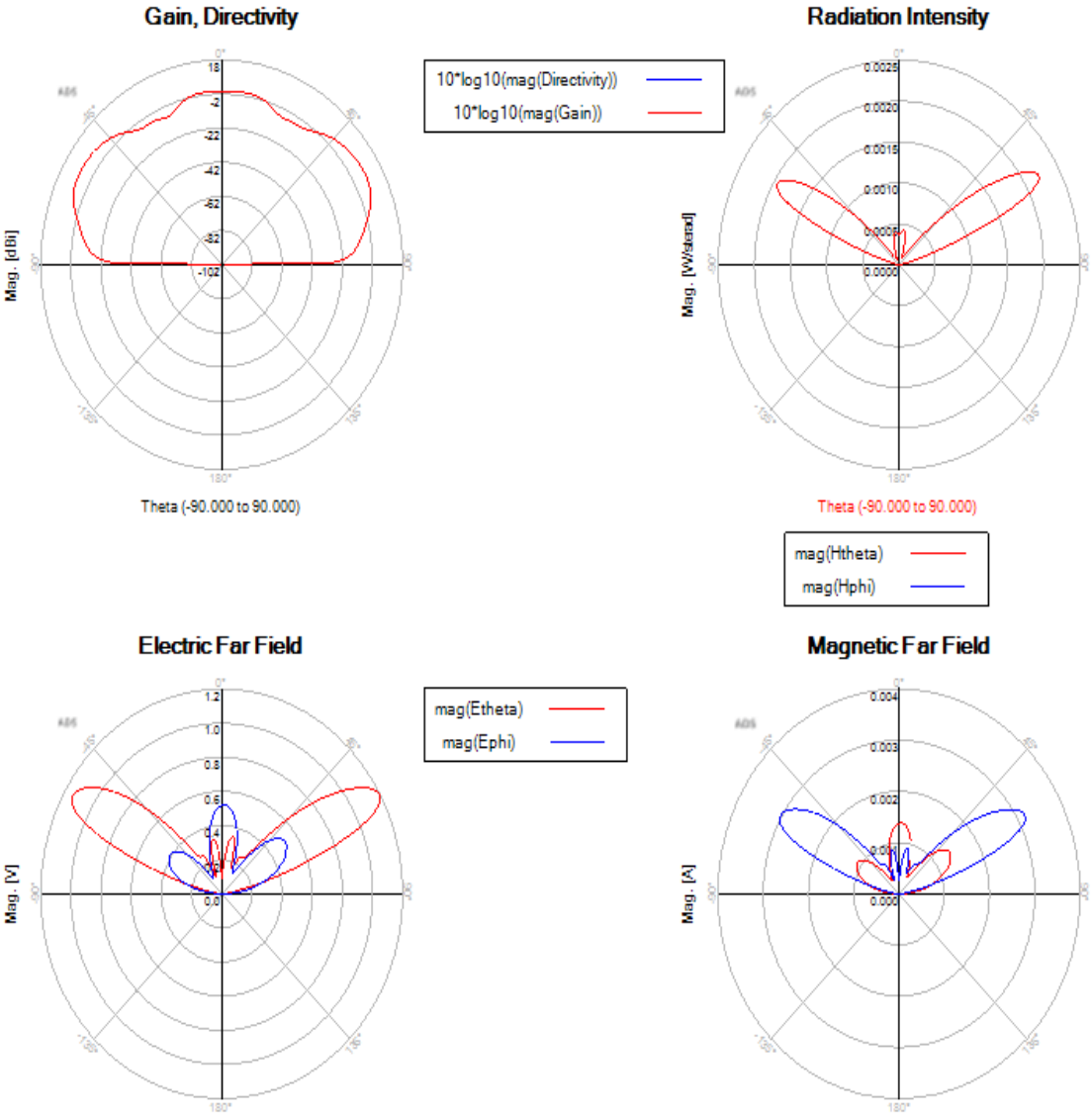

Fig.4.16. 2-D pattern of all the parameters of the proposed antenna

Figure.4.17 presents antenna patterns of the developed antenna structure and dual switched beams with dough-nut shaped pattern are observed

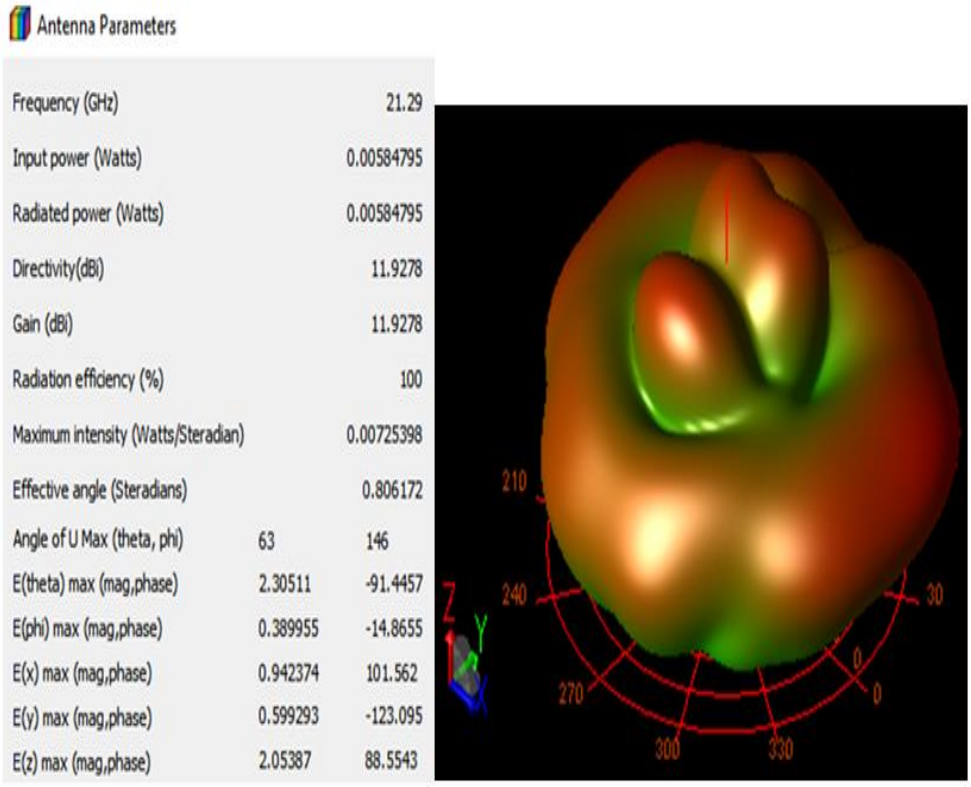

Fig.4.17. 3-D radiation pattern of the antenna

The slot dimensions are varied using ADS-2016 momentum to layout converter cum tuner. The performance parameters are deteriorated with the 1% variations in the dimensions of the swastika slot. Table.4.2 presents the performance aspects of the developed prototype.

Table.4.2. Performance parameters of the proposed antenna

Gain (dB)	**Bandwidth (GHz)**	**Directivity (dB)**	**Efficiency (%)**
11.92	3.2	11.92	100

4.4. Conclusions

In this chapter, two types of patch antennas loaded with splattered ring EBG structure and swastika shape EBG structure are designed and studied.

Overall volume of dumbbell is antenna is 25 × 30 × 1.524 mm^3. The antenna exhibits a wide impedance bandwidth with the frequencies ranging from 10.8GHz to 31GHz. The antenna patterns are steady throughout the operational frequency range. A peak radiation efficiency of 91.06% is noticed in the operational frequency band. The developed antenna is an apt candidate for high bandwidth and data rate purposes especially for 5G applications.

Overall dimensions of swastika EBG loaded split ring slotted patch antenna are 29.525 x 19.5 x 2.5mm^3. By introducing swastika EBG, it is observed that bandwidth of 3.2GHz with the gain of 11.92dB is observed in the designed antenna structure. The developed prototype can be suitably used for point-to-point applications. In the future the structure is expected to be modified for Nantenna using ADS-2016 software.

Though this chapter presents the implementation of different types of EBG structures like swastika and double splattered ring, the miniaturization at lower gigahertz frequencies (2GHz – 6GHz) is not attained by the antennas designed in this chapter. Therefore, miniaturization at the lower gigahertz frequency range is achieved by the antenna presented in the fifth chapter.

CHAPTER 5

The design and analysis of metamaterial and DGS loaded patch antenna

5.1. Introduction

In the last two chapters, the concept of high impedance surfaces was proposed and discussed. Based on these concepts, high gain has been achieved in different antennas i.e. rectangular, circular and dumbbell antennas. Miniaturization cannot be achieved in conventional patch antennas. Miniaturization in the previous chapters were achieved using radiating stubs, high impedance surfaces/AMCs like defective ground structure, electromagnetic bandgap structure, metamaterials. In the third chapter, different HIS and their contribution to the antenna's performance parameters were briefly discussed. These structures highly contribute to the miniaturization if their size is very less compared to the incident EM wave.

Literature reveals, based on patch antennas and structures to achieved the desired miniaturization at lower gigahertz frequency range. In [104], an antenna with Meander-Koch DGS operating at 5GHz is presented. The designed antenna is miniaturized by 61.83%, thereby making it electrically small. The slotted antenna in [105] operates at 2.45GHz. etching of slots increases electrical length of the surface current on the patch and thereby making the antenna resonate at lower gigahertz frequency range. This longer path of surface current facilitates the structure to resonate at 2.45GHz. The proposed patch antenna in [106] operates at 2.5GHz, 3.47GHz, and 5.75 GH. Miniaturization is achieved in the design by loading it on the cascaded E-type Defective ground plane in amalgamation with F-shaped slot. Other types of slots like 'U' and 'H' are loaded on the radiating monopole to achieve multiband characteristic. Degrees of miniaturization of 82.4% and 73.5% are achieved with the structure in [106] when compared to the conventional multiband antenna.

In this chapter, we explore the development of the metamaterial and DGS loaded patch antenna. The patch is operational at 5.2GHz and 8.25GHz. The loading of high impedance surfaces enhances the throughput of the developed structure as discussed in the third chapter. The designed antenna exhibits efficiencies of 61% and 69.7% at 5.2GHz and 8.25GHz respectively.

Figure.5 presents the design methodology of designed antenna.

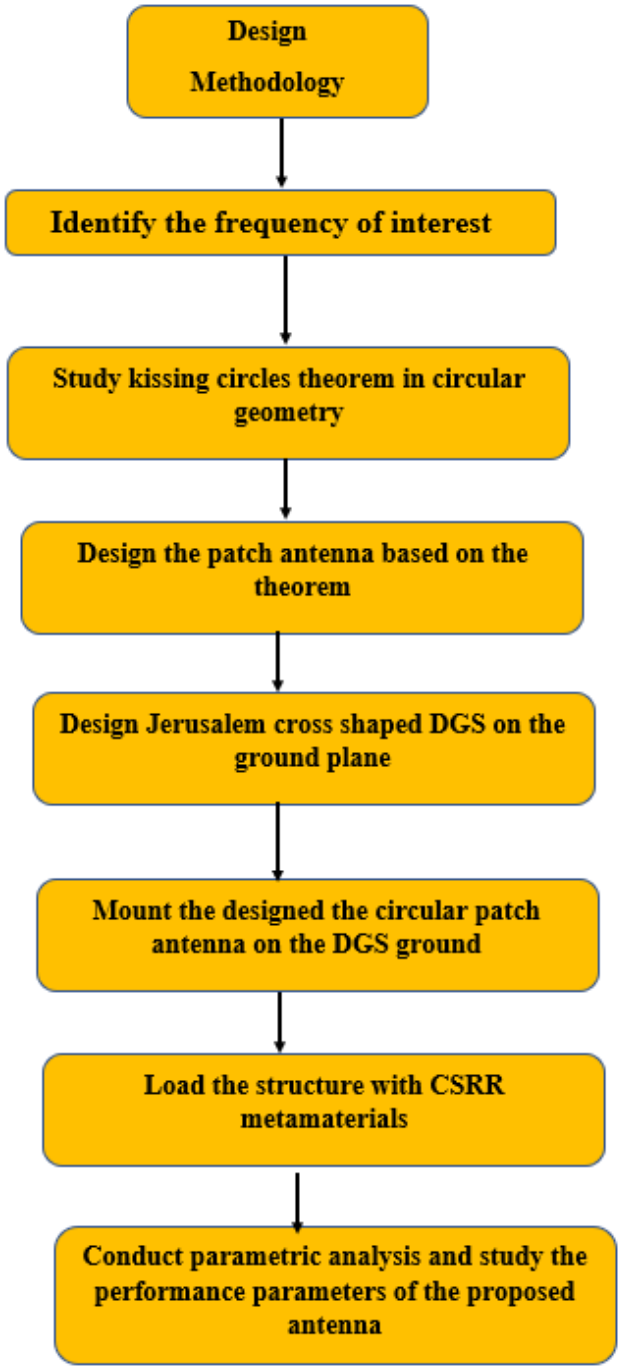

Fig.5. Designed methodology of the antenna proposed in chapter-5

5.2. Detailed design of the proposed patch antenna

The designed structure is printed on FR-4(lossy) substrate (ε_r=4.4) with the height of 1.524mm. The frequencies of operations are 8.25GHz and 5.2GHz. For f_r'= 8.15GHz, the effective radius corresponding to 8.15GHz is obtained from eq.(1.2) and eq.(1.3).

Using the above design equations, effective radius is evaluated as 8.25mm and the corresponding radius (r) is evaluated as 7.5mm. Similarly, for f_r''=5.15GHz, the radii of the design are evaluated as:

$$f_r'' = \frac{1.8412*c}{2\pi(r_{2e}+r_{1e})\sqrt{\varepsilon_r}} \quad (5.1)$$

$$r_{1e} + r_{2e} = (r_1 + r_2)\left[1 + \frac{2h}{\pi(r_1+r_2)\varepsilon_r}\left\{\ln\left(\frac{(r_1+r_2)}{2h}\right) + (1.41\varepsilon_r + 1.77) + \frac{h}{(r_1+r_2)}(0.268\varepsilon_r + 1.65)\right\}\right]^{\frac{1}{2}} \quad (5.2)$$

Where, r, r_1 and r_2 is the radii of the middle and external patches and h the thickness of the dielectric. The design of the developed antenna is derived from basic geometric theorem called "Kissing circle's theorem" which states that if three circles of radii r, r_1 and r_2 (where $r > r_1 > r_2$) touch externally then $\frac{1}{\sqrt{r_2}} = \frac{1}{\sqrt{r}} + \frac{1}{\sqrt{r_1}}$. By fixing r_1=2.5mm and substituting r=7.5mm obtained from equation (5.2), the diameter ($2r_2$) of the small patch is 3mm. Figure.5.1.(a) presents the prototype of designed antenna. The antenna is a fed with microstrip lines with the dimensions (l, l_1, l_2 and l_3) 4mm, 5mm, 11mm and 6mm respectively. The widths (w, w_1, w_2 and w_3) of the feed lines are 2mm, 2mm, 3mm and 3mm respectively. The whole patch is printed on the ground plane having total area of 30mm x 30mm and with DGS cell. A layer of foam with (ε_r=1.07) and overall volume of 10 x 23 x 2mm^3 is sandwiched between the antenna and the FR-4 substrate. Figure.5.2.(b) shows the fabricated patch antenna. Parametric analysis on the impact of width of foam dielectric over the operational bandwidth is carried out and studied in the further sections.

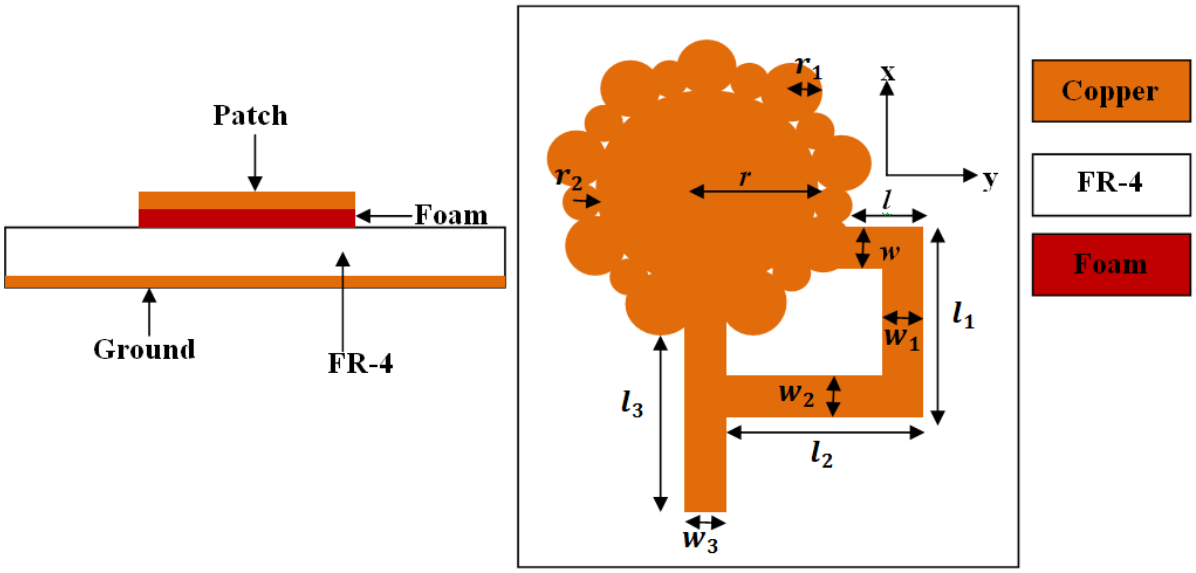

Fig.5.1.(a). Proposed antenna

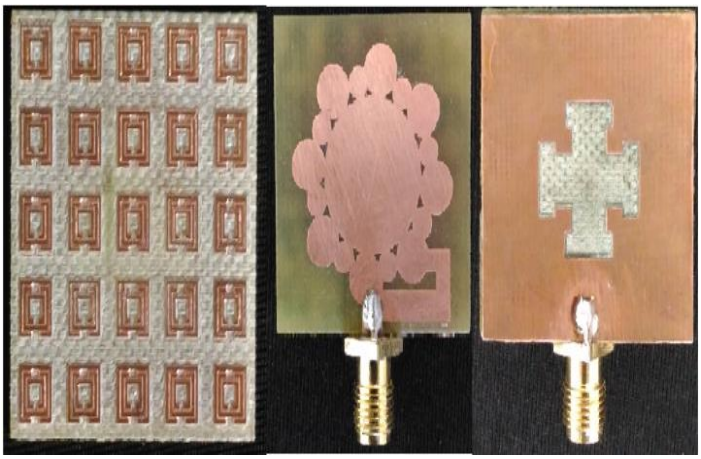

Fig.5.1.(b). Top and bottom views of the fabricated antenna

The required design aspects are obtained at the desired frequencies by optimizations and by carrying out parametric analysis on the structural features of the antenna that effects its performance. Table.5.1 presents the design specifications of the proposed structure.

Table.5.1 Parameters of the proposed antenna (see Fig.5.1.(a))

Parameters	r	r_1	r_2	l	l_1	l_2	l_3	w	w_1	w_2	w_3
Values(mm)	7.5	2.5	1	4	5	11	6	2	2	3	3

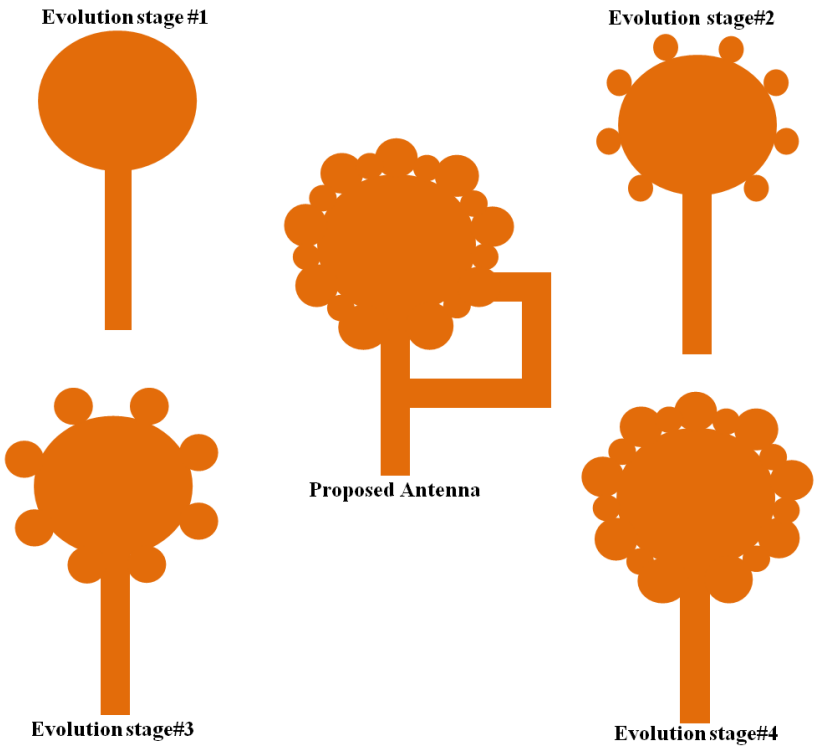

(a)

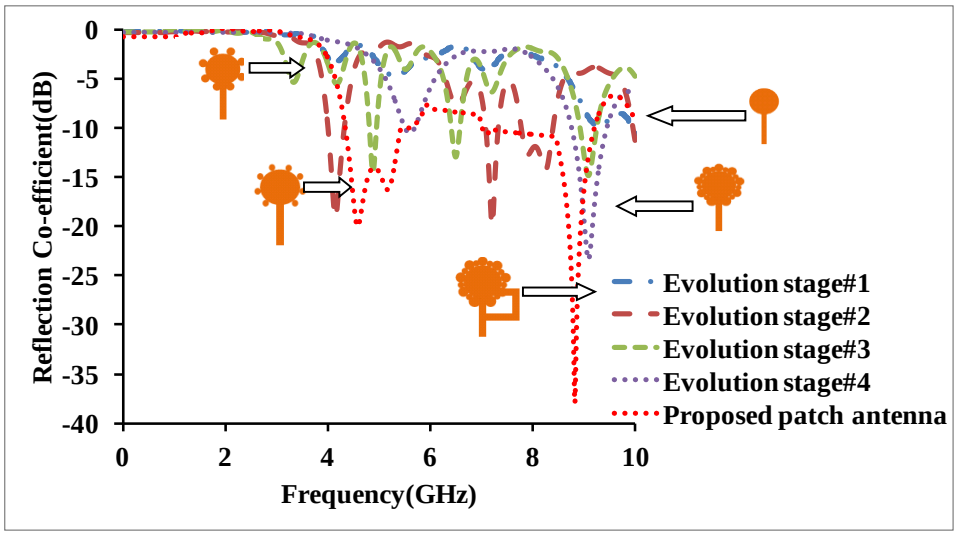

(b)

Fig.5.2. (a). Development stages of the antenna. **(b).** Impedance bandwidth plots of development stages of the antenna.

Figure.5.2.(a) presents the evolution stages of the developed structure. Figure.5.2.(b) presents the impedance bandwidth curves of the antennas presented in the evolution stages. The design developed in 1st development stage of figure.5.2.(a) is a basic circular patch antenna. From figure.5.2.(b) (thick blue line), the antenna in stage#1 resonates at 9.62GHz and the impedance bandwidth (S_{11}<-10dB) is about 110MHz. The addition of small circular patches on the

circumference of the antenna in the 1st development stage makes the resultant structure operational at 4.1GHz, 7.34GHz and 8.1GHz. The impedance bandwidths are observed to be 242MHz, 125MHz and 620MHz respectively, as presented in figure.5.2.(b) and represented in red curve. When larger radii radiators are printed on the exterior surface of the patch presented in 1st development stage, the resultant patch antenna resonates at 4.57GHz, 6.25GHz and 8.82GHz with the operational bandwidths of 112MHz, 223MHz and 312MHz respectively, as presented in figure.5.2.(b) and represented in green curve. The smaller and bigger radiators are attached on the exterior boundaries of the antenna in the 1st development stage to form the antenna presented in 4th development stage. The resultant antenna resonates at 5.52GHz and 9.15GHz with the operational bandwidths of 100MHz and 405MHz respectively, as presented in figure.5.2.(b) as represented by dotted purple curve. In the last stage, the developed and final antenna is obtained by feeding the antenna in 4th development stage in a two-way through microstrip feed. This possesses operational frequencies namely 4.57GHz and 5.15GHz with the operational bandwidths of 1.25GHz and 2.2GHz respectively, as presented in figure.5.2.(b) and represented in red dotted curve. Jerusalem slot is assumed as two dumbbells placed perpendicularly. Parallel L-C tank circuit is considered as the electrical equivalent of a dumbbell. When a slot is created on a ground plane, the electrical length increases by introducing additional resistance, inductance and capacitance and thereby increasing effective inductance and capacitance. Due to this, the operational frequency shifts towards lower gigahertz frequencies. Apart from the frequency shift, return loss and harmonics are reduced. Figure.5.3 presents the designed DGS slot. The overall area of the slot is obtained as 15mm x 15mm after the optimization. The dimensions of the outer arms are obtained as 10mm and widths (w'') of these arms are obtained as 5mm each. The dimensions of the ends of horizontal cross are 7mm and 2.5mm.

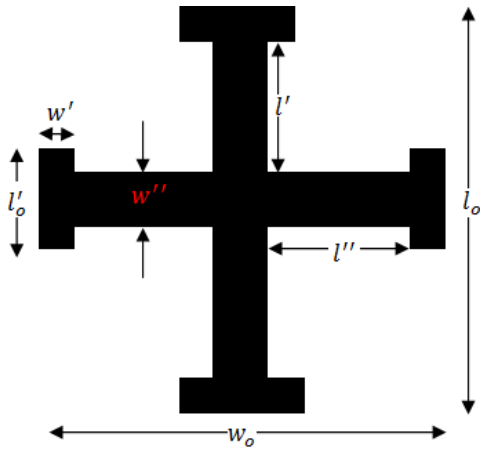

Fig.5.3. Proposed Jerusalem cross shape DGS

The proposed and implemented CSRR metamaterial cell is presented in figure.5.4. The lengths of the concentric rings are 3mm, 2mm and 1.5mm respectively. The dimension(s) of the outer ring is/are 0.25mm and dimensions of the cuts (d_o, d_1 and d_2) of the rings are 1mm, 0.75mm and 0.5mm respectively.

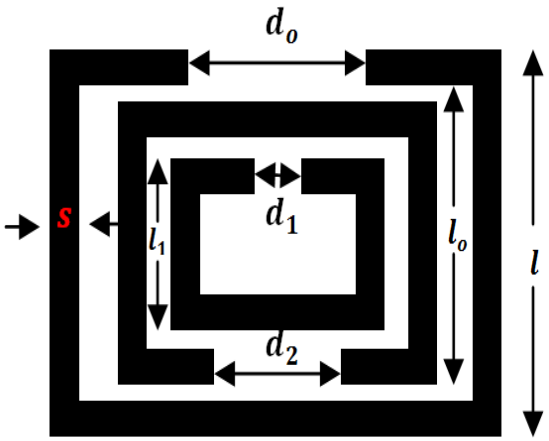

Fig.5.4. A unit cell of the triple CSRR metamaterial

The spacings (both horizontal and vertical) between the metamaterial cells are optimized to 5mm each. The cell dimensions and spacings are carefully chosen and optimized as performance specifications of the patch depend on the overall volume of the cell and spacing between the cells. A total of 25 metamaterial cells are embedded inside the substrate to obtain the best results. These are loaded inside the dielectric at a height of 0.762mm and parametric analysis is done to optimize the design and to achieve satisfactory results. All the iterations are not presented in this chapter as they produce undesired results. The brief study on the variation in the structural features of the patch antenna, DGS cell and metamaterial cells on the antenna's performance is accomplished in the further sections in this chapter.

5.3. Mathematical analysis

Green's function (G) plays an important role to obtain the radiating fields in a patch antenna. Laplace functions serve as a basis to compute Green's functions. To start with the proposed patch antenna, the surface on which the Green's function is to be computed is a cylinder with the thickness of 't'µm.

$$\nabla^2 G = \frac{1}{\rho}\frac{\partial}{\partial \rho}\left(\rho \frac{\partial G}{\partial \rho}\right) + \frac{1}{\rho^2}\frac{\partial^2 G}{\partial \theta^2} + \frac{\partial^2 G}{\partial z^2} \tag{5.3}$$

$$\nabla^2 G\,(\rho) + k_c^2 G\,(\rho, r_o) = \frac{1}{\rho}\delta(\rho)\delta(\theta)\delta(z) \tag{5.4}$$

$$G(\rho) = \frac{1}{8\pi^3} \iiint_0^{k_x k_y k_z} \tilde{g}(k)\, e^{ik.\rho} dk_x dk_y dk_z$$

Where $G(\rho)$ and $\tilde{g}(k)$ form Fourier transform pairs

$$\nabla^2 G(\rho) = \frac{1}{4\pi^2 t} \iint_0^{\rho,\psi} \tilde{g}(\rho)(-\rho^2) e^{i(\rho\cos\psi\rho\cos\theta + \rho\sin\psi r'\sin\theta)}\, \rho d\rho d\psi$$

$$\nabla^2 G(\rho) + k_c^2 G(\rho) = \frac{1}{4\pi^2 t} \iint_0^{r',\psi} \tilde{g}(r')(-r'^2) e^{i\rho r'\cos(\psi-\theta)} r' dr' d\psi +$$

$$\frac{k_c^2}{4\pi^2 t} \iint_0^{\rho,\psi} \tilde{g}(\rho) e^{i\rho r'\cos(\psi-\theta)}\, r' dr' d\psi \tag{5.5}$$

$$\tilde{g}(r') = \iiint_0^{\rho,\theta,z} \frac{1}{\rho} \delta(\rho)\delta(\theta)\, e^{-i\rho r'\cos(\psi-\theta)} r' dr' d\theta dz = 1 \tag{5.6}$$

$$\tilde{g}(r') = \frac{t}{k_c^2 - r'^2}$$

Therefore,

$$G(\rho) = \frac{1}{4\pi^2} \iint_0^{r',\psi} \frac{1}{k_c^2 - r'^2}\, e^{i\rho r'\cos(\psi-\theta)} r' dr' d\psi$$

$$G(\rho) = \frac{1}{2\pi} \int_0^{\infty} \frac{1}{k_c^2 - r'^2} J_o(\rho r') r' dr' = \frac{1}{4\pi k_c} \int_0^{\infty} [J_o(\rho r')][\frac{1}{k_c - r'} + \frac{1}{k_c + r'}]] r' dr' \tag{5.7}$$

$$G(\rho) = \frac{1}{4\pi\rho k_c} [\cos(\rho\beta_c) + \sin(\rho\beta_c) \tag{5.8}$$

$$G(\rho) = \sum_{n=-\infty}^{\infty} J_n\left(\frac{p_{kl}}{r}\rho\right) \sum_{m=-\infty}^{\infty} A_m + \sum_{n=-\infty}^{\infty} J_n\left(\frac{p_{kl}}{r_1 + r_2}\rho\right) \sum_{m=-\infty}^{\infty} A_m \tag{5.9}$$

$$A_m = \frac{1}{\sum_{m=-\infty}^{\infty} J'_m\left(\frac{p_{kl}}{r}\rho\right)} + \frac{1}{\sum_{m=-\infty}^{\infty} J'_m\left(\frac{p_{kl}}{r_1 + r_2}\rho\right)} \tag{5.10}$$

$$G(\rho) = \sum_{n=-\infty}^{\infty} \left[J_n\left(\frac{p_{kl}}{r}\rho\right) + J_n\left(\frac{p_{kl}}{r_1 + r_2}\rho\right)\right] \left[\frac{1}{\sum_{m=-\infty}^{\infty} J'_m\left(\frac{p_{kl}}{r}\rho\right)} + \frac{1}{\sum_{m=-\infty}^{\infty} J'_m\left(\frac{p_{kl}}{r_1 + r_2}\rho\right)}\right] \tag{5.11}$$

Where, r, r_1 and r_2 are the radii of the central and outer sections attached to the circumference of the proposed patch

The radiating fields in the antenna structure obtained and studied with the help of cavity model as discussed in chapter-1. The structure is considered as cylindrical cavity and the mathematical computations are accomplished by considering the designed structure as a stack of different cylindrical cavities with discrete dimensions. The ends of the patch are treated as open circuit and open boundary conditions are considered to compute the fields. The patch acts as capacitor with the charges distributed on its bottom and top layers. The charges are responsible for the

cancellation of tangential fields on all the walls of the enclosed antenna structure. The electric lines are radiated upwards.

Electric field in z-direction is the root of below presented equation:

$$(\nabla^2 + \beta^2)\overline{E} = 0. \quad (5.12)$$

Where $\beta=\omega\sqrt{\mu\varepsilon}$ is a propagation constant of the structure. $\overline{E}$ is the electric field directed towards z-axis and ∇^2 is the Laplacian operator.

$$\overline{E} = E_o J_n(\rho)\cos(n\phi)$$

$$H_\phi = \frac{-j\beta}{\omega\mu_o} J_n'(\rho)\cos(n\phi)$$

Where, 'β ' is the propagation constant and ϕ varies from 0 to 2π. Boundary conditions are applied on magnetic field H_ϕ.

$H_\phi|_{r\ \&\ (r_1+r_2)} = 0$. Different modes propagating supported by the antenna are obtained from the roots of the equation. The surface currents are obtained from the respective equivalence principles.

$$\overline{M} = 2\overline{E_z}\hat{\phi}$$

Electric vector potential ($\overline{F}$) is obtained by:

$$\overline{F} = \frac{\varepsilon}{4\pi}\frac{e^{-j\beta_o r}}{r}\iint \overline{M}\, e^{j\beta_o r.\bar{r}} dS$$

$'\overline{r}'$ is the position of the source and 'β_o' is the propagation constant.

The electric fields in the space are computed as follows:

$$E_\theta = \frac{\varepsilon}{4\pi}\frac{e^{-j\beta_o r}}{r}\sum_{n=-\infty}^{\infty}\left[J_n\left(\frac{p_{kl}}{r}\rho\right) + J_n\left(\frac{p_{kl}}{r_1+r_2}\rho\right)\right]\left[\frac{1}{\sum_{m=-\infty}^{\infty} J_m'\left(\frac{p_{kl}}{r}\rho\right)} + \frac{1}{\sum_{m=-\infty}^{\infty} J_m'\left(\frac{p_{kl}}{r_1+r_2}\rho\right)}\right]\left[[J_{n+1}(\beta_o r\sin\theta) - J_{n-1}(\beta_o r\sin\theta)] + [J_{n+1}(\beta_o(r_1+r_2)\sin\theta) - J_{n-1}(\beta_o(r_1+r_2)\sin\theta)]\right]\cos(n\phi) \quad (5.13)$$

$$E_\phi = \frac{\varepsilon}{4\pi}\frac{e^{-j\beta_o r}}{r}\sum_{n=-\infty}^{\infty}\left[J_n\left(\frac{p_{kl}}{r}\rho\right) + J_n\left(\frac{p_{kl}}{r_1+r_2}\rho\right)\right]\left[\frac{1}{\sum_{m=-\infty}^{\infty} J_m'\left(\frac{p_{kl}}{r}\rho\right)} + \frac{1}{\sum_{m=-\infty}^{\infty} J_m'\left(\frac{p_{kl}}{r_1+r_2}\rho\right)}\right]\left[[J_{n+1}(\beta_o r\sin\theta) - J_{n-1}(\beta_o r\sin\theta)] + [J_{n+1}(\beta_o(r_1+r_2)\sin\theta) - J_{n-1}(\beta_o(r_1+r_2)\sin\theta)]\right]\cos\theta\sin(n\phi) \quad (5.14)$$

Figure.5.5 shows the variation of Green's function with the distance from the radiator.

From the plot presented in the figure.5.5, it can be inferred that the function is maximum at near to the source and decreases if the observation point moves away from the source.

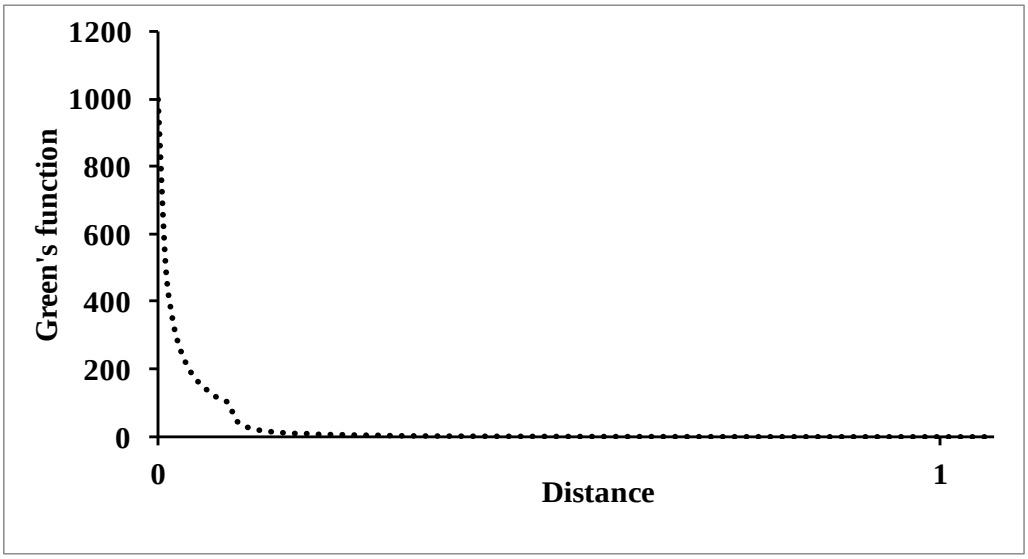

Fig. 5.5. Plotted Green's function of the proposed patch antenna

5.4. Design analysis

The throughput of the structure depends on its various structural features like dimensions of DGS, number of metamaterial cells, thickness of the foam substrate. These structural features effect operational bandwidth of the patch. The impact of the structural features on the operational bandwidth is investigated and discussed in this section. Fig.5.6.(a) presents the fluctuation in the impedance bandwidth by changing the number of metamaterial cells. The resonant frequency shifts towards right side (towards upper gigahertz range) with the decrease in the number of metamaterial cells. This fluctuation in the frequency degrades the gain at the operational frequency. With 9 metamaterial cells, the patch possesses operating frequencies at 3.2GHz, 4.01GHz and 8.1GHz. The impedance bandwidths at these frequency ranges are 101Mz, 189MHz and 301MHz. The gains at these resonant frequencies are 2.1dBi, 3.21dBi and 4.8dBi as presented in figure.5.6.(d) and represented in dashed green line. A single metamaterial cell introduces two resonant frequencies at 3.85GHz and 8.02GHz with the impedance bandwidths being 262MHz and 980MHz at these frequency ranges. The gains at these resonant frequencies are 3.2dBi and 2.6dBi as presented in figure.5.6.(d) and represented in dashed red curve. A basic flower shaped patch antenna resonates at 7.8GHz and 9.56GHz with the impedance bandwidths being 78MHz and 52MHz respectively. The gains at these resonant frequencies are 1.09dBi and 1.99dBi as presented in figure.5.6.(d) as represented blue dotted curve.

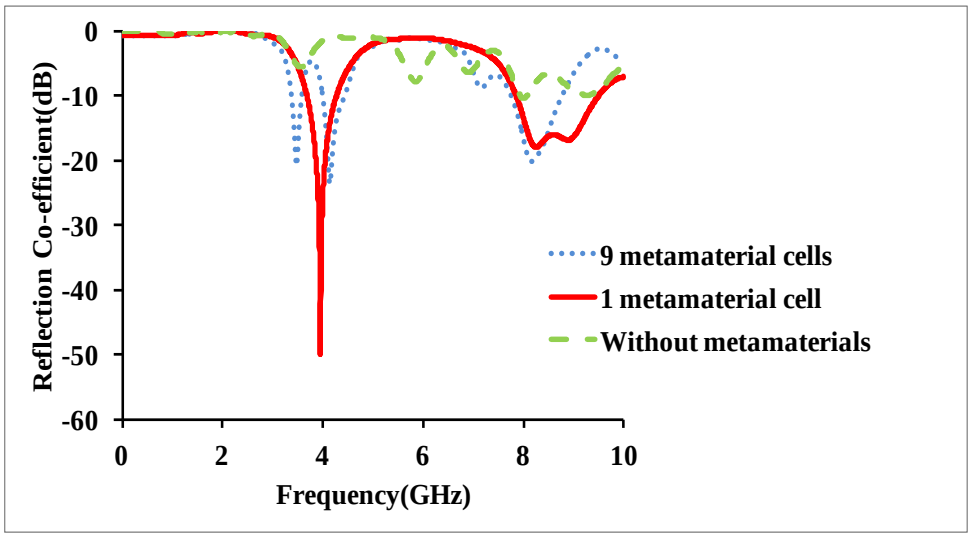

(a)

The proposed antenna becomes multi-frequency with the variation in the height of the foam layer. Figure.5.6.(b) presents the impact of height of the foam over the operational frequency range. For the foam thickness of 1mm, the developed structure resonates at 4.25GHz, 4.52GHz and 8.15GHz with the impedance bandwidths being 1.1GHz and 612MHz respectively. The patch resonates at 2.52GHz, 6.72GHz and 8.12GHz with the foam thickness of 0.5mm. The impedance bandwidths at these frequency ranges are reduced to 115MHz, 560MHz and 430MHz. When the foam substrate is not introduced, the proposed structure resonates at 2.61GHz, 7.72GHz and 9.81GHz respectively with the impedance bandwidths being 120MHz, 542MHz and 631MHz respectively. The decrease in the foam thickness deteriorates the antenna patterns and increasing in its height increases overall dimensions of the antenna. Hence, a trade-off must be maintained to meet the design requirements. Increase in the foam thickness beyond 2mm will yield undesirable outcomes and therefore, they are not presented in this chapter.

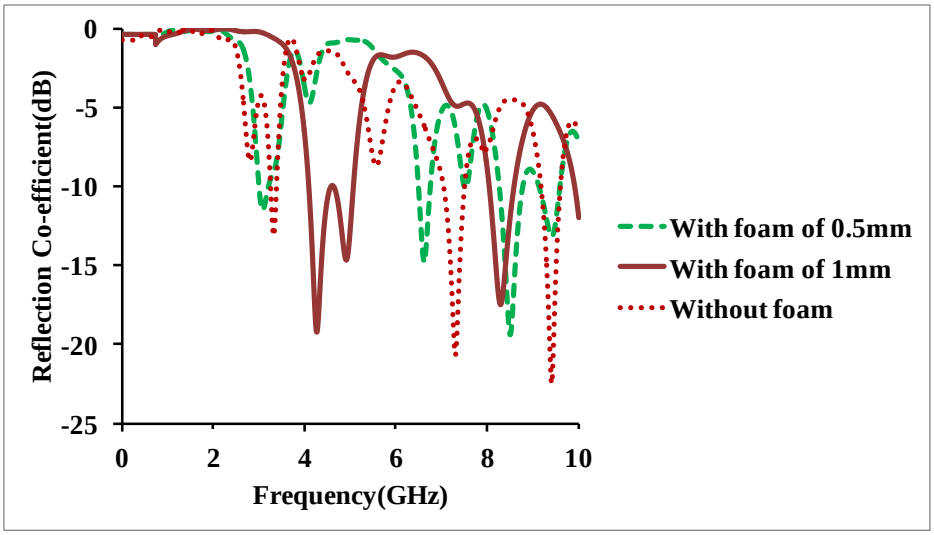

(b)

The variation in the area of Jerusalem DGS does not shift the operational frequencies but it degrades the operational bandwidth of the patch antenna. Figure.5.6.(c) presents the variation in the impedance bandwidth with the variation in the area of the DGS cell. At 'L' =12mm, the patch resonates at 2.67GHz, 4.57GHz and 8.36GHz with the impedance bandwidths being 112MHz, 201MHz, and 156MHz respectively. With the decrease in the 'L' to 9mm, antenna operates at 4.62GHz and 8.43GHz with the operational bandwidths being 1.01GHz and 762GHz at the frequency ranges. The variation in the 'L' below 9mm has little impact on the impedance bandwidth. Hence, the parametric analysis for length of DGS cell below 9mm is not presented in this chapter.

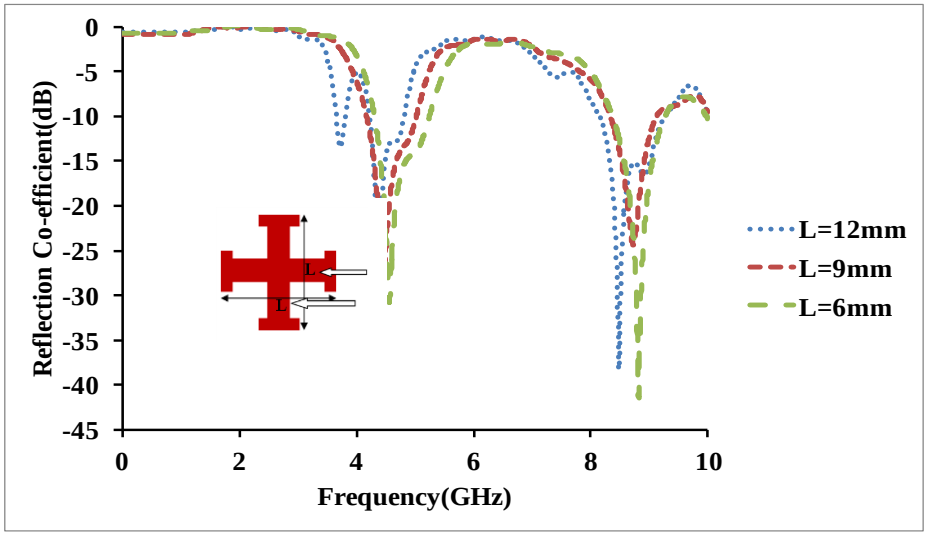

(c)

A trade-off should be maintained between number of metamaterial cells, area of DGS cell and thickness of foam substrate to avoid the degradation of performance specifications of the designed structure. The increase in the area of the Jerusalem cell enhances gain with the deterioration in the operational frequency range. Increase in the area of DGS cell beyond certain value degrades gain, impedance bandwidth and distorts radiation patterns. Figure.5.6.(d) presents the variation in the gain with the metamaterial cells. With 9 metamaterial cells, gain values of -3.2dBi and 1.2dBi are obtained at 5.2GHz and 8.25GHz as represented in dashed green curve. With one metamaterial cell, gain values of -2.8dBi and 1.2dBi are obtained at 5.2GHz as represented in dashed red curve. A basic flower shaped patch antenna without metamaterial possesses gains of -5dBi and -2.1dBi at 5.2GHz and 8.25GHz represented in dotted blue curve.

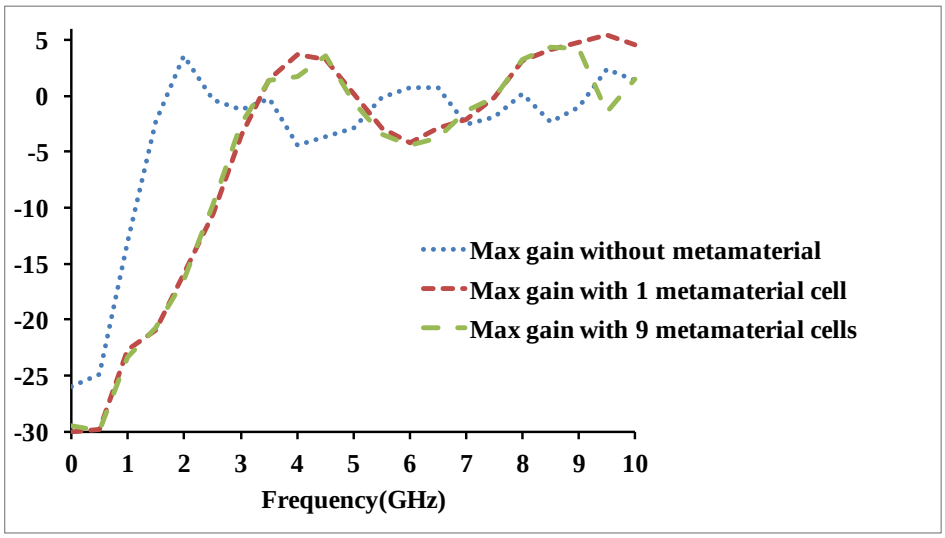

(d)

Fig.5.6. (a). Effect of the metamaterial cells on the impedance bandwidth of the designed antenna. **(b).** Effect of the foam thickness over the impedance bandwidth of the designed antenna. **(c).** Impact of the dimensions of Jerusalem DGS on the impedance bandwidth of the designed antenna. **(d).** Impact of number of metamaterial cells on the gain of flower patch antenna.

5.5. Outcomes and disquisitions

The optimized dimensions of Jerusalem DGS are obtained as 15mm x 15mm. By introducing the foam of 2mm, the antenna gives best results.

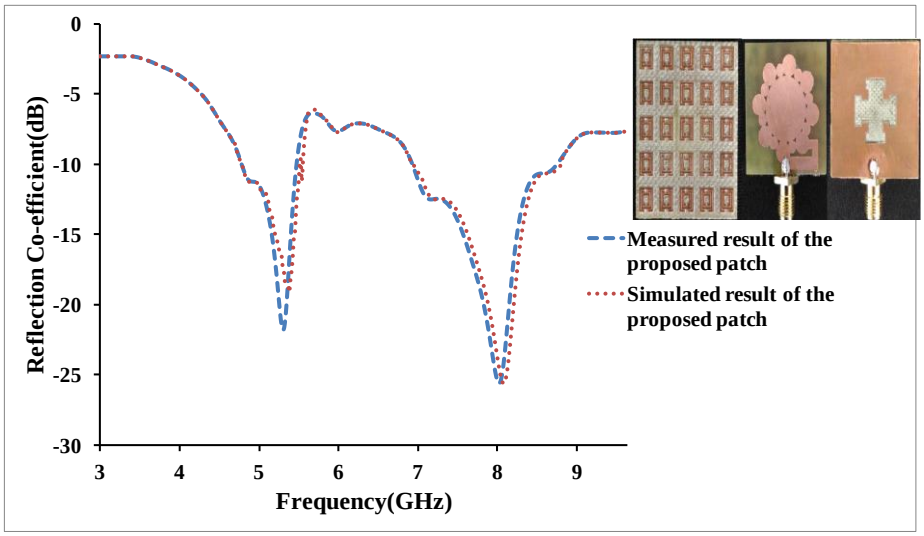

Fig.5.7. Return loss of the designed antenna

The proposed prototype is fabricated and measured. Figure.5.7 presents the simulated and measured impedance bandwidths of the developed antenna. Measured impedance bandwidths of 1.18GHz and 2.17GHz are obtained in the bands of 4.95GHz-6.15GHz and 7.1GHz-9.3GHz respectively. The measured results are in close proximity with that of simulated. The proposed antenna possesses radiation efficiencies of 61% and 69.7% at 5.25GHz and 8.25GHz as presented in figure.5.8.

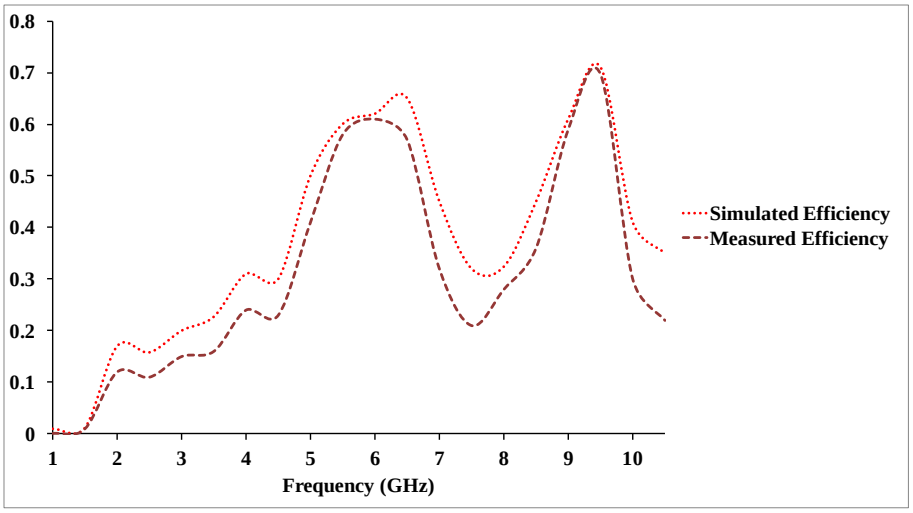

Fig.5.8. The simulated and measured efficiency of the proposed antenna

Initially, antenna patterns of the prototype are simulated in CST-microwave studio and the measurements are accomplished using an anechoic chamber using measurement apparatus comprising of double ridge horn antenna acting as test antenna. Figure.5.9 presents the measured and simulated co-polar radiation patterns at 5.2GHz. A gain of 3.93dBi is obtained in radiation planes through simulations carried out in CST. The measured gains of 3.75dBi and 3.8dBi are obtained at 5.2GHz. Simulated gain values of 4.92dBi and 5.03dBi are observed in E ($\varphi=90^{o}$) and H ($\varphi=0^{o}$) planes at 8.25GHz. The measured gains of 5.02dBi and 4.56dBi are obtained at 8.25GHz. The measured plots are in close agreement with that of simulated.

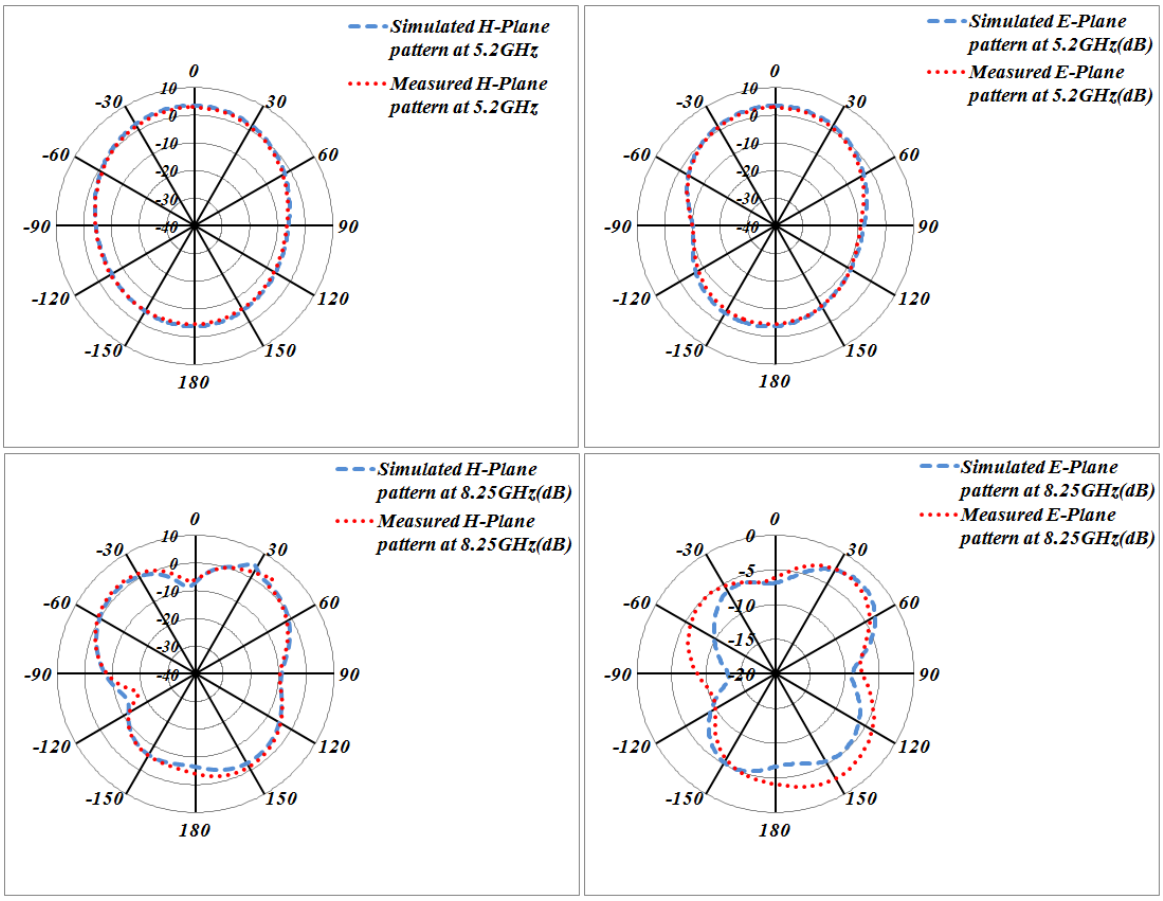

Fig.5.9. Radiation patterns of the patch antenna

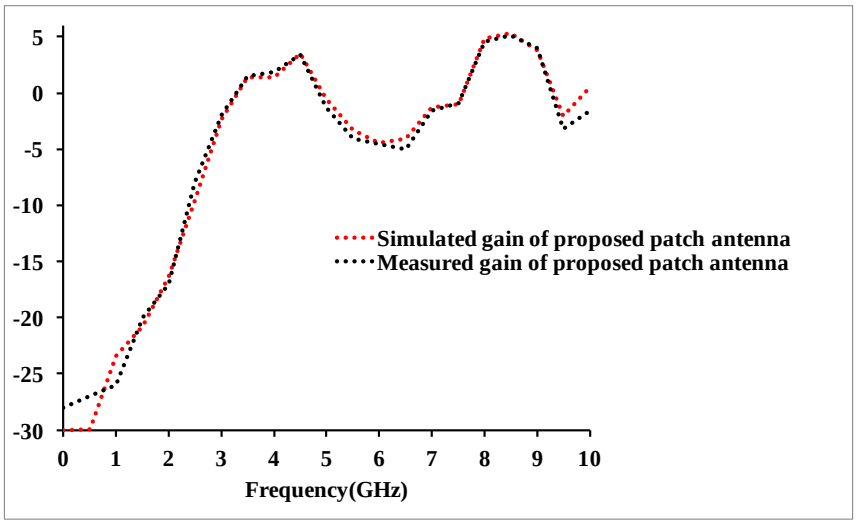

Fig.5.10. Gains of the patch antenna

Figure.5.10 presents the gains of the designed and fabricated antennas. A gain of 3.75dBi is measured at 5.2GHz and 5.02dBi at 8.25GHz. The properties of metamaterial are studied with the help of Nicolson-Ross-Weir method. This method is used to extract s-parameters The method is accomplished by deriving scattering parameters and further mathematical computations are done in MATLAB. Figure.5.11.(a) and figure.5.11.(b) show the magnitude and phase plots of S_{11} and S_{21} for CSRR unit cell which obtained in CST microwave studio. Permittivity and permeability plots are obtained in MATLAB.

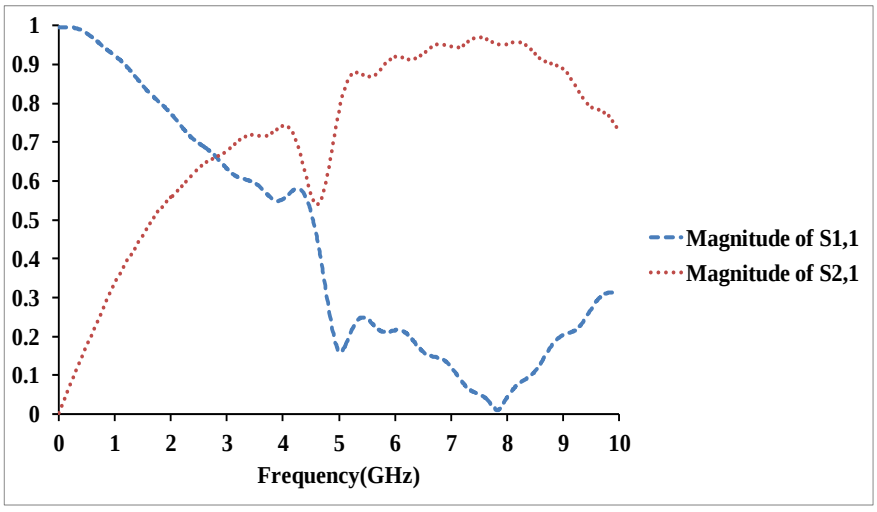

(a)

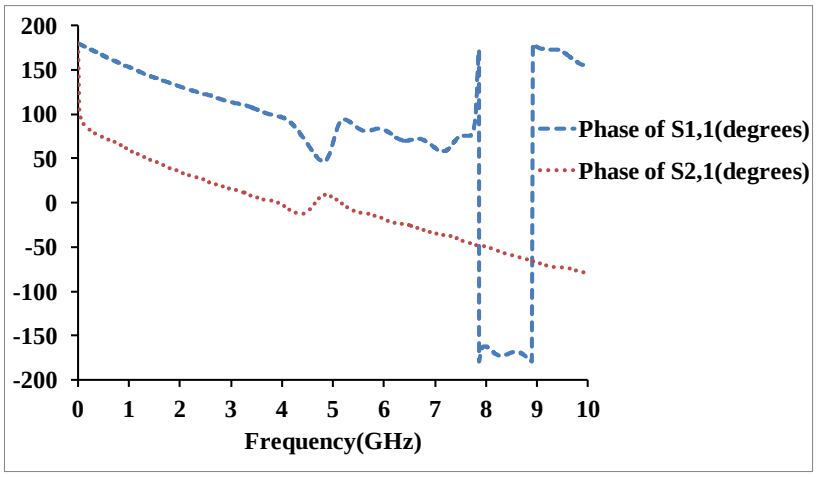

(b)

Fig.5.11. (a). Magnitude plot of the insertion loss and return loss of a unit metamaterial cell

(b). Phase plot of the insertion loss and return loss of a unit metamaterial cell

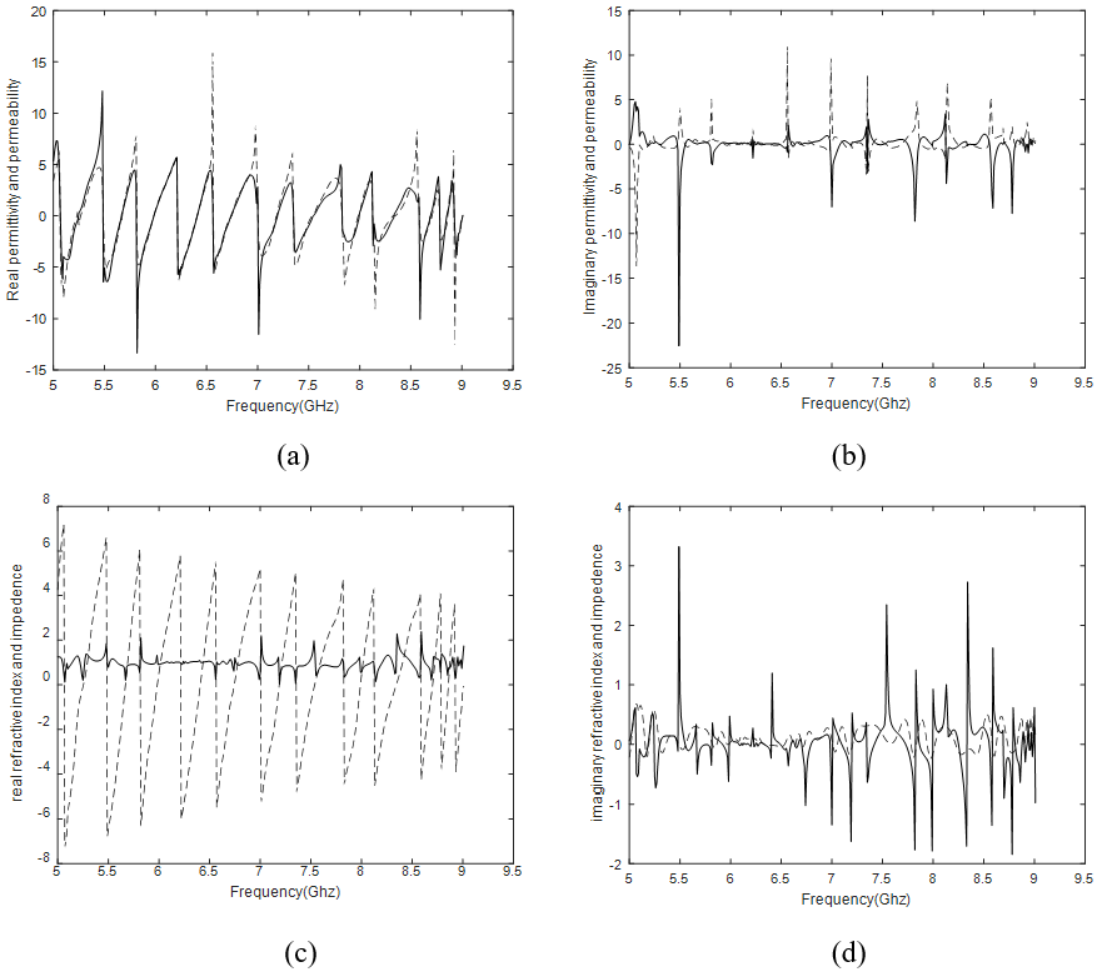

Fig.5.12.(a). The real part of permittivity and permeability. **(b).** The imaginary part of permittivity and permeability. **(c).** The real part of refractive index and impedance. **(d).** Imaginary part of refractive index.

From the figure.5.12.(a), the permeability and permittivity are negative at 5.2GHz and 8.25GHz. From the plots, it is noticed that the implemented metamaterial possesses Double Negative (DNG) property. The permittivity and permeability plots are nearly periodic in the frequency range of 5GHz-9GHz. Figure.5.12.(b) presents the complex permittivity represented in thick curve and permeability represented in dotted curve. Figures 5.12.(c) and 5.12.(d) presents the plots of real part of index of refraction, real part of impedance, complex part of index of refraction, and complex part of impedance. The current confinement in the proposed structure at 5.2GHz, and 8.25GHz are presented in figure.5.13. From the figure, it is noticed that the current is confined on Jerusalem DGS slot and the metamaterial array especially on the edges of the metamaterial cells.

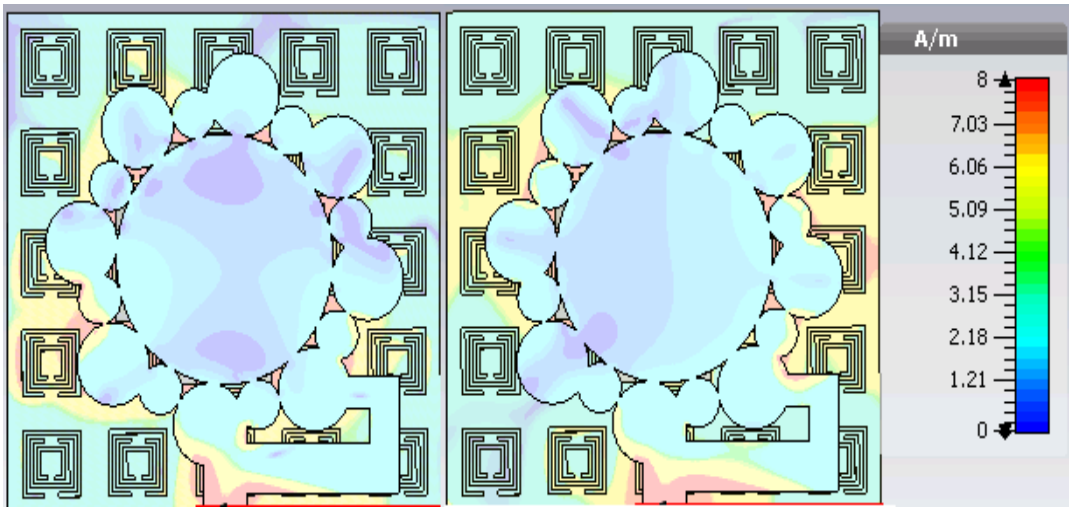

Fig.5.13. Surface current distribution in the proposed patch antenna

The detailed contrast of the developed and the preceding antennas is presented in table.5.2. From the tabular data, it can be noticed that the designed antenna is superior with regard to gain, bandwidth and overall active area.

Table.5.2. Comparison of present work with various developed antennas

Reference	Dimensions of the patch (mm^2)	Area(mm^2)	Centre Frequency (GHz)	Bandwidth (GHz)	Gain (dBi)	Application (s)
[107]	30 x 30	900	2.4/5.5	0.08/0.51	Not mentioned	Not mentioned
[108]	70 x 50	3500	1.71/2.28/ 3.03/ 3.84	2.78	2.85/2.98/ 4.04/4.73	L- and S-band applications
[109]	14 x 18	212	2.28/6.74	0.07/0.09	1/5.8	S- and C-band applications
[110]	10 x 12.5	125	6.62/7.52/ 8.96/12.37 /12.8/ 13.75/14.1 5	0.27/0.33 /0.353 /0.46/0.48/0 .56 /1	3.25/3.35/ 3.53/4.45/ 8.7	4G applications
[111]	60 x 60	3600	3.18/4.31/ 6.42/ 7.58/11.28 / 12.64	0.108/0.10/ 0.142/0.112 /0.008/ 0.036	2.32/1.25/ 3.89/4.1/6. 74/ 7.2	Space and military applications
[112]	46.4 x 46.4	2152.96	2.55/5.25	Not mentioned	6/7.2	WiMAX/W LAN
[113]	12 x 13.5	162	2.9/4.2	1.6/1	5-6	WLAN
[114]	25 x 35	875	2.45/3.55	1.6/0.5	8.9	Bluetooth/I OT/ 5G
[115]	32.7 x 39.5	1291.65	2.4/2.6	Not mentioned	3.65/4.71	Bluetooth
[116]	46 x 44	2024	1.07/ 3.119/ 4.089/ 5.683/6.51 4	Not mentioned	Not mentioned	L-/S-/C-band applications
[117]	48 x 41	1968	2.5/3.51	0.25/0.37	4.08/5.024	WLAN/ Bluetooth/ ZigBee/Wi-Max/ IMT band applications

[118]	27 x 10	270	14.25	3.7	6.2	Air-to-Ground Communications
[119]	25 x 25	625	3.23/4.93/ 7.09	4.99	1.1/0.8/1.02	S-/C-band applications
[120]	30 x 24.8	744	3.3/5.5/7.3 /9.9	0.11/0.28/1.01/ 0.56	0.7/0.65/1.1/ 1.7	WiMAX, and X-band applications
[121]	17 x 23	391	4.4/6.8/9.6	4.35	7.5	WiMAX, and X-band applications
[122]	20 x 16	320	2.4/5.2	0.31/0.21	2.7/2.5	WLAN
[123]	15 x 15	225	0.5/1/1.57/ 1.7/ 2.43/2.8/3.05	2.55	0.1/0.8/-0.5/1.9/-1/1.2/0.9	GPS/Blueto oth/WiFi
[124]	50.9 x 33	1679.7	2.9/3.4/7.5	0.2/4.2	2.1/1.3	UWB applications
Proposed Antenna	23.5 x 16	376	5.25/ 8.25	1.2/2.2	3.75/5.2	WLAN/WiMAX

5.6. Conclusion

In this chapter, metamaterial loaded antenna mounted on the DGS ground plane is developed. The present study concludes that the specifications of the designed antenna are controlled by implementing multilayer substrate, introducing metamaterial cells, Jerusalem shaped DGS slot on the ground layer, dual feed. Overall volume of the design is reduced with the impedance bandwidth being 1.2GHz and 2.2GHz in the frequency ranges of 4.9GHz~6.1GHz and 7.1GHz~9.3GHz respectively. The designed antenna is suitable for WLAN/WiMAX applications.

Beam switching/sweeping plays a vital role in the modern-day communications. Beam-switching is desirable with high gain with low cross-polarization levels. This feature cannot be achieved with the antenna proposed in this chapter. Hence, slotted waveguide antenna discussed in the sixth chapter is a suitable candidate for high gain beam switching/sweeping applications.

CHAPTER 6

Design and analysis of a double broken ring meta post loaded slotted waveguide antenna array

6.1. Introduction

Extending the work performed in the fifth chapter, a slotted waveguide antenna array loaded with metamaterial posts for beam-switching is addressed here. Patch antennas have many limitations when they are deployed in beam-forming and beam-switching applications. Beam forming is a challenging objective to meet in electrically small antennas. To obtain better results, slotted array waveguide antenna is opted.

In this chapter, meta-post loaded slotted waveguide antenna is explored.

The second design (broken ring slotted patch antenna) in the chapter-2 is wrapped along with ground layer. The broken ring slots on the radiator are converted to meta posts to form a rectangular cavity. This yields simple meta-post loaded waveguide. This structure acts as a simple bandpass filter. When the slots are etched on the waveguide with appropriate dimensions, meta-post loaded slotted waveguide antenna array is formed. This antenna is devised to operate in the frequency band ranging from 3GHz to 4.5GHz. In India, high data rate systems are slowly shifting towards sub-6GHz window. Sub-6GHz window includes the frequency ranging from 3GHz to 4.5GHz. 5G technology has been introduced by the Government of India by allotting frequency band ranging from 3GHz- 4.5GHz. This frequency allotment has paved way to the research in 5G technology in direction of its features which include MIMO, beam-sweeping/switching etc. devices. Beam-sweeping/switching feature occupies a vital place in enhancing data rates in the 5G communication systems.

In literature, various structures are presented to achieve beam-switching and high gain.

In [125], a slot loaded circular waveguide antenna resonating at 2.8GHz is presented. The proposed is omnidirectional in the E-plane, and exhibits approximately “8” radiation pattern in H-plane. Beam-switching is achieved in [126] by rotating the dielectric slabs. A deflection of 14^{o} degrees is achieved at 9.35GHz. A beam-steerable slotted waveguide antenna in [127] possesses beam sweeping feature with beams swept from 17 ° to 73 °. The beam sweeping is accomplished by varying the voltage of the antenna from 11 Volts to 2.8 Volts. The variation in the voltage is reflected through the fluctuation in the capacitances of varactors from 0.2 pF

to 0.5 pF.

In this chapter, detailed design methodology of meta-post loaded slotted waveguide antenna array is presented. Figure.6. presents the design methodology of the antenna presented in chapter-6.

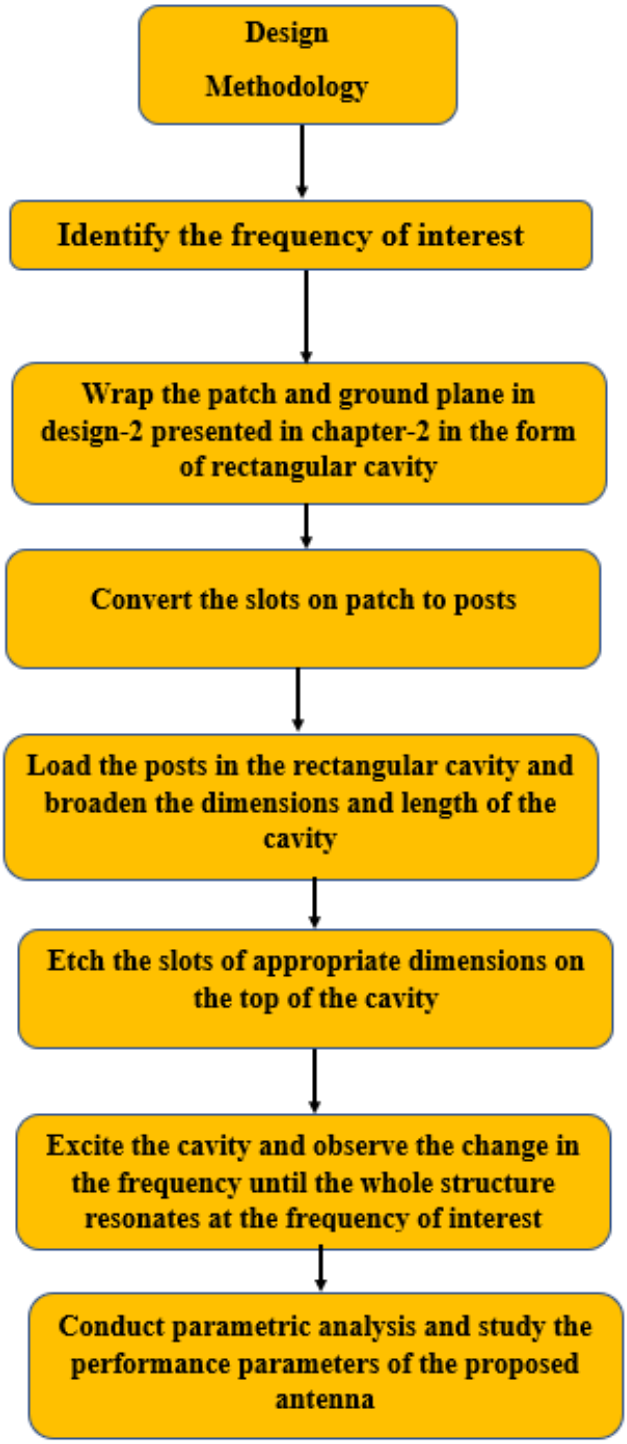

Figure.6. Design methodology of the antenna presented in chapter-6

6.2. Detailed design of the proposed antenna

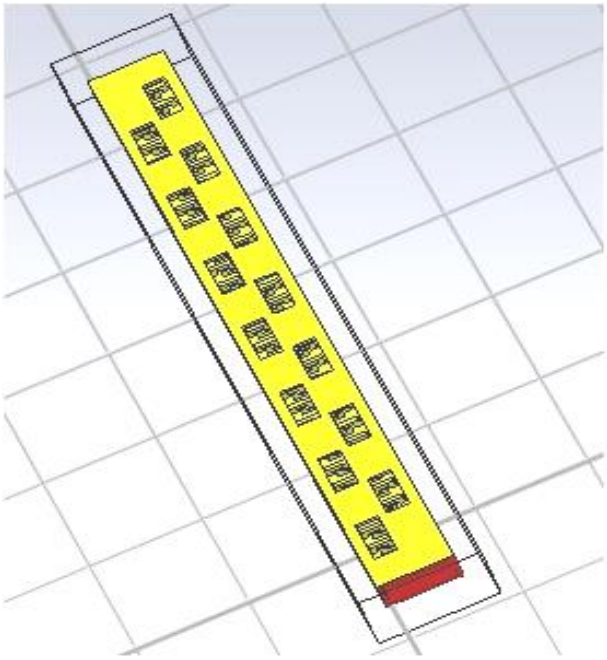

Fig.6.1.(a). Slotted waveguide antenna

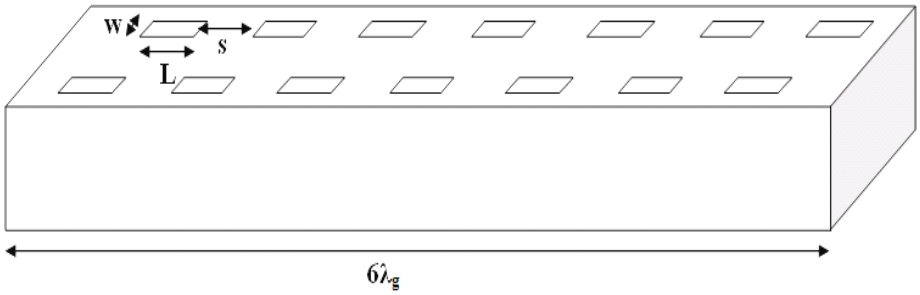

Fig.6.1. (b). Dimensions of the slots

The designed slotted waveguide antenna are having dimensions (a x b) of 24" x 12". TE_{10} mode is used to excite the antenna. Waveguide has a total length of $6\lambda_g$. Waveguide is etched with 14 slots on its top as presented in figure.6.1.(a). The designed slotted waveguide antenna resonates in the frequency window of 3GHz~ 4.5GHz. The structural aspects of the designed antenna are presented with the help of figure.6.1.(b). The radiating frequency of each slot is obtained as 4GHz and length of the slot (L) is 48mm. Slot width is of quarter wavelength and is obtained as 24mm. The slots are etched in such a way that they are at a distance of $\lambda_g/4$ from the both the ends. The meta posts are shorted to the walls of waveguide. The structure of the designed meta-post cell is presented in figure.6.2. The width (d) of the broken rings is 4mm. The dimension of the meta-post cell is of quarter wavelength and is obtained as 48mm. The breadth (U) is of the post is fraction of guided wavelength and is obtained as 24mm. To achieve the beam-switching/sweeping feature, 33 meta-posts are shorted inside the waveguide. The

spacings (s_o, s_1, s_2, w_o & w_1) are $\lambda_g/48$, $\lambda_g/32$, $\lambda_g/48$, $\lambda_g/48$ and $\lambda_g/48$ respectively. The posts are placed with a spacing of 28mm.

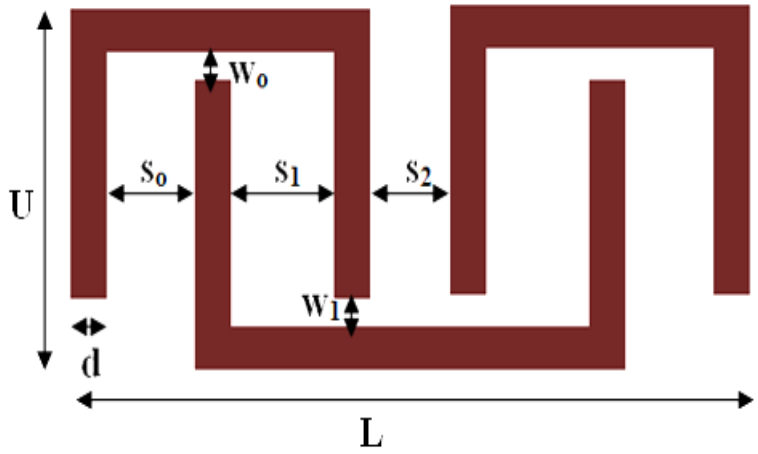

Fig.6.2. Proposed meta post cell.

Figure.6.3 presents the electrical model of the designed metapostcell.

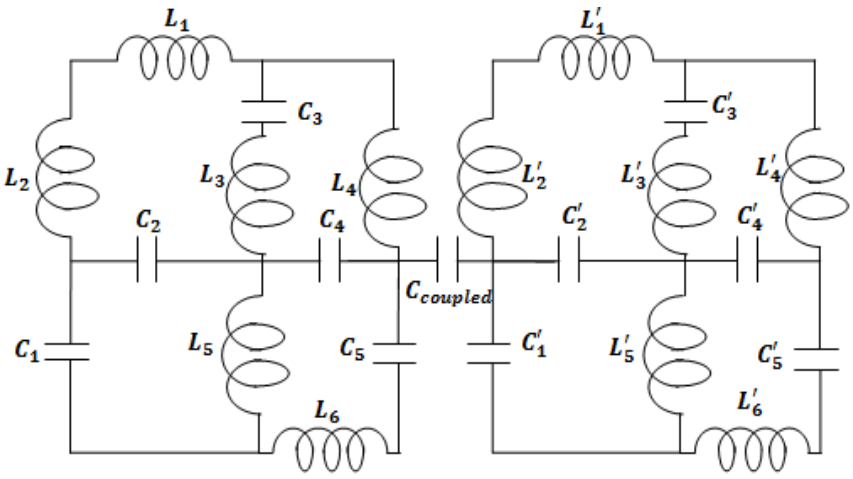

Fig.6.3. Electrical model of the unit cell.

6.3. Optimization and design analysis

The impact of meta-posts over the impedance bandwidth depends on the number of meta-posts loaded inside the waveguide. The change in the bandwidth with the meta-posts is presented in the figure.6.4. The fluctuation in the bandwidth is noticed by changing the quantity of meta-posts from 12 to 24. When 12 meta-posts are embedded inside the waveguide, the proposed antenna operates at 3GHz, 3.1GHz, 3.21GHz and 3.64GHz with the impedance bandwidths of 110MHz, 213MHz, 178MHz, and 123MHz respectively. When 24 meta-posts are shorted inside the waveguide, it operates at 3GHz and 4.5GHz with the impedance bandwidths of 112MHz, 312MHz respectively. When 30 meta-posts are deployed, the antenna operates at 3.32GHz with the operational bandwidth of 212MHz. The enhancement of number of meta-

posts beyond 30 enhances the impedance bandwidth in the desired frequency window.

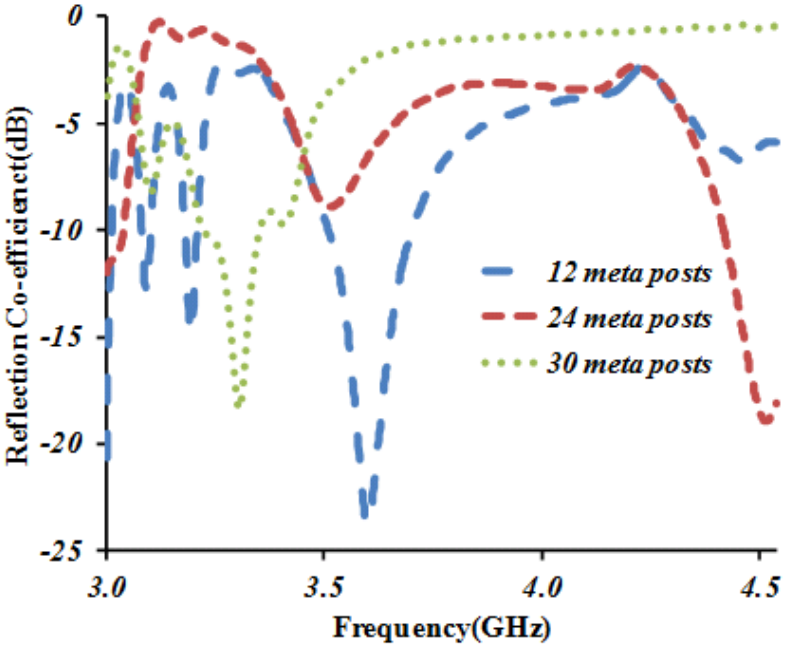

Fig.6.4. Variation in the impedance bandwidth with the number of meta-posts.

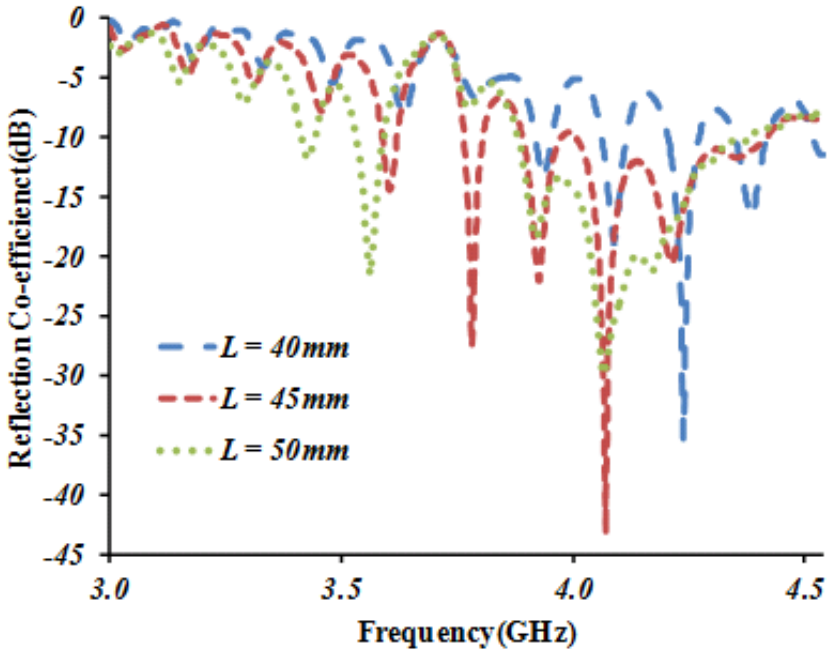

Fig.6.5. Impact of dimensions of the slot on the impedance bandwidth.

The impact of dimensions of the radiating slot over the operational or impedance bandwidth is presented in the figure.6.5. If the slot length is changed from its conventional length, the waveguide antenna exhibits multi-frequency characteristic and the same time, the fluctuation in the slot length reduces operational bandwidth.

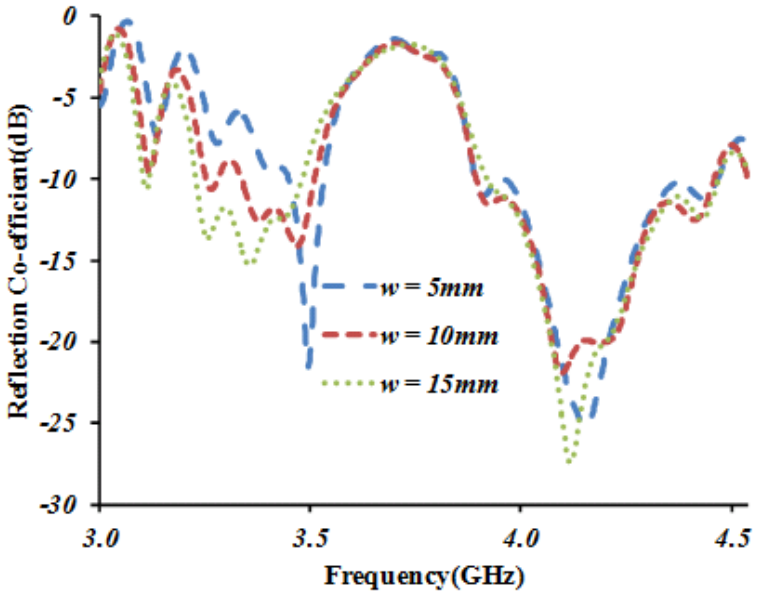

Fig.6.6. Impact of the slot width over the impedance bandwidth of the designed antenna

The impact of the radiating slot width over the operational frequency range is illustrated using figure.6.6. The operational bandwidth increases drastically when width of the slot is tuned to 20mm. Unacceptable results are observed if the width of slot is increased beyond 20mm.

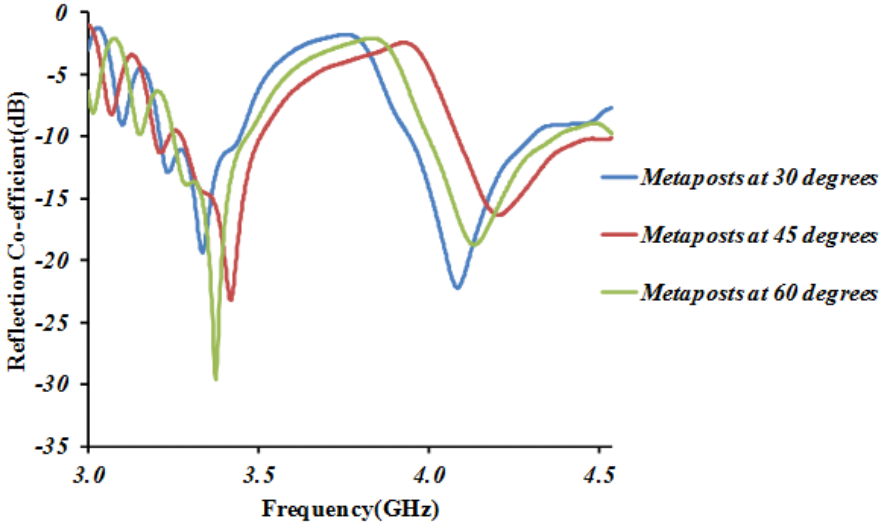

Fig.6.7. Variation of impedance bandwidth with the inclination of meta-posts

The fluctuation of return loss with the variation in the angle of tilt of meta-post is presented in figure.6.7. The degradation in the bandwidth is notice with the step-wise increment in the tilt of post. The increase in the tilt not only degrades the bandwidth but also shifts the resonant frequency. To achieve the best results, meta-posts are shorted perpendicularly to the inner axis of the antenna. With the increase in the inclination beyond 60 degrees, the feature beam sweeping cannot be accomplished. Hence, the parametric analysis is restricted to the inclination of meta-post of 60 degrees.

6.4. Results and Discussions

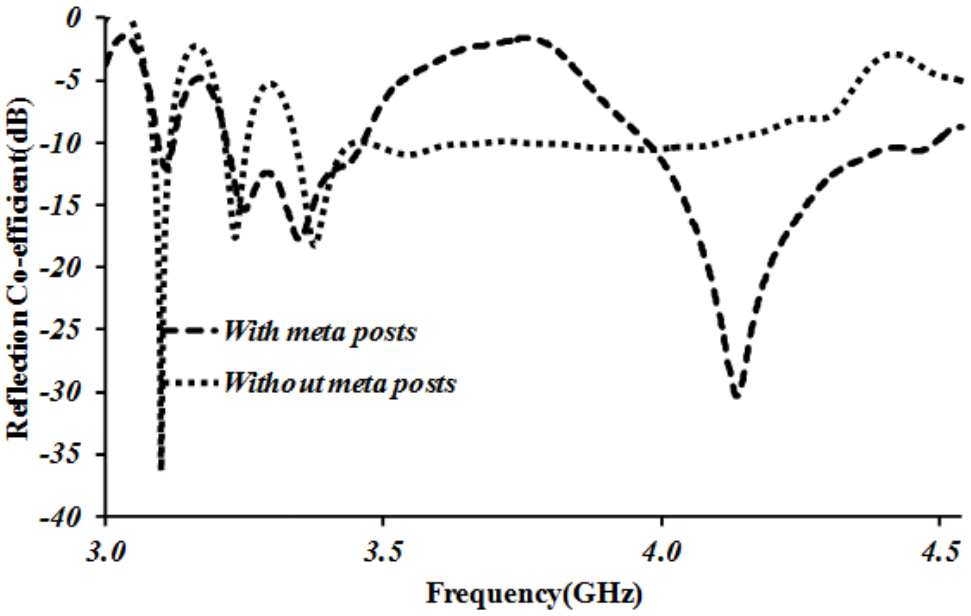

Fig.6.8. Impedance bandwidth of the designed antenna

The operational bandwidth of the basic slotted waveguide antenna array and the designed antenna is presented in figure.6.8. The designed antenna is designed to operate at three different sub-bands namely 3.1GHz, 3.32GHz and 4.1GHz.

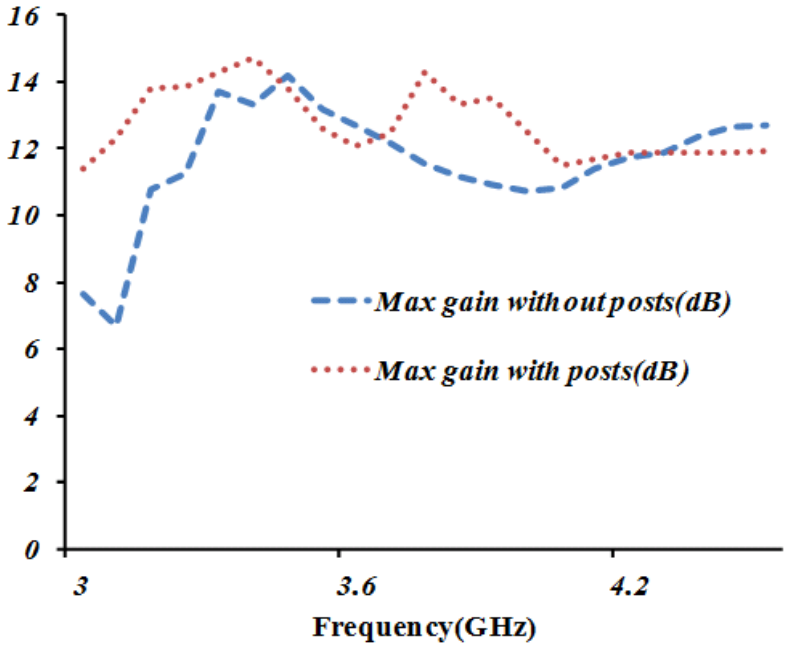

Fig.6.9. Gains of the antenna with and without meta-posts

The gains of designed structure and basic slotted waveguide antenna are shown in figure.6.9. An improvement in the gain is observed in the meta-post loaded antenna. The gains vary from 12.1dBi – 14.5dBi in the frequency range of 3.32GHz – 4.1GHz respectively.

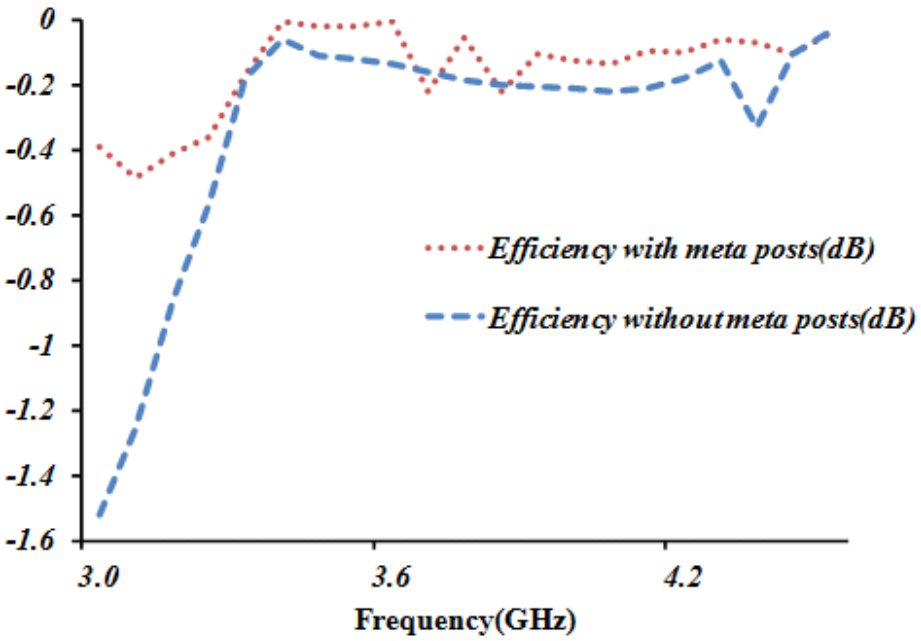

Fig.6.10. Efficiencies of slotted waveguide antenna with and without meta posts

The efficiencies of the designed structure before and after insertion of meta-posts are presented in figure.6.10. The efficiencies vary from 94% to 99% in the frequency range of 3GHz – 4.2GHz. Meta-post loaded antenna is highly efficient than slotted waveguide antenna without meta-post.

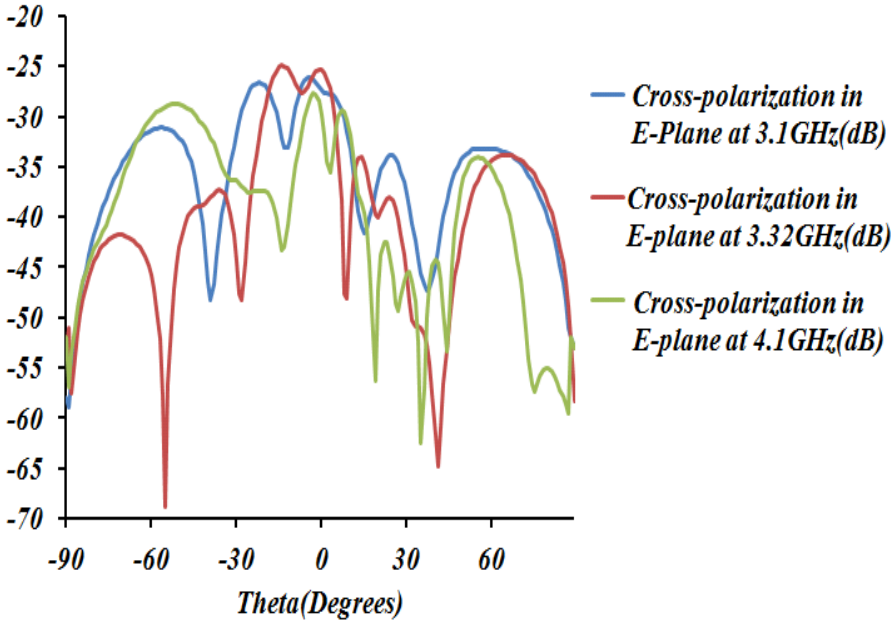

Fig.6.11.a. Cross polarization in E-plane

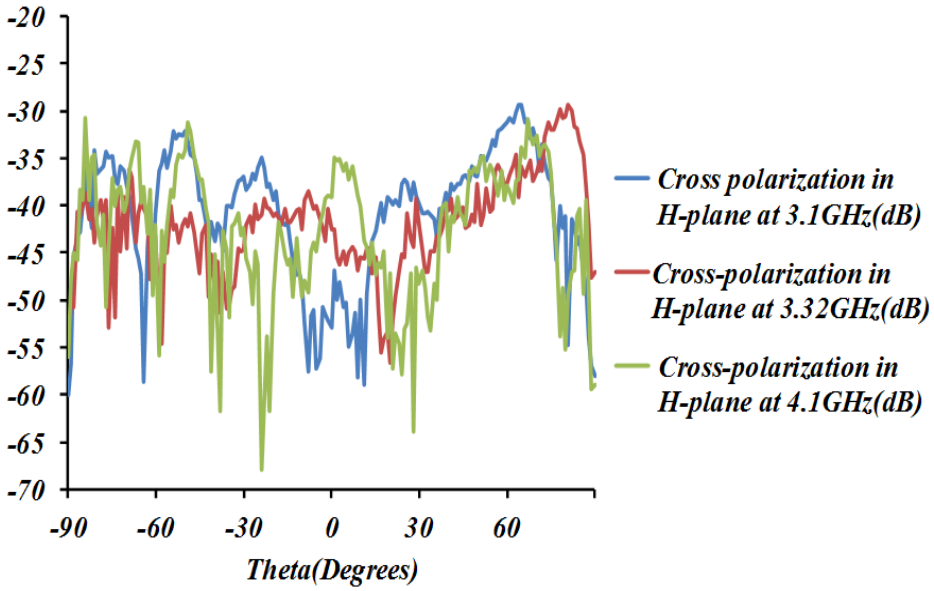

Fig.6.11.b. Cross polarization in H-plane

Cross-polarization levels of designed structure are illustrated using figure.6.11.(a) and 6.11.(b). It is observed that the cross-polarization levels are below -60dB at the frequencies of operation when the antenna is loaded with meta-posts.

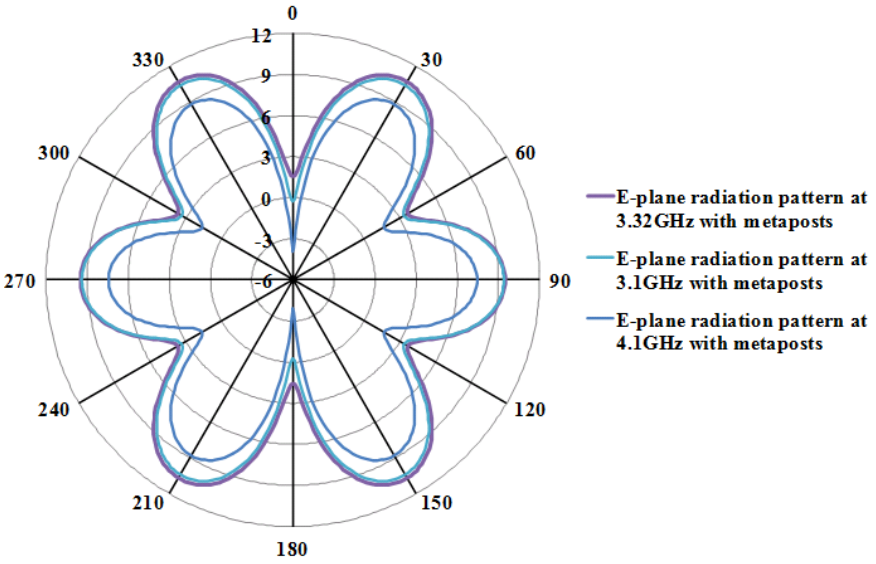

Fig.6.12.(a). Radiation patterns in E- plane.

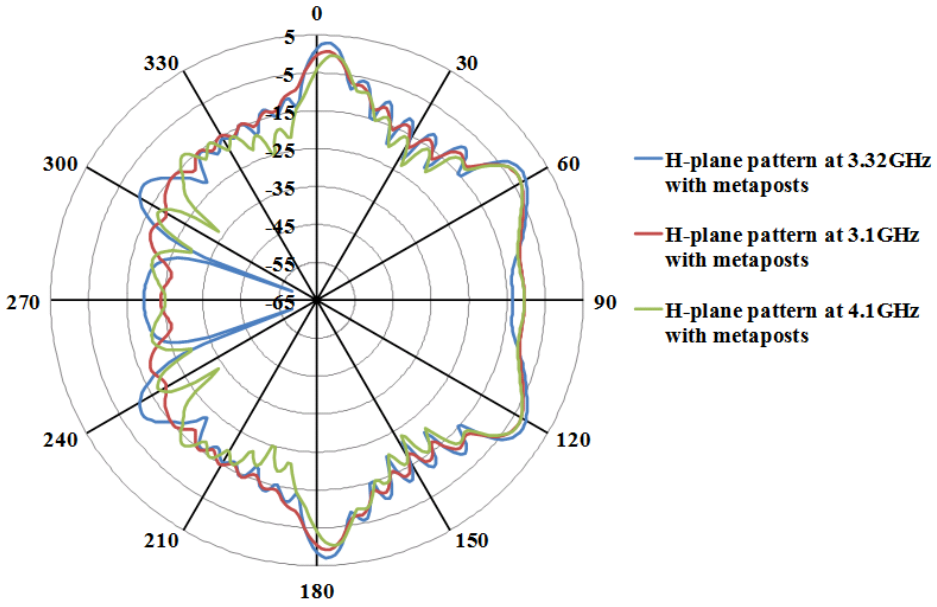

Fig.6.12.(b). Radiation patterns in H-plane.

The antenna patterns of the designed in all the planes at the radiating frequencies are illustrated using figure.6.12.(a) and 6.12.(b). In E-plane, the antenna exhibits flower-shaped radiation pattern. In H-plane, it exhibits dumbbell shaped radiation pattern

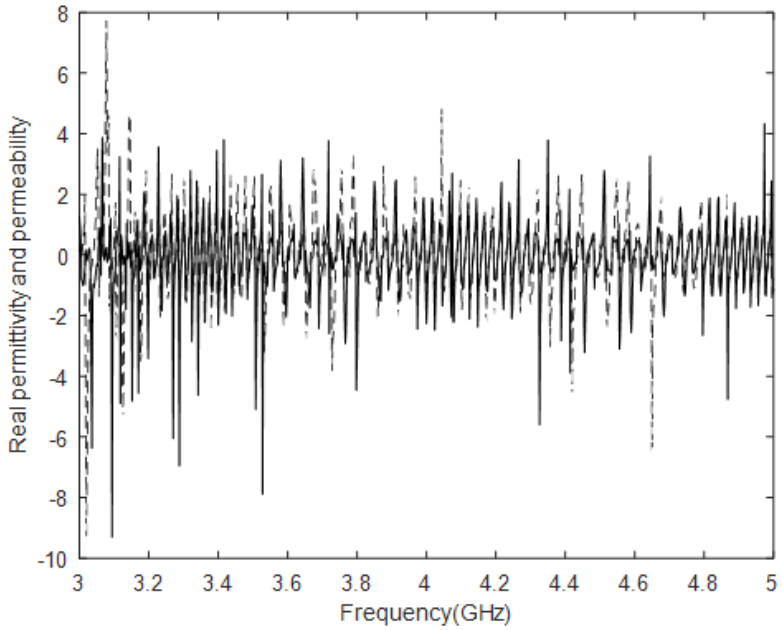

Fig.6.13.(a). Real part of permittivity and permeability of an unit cell meta-posts.

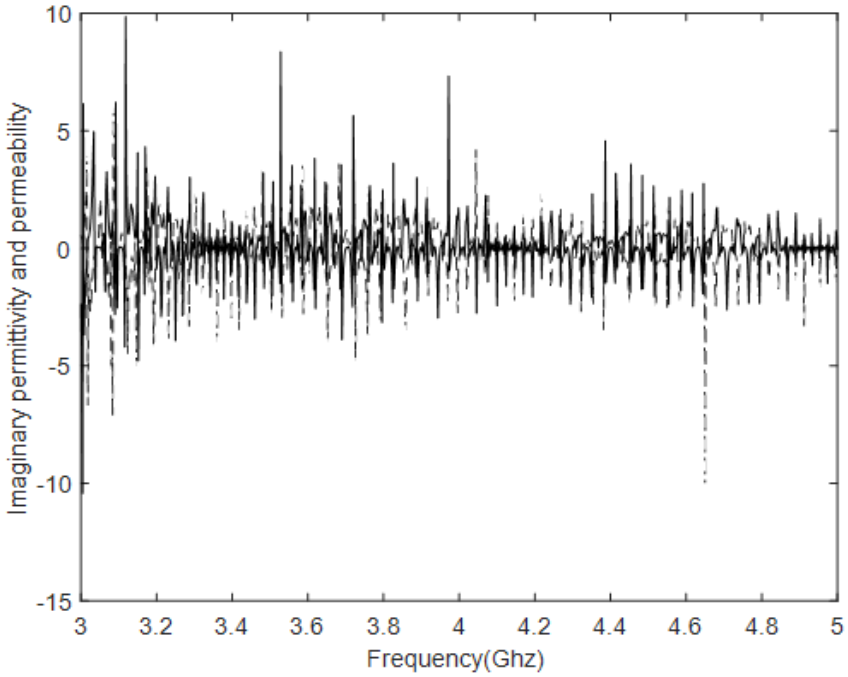

Fig.6.13.(b). Imaginary part of permittivity and permeability of an unit cell meta post

Nicholson-Ross-Weir method is used to compute permittivity and permeability. This method is implemented for obtaining S-parameters from CST-microwave studio. Mathematical calculations are done in MATLAB for obtaining permittivity and permeability plots. It is observed that the proposed meta-post possesses double negative (DNG) characteristics in the frequencies ranging from 3GHz to 4.5GHz as shown in figure.6.13.(a). It is inferred that the meta-post is Double Negative (DNG). Imaginary permittivity and permeability plots are presented in figure.6.13.(b). The DNG feature in the meta-post makes the proposed antenna radiate in all the directions especially in the reverse directions. This feature helps the antenna to acquire beam-sweeping/switching characteristic which is essential in 5^{th} generation systems. Table.1 shows the comparison of designed antennas with the developed waveguide antennas.

Table. 6.1 Comparison of designed antennas with the developed waveguide antennas

Reference	Frequency Bands (GHz)	Bandwidth (GHz)	Gain (dBi)
[128]	2.25 & 4.91	Not mentioned	14.6 & 17.1
[129]	3	Not mentioned	17
[130]	2.5~4.9	Not mentioned	11.12 & 18.9
[131]	3	Not mentioned	16.6
This work	3.1, 3.32 & 4.2	0.11, 0.24 & 0.54	11.3, 14.1&12.6

6.5. Conclusion

The designed slotted waveguide antenna array is devised and analyzed in this chapter. This exhibits the beam switching (sweeping the beam across all the angles) characteristic which is an essential feature for 5^{th} generation systems and C-band communications. If the meta-post is further broken and evolved into quadruple broken post then the radiation beams can be increased to sweep across all the angles. A wide bandwidth, multifrequency feature, enhanced gain and improved efficiency set the designed antenna apt for 5^{th} generation and C-band satellite communications.

Meta post loaded slotted array waveguide antenna is apt for high gain applications. But complex and bulky nature of this antenna makes it prone to high ohmic losses and radiation deflections. Hence, stable radiation patterns cannot be achieved with these types of structures. The solution to these problems is to design concatenated antennas as discussed in the seventh chapter.

CHAPTER 7

Concatenated Antennas

7.1. Introduction

In the preceding chapters, the importance of gain enhancement and miniaturization were discussed. The reduction the active area is an important specification in the patch antennas. To meet this specification, different types of EBG structures were presented in the previous chapters.

PBG and EBG structures facilitate antennas to radiate at multi-frequencies with a reasonable guard band between the frequencies of interest. These structures eliminate spurious radiations due to surface waves and improve antenna's performance [133]-[136]. These structures possess the reconfigurable characteristic which is an essential feature in the upcoming generations of wireless communications.

Apart from the multiband switching in 5G, gain improvement is required and it is challenging to achieve enhanced gain along with the compatibility. EBG and PBG structures are suitable candidates in achieving enhanced performance parameters with reasonable compatibility [137]-[138]. These structures further introduce multi-frequency feature in the patch antenna and thereby making the resultant prototype suitable candidate for advanced communications [139]-[140].

This chapter presents the concept of concatenated antennas by mounting the oval ring patch antenna discussed in the second chapter on the ground plane with serpentine patch antenna discussed in second chapter serving as EBG structure.

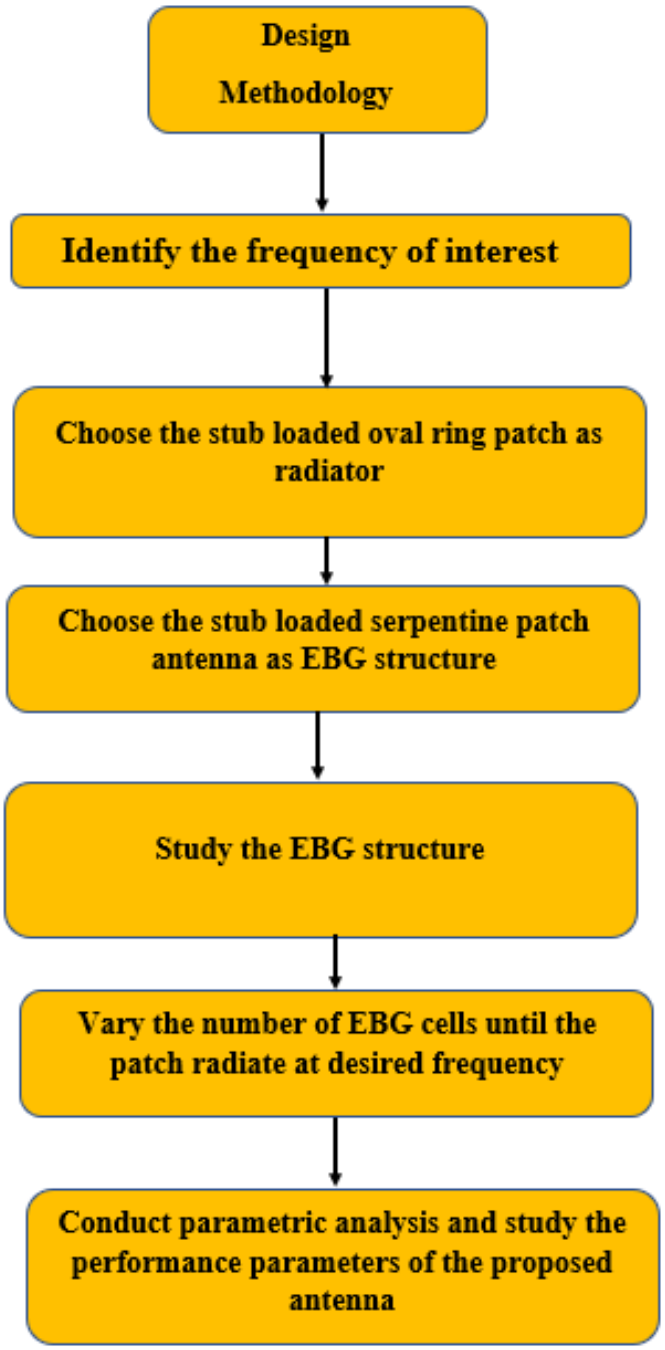

Fig.7. Design methodology of antenna in chapter-7.

7.2. Detailed design of the antenna

The oval patch antenna loaded with stubs presented in chapter-2 is chosen as radiating element. This antenna is printed on RT/duroid-5880 (ε_r = 2.2) having the height of 0.8mm. The designed structure has a volume of 18 x 18 x 0.8mm^3. The proposed is loaded on the ground plane etched with serpetine shaped EBG slots. The shape of the EBG cell is derived from the stub loaded serpentine shaped patch antenna discussed in chapter-2. As disccused in chapter-2, this antenna antenna operates at lower giga-hertz frequencies. Thus, this antenna is used as a basis to achieve the required degree of miniaturization. The ground plane consists of 12 EBG cells to achieve desired results. Parametric analysis is carried out in the further sections to study the impact of number of EBG slots over the operational bandwidth of the designed antenna. The proposed EBG cell is presented in the figure.7.1. The analysis has also been carried out on serpentine patch antenna with stub loaded oval ring as HIS ground plane. But the design has not yielded desired results.

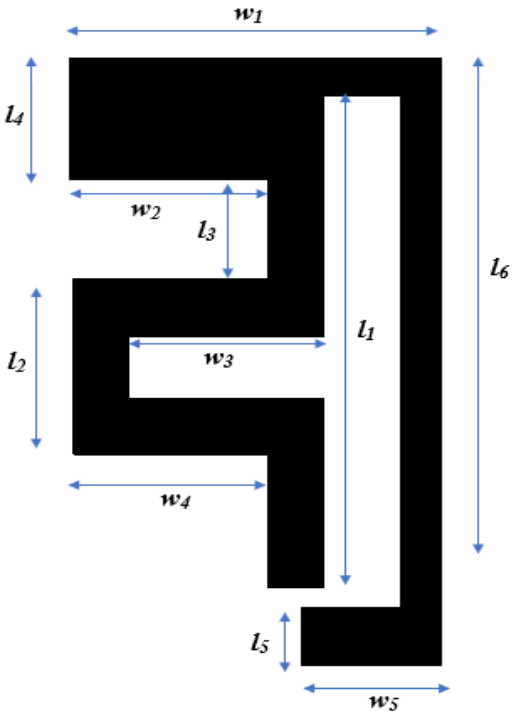

Fig.7.1. Proposed serpentine cell.

The comprehensive dimensions of EBG are retrieved from chapter-2. The design aspects of the proposed EBG cell are disclosed in the table.7.1.

Table.7.1 Detailed dimensions of serpentine EBG cell

Dimension	l_1	l_2	l_3	l_4
Value(mm)	1	0.4	0.2	0.3
Dimension	l_5	l_6	w_1	w_2
Value(mm)	0.1	1.1	0.3	0.15
Dimension	w_3	w_4	w_5	
Value(mm)	0.2	0.25	0.15	

The designed antenna along with the EBG ground layer are presented in figure.7.2. The detailed spacings between the EBG cells are also disclosed.

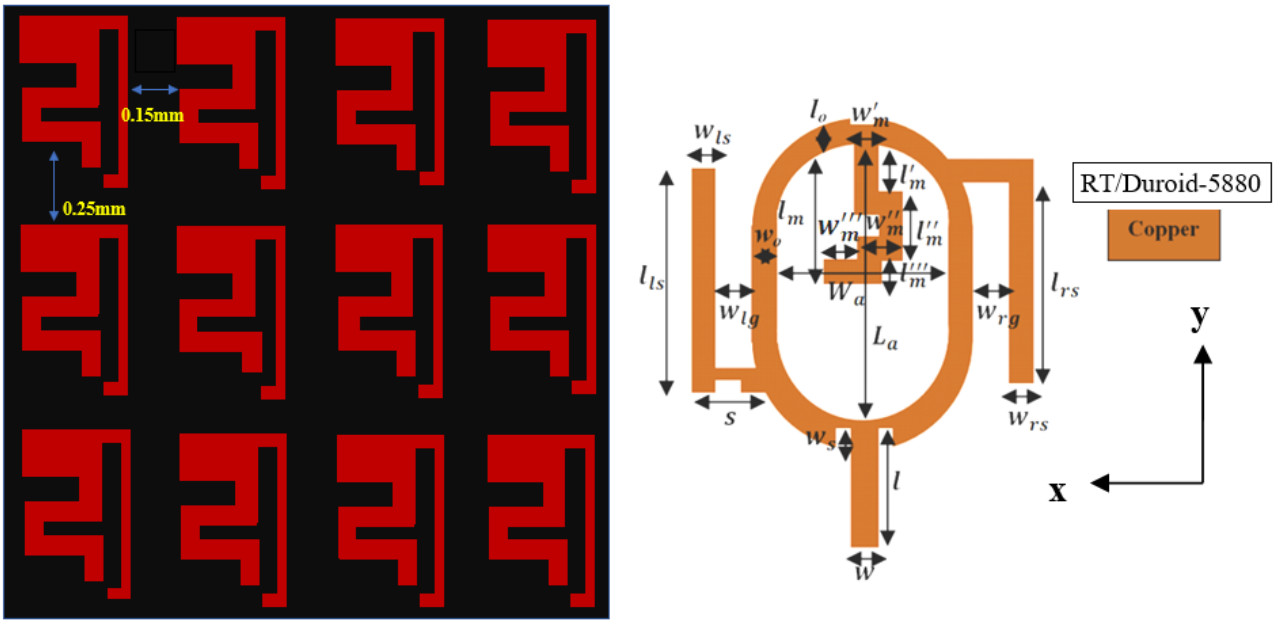

Fig.7.2. Proposed structure of the designed antenna.

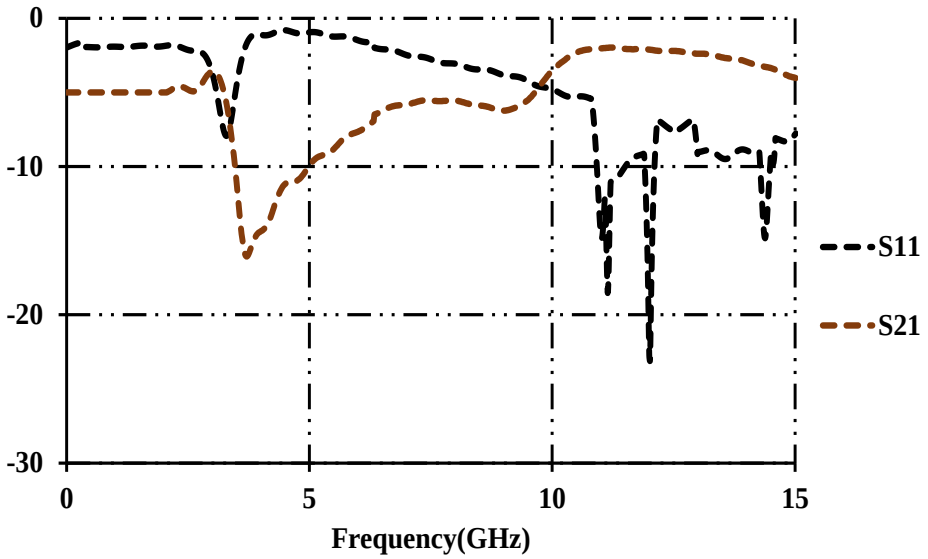

Fig.7.3. Return and insertion losses of unit EBG cell.

The return and insertion losses of a unit EBG cell are presented in figure.7.3. It is observed that EBG cell resonates at the operational frequencies as that of the patch. This favours in shifting the resonant frequency in the antenna towards lower gigahertz range. The fluctuation in the impedance bandwidth with the EBG cells is presented in figure.7.4. The decrease in the EBG cells lowers the degree of miniaturization. Therefore, 12 EBG cells are chosen to get the better results. Resonant frequencies are tuned either by varying the number of EBG cells on the ground plane or by varying the area of the cells. Increase in the number of EBG cells beyond 12 yields undesired results and hence, they are not disclosed in the present chapter.

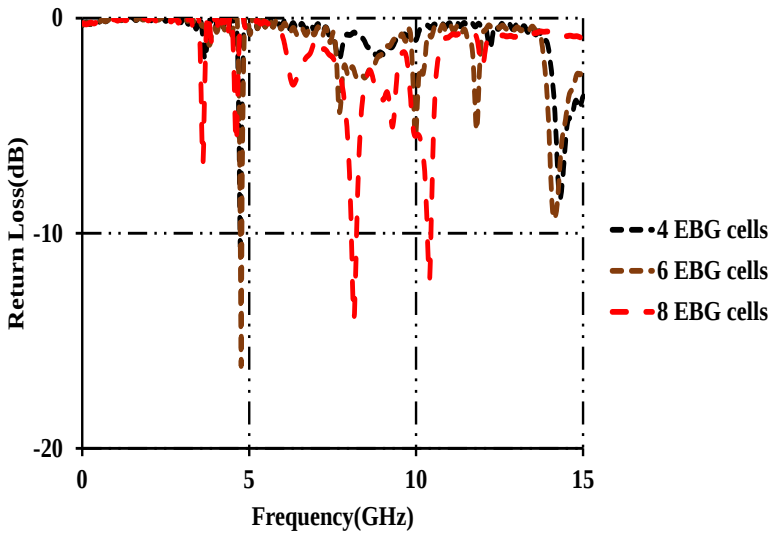

Fig.7.4. Impact of EBG cells on the reflection coefficient of the antenna.

7.3. Outcomes and Disquisitions

The impedance bandwidths of the antenna with and without EBG are presented in figure.7.5. By mounting on EBG ground, the patch is miniaturized by 89.1%.

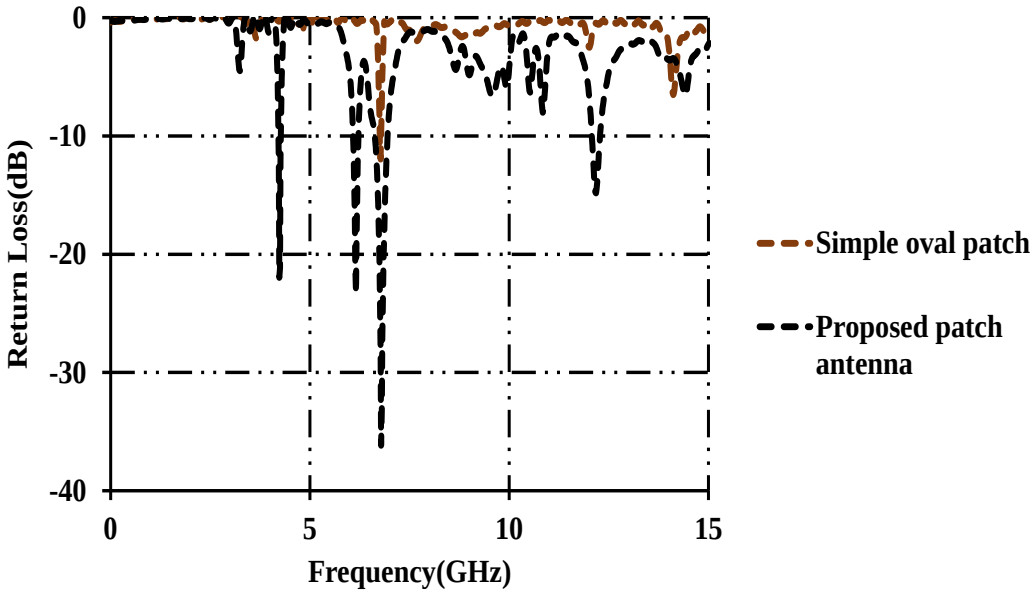

Fig.7.5. Impedance bandwidths with EBG structure and without EBG structure.

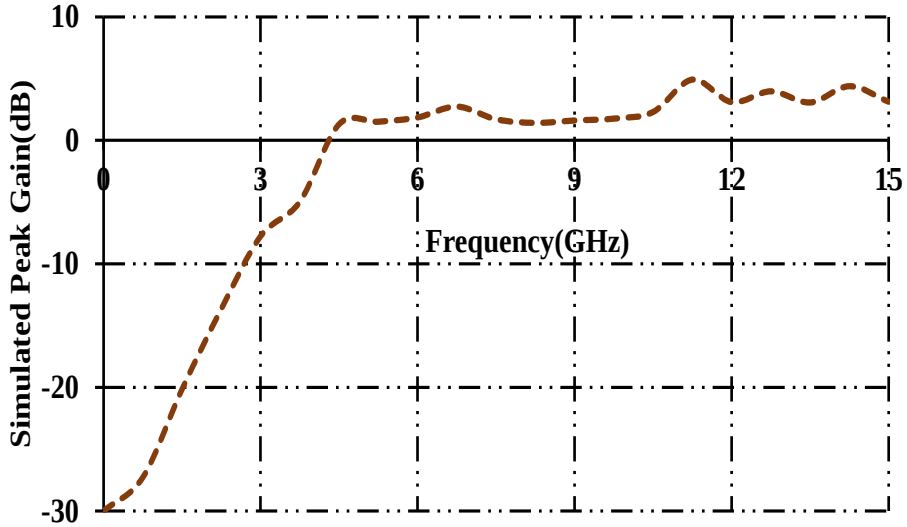

Fig.7.6. Peak gain of the designed antenna

The maximum gains of the developed patch are presented in figure.7.6. The gains ranging from 1.1dBi to 2.8dBi are noticed at all the operational frequencies. It is observed that the gain is stable at all the operational frequencies. As presented in figure.7.7.(a), the current is guided towards the radiating stubs and some current is confined to the ground layer. Current is

confined on the circumference of the oval at 6.15GHz as presented in figure.7.7.(b). From the figure.7.7.(c), it is seen that the current-density at 6.78GHz is diverted towards the ground plane and the current on the patch decreases drastically. Current is equally concentrated on ground plane and the patch at 12.15GHz as presented in figure.7.7.(d). The electrical length of the design is increased by introducing meander lines which will divert the surface currents through a longer path and thereby shifting the frequencies towards the lower gigahertz range.

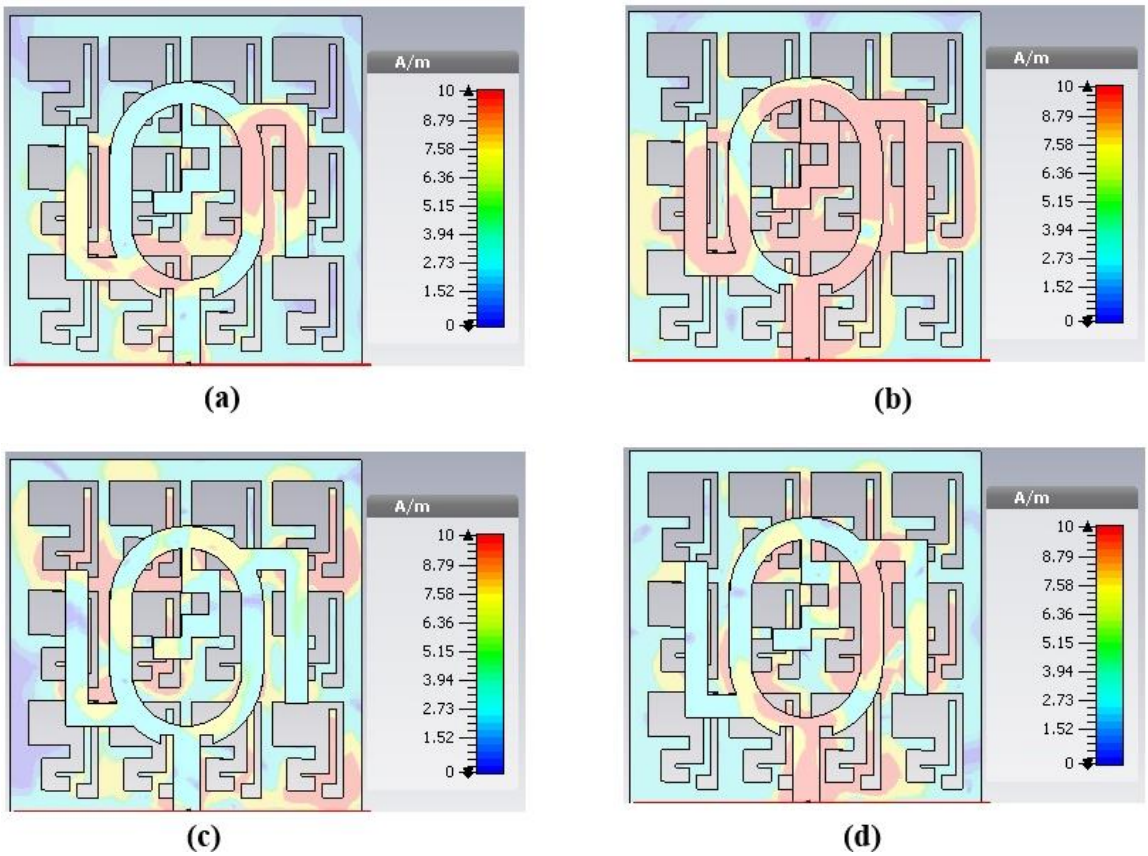

Fig.7.7. Distribution of current densities at (a).4.28GHz. (b).6.15GHz. (c).6.78GHz. (d).12.15GHz

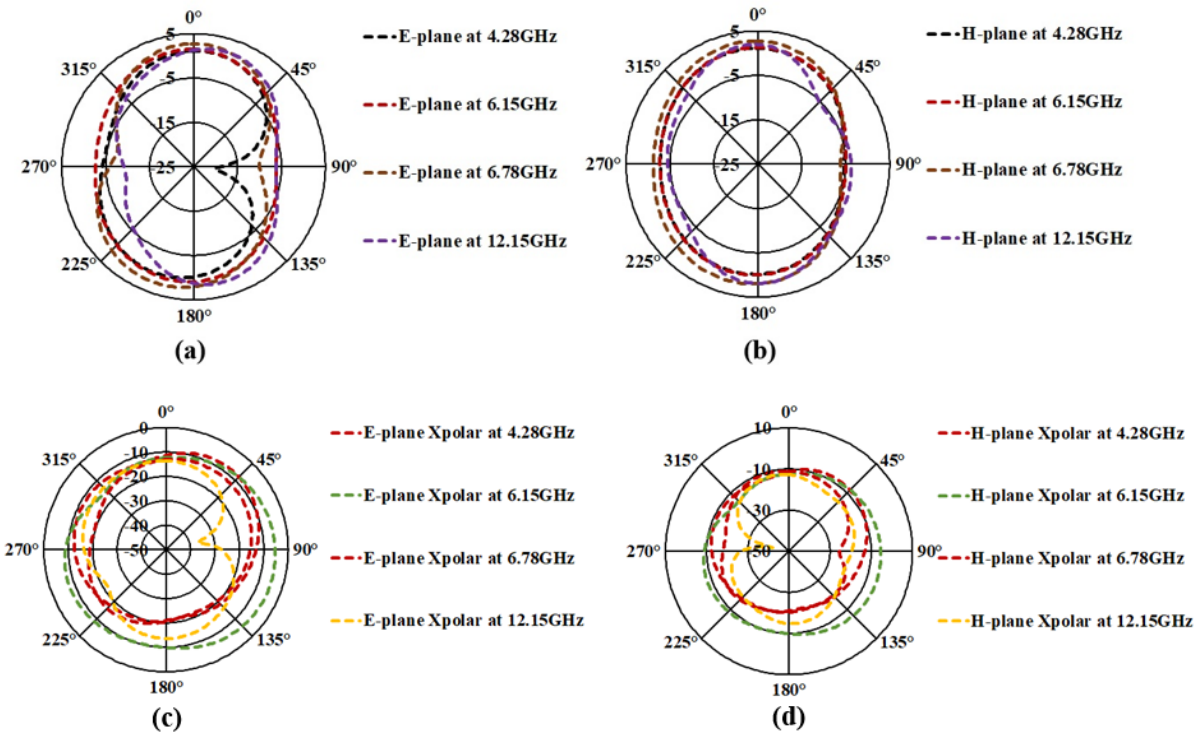

Fig.7.8. Radiation patterns at 4.28GHz, 6.15GHz, 6.78GHz and 12.15GHz.

The antenna patterns in both the radiating planes are observed in CST-MWS package. The radiation patterns in E-planes are presented in figure.7.8.(a) and figure.7.8.(c). The designed structure possesses bidirectional radiation patterns in E-plane at all the resonant frequencies. The radiation patterns in H-planes are presented in figure.7.8.(b) and figure.7.8.(d). The radiation patterns are bidirectional in shape in H-planes at all the frequencies of operation. As the frequency increases, the patch supports common mode currents which will distort the antenna patterns. For the same reason, these patterns are slightly distorted at 12.15GHz. Cross-polarization component is below -10dB at all the resonant frequencies.

A weigh up between the present work and the existing EBG antennas is presented in table.7.2. The designed structure is superior in terms of active area, gain and is suitable for multi-frequency applications.

Table.7.2 Weighing up the designed antenna with the preceding PBG/EBG antennas

Reference	Area (mm^2)	Frequency(ies) (GHz)	Peak Gain(s) (dBi)
[141]	800	2.45	4.48
[142]	3600	4.57 and 5.06	1.87 and 1.56
[143]	3354	3.76, 7.5 and 11.84	8, 9.5 and 9.7
[144]	896	4, 6,8,10,14 and 17	4 - 6
[145]	81.37	9.7	7.7
Proposed antenna	**70**	**4.28, 6.15, 6.78 and 12.15**	**1.1, 1.3, 2.8 and 2**

7.4. Conclusion

This chapter presents the concept, design and parametric analysis of concatenated antennas. The oval ring patch radiator discussed in the 2nd chapter is mounted on the EBG structure wherein the EBG slot is etched in the shape of stub loaded serpentine patch antenna. Overall volume of designed antenna is $18 \times 18 \times 0.8mm^3$. The antenna operates at 4.28GHz, 6.15GHz, 6.78GHz and 12.15GHz. The designed antenna is miniaturized by 89.1% by using the suggested EBG structure. The antenna patterns and the gain of antenna are almost steady and constant at frequencies of operation. The antenna is an apt candidate for C- and K_u-band communications.

CHAPTER 8

Conclusion

This chapter is mainly separated into two segments: (i) conclusions of the complete research work, which have been discussed in the presented thesis, and (ii) the impending purview of the given research work.

This thesis mainly concentrated on the miniaturization, high gain, stable gain high bandwidth, stable radiation patterns and beam sweeping/ switching.

8.1 Conclusion of the Presented Work

In the first chapter, a brief introduction different conventional microstrip patch antennas and their limitations were discussed. Next, a brief literature survey was conducted about the improvised patch antennas. Next, the modal analysis was studied in to identify the higher order propagation modes in the patch antennas which were described in the further chapters. In the end, different types of models like transmission model and cavity model were discussed to study the radiating fields in the patch antennas. This introduction laid the foundation that is essential to appreciate the work performed in this thesis.

In the second chapter, we started with two conventional rectangular patch antenna and oval patch antenna. But it was found that gain and efficiencies are low in these designs. To counter these problems, the gain enhancement was achieved using quarter wavelength stubs. Two types of antennas i.e. serpentine patch antenna loaded with stubs (Design-1) and oval ring patch antenna loaded with stubs (Design-2) were developed. On the other hand, bandwidth degrades with the increase in the gain. This counter this problem, partial ground plane is deployed in design-1. The variation in the bandwidth and the gain were studied using parametric analysis and design-1 and 2 were optimized accordingly.

In the third chapter, we introduced dumbbell shaped high impedance surfaces (HIS) are designed and studied. Stub-loaded antennas lack essential features like high gain, stable gain and might not be useful for many applications due to it. The antenna's throughput is improved by mounting it on the high impedance surfaces such as DGS, EBG and metamaterials. The oval

ring antenna discussed in 2nd chapter is mounted on dumbbell-shaped high impedance surfaces. The impact of these surfaces over the antenna's throughput is discussed.

In the fourth chapter, we explored two types of EBG loaded patch antennas after getting motivation from second chapter. These antennas are designed to achieve high bandwidth without degradation in gain and efficiency. In the first design (dumbbell patch antenna mounted on splattered ring EBG), a wide bandwidth of 20.2GHz is observed. A peak gain and efficiency of 9.01dB and 91.2% are observed across the operational bands. In the second design (Swastika shaped EBG bandwidth of 3.2GHz is observed. A peak gain of 11.92dBi is observed at 21.29GHz. These antennas are highly useful for high data rate communications.

In the fifth chapter, we explored a flower shaped patch antenna mounted Jerusalem cross shaped DGS and loaded with CSRR metamaterials. This antenna is designed to meet the requirements of miniaturization at lower gigahertz frequency range. The proposed structure with and without DGS and metamaterials is analysed to see whether antenna's performance parameters micht be improved. We showed that by using DGS and metamaterial together, the overall active area of antenna is significantly reduced with the improved impedance bandwidth of 26.50%.

Extending the work performed in the fifth chapter, we designed a meta-post loaded slotted waveguide antenna array in the sixth chapter. This antenna is designed by wrapping design-2 in chapter-4 in such a way that it forms a rectangular waveguide antenna. The slots on the patch are converted into meta-posts and loaded inside the waveguide. Extending its dimensions enhances performance specifications of the proposed antenna. The developed antenna possesses high gain and beam-switching property. This antenna fulfils the beam-switching requirements not only for 5G technology but also for latest wireless communications.

In the seventh chapter, we designed concatenated antennas. High impedance surfaces enhance the performance parameters and at the same time, these surfaces often induce ohmic losses. Proper dimensions of HIS cell must be chosen to get desired results. To circumvent this problem, concatenated antennas are introduced. The basic methodology to design this antenna is to deploy the 1st design chapter-2 as EBG and design-2 in chapter-2 as radiator. The features of two antennas are amalgamated to achieve improved performance of the proposed antenna. The volume of antenna is $18 \times 18 \times 0.8mm^3$. The designed antenna radiates at 4.28GHz, 6.15GHz, 6.78GHz and 12.15GHz. The antenna is miniaturized by 89.1% loading it on the

EBG ground with serpentine shaped slots. The antenna patterns and the gain of antenna are almost steady and constant at frequencies of operation.

8.2. Subsequent ambit of the thesis

This thesis gives the concepts of various stub-loaded patch antennas, and high impedance surfaces for achieving miniaturization, high gain, high efficiency, high bandwidth, stable radiation patterns, and beam-switching. A new concept of concatenated antennas is introduced in this thesis. This thesis conducted study on different dumbbell shaped high impedance surfaces and their impact on stub loaded oval ring patch antenna. This thesis also concentrated on basic designs of antennas, so these designs can further be developed to accomplish hyper wide-bandwidth. In miniaturized antennas, it is difficult to maintain high gain up to higher frequencies and at the same time it is difficult to maintain stable radiation patterns. Artificial intelligence devices must be used to direct the radiation leakages towards the antennas. These artificial devices direct the current on the patch with improved power gain and reduce the eddy current losses. Further, many techniques can be developed to improve the quality of communication from one place to another by introducing MIMO, fractal antennas, superstrates, Substrate Integrated Waveguide etc.

References

1. Ranjan Mishra, “An Overview Of Microstrip Antenna”, *HCTL Open International Journal of Technology Innovations and Research (IJTIR)*, Vol.21, issue.2, 2016. pp.1-17. DOI: 10.5281/zenodo.161524.

2. Ashish Jadhav, Nagashettappa Biradar, Husain Bhaldar, Mahesh Mathpati, Renuka Wadekar , and Manoj Deshmukh, “Multiband Circular Microstrip Patch Antenna for Wireless Applications”, *Wireless Personal Communications.*2022. DOI:https://doi.org/10.1007/s11277-022-09948-9.

3. Aakash Bansal, and Richa Gupta, “A review on microstrip patch antenna and feeding techniques”, *International Journal of Information Technology*, Vol.12, 2020.pp.149-154. DOI:https://doi.org/10.1007/s41870-018-0121-4

4. Zhan-Hong Zeng, Jian-Qi Li, Jia-Sheng Lin, Guan-Xiong Chen, and Xiao Zhang, “A New Perspective on E-shape and U-slot Patch Antennas: Current Reshaping, Patterns Correction, and Polarization Reversal”, *IEEE-International Conference on Microwave and Millimeter Wave Technology (ICMMT)*, 2020.pp.1-3. DOI: 10.1109/ICMMT49418.2020.9386975

5. Ali I. Abdalla, and Israa Hazem Ali, “Design and Modification of multiband M-slot patch antenna for wireless applications”, *IEEE-International Conference on Smart Communities: Improving Quality of Life Using ICT, IoT and AI (HONET)*, 2020. pp.1-4. DOI: 10.1109/ICMMT49418.2020.9386975.

6. Ajay Yadav, and R.P. Yadav, “Quarter wavelength parasitic stub loaded polarization reconfigurable patch antenna”, *Electromagnetics*, Vol.41, issue.6, 2021.pp.459-467. https://doi.org/10.1080/02726343.2021.2003026.

7. K.P.Ray, S.Nikhil, and A.Nair, “Compact Tunable and Dual band Circular Microstrip Antenna for GSM and Bluetooth Applications”, *International Journal of Microwave and Optical Technology*, Vol.4, issue.4, 2009. pp.205-210.

8. Amir Jafargholi, Ali Jafargholi, Jun H. Choi, Mehdi Veysi, and Ali Soleimani, “Microstrip patch back radiation reduction using metamaterial superstrate”, *IET-microwave, antenna and propagation*, Vol.14, issue.2, 2020. Pp.158-164. https://doi.org/10.1049/iet-map.2018.623.

9. Hilal M. El Misilmani,Mohammed Al-Husseini,Karim Y. Kabalan, “Design procedure for planar slotted waveguide antenna arrays with controllable sidelobe level ratio for high power microwave applications”, *Engineering Reports*, Vol.2, issue.10, 2020, pp.1-15. https://doi.org/10.1002/eng2.12255.

10. Wai Yan Yong, Abolfazl Haddadi, Thomas Emanuelsson and Andres Alay, “A Bandwidth-Enhanced Cavity-Backed Slot Array Antenna for mmWave Fixed-Beam Applications”, *IEEE-Antenna and propagation letters*, Vol.19, issue.11, 2020, pp.

11. E.Baum, Carl. *Sidewall Waveguide Slot Antenna For High Power*. Air Force Office of Scientific Research., 2005. Print.

12. Li, J.-Y., L.-W. Li, and Y.-B. Gan, "Method Of Moments Analysis of Waveguide Slot Antennas Using The EFIE". *Journal of Electromagnetic Waves and Applications* Vol.19, issue.13, 2005.pp. 1729-1748. https://doi.org/10.1163/156939305775696810.

13. Itoh, Keiichi, Katsumasa Miyata, and Hajime Igarashi, "Evolutional Design Of Waveguide Slot Antenna With Dielectric Lenses", *IEEE Transactions on Magnetics*, Vol.48, issue.2, 2017. pp.779-782. DOI: 10.1109/TMAG.2011.2176320.

14. Sekretarov, S. and Vavriv, D.M., "A Wideband Slotted Waveguide Antenna Array for SAR Systems", *Progress In Electromagnetics Research M*, issue.11, 2010, pp. 165–176. doi: 10.2528/pierm10010606

15. Qiang Fu, Cheng Lee Fan, Li Sijia, Gang Wang, and Xiang-Yu Cao, "Ultra-Broad Band Radar Cross Section Reduction Of Waveguide Slot Antenna With Metamaterials", *Radioengineering*, Vol.25, issue.2, 2016. Pp.241-246. DOI: 10.13164/re.2016.0241

16. Keltouma Nouri, Tayeb Habib Chawki Bouazza, Boubakar Seddik Bouazza, Mehdi Damou, Kada Becharef, and Salima Seghier, "Design of Substrate Integrated Waveguide Multi-band Slots Array Antennas", *International Journal of Information and Electronics Engineering, Vol. 6, No.4*

17. Yousefbeigi, M. and Shahabadi, M., "Substrate-integrated-waveguide feed network for microstrip antenna arrays", *Microwave and Optical Technology Letters*, Vol.51, issue.7, 2009, pp. 1619–1621. doi: 10.1002/mop.24412.

18. Clauzier, S., Le Coq, L., Avrillon, S., Colombel, F., Rochefort, E. and Himdi, M., "Slotted waveguide antenna with a near-field focused beam in one plane", *IET Microwaves, Antennas & Propagation*, Vol.9, issue.7, 2015, pp. 634–639. doi: 10.1049/iet-map.2014.0479

19. G. Srivastava,A. Mohan, "High gain SIW cavity backed differential slot antenna for X-band applications", IET-Electronics letters, Vol.54, issue.24, 2018, pp.1361-1362. https://doi.org/10.1049/el.2018.6390.

20. Mehmet A. Belen. Filiz Güneş. Alper Çalışkan. Peyman Mahouti. Salih Demirel, Aysu Yıldırım, "Microstrip SIW Patch Antenna Design for X band Application", *IEEE Microwave, Radar and Wireless Communications (MIKON), 2016- 21st International Conference*, pp.1-3.doi**:** 10.1109/MIKON.2016.7492095.

21. Sam Leme, and Hendrik Rogier, "SIW textile antennas as a novel technology for UWB RFID tags",*IEEE RFID Technology and Applications Conference (RFID-TA)*, 2014.pp.1-5. doi: 10.1109/RFID-TA.2014.6934239.

22. Massimiliano Casaletti, Guido Valerio, Josip Seljan, Mauro Ettorre, and Ronan Sauleau, "Efficient analysis of SIW-based antenna geometries through a rigorous MoM mode-matching approach", *IEEE Antennas and Propagation Society International Symposium (APSURSI)*. pp.1-2. .doi**:** 10.1109/APS.2013.6711026

23. R.F.Harrington and J.R.Mautz,"Theory of Characteristic Modes for Conducting Bodies," *IEEE Transactions on Antennas and Propagation*, AP-19, 5, September 1971, pp. 622-628.

24. Ajit Rajput, Manorma Kushwah, and Jitendra Dodiya, "Microstrip antenna design using transmission line model in hexagonal shape with probe feed", *IEEE-International Conference on Electrical, Electronics, and Optimization Techniques (ICEEOT)*, 2016. pp.1-4. DOI:10.1109/ICEEOT.2016.7755475.
25. Hong-li Peng, Zheng Tang, Yao-ping Zhang, and J. Mao, "Cavity Model Analysis of a Dual-Probe-Feed Circular Microstrip Patch Antenna", *IEEE- Antennas and wireless propagation letters*, 2016. pp.1-4. DOI:10.1109/LAWP.2015.2427368.
26. Verma R.K., and Srivastava D.K, "Bandwidth Improvement of Stub Loaded Compact Ultra-Wideband Microstrip Patch Antenna for C/X-Band Applications", *Wireless Personal Communications*, 120, 2021.pp.185–202. https://doi.org/10.1007/s11277-021-08441-z
27. A.G. Ambekar., A.A.Deshmukh.,and K.P.Ray, "Stub Loaded Semi-annular Ring Microstrip Antenna for Multiband Dual-Polarized Response", *Proceedings of International Conference on Wireless Communication . Lecture Notes on Data Engineering and Communications Technologies*, Vol 36, 2020, Springer, Singapore. https://doi.org/10.1007/978-981-15-1002-1_10.
28. Ambekar, A.G., Deshmukh A.A., and Chavali V.A.P, "Stub Loaded A-Shape Microstrip Antenna for Dual Polarized Multiband Response", *Proceedings of International Conference on Wireless Communication. Lecture Notes on Data Engineering and Communications Technologies*, Vol 92. Springer, Singapore. https://doi.org/10.1007/978-981-16-6601-8_16.
29. Amandeep Kaur Sidhu, and Jagtar Singh Sivia, "Microstrip Rectangular Patch Antenna for S and X band applications", *IEEE-International Conference on Wireless Communications, Signal Processing and Networking (WiSPNET)*, September 2016. pp.248-251. 10.1109/WiSPNET.2016.7566130.
30. Mohamed Nabil Srifi, Mourad Meloui and Mohamed Essaaidi, "Rectangular Slotted Patch Antenna for 5-6GHz Applications", *International Journal of Microwave and Optical Technology*, Vol.5,issue.2 2014, ,pp.52-57.
31. Rabbani, Muhammad, Ghafouri-Shiraz, and Hooshang, "Design of dual and Wideband Rectangular Patch Antenna for C and X Band Applications", *Advanced Electromagnetics*, 2018, Vol.10, issue.5.pp.145-150. DOI: https://doi.org/10.7716/aem.v7i5.933.
32. Farohaji Kurniawan, Josaphat T. Sri Sumantyo, Koichi Ito, Hiroaki Kuze, and Steven Gao, "Patch Antenna Using Rectangular Centre Slot and Circular Ground Slot for Circularly Polarized Synthetic Aperture Radar (CP-SAR) Application", *Progress In Electromagnetics Research*, 2017, 160,.pp. 51-61. doi:10.2528/PIER17082903.
33. M. Sekhar , S Naga kishore Bhavanam , and P. Siddaiah, "Triple frequency circular patch antenna", *IEEE International Conference on Computational Intelligence and Computing Research*, 2014.pp.1052-1056. DOI: 10.1109/ICCIC.2014.7238527.
34. R. Kiruthika, T. Shanmuganantham, and Rupak Kumar Gupta, "A novel dual band microstrip patch antenna with DGS for X-band applications", *IEEE International Conference on Computer, Communication and Signal Processing (ICCCSP)*, 2017. pp.1-5. DOI: 10.1109/ICCCSP.2017.7944078.

35. NayanSarker, Md. Aminul Islam, and M. Rubaiyat Hossain Mondal, "Two Novel Multiband Centimetre-Wave Patch Antennas for a Novel OFDM Based RFID System", *Journal of Communications*, Vol.13, issue.6. pp.303-316. DOI: 10.12720/jcm.13.6.303-316.

36. Vivek Singh, Brijesh Mishra, and Rajeev Singh, "A Compact and Wide Band Microstrip Patch Antenna for X-Band Applications", *IEEE-Second International Conference on Advances in Computing and Communication Engineering*, October 2015. pp.296-300. DOI: 10.1109/ICACCE.2015.135.

37. Abhinav Anand, and Priyadarshi Suraj, "Design of a stacked microstrip patch antenna for X-band communication", *IEEE-4th International Conference on Recent Advances in Information Technology (RAIT)*, June 2018. pp.1-5. DOI: 10.1109/RAIT.2018.8389017.

38. R. Kiruthika, T. Shanmuganantham, and Rupak Kumar Gupta, "A Fan Shaped Triple Band Microstrip Patch Antenna with DGS for X-band Applications", *IEEE-International Conference on Control, Instrumentation, Communication and Computational Technologies (ICCICCT)*, July 2017, pp.292-297. DOI: 10.1109/ICCICCT.2016.7987962.

39. Parul Dawar, N. S. Raghava and Asok De, "Tunable and directive metamaterial-inspired antennas for 'C' Band Applications", *International Journal of Microwave and Optical Technology*, 2015, Vol.10, issue.3, pp.168-175.

40. M. Samsuzzaman, and M. T. Islam, "Inverted S-Shaped Compact Antenna for X-Band Applications", *The Scientific World Journal*, 2014, 2014, pp.1-11. DOI: 10.1155/2014/604375.

41. M. M. Islam, M. T. Islam, M. R I Faruque, and W. Hueyshin, "Design of an X-band microstrip patch antenna with Enhanced bandwidth", *IEEE-2nd International Conference on Advances in Electrical Engineering (ICAEE 2013)*,2014, pp.313-317. DOI: 10.1109/ICAEE.2013.6750355.

42. J. Anguera, C. Puente, and C. Borja, "A Procedure to Design Wide-Band Electromagnetically-Coupled Stacked Microstrip Antennas Based on a Simple Network Model", *IEEE Antennas and Propagation Society International Symposium, II*, 1999. pp.944-947. DOI: 10.1109/APS.1999.789468.

43. S. Risco, J. Anguera, A. Andújar, A. Pérez, and C. Puente, "Coupled Monopole Antenna Design for Multiband Handset Devices", *Microwave and Optical Technology Letters*, Vol.52, issue.10. pp. 359-364, https://doi.org/10.1002/mop.24893.

44. A. Kandwal, "Compact Dual Band Antenna Design for Ku / Ka Band Applications", *Advanced Electromagnetics (AEM),*Vol.6, issue.4, 2017.pp.1-5. https://doi.org/10.7716/aem.v6i4.450.

45. Brijesh Mishra, "An ultra compact triple band antenna for X/Ku/K band applications", *Microwave and Optical Technology Letters*, Vol. 61, issue.7, 2019. pp.1857-1862.https://doi.org/10.1002/mop.31812.

46. M. M. Islam, M. T. Islam, and M. R. I. Faruque, "Dual-Band Operation of a Microstrip Patch Antenna on a Duroid 5870 Substrate for Ku- and K-Bands", *The Scientific World Journal(Hindawi)*, 2013. pp.1-10. https://doi.org/10.1155/2013/378420.

47. LamyaeAkrou, OtmanAghzout, Henrique Silva, and Mohamed Essaaidi, “Design of Compact Multiband Antenna with Band-Rejection Features for Mobile Broadband Satellite Communications”, *Progress In Electromagnetics Research C*, Vol.68, 2016. pp.95-106.https://doi.org/10.2528/PIERC16073103.

48. SoufianLakrit, Hassan Ammor, SoufianeMatah, Radouane Karli, Adil Saadi,Jaouad Terhzaz, and Abdelwahed Tribak, “A new small high-gain wideband rectangular patch antenna for X and Ku bands applications”, *Journal of Taibah University for Science*,Vol.12, issue.2,2018. pp.202-207. https://doi.org/10.1080/16583655.2018.1451105.

49. M. R. Ahsan , Mohammad Tariqul Islam, M. T. Islam , M Habib Ullah, M. Habib Ullah, Rabah W Aldhaheri, R. W. Aldhaheri, M M Sheikh, and M. M. Sheikh, “A new design approach for dual-band patch antenna serving Ku/K band satellite communications”, *International Journal of Satellite Communications and Networking*, Vol.34, issue.6, 2016.pp.759-769.https://doi.org/10.1002/sat.1130.

50. Manish Sharma, Yogendra Kumar Awasthi, and Himanshu Singh, “Planar high rejection dual band-notch UWB antenna with X & Ku-bands wireless applications”, *International Journal of Microwave and Wireless Technologies*, Vol.9, issue.8, 2017. pp.1725-1733. https://doi.org/10.1017/S1759078717000393.

51. Nagendra P. Yadav, Guozhen Hu,and Zhengpeng Yao, “Parallel Notch and H Shape Slot Loaded Compact Antenna for X and Ku Band Applications”, *Open Journal of Antennas and Propagation(Scientific Research Publishing)*,Vol.7, issue.2,2019. pp.13-21, DOI: https://doi.org/10.4236/ojapr.2019.72002

52. Ankur Dalmiya, and Om Prakash Sharma, “A novel design of multiband Minkowski fractal patch antenna with square patch element for X and Ku band applications”, *International Conference on Recent Advances and Innovations in Engineering (ICRAIE)*,2016.pp.1-6.

53. Mohd G. Siddiqui, Abhishek K. Saroj, Devesh, and Jamshed A. Ansari, “Multi-Band Fractaled Triangular Microstrip Antenna for Wireless Applications”, *Progress In Electromagnetics Research M*, Vol.65, 2018. pp.51-60, https://doi.org/10.2528/PIERM18011027.

54. Parul Dawar, N.S.Raghava, and Asok De.”A novel metamaterial for miniaturization and multi-resonance in antenna” ,*Cogent Physics*, Vol.2, issue.1, 2015, pp.1-13, https://doi.org/10.1080/23311940.2015.1123595.

55. Md. JubaerAlam, M. R. I. Faruque, M. T. Islam, “Split quadrilateral multiband microstrip patch antenna design for modern communication system”, *Microwave and Optical Technology Letters*, Vol.59, issue.7,2017. Pp. 1530-1538, https://doi.org/10.1002/mop.30587.

56. M. Samsuzzaman, M. T. Islam, N . Misran, and M.A. Mohd Ali, “Dual band X shape Microstrip Patch Antenna for Satellite Applications”, *The 4th International Conference on Electrical Engineering and Informatics (ICEEI 2013)*,2013.pp. 1223-1228.

57. Muhammad Asad Rahman, Eisuke Nishiyama, and Ichihiko Toyoda, “A Dual-Band Slot-Embedded Microstrip Antenna for Dual-Polarization Operation”, *Progress In Electromagnetics Research M, Vol.*63, 2018. pp.141-149. https://doi.org/10.2528/PIERM17100501.

58. Gurpreet Singh Saini, and Rajeev Kumar, "A low profile patch antenna for K_u-band applications", *International Journal of Electronics Letters,*Vol.9, issue.1, 2019. pp.1-12. https://doi.org/ 10.1080/21681724.2019.1661018.

59. Md. Rokunuzzaman, M. T. Islam, Baharudin Yatim, and Mhd FairosAsillam., "A Compact Coupled-Line Multiband Microstrip Antenna", *14th International Symposium on Microwave and Optical Technology (ISMOT 2013),* Vol.9,issue.1, 2014.pp. 29-33.

60. M. Habib Ullah, M. T. Islam, and J. S. Mandeep, "Printed Prototype of a Wideband S-Shape Microstrip Patch Antenna for Ku/K Band Applications", *Applied Computational Electromagnetics Society Journal, Vol.*18, issue.4, 2014. pp.307-313,

61. Brijesh Mishra, Vivek Singh, Rakesh Kumar Singh, and Neha Singh,Rajeev Singh, "A compact UWB patch antenna with defected ground for Ku/K band applications", *Microwave and Optical Technology Letters,* Vol.60,issue.1, 2018.pp.1-6.https://doi.org/ 10.1002/mop.30911.

62. M. R. Ahsan, M. Habib Ullah, F. Mansor, N. Misran, and T. Islam, "Analysis of a Compact Wideband Slotted Antenna for Ku Band Applications", *International Journal of Antennas and Propagation*, 2014, pp.1-6. https://doi.org/10.1155/2014/423495.

63. Hossein Malekpoor, and Mehdi Hamidkhani, "CPW-fed printed tapered slot antenna loaded by a wideband stacked artificial magnetic conductor with a progressed performance", *International Journal of Microwave and Wireless Technologies,* 2022.pp.1-10. doi:10.1017/S1759078722000046.

64. Yue GE, Yongjiu ZHAO, and Jiaqing CHEN, "Wideband RCS Reduction and Gain Enhancement for a Patch Antenna with Broadband AMC Structure", *Radioengineering*, Vol.28, issue.1, 2019. pp.45-52. DOI: 10.13164/re.2019.0045

65. Amit Baran Dey, and Wasim Arif, "Design of Flexible and High Gain AMC based Patch Antenna for X-band applications", *IEEE-TENCON,* 2019.pp.1-5. DOI: 10.1109/TENCON.2019.8929449.

66. Debajyoti Chatterjee and Anjan Kumar Kundu, "Study of Miniaturized Patch Microstrip Antenna with Circular Slot and SRR Optimization", *2019 URSI Asia-Pacific Radio Science Conference (AP-RASC)*, 2019, pp.1-4. DOI: 10.23919/URSIAP-RASC.2019.8738443

67. P.Dawar, N.S.Raghava and Asok De, "UWB and miniaturized meandered stripline fed metamaterial loaded antenna for satellite applications", *IOP Conference Series Materials Science and Engineering*, 377(1):012080, 2018, pp.1-11. DOI: 10.1088/1757-899X/377/1/012080.

68. Parul Dawar, N.S.Raghava and Asok De, "UWB, miniaturized and directive metamaterial loaded antenna for satellite applications", International Journal of Networked and Distributed Computing, Vol.6, issue.1, 2018, pp.24-34. DOI: https://doi.org/10.2991/ijndc.2018.6.1.3.

69. Parul Dawar, N.S.Raghava and Asok De, "S-Shaped Metamaterial Ultra-Wideband Directive Patch Antenna", *Radioelectronics and Communications Systems,* Vol.61, pp.2018, pp. 394-405. DOI: https://doi.org/10.3103/S0735272718090029.

70. Parul Dawar, N.S.Raghava and Asok De, "High gain, directive and miniaturized metamaterial C-band antenna", Cogent *Physics*, Vol.3, issue.1, 2016, pp.1-12. DOI: https://doi.org/10.1080/23311940.2016.1236510..

71. Parul Dawar, N.S.Raghava and Asok De, "Ultra Wide Band, Multi-resonance Antenna Using Swastika Metamaterial" , *International Journal of Microwave and Optical Technology*, Vol.11, No.6, 2016, pp.413-420. IJMOT 2014-11-645. IJMOT-2016-6-1035.

72. N.S.Raghava and Asok De, "Photonic Bandgap Stacked Rectangular Microstrip Antenna for Road Vehicle Communication", *IEEE Antennas and Wireless Propagation Letters*, Vol.5, 2006, pp.421-423. DOI: 10.1109/LAWP.2006.883950.

73. N.S. Raghava , Asok De, Nitish Kataria and Sarthak Chatterjee, "Stacked Patch Antenna With Cross Slot Electronic Band Gap Structure", *International Journal of Information and Computation Technology*, Vol.3, No.5, 2013, pp.1-4, arXiv:1310.6259.

74. Anand Kumar , Dinesh Kumar V , Jitendra Mohan and Hari Om Gupta, "Investigation of grid metamaterial and EBG structures and its application to patch antenna", *International Journal of Microwave and Wireless Technologies*, Vol.7, issue.6, 2014, pp.705-712. DOI: https://doi.org/10.1017/S1759078714000944.

75. Raimi Dewan, Mohamad Kamal Abd Rahim, Mohamad Rijal Hamid, Mohamed Himdi, Huda Bin A. Majid, and Noor Asmawati Samsuri, "HIS-EBG Unit Cells for Pattern and Frequency Reconfigurable Dual Band Array Antenna", *Progress In Electromagnetics Research M, Vol. 76, 2018. pp.123-132. doi:10.2528/PIERM18090202.*

76. Kirti Inamdar, Y. P. Kosta and S. Patnaik, "Criss-cross metamaterial-substrate microstrip antenna with enhanced gain and bandwidth", *Radioelectronics and communication systems*, Vol.59,2015. pp.69-74. https://doi.org/10.3103/S073527271502003X.

77. A.Choudhary, N.S.Raghava and Asok De, "A highly efficient Rectangular Microstrip Antenna with hexagonal holes as an Electromagnetic Bandgap structure in the ground plane", International Conference on Recent Advances in Microwave Theory and Applications, 2008, pp.152-153. DOI: DOI:10.1109/AMTA.2008.4763076.

78. N. S. Raghava and Asok De, "A Novel High-Performance Patch Radiator", *International Journal of Microwave Science and Technology*, Volume 2008, Article ID 562193, 2008, pp.1-4. DOI: doi:10.1155/2008/562193.

79. N.S.Raghava and Asok De, "Effect of air gap width on the performance of a stacked square Electronic Band gap Antenna", International Journal of Microwave and Optical Technology, Vol.3, issue.5, 2009, pp.315-317. IJMOT-2009-6-443.

80. Karteek Viswanadha and N.S.Raghava, "Design and analysis of a dual- polarization multiband oval ring patch antenna with L-stubs and folded meander line for C-band/X-band/ Ku-band/ K-band communications", *International Journal of Electronics*, 2020, pp.1-22. DOI: 10.1080/00207217.2020.1793411.

81. Rothwell, E. J., Frasch, J. L., Ellison, S. M., Chahal, P. and Ouedraogo, R. O, "Analysis of the Nicolson–Ross–Weir method for characterizing the electromagnetic properties of engineered materials", *Progress in Electromagnetics Research*, Vol.157, 2016, pp.31–47.DOI: 10.2528/PIER16071706.

82. Wei He, Ronghong Jin, Junping Geng, "E-Shape patch with wideband and circular polarization for millimeter-wave communication", *IEEE Transactions on Antennas and propagation*, Vol.56, Issue.3, 2008, pp.893-895.

83. Nasimuddin, Zhi Ning Chen and Xianming Qing, "Asymmetric-Circular Shaped Slotted Microstrip Antennas for Circular Polarization and RFID Applications", *IEEE Transactions on Antennas and propagation*,Vol.58, Issue.12, 2010, pp.3821-3828.

84. Norbahiah Misran, Mohammed N. Shakib, Mohammad T. Islam, and Baharudin Yatim, "Analysis of broadband slotted microstrip patch antenna" , *IEEE international conference on computer and information technology*, ISBN: 978-1-4244-2135-0, 2008, Bangladesh, pp.758-761.

85. Nasimuddin, Zhi Ning Chen and Xianming Qing, "Slotted Microstrip Antennas for Circular Polarization with Compact Size", *IEEE Transactions on Antennas and Propagation,* Vol.55, Issue.2, 2013, pp.124-137.

86. KK Sharma and Ravi Kumara Goyal, "Slotted microstrip patch antenna at 60GHz for point to point communication", IEEE international conference on communication networks, ISBN: 978-1-5090-0051-7, Gwalior, 2015, pp.371-373.

87. Sourabh Kumar, and Dinesh Kumar Vishwakarma, "Miniaturized curved slotted patch antenna over a fractalized EBG ground plane," *International Journal of Microwave and Wireless Technologies*, Vol. 9, issue.3, 2017. pp.599-605. DOI: https://doi.org/10.1017/S1759078716000052.

88. Ankit Kumar Patel, Shekhar Yadav, Nagesh Kallollu Narayaswamy and Brijesh Mishra, "UWB Multilayer Patch Antenna with EBG Structure for IEEE-C, X, Ku and K Band Applications", *Wireless Personal Communications*, Vol.121,2021. pp.1405-1422. https://doi.org/10.1007/s11277-021-08676-w.

89. R. Sanmuga Sundaram, M. Manikandan, P. Suresh and V. Mariselvam, "A novel EBG backed circular patch antenna for smart devices with multiband applications in smart cities", *International Journal of System Assurance Engineering and Management*, Vol.13, 2022.pp.757-763. https://doi.org/10.1007/s13198-021-01609-7.

90. Taksala Devapriya Amalraj, and Robinson Savarimuthu, "Design and Analysis of Microstrip Patch Antenna Using Periodic EBG Structure for C-Band Applications", *Wireless Personal Communications, Vol.109, 2019, pp.2077-2094.* https://doi.org/10.1007/s11277-019-06669-4.

91. Hongchan Kim,KyuBong Yeon,Wonjong Kim, and Chul Soon Park, "Design and implementation of electromagnetic band-gap embedded antenna for vehicle-to-everything communications in vehicular systems", *ETRI Journal*, Vol.41, issue.6, 2019.pp.731-738. https://doi.org/10.4218/etrij.2017-0197.

92. Sree Pramod Pinapati,Joshua Brittain,Adrian Caldow, and Christophe Fumeaux, "Wearable textile EBG-inspired bandwidth-enhanced patch antenna", IET- Microwave, antennas and propagation, Vol.15, issue.15, 2020.pp.2011-2019. https://doi.org/10.1049/iet-map.2019.1025.

93. Encheng Wang,and Qiuping Liu, ”GPS Patch Antenna Loaded with Fractal EBG Structure Using Organic Magnetic Substrate”, Progress In Electromagnetics Research Letters, Vol. 58, 2016. Pp.23–28.

94. Ameya A. Kadam, and Amit A. Deshmukh, “Pentagonal Shaped UWB Antenna Loaded with Slot and EBG Structure for Dual Band Notched Response”, Progress In Electromagnetics Research M, Vol. 95, 2020.pp. 165-176.

95. Nagendra Kushwaha, and Raj Kumar, “Study of different shape Electromagnetic Band Gap (EBG) structures for single and dual band applications”, The Journal of Microwaves, Optoelectronics and Electromagnetic Applications, Vol.13, issue.1, 2014. pp.16-30. DOI: 10.1590/S2179-10742014000100002.

96. Mekala Harinath Reddy, D. Sheela, Abhay Sharma, and J. J. Tiang, “A novel microstrip antenna loaded with EBG and ELC for bandwidth enhancement”, *Analog Integrated Circuits and Signal Processing*, Vol. 109, 2021. Pp.115-126. https://doi.org/10.1007/s10470-021-01935-7.

97. Ramesh Garg, Prakash Bhartia, Inder J. Bahl, and A. Ittipiboon, “Microstrip Antenna Design Handbook”, Arttech publishers, 2000.

98. Sudeep Baudha, Harshit Garg, and Manish Varun Yadav, “Dumbbell Shaped Microstrip Broadband Antenna”, *Journal of Microwaves, Optoelectronics and Electromagnetic Applications,* Vol.18, 2019. pp.33-42. https://doi.org/10.1590/2179-10742019v18i11371

99. Tapesh Bhandari and Sudeep Baudha, “An UWB Compact Microstrip Antenna for S Band, C Band and X Band Applications”, *12th European Conference on Antennas and Propagation (EuCAP 2018)*, 2018. pp.1-5. 10.1049/cp.2018.1014.

100. Baudha Sudeep and Kumar V.Dinesh, “A Compact Broadband Printed Circular Slot Antenna with Stair Shaped Ground Plane”, *Progress In Electromagnetics Research Letters*, Vol.74, 2018. pp.9-16. doi:10.2528/PIERL17120305.

101. Han-Ul Bong, Minjoo Jeong, Niamat Hussain, Seung-Yeop Rhee, Sang-Keun Gil, and Nam Kim, “Design of an UWB antenna with two slits for 5G/WLAN notched bands”, *Microwave and Optical Technology Letters*, Vol.61, issue.5, 2019. pp.1-6. https://doi.org/10.1002/mop.31670.

102. Boualem Hammache, Abderraouf Messai, Idris Messaoudene, and Tayeb A. Denidni, “A compact ultra-wideband antenna with three C-shaped slots for notched band characteristics”, *Microwave and Optical Technology Letters*, Vol.61, issue.1, 2019. pp.275-279. https://doi.org/10.1002/mop.31670

103. Jiwan Ghimire and Dong-You Choi, “Design of a Compact Ultrawideband U-Shaped Slot Etched on a Circular Patch Antenna with Notch Band Characteristics for Ultrawideband Applications”, *International Journal of Antennas and Propagation*, Vol.2019, 2019.pp.1-10. https://doi.org/10.1155/2019/8090936.

104. Kakani Suvarna, Nallagarla Ramamurthy, and Dupakuntla V. Vardhan, “Gain Enhanced Characteristics of Miniaturized Antenna for 5 GHz WLAN Application”, Progress in Electromagnetics, Vol. 124, 2022. pp.23–32.

105. Jai Magnal, Gaurav Varshney, and Anvesh Kumar, "Miniaturization of a Conventional WLAN 2.45GHz Patch Antenna using Slot Insertion Technique", *IEEE-11th International Conference on Computing, Communication and Networking Technologies (ICCCNT)*, 2020. pp.1-7. DOI: 10.1109/ICCCNT49239.2020.9225664.

106. Tanweer Ali, and Rajashekhar Biradar, "A triple-band highly miniaturized antenna for WiMAX/WLAN applications", *Microwave and Optical Technology Letters*, Vol.60, issue.2, 2018.pp.466-471. DOI: 10.1002/mop.30993.

107. Xiaosheng Guo, Weiwei Liao, Qingfeng and Zhang Yifan Chen, "A dual-band embedded inverted T-slot circular microstrip patch antenna," *IEEE 5th Asia-Pacific Conference on Antennas and Propagation (APCAP)*, Taiwan, 2016. pp.151-152. DOI: 10.1109/APCAP.2016.7843143.

108. Bhupendra K. Shukla, Nitesh Kashyap, and Rajendra K. Baghel. "Circular Slotted Elliptical Patch Antenna with Elliptical Notch in Ground", *Progress In Electromagnetics Research C*, Vol.74, 2017.pp.181-189.

109. Avisankar Roy,Sunandan Bhunia, Debasree C. Sarkar, and Partha P. Sarkar, "Slot Loaded Compact Microstrip Patch Antenna for Dual Band Operation", *Progress In Electromagnetics Research C*, Vol.73, 2017. pp.145-156.

110. Mohamed A. Abdelaal and Hussein Hamed Mahmoud Ghouz, "New Compact Circular Ring Microstrip Patch Antennas", *Progress In Electromagnetics Research C*, Vol.46,2018. pp. 135-143.

111. Deepanshu Kaushal and T.Shanmuganantham, "Parametric enhancement of a novel microstrip patch antenna using Circular SRR Loaded Fractal Geometry", *Alexandria Engineering Journal*, Vol.57, issue.4, 2018.pp.2551-2557. https://doi.org/10.1016/j.aej.2017.08.021.

112. Mukesh Kumar Khandelwal, Binod Kumar Kanaujia, Santanu Dwari, Sachin Kumar and A.K.Gautam. "Analysis and design of dual band compact stacked Microstrip patch antenna with defected ground structure for WLAN/WiMax applications", *AEU - International Journal of Electronics and Communications*,Vol. 69, issue.1,2015. pp.39-47. https://doi.org/10.1016/j.aeue.2014.07.018.

113. Azadeh Pirooj, Mohammad Naser-Moghadasi, Ferdows B. Zarrabi, and Alireza Sharifi, "A Dual Band Slot Antenna for Wireless Applications with Circular Polarization", *Progress In Electromagnetics Research C*, Vol.71,2017. pp. 69-77.

114. Qasim Awais, Hassan Tariq Chattha, Mohsin Jamil, Yang Jin, Farooq Ahmad Tahir, and Masood Ur Rehman, "A Novel Dual Ultrawideband CPW-Fed Printed Antenna for Internet of Things (IoT) Applications", *Wireless Communications and Mobile Computing*, 2018. pp.1-9. https://doi.org/10.1155/2018/2179571.

115. Sachin Kumar, Alind P. Singh , and Mukesh K. Khandelwal, "Theoretical Analysis and Design of Dual Band DGS Antenna with Small Frequency Ratio for Wi-Fi and WiMAX Applications", *Progress In Electromagnetics Research M*, Vol.62, 2017. pp.153-166.

116. Abhishek K. Saroj, Mohd. G. Siddiqui, Mukesh Kumar, and Jamshed A. Ansari, "Design of Multiband Quad-Rectangular Shaped Microstrip Antenna for Wireless Applications", *Progress In Electromagnetics Research M*, Vol.59, 2017, pp. 213-221.

117. Amanpreet Kaur, Rajesh Khanna and Machavaram Kartikeyan, "A multilayer dual wideband circularly polarized microstrip antenna with DGS for WLAN/Bluetooth/ZigBee/Wi-Max/ IMT band applications", *International Journal of Microwave and Wireless Technologies*, Vol.9, issue.2, 2015. pp.317-325. DOI: 10.1017/S1759078715001294.

118. L. A. R. Ramirez and J. C. A. Santos, "Design, Simulation, and Optimization of an Irregularly Shaped Microstrip Patch Antenna for Air-to-Ground Communications, International Journal of Antennas and Propagation", 2017. pp.1-9. https://doi.org/10.1155/2017/5156263.

119. Puneet Khanna, Amar Sharma, Kshitij Shinghal, and Arun Kumar, "A Defected Structure Shaped CPW-Fed Wideband Microstrip Antenna for Wireless Applications", *Journal of Engineering*, 2016.pp.1-7. https://doi.org/10.1155/2016/2863508

120. Tanweer Ali, Mohammad Saadh Aw and Rajashekhar C. Biradar, "A fractal quad-band antenna loaded with L-shaped slot and metamaterial for wireless applications", *International Journal of Microwave and Wireless Technologies*,Vol.10, issue.7 2018. pp.826-834. doi: 10.1017/S1759078718000272.

121. Sumeet S. Bhatia , Aditi Sahni, and Shashi B. Rana, "A Novel Design of Compact Monopole Antenna with Defected Ground Plane for Wideband Applications", *Progress In Electromagnetics Research M* ,Vol. 70, 2018. pp. 21-31.

122. Tanweer Ali and Rajashekhar C. Biradar, "A compact hexagonal slot dual band frequency reconfigurable antenna for WLAN applications", *Microwave and Optical Technology Letters*, Vol.59, issue.4,2016. pp. 958-964. https://doi.org/10.1002/mop.30443.

123. Mohammad Alibakhshikenari, ErnestoLimiti, Mohammad Naser-Moghadasi, Bal S.Virdee, and R.A.Sadeghzadehd, "A new wideband planar antenna with band-notch functionality at GPS, Bluetooth and WiFi bands for integration in portable wireless systems", *AEU - International Journal of Electronics and Communications*, Vol.72, 2017.pp. 79-85. https://doi.org/10.1016/j.aeue.2016.11.023.

124. Siddhant Arun Goswami, and Deepak Karia, "A compact monopole antenna for wireless applications with enhanced bandwidth", *AEU - International Journal of Electronics and Communications*, Vol.72, 2017.pp.33-39. https://doi.org/10.1016/j.aeue.2016.10.024.

125. Zhengxin Fang, "Design of S band Cylindrical Waveguide Slot Omnidirectional Antenna", *SPACOMM 2018 : The Tenth International Conference on Advances in Satellite and Space Communications*, 2018. pp.48-50..

126. Amirhossein Ghasemi, and Jean-Jacques Laurin, "A Continuous Beam Steering Slotted Waveguide Antenna Using Rotating Dielectric Slabs",*IEEE Transactions on Antennas and Propagation*, Vol.67, issue.10, 2019. pp. 6362 – 6370. DOI: 10.1109/TAP.2019.2925272.

127. Amirmasoud Ohadi, and George V. Eleftheriades, "A Beam-steerable Slotted Waveguide Antenna With Tunable Impedance Walls", *IEEE International Symposium on Antennas and Propagation and North American Radio Science Meeting*, 2020. pp.1-2. DOI: 10.1109/IEEECONF35879.2020.9330412.

128. I. F. da Costa, R. A. Santos, S. C. Patricio, J. A. J. Ribeiro, D. H. Spadoti, A. Bogoni, and Arismar Cerqueira S, "A dual-band slotted waveguide antenna array for radars applications", *SBMO/IEEE MTT-S International Microwave and Optoelectronics Conference (IMOC)*, pp.1-4, January 2016.

129. M. Al-Husseini, A. El-Hajj , and K. Y. Kabalan, "High-gain S-band Slotted Waveguide Antenna Arrays with Elliptical Slots and Low Sidelobe Levels", Progress In Electromagnetics Research Symposium Proceedings, Stockholm, Sweden, pp.1821-1824, August 2013.

130. Cerqueira S. Arismar, I. F. da Costa, Sergio Pinna, Suzanne Melo, Francesco Laghezza, Filippo Scotti, Paolo Ghelfi, Danilo Spadoti, and A. Bogoni, "A novel dual-polarization and dual-band slotted waveguide antenna array for dual-use radars", *10th European Conference on Antennas and Propagation (EuCAP)*, 2016. pp.1-4.

131. Hilal M. El Misilmani, Mohammed Al-Husseini, and Karim Y. Kabalan, "Design of Slotted Waveguide Antennas with Low Sidelobes for High Power Microwave Applications", *Progress In Electromagnetics Research C*,2015. pp.15-28.

132. Jasmine Saini and Manoj Kumar Garg, "PBG structured compact antenna with switching capability in lower and upper bands of 5G" *Progress In Electromagnetics Research M*, Vol. 94, pp.19-29,2020. DOI:10.2528/PIERM20022202.

133. Taksala Devapriya Amalraj and Robinson Savarimuthu, "Design and Analysis of Microstrip Patch Antenna Using Periodic EBG Structure for C-Band Applications", *Wireless Personal Communications*, Vol.109, pp.2077–2094, 2019. https://doi.org/10.1007/s11277-019-06669-4.

134. Yahiea Alnaiemy and Lajos Nagy, "Improved Antenna Gain and Efficiency Using Novel EBG Layer", *IEEE-International Conference of System of Systems Engineering*, 2020. pp.271-276..

135. Urmi Das and Nusrat Jahan, "Dual Band Rectangular Slotted Electromagnetic Band Gap Structure Design for improving Microstrip Patch Antenna Performance", *IEEE-11th International Conference on Electrical and Computer Engineering*, 2020. pp.97-100.

136. Nigar Berna Tesneli, Cemile Tangel and Ahmet Yahya Tesneli, "Performance Improvement of a Microstrip Patch Antenna by Using Electromagnetic Band Gap and Defected Ground Structures", *IEEE-2nd International Conference on Electrical, Communication and Computer Engineering (ICECCE)*, pp.1-4, 2020.

137. Garima Joshi and R.Vijaya, "Dual Band Microstrip Patch Antenna using Uniplanar EBG of Aperture type FSS", *IEEE-Indian Conference on Antennas and Propagation (InCAP)*, 2019.pp.1-4.

138. Anand C Konnur, Arun S Tigadi, PrabhakarManage and Shambulingappa K Vadeyanpur, "High gain patch antenna using EBG structures for WiMAX application", *International Conference on Recent Innovations in Engineering and Technology (ICRIET 2020)*, Vol.1070,pp.1-9, 2020.

139. Mohammad Ismail Zaman, Farzad Tavakkol Hamedani and Hana Amjadi, "A New EBG structure and its application on microstrip patch antenna", *IEEE-International Symposium on Antenna Technology and Applied Electromagnetics*, pp.1-3, 2012.

140. Jamal Zaid, Mohammadmahdi Farahani, Arun Kesavan and Tayeb A. Denidni, "Miniaturized microstrip patch antenna using Electromagnetic Band Gap (EBG) structures for multiport passive UHF RFID-tag applications", *IEEE-International Symposium on Antennas and Propagation & USNC/URSI National Radio Science Meeting*, pp. 2459-2460, 2017.

141. Saurabh Singh and Sudhanshu Verma, "Printed compact asymmetric dual L-strip fed split-ring shaped EBG-based textile antenna for WBAN applications", *Microwave and Optical Technology Letters*, Vol.62, issue.12, 2020. https://doi.org/10.1002/mop.32512

142. Xiaoyan Zhang, Zhaopeng Teng, Zhiqing Liu and Bincheng Li, "A Dual Band Patch Antenna with a Pinwheel-Shaped Slots EBG Substrate", *International Journal of Antennas and Propagation*, Vol.2015, pp.1-8,2015. http://dx.doi.org/10.1155/2015/815751.

143. El Amjed Hajlaoui, "New triple band electromagnetic band gap microstrip patch antenna with two shaped parasitic elements", *Journal of Computational Electronics*, Vol.17, pp.452-457, 2018. https://doi.org/10.1007/s10825-017-1100-x.

144. Taha Ahmed Elwi, Ahmed Imad Imran and Yahiea Alnaiemy, "A Miniaturized Lotus Shaped Microstrip Antenna Loaded with EBG Structures for High Gain-Bandwidth Product Applications", *Progress In Electromagnetics Research C*, Vol. 60, pp.157-167, 2015. doi:10.2528/PIERC15101804.

145. O. Borazjani , M. Naser-Moghadasi ,J. Rashed-Mohassel and R. A. Sadeghzadeh, "Bandwidth improvement of planar antennas using a single-layer metamaterial substrate for X-band application", *International Journal of Microwave and Wireless Technologies*, Vol.12, issue.9, pp.906-914,2020. doi:10.1017/S1759078720000264.